Facoltà di Scienze Matematiche Fisiche e Naturali

Dipartimento di Chimica

XXVI Ciclo Dottorato in Chimica Analitica e Dei Sistemi Reali

DEVELOPMENT OF ANALYTICAL METHODOLOGIES FOR THE MONITORING OF THE ATMOSPHERIC PARTICULATE MATTER

Relatore

Dott.ssa Silvia Canepari

Dottorando

Carmela Farao

Matricola 1101006

ANNO ACCADEMICO 2013/2014

SUMMARY

ABSTRACT

The present research project focused on the development of analytical methodologies for the monitoring of the atmospheric Particulate Matter.

Particulate matter (PM) is one of the main pollutants exceeding the ambient standards for air quality in Europe. In Italy, the mass concentration standards are overcome many times per year, mainly due to the unfavourable meteorological conditions (especially in the Po Valley regions) and to the transportation of the air masses coming from the Sahara Desert (Southern and Central regions). The direct and indirect influence of the PM on human health, global climate change and reduced visibility have led to numerous studies in the last past decades, focusing upon its complex composition, toxicology and the source attribution. The particulate matter is constituted by an heterogeneous mix of components, characterized by a variable chemical composition and different chemical-physical properties that greatly influence its deposition and distribution. For these reasons nowadays it is still very difficult to develop efficient abatement strategies to protect both human health and environment. To achieve these specific objectives it is necessary to focus on some issues that are still not resolved, by taking advantage of both the analytical chemistry and the statistical methods.

One of the "open" issues is the determination of water content in PM. Water plays an important role in the formation of the secondary species starting from gaseous precursors. It is well known that these species undergo gas-particle equilibria influencing the sampling phase and altering the results of the monitoring campaigns but, given the great variability of the measured concentrations, to date, a clear interpretation of these processes has still not been found. More information could be obtained by determining the water content in PM. Moreover, the knowledge of the water amount sampled together with the atmospheric particles on appropriate media could be very useful to establish the water influence on the PM mass concentration as well. Till now, the water determination has been carried out mostly by indirect methods estimating the water adsorbed on not-sampled particles. During the present project a simple method to determine water in PM samples has been optimized and validated, based on the Karl-Fisher theory. The potentialities of the thermal desorption were also explored to study the different types of water linked to the particles. After the validation, this methodology has been then applied to real PM samples collected in geographical areas characterized by several emission sources (traffic, industries, etc.), demonstrating that water is a relevant component of the PM and it influences in a significant way the PM mass concentration especially in samples very rich of secondary inorganic compounds or

natural sand. Moreover the type of water present in the atmospheric particles is strictly dependent on the PM chemical composition.

The second part of this project concerned the measurements of the PM at high temporal resolution. Sampling and analysis of PM in real time at high time resolution allow to have some precious information about the temporal variability of the atmospheric pollutants' concentration, that usually are lost with the 24-hours sampling time. Our attention was focused on a new device able to sample and analyze in real time the atmospheric inorganic ions, the Particle Into Liquid Sampler coupled with the Ion Chromatography (PILS-IC). The instrument in its original configuration is affected by some limits, the high detection limit values that make difficult to apply it in low polluted areas and the low time resolution due to the analysis of the solution contained in the chromatographic loop only at the injection time into the column. These limits were solved modifying the original instrumental configuration, inserting a pre-concentration system. The new optimized system was then validated and applied to a monitoring campaign. The results have been compared with those obtained by other analytical techniques aimed to measure the same species, showing good performance of the new system. The data obtained by using this system were also useful to understand the chemical form in which the ions were present in the atmosphere at the sampling time and allowed to isolate some *hot spot* pollution events.

The last part of the present project has been carried out at the University of Birmingham (United Kingdom) under the kindly supervision of Prof. Roy M.Harrison and focused on the traceability of the PM emission sources. The knowledge of the emission sources is one of the main objectives in the PM studies, as it is necessary for developing efficient abatement strategies. The Source Apportion techniques are very helpful to reach this objective. In particular, the Positive Matrix Factorization receptor model (PMF) was applied to identify and quantify the PM sources at an industrial area of the Po Valley. This model is very useful to manage large databases coming from the chemical analysis of PM collected during long monitoring campaigns and is able to determine the main PM sources by looking at the correlation of the variables (measured species) at the monitored receptor sites. The variables to process by the model have been chosen with the support of a detailed chemical characterization of PM using a fractionation methodology based on the elemental solubility. The main PM sources in the Po Valley have been identified with the secondary nitrate and the biomass burning, although the industrial nature of the monitored area.

Because of the wideness of the topics they will be treated in separated chapters.

Chapter 1 – ATMOSPHERIC PARTICULATE MATTER

1.1 Introduction: definitions and classifications

Particulate matter (PM) is the term used for a mixture of solid and liquid particles suspended in the atmosphere, with an aerodynamic diameter ranging between 0.01 and 100 μm. The heterogeneous composition of these particles takes in soot, dust, differently originated salts, fly ashes, trace metals and biological micro-organisms (viruses, bacteria, fungi, spores and pollen) (Manahan 2000; EPA 1997).

A first general classification of PM can be made considering the emission sources, which are distinguished in:

• *Natural sources*: volcanic eruptions, forest fires, erosion and disintegration of rocks, plants (pollen and plant residues), spores, sea spray.

• *Anthropogenic sources*: combustion engines (trucks, cars, airplanes), domestic heating (especially coal and wood), road surface abrasion, brakes and tires wear, construction works, industries, agricultural processes, incinerators and power plants, tobacco smoke.

On a global level, the masses of particulate matter produced by natural causes take precedence over those produced by human activities. The anthropogenic sources are, however, able to introduce into the atmosphere a greater amount of particles toxicologically harmful for the health and the environment. In addition, these sources tend to concentrate spatially, making some areas (urban and industrial sites) more at risk than others.

Atmospheric particles may also be classified as primary or secondary depending on its mechanism of formation.

Primary particles are directly emitted into the atmosphere consisting of fuel combustion, surface erosion and windblown dusts, and mechanical break-up from for example, quarrying and construction activities. *Secondary particles* are those formed in the air, generally by chemical reactions of gaseous precursors, sulphur dioxide (SO_2), nitrogen oxides (NO_x) and ammonia (NH_3) to form particulate sulphates and nitrates, as well as organic aerosols formed from the photochemically-induced oxidation of volatile organic compounds (EC 2004e).

The heterogeneous character of PM makes necessary to introduce different detailed classifications, each of them evidencing its peculiar physical – chemical properties.

Differently originated particles show very different sizes and shapes as it can be seen in Figures 1.1 a-b.

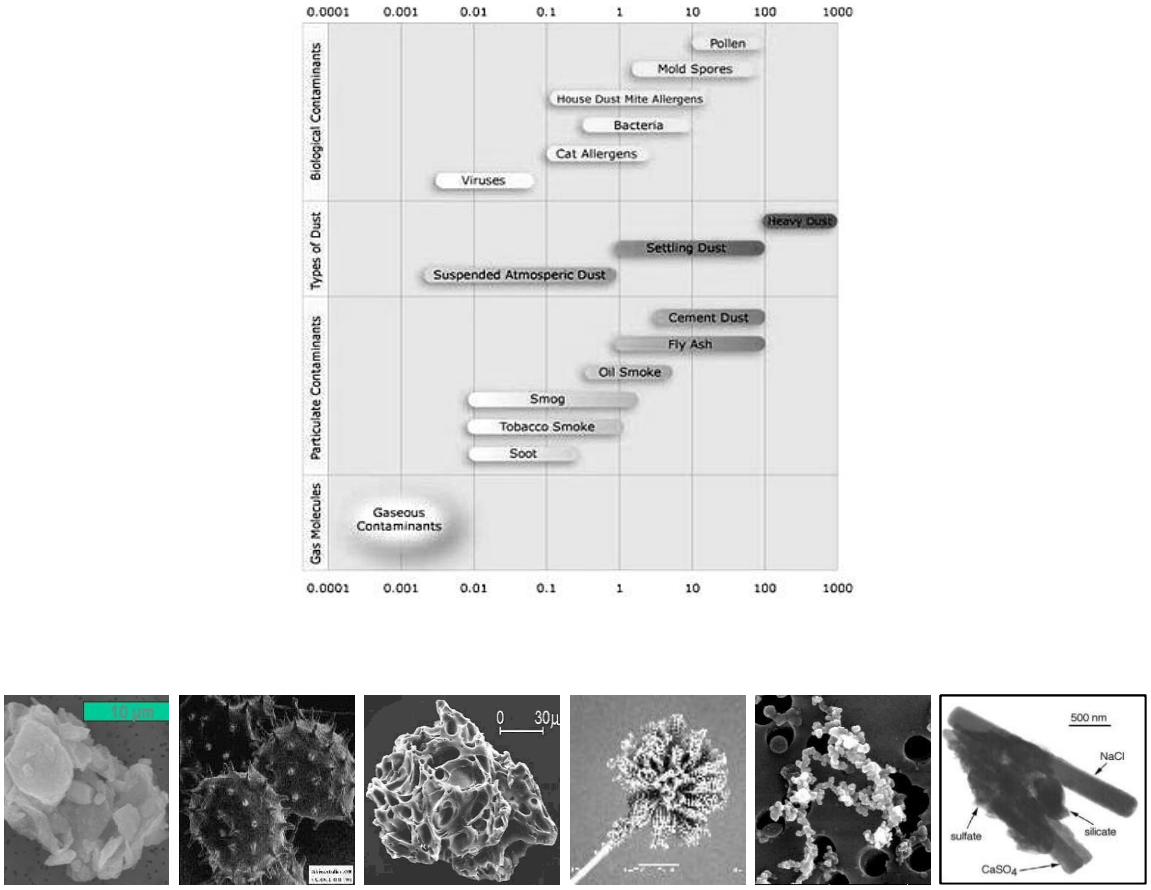

Fig. 1.1 (Upper panel). Size distribution in micrometres of various types of atmospheric particulate matter. (Lower panel). Scanning electron or transmission electron microscope images. From the left to the right: desertic particle (A. Gaudichet, LISA); hibiscus pollen :http://uq.edu.au/nanoworld); ash particle from the eruption of Mount St. Helens (http://volcanoes.usgs.gov); indoor moulds (M. Boissier, CSTB); soot particle (MPI for Chemistry Mainz); mineral dust from marine throposphere (Copyright © 1999, The National Academy of Sciences) http://www.env.leeds.ac.uk/envi2150/oldnotes/lecture4/gases.html

Although the atmospheric particles have not a regular shape, they can be classified referring to the *aerodynamic diameter* (a.d.), defined as the diameter of a unit-density spherical particle ($1 g/cm^3$) having the same aerodynamic properties (sedimentation rate) of a given particle (John 2001).

Regarding the dimensional characteristics, atmospheric particles are divided in three different sub-classifications: *modal*, based on the mechanisms of particle formation and consequently on their number, surface area and mass distribution (Whitby 1978); *dimensional (size) cut-off*, based on the efficiency of the sampling head device during the PM collection and *dosimetric*, based on the particles' ability to enter and penetrate into the respiratory system.

1.1.1Modal classification

By plotting the number of suspended particles versus their size it will generate a multimodal distribution, as showed in fig 1.2. This refers to the classification by Whitby in 1978 later updated by the EPA in 1997 (John 2001).

Particles with less than 0.1 µm aerodynamic diameter ("ultra-fine" fraction) are found in the *nucleation* mode, including combustion and gas – particle processes. The *accumulation* mode considers those particles having an aerodynamic diameter between 0.1 and 2.5 µm, generated by coagulation and condensation mechanisms involving nucleation particles, giving altogether the so called "fine" fraction. Finally, the *coarse* mode includes particles with an aerodynamic diameter higher than 2.5 and up to 100 µm, which originate from mechanical processes, such as erosion and abrasion, re-suspension of dust and fragments of organic and vegetable materials, air masses transported from marine or desertic sites (John 2001; Puxbaum 1991). However, by current convention (EC 1997) particles between 2.5 and 10 µm are called "*coarse particles*", whereas particles less than 2.5 µm are called "*fine particles*" and the expression "*ultrafine particles*" is used mostly in health related literature as notion for particles less than 0.1 µm.

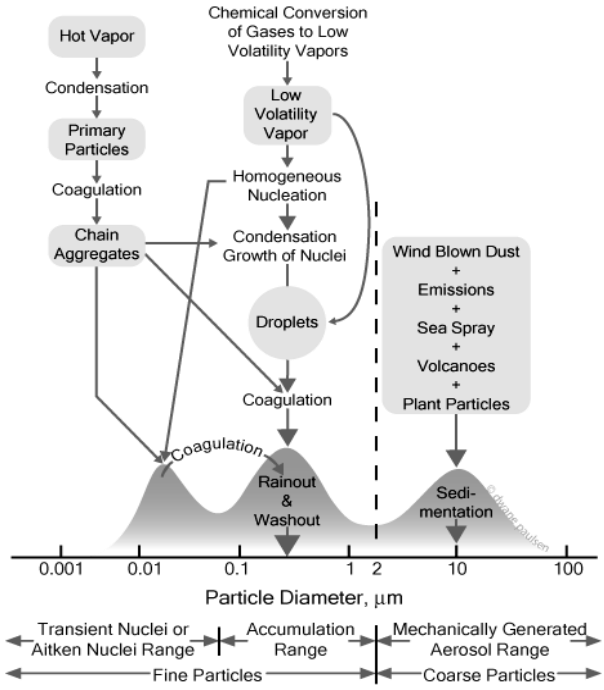

Figure 2.1. The three ranges for atmospheric particles and the processes leading to their formation.

1.1.2 Size cut – off classification

This kind of classification refers to the technical specifications of the PM sampling devices.

PM_X is the fraction of particulate matter that has been collected by a selective inlet impactor with a 50% efficiency cut-off at X μm aerodynamic diameter (EC 1997). Indeed, the instruments usually used in the air sampling stage collect particles that fall within a size range rather than one single size. The most commonly available sampling heads for commercial samplers collect mainly the PM_{10} and $PM_{2.5}$ fractions, being the most interesting for both health/environmental effects and investigations on the life-cycle of airborne particles. Nowadays, the PM_1 fraction is gaining more attention, as smaller particles have potentially higher toxicity and capability to infiltrate into the pulmonary system.

Therefore, the "*fine*" fraction will be intended for $PM_{2.5}$ fraction, while the "*coarse*" fraction will be intended to include particles with aerodynamic diameter between 2,5 and 10 μm, that is the difference between PM_{10} and $PM_{2.5}$ (EPA 1999).

Conventional PM_{10} and $PM_{2.5}$ samplers show a 50% efficiency in collecting particles with 10 ± 0.5 μm or 2.5±0.5 μm aerodynamic diameter.

1.1.3 Dosimetric classification

The dosimetric classification is based on the capability of airborne particles to enter, infiltrate, deposit and react with the different zones of the respiratory system, as showed in figure 1.3. These actions depend on the particle chemical composition, size and solubility.

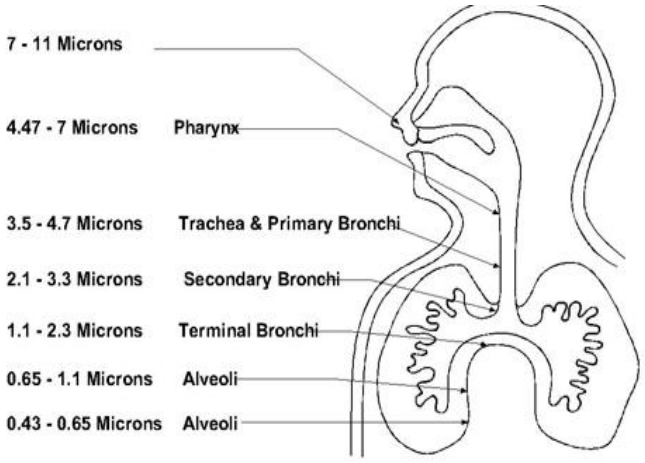

Fig.1.3: Potential deposition of particles with different sizes into the respiratory system (http://www.acrd.bc.ca/cms.asp?wpID=314).

Particles greater than 10 μm a.d. are mainly deposited in the upper system, particles between 5 and 10 μm are deposited in the trachea and pharynx, and particles of less than 2 μm penetrate significantly into the bronchi and alveoli.

Therefore, under this classification particles are identified by four fractions: *inhalable*, particles which pass into the nose and mouth; *thoracic*, particles which deposit within the lower respiratory tract, including particles that reach lungs; *respirable*, particles penetrating significantly up to the gas-exchange region of alveoli; *respirable "high risk"* fraction, which refers to the harmful effects of the respirable fraction on children and people suffering from cardio-pulmonary diseases (Mark 1999).

1.2 Chemical composition of particulate matter

The chemical composition of the particulate matter is very complex and includes a large number of species. It can be divided into two major classes:

- The *macro-components*: inorganic ions, elements and carbon-containing compounds that exceed more than 1% of the PM mass;
- The *micro-components*: metals present in trace amount (< 1% of PM mass).

The species present in PM depend on the nature of the emission sources , but also on the chemical-physical processes occurring in the atmosphere and the location of the monitoring site.

Furthermore, the chemical composition changes by varying the particle size: recent environmental studies show that the majority of the *fine* fraction is constituted by chemical species such as elemental carbon (EC), sulphates (normally present as ammonium salts) and various organic compounds of primary and secondary origin; the *coarse* fraction is mainly formed by elements coming from the earth's crust (Ca, Al, Si, Mg, Fe) and some bio-organic materials such as pollen, spores, plants and animal wastes.

1.2.1 PM macro-components

Among the macro-components it can be found anions, (Cl^-, NO^{3-}, SO_4^{2-}, CO_3^{2-}, SiO_4^{4-}), cations (Na^+, NH_4^+, K^+, Mg^{2+}, Ca^{2+}) and some of elements (Al, Si, Fe). In addition a relevant fraction of the macro-components is constituted by EC-containing compounds and organic matter. It is possible to

further subdivide the ions in reference to their primary or secondary nature. The primary ions are *chlorides* – coming from marine aerosol or from the waste incineration-, *sodium*- coming from marine aerosol and partly from the soil-, *calcium*- coming from soil, wood combustion, fires and industrial activities-, *magnesium*- coming from marine aerosol and soil-, *potassium*- coming from the earth's crust, biomass combustion and agricultural fertilization-, *sulphates*- mainly present as secondary species but a minimal part comes from the marine aerosol-, *silicates and carbonate*- mainly present in the earth's crust.

On the contrary, the gaseous precursors for the secondary compounds formation are *sulphide oxides* and *nitrogen oxides* – coming mainly from coal and fuel combustion processes, e.g. power plants, heating plants, vehicular traffic- and *ammonia*- coming from the microbiological activity of the soil and sea; it can be formed also by reduction of NO_x; it is emitted by stock farms and, on a urban local scale, by the vehicular exhausts.

These gaseous precursors give rise to acid-base reactions in the atmosphere leading to the formation of salts, such as sulphate and ammonium nitrate.

In general, the formation and the composition of the secondary particles depends largely on the acid-base reactions, oxidation processes, gas-particle interactions that from gaseous precursors give rise to several products (as discussed in the next paragraphs). These reactions mainly involve the inorganic species and influence their solubility and their transferability to the surrounding environment.

1.2.2 Carbon containing compounds

The total carbon fraction present in the PM, occurring for 20-60% of the total mass, can be divided into organic carbon (OC) and elemental carbon (EC). Their presence is due to some changes in the physical conditions during the combustion process that lead to a deviation from an ideal combustion. Indeed, besides of CO_2 and H_2O, also other organic gas (such as CH_4, hydrocarbons and volatile organic compounds) are released in the atmosphere. Along with these also solid particles, such as soot and aerosol particles are released.

The EC is directly emitted into the atmosphere by combustion processes either as single particles or clusters with variable shape and size (Barone et al., 2006).

The OC fraction is constituted by a complex mix of numerous compounds. Lots of studies have been done to attempt their identification and classification but, nowadays, only few classes are

known. Some of these are very harmful to the human health such as alkanes, benzoic acids, benzaldehydes, phenols, furans, carboxylic acids, polycarboxylic aromatic acids, aliphatic acids, polycyclic aromatic hydrocarbons (PAHs), polycyclic aromatic ketones, sterols and pesticides. Primary organic compounds come from combustion processes and from geological and natural sources, e.g. meat cooking, paving roads, chimney emissions, forest fires and cigarette smoke (Gelencsér et al., 2000), while secondary organic compounds come some reactions occurring in the atmosphere involving volatile organic compounds (VOCs) and oxidant species such as O_3 and OH radical.

1.2.3 PM micro-components

PM includes also a great number of elements with a variable percentage depending on the different nature and origin of the particles. Trace metals coming from natural sources are related to the geological composition of the earth's crust. Also, their suspension in the air is due to the physical, chemical, biological and meteorological processes, such as the particles resuspension from the soil by wind, the volcanoes (which emit Cd, Hg, As, Cr, Cu, Ni, Pb and Sb), the sea spray (which leads to an enrichment in Cd, Cu, Ni, Pb and Zn) and the forest fires (which may originate metals such as Cu, Pb and Zn) (Pacyna, 1999).

The release of trace metals into the atmosphere by anthropogenic activity is much more significant and is attributable to the various industrial processes, the production of electricity, the combustion of fossil fuels to generate heat and to the vehicular traffic: these sources are responsible for more than 50% of the total emissions of Cr, Mn and V and for 20-30% of the annual release into the atmosphere of metals such as Cu, Mo, Ni, Pb, Sb, as, Se, Hg, Sn and Zn (Moore,1994). Other sources of trace metals can be identified with the waste incineration and paved roads: the latter emits Al, Si, K, Ca, Ti and Fe, mainly contained in the *coarse* fraction, while the first releases in atmosphere elements mainly included in the *fine* fraction such as Cu, Zn, Cd, Sb, Pb and Ca, Cr, Mn, Ni (Abbas et al., 2001; Phongphiphat et al., 2011). By studying the metal distributions and their emission sources, it may have more information about the interpretation of the environmental pollution phenomena. An example is given by the use of Ni and V as tracers, which are released mainly during the combustion of oils. As their concentration coming from natural sources is very low, they are used as indicators of local anthropogenic pollution, such as the production of electrical energy (Claes et al., 1999).

1.3 Chemical reactions of particulate matter

Atmospheric particles undergo a large number of different homogeneous and heterogeneous chemical reactions influencing their chemical composition, degradation rates and residence time in the atmosphere.

Heterogeneous reactions directly or indirectly affect the degradation rates of airborne chemicals and modify their atmospheric residence times. According to their surface properties, aerosol particles interact with gaseous species, radicals and other reactive intermediates.

Typical heterogeneous processes occur on either solids or supercooled liquids in the polar winter stratosphere (Schurath and Naumann, 1998). Extensive laboratory studies have confirmed that these reactions convert chlorine and bromine into photoactive halogen compounds that catalyze the destruction of ozone under the sunlight action.

Heterogeneous reactions between gases and particulate matter must also be considered in the troposphere, particularly in the polluted boundary layer where the aerosol particles are more abundant. They can occur between the gaseous species (ozone, H_2O radicals, SO_2 and HNO_3) and the mineral dust. Obviously, these reactions have a direct impact on the environmental SO_2 and NO_x, which can be directly degraded by heterogeneous processes on particles.

Heterogeneous interactions of NO_2 with aerosol particles are of extreme interest because they are a likely night-time source of HONO. Also the heterogeneous reaction between soot particles and (PAHs) has to be mentioned. The PAHs condense on the particles when the temperature drops after the soot particles have been formed at very high temperatures.

Finally, other heterogeneous processes involving reactive gaseous species and various types of particulate to be cited are the chemisorption of radicals on diesel or aircraft soot, the solubilisation of metals in mineral dusts, the gas-to-particle conversion of particles coated with organic species and the pH dependent uptake of acidic/alkaline gases in sea salt particles.

Many reactions, indeed, involve the inorganic components of atmospheric particulate influencing its acidic properties and therefore affecting the solubility of the chemical components and their environmental mobility.

In the atmosphere mineral and organic acids may exist both in the particulate and gaseous forms. The latter (mainly formic, acetic and oxalate acids) tend to be not dissociated, irrespective of the

phase in which they are, and therefore less relevantly affect the particles' acidity. Conversely, mineral acids are the main responsible for this, being the largest fraction of acidic species in the atmosphere. Main mineral acids in the particulate form are sulphuric acid (H_2SO_4) and bi-sulphate ion (HSO_4^-), while nitric, nitrous and chloridric acids (HNO_3 , HNO_2 , HCl) are prevalent in the gaseous phase. Particularly, the H_2SO_4 is the main component in acid particulates, due to the reaction of SO_2 (highly hygroscopic) with water vapour under oxidation conditions (2) (Polyak 2001).

$$2\ SO_2 + O_2 + 2\ H_2O \rightarrow 2\ H_2SO_4 \quad (1)$$

In the presence of alkaline pollutants such as ammonia and calcium oxide the H_2SO_4 gives the following reactions (3-4):

$$H_2SO_4\ (aq) + 2\ NH_3\ (g) \rightleftharpoons (NH_4)_2SO_4\ (aq) \quad (2)$$

$$H_2SO_4\ (aq) + CaO\ (s) \rightleftharpoons CaSO_4\ (aq) + H_2O \quad (3)$$

whereas in the case of dry conditions the water easily leaves the aerosol giving rise to the formation of salt particles.

Conversely, the main atmospheric mechanism giving HNO_3 is the reaction of the $OH^\bullet$ radical with NO_2:

$$OH^\bullet + NO_2 + M \rightarrow HNO_3 \quad (4)$$

Laboratory experiments have shown that the reaction of $OH^\bullet$ with NO_2 is approximately 10 times faster than that of $OH^\bullet$ with SO_2; consequently, the conversion of SO_2 to gaseous H_2SO_4 is slowed down until the conversion of NO_2 is complete.

A second pattern of HNO_3 formation is hereafter given by:

$$NO_2 + O_3 \rightarrow NO_3^\bullet + O_2 \quad (5)$$

$$NO_3^{\bullet} + NO_2 \rightarrow N_2O_5 \quad (6)$$

$$N_2O_5 + H_2O\,(l) \rightarrow 2HNO_3\,(aq) \quad (7)$$

However, since the reaction of N_2O_5 with water is slow, the presence of nitric acid in the atmosphere is mainly due to the reaction (5) of NO_2 with $OH^{\bullet}$.

Similarly to sulphates, nitrate particles originate by oxidation reactions of nitrogen oxides to HNO_3, mainly in the gaseous phase, with consequent reaction with ammonia to form particulate ammonium nitrate by a similar mechanism as for reaction (2):

$$HNO_3 + NH_3 \rightleftharpoons NH_4NO_3 \quad (8)$$

Ammonia is the only alcaline gas present in the atmosphere at a sufficiently high concentrations to influence the acid-base equilibria, being the unique species able to reduce the acidity of the atmosphere. The knowledge of these equilibria, in terms of thermodynamic constants and of initial species, allow to make previsions on the chemical composition of particulates under given thermodynamic conditions of the atmosphere. It is well known, indeed, that ammonia preferably reacts with H_2SO_4 and only after its complete neutralization it also reacts with HNO_3.

While the chemical reactions involving inorganic species are known and have been studied for a long time, the reactions involving organics are very complex to understand as they involve a large number of intermediates, mostly radicals, so that an accurate description of these mechanisms is not possible. In general the volatile organic compounds are oxidized under atmospheric conditions by O_3 , OH• and $NO_3^{\bullet}$. The main product of this reaction is the alkyl peroxide radical ($RO_2^{\bullet}$) which reacts very quickly, by adding polar functional groups containing sulphur or nitrogen, leading to the formation of less volatile products that may condense on the existent particulate matter.

However, most of the species involved in these reactions have not yet been identified and the theoretical models that try to describe these processes do not always agree with the experimental observations (Schurath and Naumann, 1998).

1.4 Gas-particle equilibria

In the previous section the reactions leading to the formation of the secondary compounds have been briefly discussed. Our attention is particularly focused on the formation of the ammonium

salts by reaction of the atmospheric sulphuric and nitric acids with the available ammonia (reactions 2 and 8). Once formed, these salts undergo gas-particle equilibria that alter their original composition not allowing, through the common methods of measurement, to know the distribution percentage of the secondary compounds between solid and vapor phase. In particular, it is highlighted in several studies as the equilibrium established in the atmosphere can be already altered since the sampling phase, under certain conditions of temperature, pressure and relative humidity (RH), by causing an artifact that affects all the subsequent analyses (Tsai et al., 1998; Bidleman, 1988).

As it will be seen later, some sampling methods designed to reduce this artifact of measurement have been developed in the last decades, although the attention seems to be focused more on quantify the error rather than to study the processes that alter the gas-particle equilibrium. These processes are very difficult to study, because the gas-particle equilibria are regulated by several factors, first of all the temporal variation of the pollutant concentrations.

The distribution between gas and particle phases also influences the distribution of semi-volatile compounds into the environmental compartments as the gaseous species can easily dissolve in the rain and fog, while the solid species can be removed by wet or dry precipitation.

Moreover gaseous species are able to penetrate into the respiratory system in agreement to their solubility while the particulate species penetrate into the respiratory system according to their aerodynamic characteristics (size, density).

1.4.1 Semi-volatile organic compounds

As already discussed previously, the organic compounds are oxidized by O_2, NO_x or light radiation giving rise both to volatile organic compounds (VOCs) characterized by high vapor pressure or to organic compound characterized by low vapor pressure that nucleate to form ultrafine particles.

Also, semi-volatile compound can be formed by oxidation, such as Polycyclic Aromatic Hydrocarbons (PAHs) and Polychlorinated Biphenyls (PCBs) that undergo gas-particle equilibria (Wittmaack and Keck, 2004). During the sampling phase, this equilibrium is inevitably alterated by temperature and relative humidity changes and, as a consequence, some organic compounds may adsorb on or evaporate from the particles. During the sampling time these changes may occur several time, so that the equilibrium will be dependent on the environmental conditions occurring during the last sampling phase. It could then occur a *positive* or *negative artifact* both causing an overestimation or an underestimation in the semi-volatile compounds determination (Gundel et al.,

1995). Because there is no method able to quantify these errors separately, it is not known which of them is the most significant according to the different sampling conditions.

1.4.2 Semi-volatile inorganic compounds

Particular attention, with regard to the solid-vapor equilibria is given to the inorganic fraction of $PM_{2.5}$, which contains most of the secondary formed particles, relevant from a toxicological point of view. As already discussed in 1.3 paragraph, secondary salts are formed by acid-base reactions. The most studied are the ammonium salts that, sometimes, can represent more than 40% of the PM total mass. During their permanence in the atmosphere they distribute between gas and particle phases according to the following reactions:

$$NH_4NO_{3(s)} \rightleftharpoons NH_{3(g)} + HNO_{3(g)} \quad (1)$$

$$(NH_4)_2SO_{4\,(s)} \rightleftharpoons H_2SO_{4\,(aq)} + 2\,NH_{3\,(g)} \quad (2)$$

$$2NH_4NO_{3(s)} + H_2SO_{4(aq)} \rightleftharpoons (NH_4)_2SO_{4(s)} + 2HNO_{3(g)} \quad (3)$$

$$NH_4NO_{3(s)} + HCl_{(g)} \rightleftharpoons NH_4Cl_{(s)} + HNO_{3(g)} \quad (4)$$

Sulphates and chlorides have the same behavior.
Also a further contribute to these equilibria can be addressed to marine sprays. Although these are transported to coastal areas mainly as SO_2 and sodium salts, such as chloride and nitrate, high concentrations of sulphates and low chloride content are found in their particulate phase. This is likely due to the oxidation of SO_2 to sulphates, whereas chloride and nitrate might be transformed to gaseous and volatile HCl, following the reactions (Ames and Malm, 2001):

$$H_2SO_4 + 2\,NaCl_{(s)} \rightleftharpoons Na_2SO_{4\,(s)} + 2\,HCl_{(g)} \quad (5)$$

$$2NaNO_{3(s)} + H_2SO_{4(aq)} \rightleftharpoons Na_2SO_{4(s)} + 2HNO_{3(g)} \quad (6)$$

As it can be seen these reactions are complex and in competition with each other, they constitute a great obstacle to the chemical characterization of the particulate material and to the study of the mechanisms of formation. Even these reactions are influenced by temperature, relative humidity

and concentration of the gaseous precursors: a recent study has demonstrated that the low winter temperatures favor the particulate NO_3^- while in summer the presence of gaseous HNO_3 is favored (Behera and Sharma, 2010). The evaporation of the ammonium salts, is one of the most important barriers to obtain accurate values in the measurements of PM concentration and is one of the most interesting aspects to be studied, considering that they can be up to 50% of the total PM mass, in areas where their concentration is particularly high. In particular the ammonium nitrate artifact is due to the evaporation (even at ambient temperature) of NH_3 and HNO_3, but also to the chemical reactions between the particles already collected and those contained in the air flow or to losses occurring during the sample storage (Sickles and Sandwick, 2008; Cheng and Tsai, 1997). The magnitude of this loss can be significant and negatively influences the $PM_{2.5}$ mass determination considering that more than 50% of the NH_4NO_3 contained in the inorganic fraction of the $PM_{2.5}$ evolves during the sampling phase.

Many information about the qualitative aspect of the semi-volatile inorganic compounds can be found in literature, rather than detailed information about their quantification. Indeed, to obtain good quality data it is necessary to perform an efficient sampling. During this phase, it is expected that the volatile part of the components is subjected to uncontrolled variation, so as to introduce a measurement uncertainty that is difficult to assess (Behera and Sharma, 2010). In the next paragraphs the sampling devices adopted to reduce this artifact will be discussed.

1.5 Permanence, transport and removal mechanisms of particulate matter in the atmosphere

Once the particles have been emitted into or formed in the atmosphere, they are subject to transport in and removal from the atmosphere by different processes, which together determine the atmospheric lifetime of the particles. Secondary formation of components on particles, i.e., takes long time and is thus connected with long-range transport.

Particle size exerts strong control over residence time in the atmosphere and over particle dispersion and removal. For example, coarse particles are removed from the atmosphere by sedimentation and precipitation (the residence time for particles >20 μm is several hours while it is 2-4 days for 2-3 μm particles). Particles in the range of 0.1-1 μm (accumulation mode and larger Aitken mode particles) exhibit the longest lifetime in the atmosphere, ranging from days to a few weeks, so that they can be transported over long distances (~ several 1000 km).

Also, greater is the particle residence time, greater will be its possibility to incur in physical-chemical reactions occurring at particles surface, resulting in some changes of its original properties and residence time in atmosphere (EC 2004b).

The most relevant physical phenomena acting on atmospheric lifetime of particulate matter are *diffusion* – which causes shifting of materials following their concentration gradient -, *sedimentation* – depending on gravitational force – and the eventual *resuspension* of soil-deposited particles, due to winds action and to prolonged lack of precipitations.

Atmospheric removal occurs also by dry or wet deposition. Removal by dry deposition takes approximatively 1 month, whereas by wet deposition residence time is around 1 week (Losno et al. 1988; Chester et al. 1988). Wet deposition is the result of different mechanisms of particulate transport to the earth's surface by various forms of precipitation, such as rain, snow and clouds, whereas dry deposition is given by all physical phenomena acting on gas, aerosols and particles removal in the absence of precipitations (Polyak 1998; Morselli 1991).

Deposition by precipitation is the dominant deposition path for fine particles. Indeed, particles in the range 0.1-1 μm often are efficient cloud condensation nuclei, easily forming cloud droplets, due to a sufficient water-soluble fraction. Wet deposition may occur by two different mechanisms, the *rain-out* and the *wash-out.* In the first case particles behave as condensation nuclei inside clouds catalysing the formation of rain drops, whilst in the second they incur into precipitations being thus mechanically trasnported on the terrestrial surface (Jennings 1999). A general scheme of the above described main residence, transport and removal mechanisms of atmospheric particles is given in figure 1.4.

Nucleation and coagulation are the most relevant chemical mechanisms of removal. In the first, over-saturation vapours condense to form particles in the liquid state, while the second process forms aggregates of larger particle due to collision or to interactions of electrostatic nature (Di Menno Di Bucchianico et al., 2002).

Finally, meteorological parameters like speed and direction of winds, temperature, relative humidity, cloudiness and intensity of solar radiation strongly contribute to both transformation and transport of the particles in the atmosphere, being mainly responsible of the atmospheric distribution and concentrations of the different particle size fractions in a given area.

1.5.1 Planetary Boundary Layer (PBL)

The PBL is the portion of the troposphere directly influenced by the earth's surface. The perturbations induced by the soil are various, the main ones include resistance to the air masses movement due to the type of orography, evaporation and transpiration processes induced by the presence of water and plants, transfer and loss of heat due to the day-night cycle and emission of pollutants. Looking at the evolution of the vertical PBL, starting from the surface , the thickness of this layer is variable in time and space, and can go from some hundreds of meters to a few kilometers (Tidblad and Kucera, 1998).

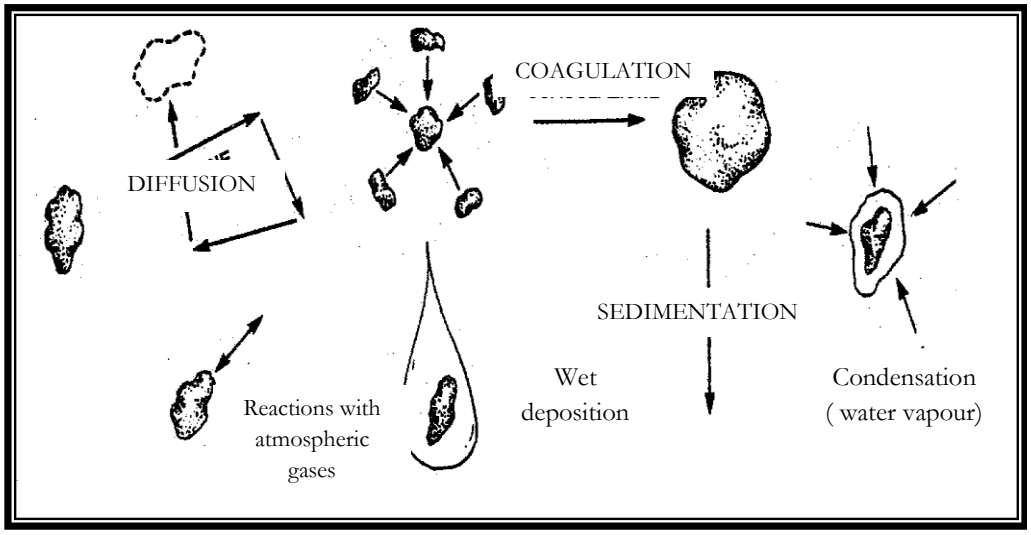

Fig. 1.4 Formation, transport and removal mechanisms of airborne particles in the atmosphere (Manahan 2000).

Normally, this variability is linked to the day-night cycle. The presence of a clear diurnal cycle of the PBL thickness and of the air temperature suggests that the PBL converts the solar energy to air masses movement [56]. At night and during the cold season, the PBL tends to shrink, while during the day and the hot season, it tends to thicken. This depends also by the wind speed and the temperature. High speed winds allow more intensive convective mixing .

This convective mixing determines the PBL expansion. At night, the PBL contracts because of the cold air is denser than hot, therefore the PBL will tend to be less deep during the cold season. The most important meteorological factors affecting the atmospheric pollution in the PBL are: the *wind*, which in the PBL is turbulent, the *atmospheric stability*, which is an indicator of atmospheric turbulence to which air remixing and pollutant dilution are attributed, the t*emperature*, which in the PBL can get very hot during the day and cooling at night, *thermal inversions*, which determine the

height of the PBL (Zannetti,1990). The inversion is a particular atmospheric and meteorological phenomenon. Normally, when the altitude increases the air temperature decreases, because , upon contact with the soil, the air heats up and decreases its specific weight getting up.

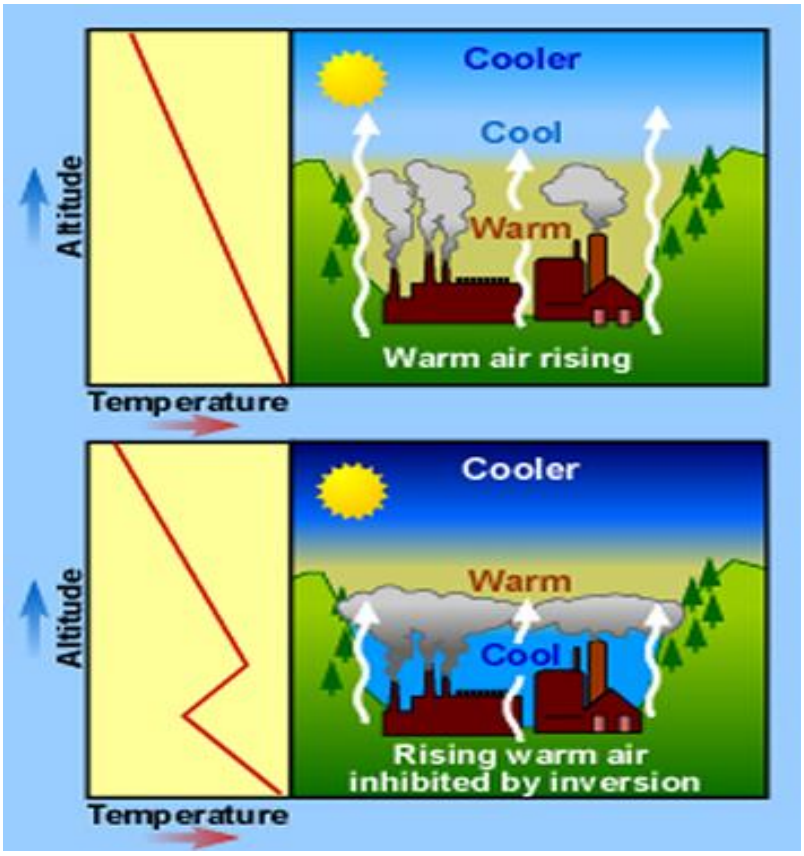

Fig.1.5:schematic picture of the thermal inversion process.

Once heated and climb in altitude, the air is subjected to a lower pressure, therefore, it expands and cools again. During a thermal inversion (Figure 1.5) the opposite phenomenon occurs: by rising, the air heats up, instead of cool down. Unstable conditions occur when the transport of heat from the ground upwards is remarkable, like in the sunny days. The thermal inversion, however, generates highly stable air, then locks each vertical mixing. The stable conditions, which typically occur in continental clear nights with low speed winds, lead to the pollutants' accumulation. The most serious pollution phenomena occur precisely in thermal inversion conditions, during which the pollutants fail to rise because are colder and therefore heavier of the surrounding air.

All these described phenomena regulate the mixing properties of the lower atmosphere, contributing also to favor or not the accumulation of the atmospheric pollutants.

Evaluation of the properties of mixing of the lower atmosphere can be effectively carried out by measuring the natural radioactivity due to Radon progeny, which will be widely discussed in the next paragraph.

1.5.2 The natural radioactivity

The use of radioactive tracers, such as radon, allows to monitor the pollutants' dispersion and diffusion in the lower atmospheric. Radon is a radioactive chemical element which has a natural origin and belongs to the family of the so-called noble or inert gases. It is colourless, odourless and tasteless, so it cannot be perceived by the senses. The Radon-222, the main isotope of this gas, is produced by nuclear decay of Radio-226, present in rocks and soils, which in turn comes from the decay of Uranium-238. Conversely to the solid nature of the other radioactive elements, radon is a gas and therefore it is characterized by a higher diffusion coefficient; also its half-life time is about four days, a particularly suitable time to measure the emitted radiation. Radon released from underground is stable and homogeneous over time and in space, at least at the time scale which the phenomena of urban pollution occur (Perrino et al., 2001). Therefore its concentration in the atmosphere depends only on the dispersion processes and the measurement of the natural radioactivity captures information on the mixing degree of atmospheric layers closer to the ground: if the lower layers of the atmosphere are well mixed (vertical mixing), the radionuclides may be diluted and the values of natural radioactivity will be low, while in the case of a stable atmosphere with limited or absent trade-off between the lower and the higher layers (thermal inversion), the radionuclides will cumulate and the natural radioactivity will assume values increasing over time (Perrino et al., 2008). Natural radioactivity is therefore a useful parameter allowing to identify the variations in pollutant concentrations due to variations of the mixed layer (i.e. the volume of air used for their dispersion) and to distinguish them from those that depend by changes in the flow emissions or chemical reactions.

1.6 Effects of particulate matter

The interest of institutions and research groups towards the air pollution has intensified in recent years. In particular, the problem of PM is one of the most difficult to solve, because of its heterogeneous and variable composition, as well as all the chemical-physical factors that influence it. However, recent environmental studies are focusing their attention on the development of

monitoring systems in urban, rural and remote areas and on the possibility to determine the chemical form and concentration of the species present in the atmosphere. To this purpose, information about concentration and chemical forms may be useful to study and explain the possible cause-effect relationships between harmful pollutants and human health (Hlavay et al., 2001).

1.6.1. Effects on human health.

The entire human population is subject to air pollution exposure because particulate matter is considered an integral part of the air we breathe. The criteria set out by international institutions to establish the dangerousness of PM are essentially based on the mass concentration and particle size fractions. This approach represents a great limitation as it is well known that the different chemical-physical forms in which a substance is present can show different environmental impact and toxicity; also the only determination of the total concentration do not provide any information about the bioavailability of the species and their interaction with the human organism. For instance, the metals' toxicity is closely related to the oxidation state in which they are present. An element can be beneficial or toxic depending on its oxidation number, e.g. Cr (III) can be an essential element for the metabolism of glucose while Cr (VI) is carcinogenic. The oxidation state can also affect the absorption and elimination time of an element. The ion Fe (II) is soluble in physiological conditions and diffuses freely through the membranes, while the Fe (III) does not easily enter into the cells and is more subject to hydrolysis in biological systems. Moreover, the mobility of an element depends on many other factors, such as solubility, pH and ionic strength. For example, Cr is not soluble in neutral water solutions, but may become soluble at a more basic pH values (Goodarzi and Huggins, 2001). However these substances undergo transformation, interconversion and degradation processes, affected by the environmental conditions, giving rise to products whose physical-chemical properties and whose toxicity are markedly different from those of the originating compounds.

At present, only few chemical species present in the atmosphere are normed:

• The Italian D.lgs 60/2002 contains the limit values and alert thresholds for NO_2, NO_x, SO_2, CO, PM_{10}, Benzene, Pb (D.lgs 60/2002).

• The D.lgs 261/2002 establishes target values for As, Cd, Ni, Hg and Benzo (a) pyrene (D.lgs 261/2002).

The gaseous NO_x and SO_2 are irritating and pungent. They form oxidizing and corrosive acids in the atmosphere. These acids form secondary salts, as previously discussed, which, because of the

small size, penetrate into the respiratory system reaching the pulmonary alveoli and causing chronic respiratory diseases such as asthma, bronchitis and emphysema (Aust et al., 2002).

Among these, the carbon monoxide is quickly adsorbed in the pulmonary alveoli, the benzo (a) pyrene is highly soluble and can cross the membrane very easily. In addition, the Polycyclic Aromatic Hydrocarbon (PAHs) as well as benzene have been classified by the IARC (International Agency for Research on Cancer) as possible or probable human carcinogens (Mastrangelo et al., 1996; Kao and Nanagas, 2006).

1.6.2. Effects on climate and environment

The PM absorbs and/or reflects the sunlight radiation as a function of the particle size and chemical composition: on one hand, particles reflect sunlight, leading to a cooling of the earth surface, on the other hand they have a role in the absorption of terrestrial infrared radiations, contributing positively to the global heating. The light attenuation, is mainly caused by the particles of secondary origin belonging to the ultrafine fraction, while the particles of the accumulation mode involve the light dispersion and cause a reduced visibility.

The light absorption is directly related to the chemical composition of the particles. For example, the carbonaceous substances absorb strongly the solar radiation (Barry and Chorley, 1992).

PM also acts on the environment through acid rains.

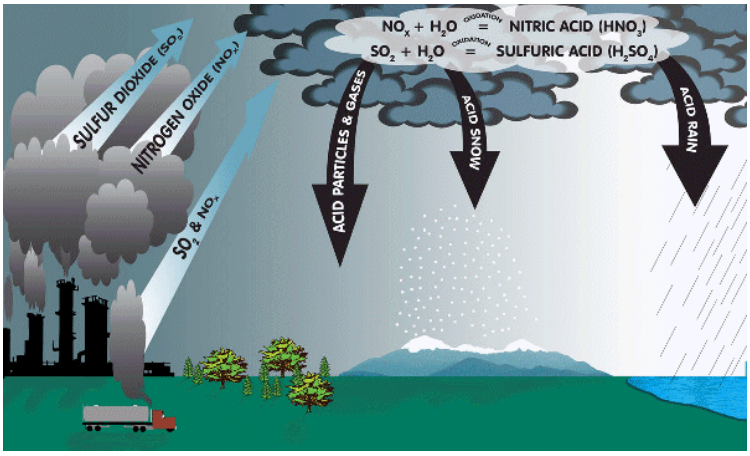

Fig. 1.6: Acid Deposition Large Graphic (http://www.dec.ny.gov/chemical/41293.html)

This phenomenon is caused mainly by atmospheric gaseous components (SO_2, SO_3, NO_x and CO_2) coming from combustion and industrial activities in general. These gases can be transformed in a

few days in acid (H_2SO_4, HNO_3, HNO_2), by means of reactions with H_2O or OH radical, giving rise to acid precipitations (fig.1.6).

The fallout on the ground of acid pollutants occurs through the wet or dry deposition. The first is the most known and occurs in the form of rain, snow, acid fog. The dry deposition consists of the fallout on the soil of acidic substances in the form of gas or microscopic particles (Morselli,1991). This phenomena can cause an alteration of the chemical composition of the groundwater, lakes, rivers and sea waters. Also the vegetation is affected by the acid rains, causing plants' weakening and resulting in a rapid decline of some forests.

Moreover, the action of acid rain is clearly visible on the monuments (historic buildings, metal statues, etc.) by action of corrosion or removal mechanical of the material, previously made friable and soluble. In the limestone monuments sulphuric acid (H_2SO_4) present in the acid depositions turns the calcium carbonate ($CaCO_3$) into calcium sulphate ($CaSO_4$), which is easily washed away by rainwater. Even metals are considerably corroded by acid rain, and in particular by the sulphuric and nitric acid, which have a strong oxidizing power, e.g. acid precipitation determine the formation of a typical green layer on copper or bronze monuments, due to copper salts (Morseli, 1991).

1.7 Regulations

The air quality standards are constantly evolving because of the increasing need to protect both resources and human health and to assure a sustainable development to the next generations. During the last decades the Italian situation has profoundly changed: most of the emissions are due to particulate matter and nitrogen oxides resulting from the natural gas combustion and to carbon monoxide from road traffic. As a result, air pollution today mainly interests the urban areas and industrial centers. The vehicular traffic is the main cause of air pollution in urban areas, in which very often the high concentrations of pollutants accumulate, due to the unfavorable atmospheric conditions. A key role is played by the European Union (EU) which has established new regulations to ensure a significant reduction of the ambient concentrations of pollutants.

The Italian D.lgs 60/2002 (transposition of the Directive 1999/30/CE), set the daily limit value for PM_{10} to 50 μg m^{-3}not to be exceeded more than 35 times a year, while 40 μg m^{-3} is the yearly average value. In 2008 the EU adopted a new directive 2008/50/CE, transposed in Italy as D.lgs 155/2010, promoting further studies in the air quality field and recognizing, for the first time, the limits of the only PM mass concentration determination. In particular, it introduced the measurement of the $PM_{2.5}$ mass concentration, considered to be potentially more dangerous to

human health, while the limit values for PM_{10} have remained unaltered. Furthermore it establishes the obligation to measure the concentration of some specific components (reported in table 1.1), useful to allow the differentiation among the background, local and regional contributions. Unlike the previous, this legislation requires the chemical characterization of samples, necessary to understand the mechanisms of formation of secondary particles. This also allows to differentiate the emission sources and to separate the contributions due to some special climatic phenomena (transport of natural dust from the desert or transport of dust from the neighboring countries), through the combination of the chemical analysis and the statistical models.

Finally this Directive allows to deduct the exceedances attributable to the phenomena just mentioned and establishes some exceptions to the sampling sites that are subject to particular weather conditions, such as the Po Valley.

Table 1.1: Species to be measured in PM according to the Directive 2008/50/CE.

Anions	**Cations**	**C-containing compounds**
SO_4^{2-},Cl^-, NO_3^-	Ca^{2+},NH_4^+,Na^+,K^+, Mg^{2+}	Elemental Carbon (EC) Organic Carbon (OC)

1.8 Sampling techniques for particulate matter

The reliability of the analytical results depends on many factors, among which the sampling method has a major importance. A lot of problems are linked to the PM sampling mainly due to its heterogeneous composition and the relatively low concentrations in which it is present in the air. The sampling step has to be carried out by taking into account the physical-chemical lability of many compounds, especially those adsorbed or bound to the particles' surface. As widely discussed in the previous paragraphs, secondary compounds give rise to gas-particle equilibria which may cause a loss/adsorption of the semi-volatile species during the sampling step, resulting in significant sampling *artifacts*. To solve this problem some appropriate sampling systems have been developed, able to quantify and to correct these errors.

Also, because of PM concentrations in the air are very low (few μg m^{-3}), to perform a chemical characterization of PM it is necessary to collect a sufficient amount of dust so that it is possible to analyze it by using the conventional analytical techniques. Unfortunately in this case many

information are lost due to the low temporal resolution, as during the long sampling time some reactions among the particles occur modifying their original characteristics. To have an high temporal resolution some appropriate sampling devices have been developed in the last decades (as it will be discussed later), able to carry out both the sampling and analyze of PM in "real-time".
Therefore, the PM sampling and analysis usually depend on the information that the operator want to achieve, taking into account all the factors affecting a good analytical performance.

1.8.1 Sampling and measurement methods of the PM_{10} and $PM_{2.5}$ fractions

The measure of airborne particulate matter is effectively defined for European regulatory purposes by the European Committee for Standardization (CEN). For PM_{10}, the European Reference Method is described in the CEN standard EN 12341, adopted by CEN in November 1998 (CEN 1998) while for $PM_{2.5}$ the standard are set in the EN 14907 adopted in 2005 (CEN 2005). They define a PM sampling inlet coupled with a filter substrate and a regulated flow device. These systems allow to sample PM according to the particle aerodynamic size. Also by increasing the sampling time, a sufficient quantity of powder can be collected to obtain both an accurate determination of the mass and of the subsequent chemical analysis. The standard samplers are constituted by a sampling head that both draw the air flow and select the particles so as to remove particles greater than a certain size. The air thus "purified" is conveyed through a filtration membrane able to retain the selected particles. Downstream of sampling line, there is pump that generate the pressure gradient necessary to the air flow. As was anticipated, the current regulation provides for the measurement of PM_{10} and $PM_{2.5}$. These samples are then constituted by all the particles contained in the *fine* mode and most of the particles belonging to the *coarse* mode, as it is shown in figure 1.7.

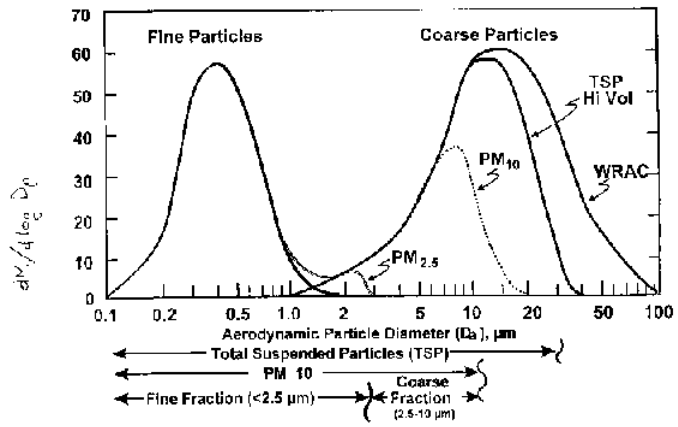

Fig.1.7: Typical size distribution of atmospheric aerosols.

The choice of setting the cut to 10 and 2.5 µm was determined by toxicological considerations, since, as already described, the particles with a.d <10 µm, can penetrate into the respiratory system, while the particles with a.d <2.5µm are considered to be particularly harmful. This choice, however, does not allow an adequate interpretation from the environmental point of view: in fact, it would be useful to distinguish the particles according to the different processes of formation, much more indicative for the identification of the emission sources. From this point of view it would be appropriate to consider separately the particles belonging to the two coarse and fine modes, because they constitute two independent sets of particles.

Samplers can be divided in two main group: the High Volume Samplers (HVS) that allow to collect high amount of dust on large filters (diameter 150 mm) and the Low Volume Samplers (LVS) that allow to collect small amount of dust (few mg) on membranes of 47 mm diameter. The flow rate is critical to maintain the PM cut point and when using the standard impactor dimension, following the criteria for the CEN standard (CEN 1998), a constant flow rate of 68 m^3h^{-1} (1133 L min^{-1}) is required for a high volume sampler and 2.3 m^3h^{-1} (38 L min^{-1}) for a low volume sampler.

In figure 1.8 an example of instrument which is in accordance with CEN standard (1998) for PM_{10} measurements is shown.

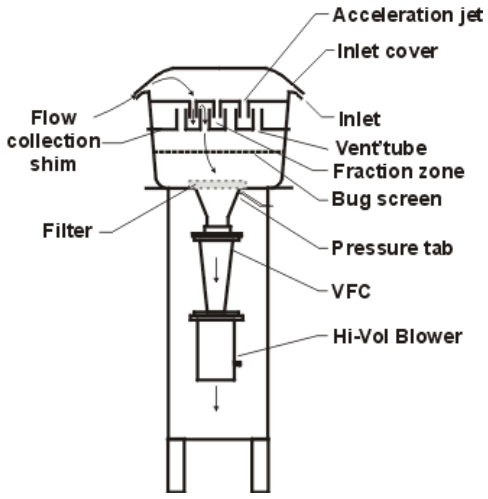

Figure 1.8. Schematic diagram of Sierra-Andersen/GMW Model 12000 with a volumetric flow controller (VFC).

Different material can be used to collect PM depending on the chemical analysis to perform after the sampling phase. In table 1.2 the advantages and disadvantages of the most used materials are reported.

Table1.2. Characteristics of the materials used to collect PM.

Filter material	Advantage	Disadvantage
Glass fiber	High retention capacity.	Release of material due to the fibrous structure.
Quartz	Resistance to high temperatures; available to analyze carbonaceous compounds by means of thermal methods.	Tendency to adsorb volatile organic compounds.
Teflon	No release of material due to the continue structure; low blank value, suitable to analyze trace elements.	Fast clogging with high PM concentrations.

The mass collected on the filter is gravimetrically measured by means of a micro-balance under ambient air conditions. All handling of filters should be made in clean air and all equipment should be stored in plastic bags in a dust free environment. It is required by EN 12341 (CEN 1998) that the filters are equilibrated, at 20° C (±1) and 50% R.H. (±5), for 48 hours. This equilibration should be performed before the filters are weighed previous to the sample collection, and after sampling, before the filter is weighed again with the collected sample. This is helpful to make the determination of mass independent from any external condition. Known the flow and the sampling time, the concentration of particulate matter in the air (in mg m^{-3}) is expressed as:

$$C = \frac{m(n) - m(b)}{F\ t}$$

Where *m(n)* is the mass of the sampled filter, *m(b)* is the mass of the blank filter, *F* is the flow value and *t* is the sampling time.

This method has some drawbacks: it is slow, it requires high sampling volumes and the conditioning procedure requires at least 48 hours. Furthermore, the main problem is the low ratio between the mass of the sampled and the blank filter. In these conditions, the uncertainty associated with the measurement is equal to 2-4%.

Alternatively, PM mass determination can be carried out automatically by measuring the attenuation of the β radiation produced by a radioactive source of C-14 placed inside the sampler. The β radiations pass through the filter before and after the sampling so that the difference in the absorption of β-rays by the filter is proportional to the concentration of PM. In this case the uncertainty of measurement is influenced especially by the stability of the β source and is equal to 1-2%.

1.8.2 Cascade impactor sampler

Besides to the PM samplers aimed to collect particles with a wide range of aerodynamic parameters, e.g PM_{10} and $PM_{2.5}$, cascade impactors allow to fractionate the particles in different restricted ranges of aerodynamic diameters. The multiple stages of a cascade impactor can be analyzed to determine aerosol mass distribution (by gravimetric analysis) or to study the chemical composition as a function of the particle size. Simultaneous data on particle size and mass or chemical composition are useful to assess health effects and particle transport in the atmosphere.

Particle impaction refers to the collection of particles on a solid plate when they deviate from the air flow streamlines due to their inertia. Particles contained in the air enter in the device by means of a nozzle and are blocked on a solid plate oriented perpendicularly to the nozzle axis. The air flow is laminar and the particles are accelerated to an uniform velocity. Larger particles are propelled from the streamlines and are collected on the plate, while smaller particles remain in the air flow. A schematic representation of a multistage cascade impactor is shown in figure 1.9.

Air flow enters at the top by means of a pump, passes through every plate and is exhausted through a back-up filter. Each impactor stage consist of a particular aerodynamic diameter range and successive stages are aimed to collect smaller particles (Hering et al., 1979).

Sampling by the cascade impactor should cause some drawbacks, depending on the sampling conditions and the physical and chemical properties of the aerosol sampled.

For example, all of the aerosol sampled in an impactor should be deposited on the collection plates or be captured by the after filter. In practice, some of the particles are collected on other interior surfaces and are typically excluded from the analysis. Wall losses result from diffusion of particles in turbulent eddies, from sedimentation of large particles Therefore, if they are significant, the total mass concentration will contain an error. Another problem occurs when particles bounce off the collection surface and they may be carried to subsequent stages, where they may stick or again

bounce off. The result is that subsequent stages collect more mass than is appropriate, and the inferred particle-size distribution is biased towards the smaller particles. This phenomenon can severely limit the utility of the collected data. Typically, sticky substances are applied to impaction surfaces to reduce particle bounce.

1.8.3 Sampling devices to reduce sampling artifacts

As already discussed in paragraph 1.5, secondary species udergo gas-particle equilibria causing positive or negative artefacts. In fact during the sampling phase there is a displacement of the equilibrium regulated by temperature, concentration and flow rate changes, kinetic effects leading to the evaporation of the sampled species (negative artifact). Also it has to take into account the influence of the sampling membrane, since many species can adsorb on the filter before, during or after the sampling (positive artifact).

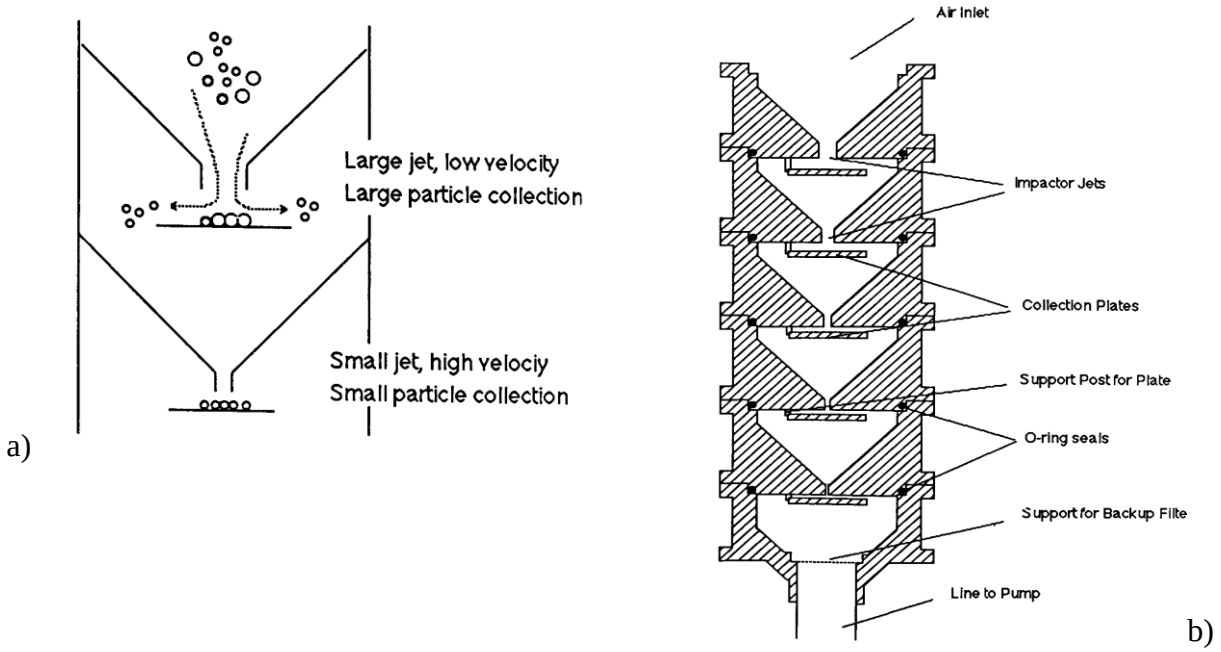

Fig.1.9: a) Scheme of two impactor stages showing large and small particle trajectory; b) Example of five-stage cascade impactor.

Since the separation of the solid and the gaseous species can be done only during the sampling phase, it was necessary to create some sampling devices able to "pick up" the gaseous components that are lost during the sampling due to variations in the equilibrium. To this purpose, the diffusion

denuder allows the selective removal of the gas phase on the device's walls and the sampling of the particles on filter membrane placed downstream. It is a cylindrical glass tube (figure 1.10) whose inner surface is coated with a substance capable of chemically reacting with the gaseous species of interest (Ferm, 1979). By means of a pump, the atmospheric air is drawn in through the denuder and, in laminar flow conditions, the molecules in the vapor phase diffuse toward the reactive or adsorbent surface (concentration gradient), while the particles are blocked on the filter (fig.1.11).

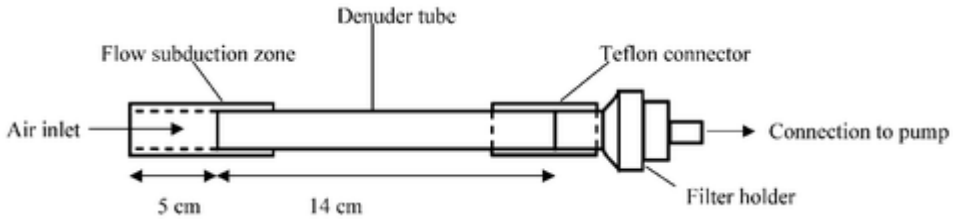

Fig.1.10 Schematic structure of a cylindrical denuder

However the cylindrical denuders are subject to some limitations, mainly due to their length and the need to operate at a low sampling rate. Indeed, a good absorption efficiency can be obtained only by operating at a flow of about 1-2 L min^{-1}. It makes the impossibility to perform short time samplings, especially in slightly polluted areas. These difficulties have been overcome by the introduction of a annular denuder, consisting of two concentric tubes placed so that air can flow through the gap between the two tubes. In general, the gaseous molecules walk lower distances before to be collected by the reactive surface and can accumulate in higher concentration (Allegrini et al. 1987).
Denuders are especially used to reduce the artifact due to the evaporation of the ammonium nitrate. They give the possibility to determine simultaneously the individual concentrations of HNO_3(gas) NO_3^-(particle), NH_3(gas) and NH_4^+(particle). The air is drawn through a series of annular denuders, and filters. The first two denuders are internally coated with sodium carbonate (Na_2CO_3) and glycerol for the collection of nitric acid and sulphur dioxide respectively, (glycerol prevents oxidation of nitrite to nitrate by ozone), the third is coated with citric acid, oxalic acid or phosphorous acid for the collection of ammonia. The coated denuders are then followed by a three-filter pack system, in which the first filter is characterized by a high collection efficiency for submicron particles, followed by a filter impregnated with potassium hydroxide for collection of nitric acid which may have evaporated from the particle filter, and a filter impregnated with oxalic acid for the collection of ammonia which may also have evaporated. Nitrous acid (HNO_2) is also absorbed in the alkaline denuders, but will normally not cause a significant interference as it is usually detected as nitrite in the sample extracts.

Regarding the Semi-Volatile Organic Compound there is not a validated sampling method to reduce the artefacts. In fact, sampling devices such as carbon-coated denuders are going to be developed but, to date, the systems are still under study. For this reason the only way to reduce and valuate the organic compound artifacts is to collect the evaporated compounds at the bottom of the sampling system. One of the most used materials involved in this phase is the PolyUrethane Foam (PUF); this material, located after the sampling filter, is extracted during the analytical phase to measure organic species such as Polycyclic Aromatic Hydrocarbons.

1.9 Analysis and chemical characterization of particulate matter

Many studies are available in literature concerning the determination and characterization of different chemical species and/or size fractions of particulate matter, eventually combined to source-apportionment applications (EPA 1999; Kleeman et al. 1998; Querol et al. 2003).

A complete chemical characterization of airborne particulate matter includes determinations of the volatile, hydrosoluble and insoluble fractions by detecting the inorganic ions, organic and elemental components. Since various different analytical methods have been developed and used for these determinations, usually data quality is variable and it is difficult a comparison among the results. This might consequently affect data interpretation in environmental research.

To this aim, the Chemical Coordination Centre (CCC) working under the EMEP Programme[1] has developed a *Manual for Sampling and Chemical Analysis* (EMEP/CCC 1996) which describes the recommended methods for the sampling and the chemical characterization of air pollutants covered by the EMEP Programme. However, where available, the manual reports the standards developed by the CEN and it is periodically revised with respect to new developments in Analytical Chemistry.

Therefore, the following brief survey of analytical methods applied to the chemical characterization of airborne particulate matter will be mainly based on information reported by the EMEP manual.

[1]. The "Cooperative programme for monitoring and evaluation of long-range transmission of air pollutants in Europe" (EMEP) was launched in 1977 as a response to the growing concern over the effects on the environment caused by acid deposition under the auspices of the United Nations Economic Commission for Europe (UN ECE). Today EMEP is an integral component of the cooperation under the Convention on Long-range Transboundary Air Pollution (CLRTAP). The programme includes three main elements: emission data, measurements of air and precipitation quality, and atmospheric dispersion models and is co-ordinated by three international centres: two centres for modelling activities and the Chemical Co-ordinating Centre (CCC) for coordination of the chemical measurements.

1.9. 1 Chemical characterization of the carbon fraction

The carbon fraction typically constitutes more of 30 % of the particulate mass and contains elemental carbon (EC) and a huge number of different organic carbon (OC) compounds. Measurements of EC and OC are important both for health and source apportionment studies, as well as for the models' validation. Indeed, the ratio between EC and OC (EC/OC) is often used as a valuable tool to understand the origin of the air masses. A variety of methods is available for the measurement of the carbon content of the aerosols (Heintzenberg and Winkler 1991); however, the distinction of organic and elemental carbon remains one of the critical issues and strongly depends on the analytical procedure of the method (EC 2004c).

The recommended method to determine EC is based on the volatilization and oxidation of the sample, and consequently determination of the evolved CO_2, either directly or after conversion to CH_4 by a flame ionization detector (FID). This procedure also gives the total carbon content, and then a quantification of the total amount of the organic materials The method is not free of artifacts, particularly the charring or incomplete removal of organic compounds may lead to the overestimation of EC.

Generally two main organic fractions are determined in PM samples, respectively Persistent Organic Pollutants (POPs), such as pesticides and PCBs, and PAHs.

These two fractions are collected by an high volume air sampler on a particle glass fiber filter followed by two plugs of polyurethane foam (PUF) to retain the volatile compounds. After the sampling both filters and PUF are extracted and cleaned up following procedures depending on the components to be determined. The components are then separated and quantified by using gas chromatography combined with mass spectrometry (GC MS) using the method of internal standard).

Table 1.3. Recommended and alternatives methods for chemical analysis of inorganic ions (EMEP/CCC 1996).

METHODS FOR CHEMICAL ANALYSIS OF INORGANIC IONS		
Component or parameter	**Recommended methods**	**Alternative**
Conductivity	Conductivity cell and resistance bridge	
Hydrogen ion (H^+)	Potentiometry (glass electrode) pH<5.0	Titration

Ammonium ion (NH_4^+)	Ion chromatography	Spectrophotometry (indophenol blue colour reaction)
Sodium ion (Na^+)	Atomic absorption spectrophotometry (AAS)	Ion chromatography
Potassium ion (K^+)	AAS	Ion chromatography
Magnesium ion (Mg^{2+})	AAS	Ion chromatography
Calcium (Ca^{2+})	AAS	Ion chromatography
Sulphate ion (SO_4^{2-})	Ion chromatography	
Nitrate ion (NO_3^-)	Ion chromatography	Reduction to nitrite and diazotation
Chloride ion (Cl^-)	Ion chromatography	Displacement of SCN^- in $Hg(SCN)_4^{2-}$, determination of coloured Fe(SCN) complex.

1.9.2 Chemical characterization of the inorganic ionic fraction

The major inorganic ions to be determined in the particulate matter are those indicated in table 1.3, which also reports the recommended analytical methods.

When the inorganic ions fraction is to be determined a special attention should be given to PM sampling, due to the eventual artefacts arising from their gas-particle phase distribution as already discussed in in paragraph 1.6.3.

As shown in table 1.4. the recommended analytical method for ionic determination is mainly the ion chromatography after filter extraction. The extraction solution is water if the sample has been collected on a teflon filter, while by extracting impregnated filters or filter packs coming from a denuder sampler, acidic or alkaline extraction solution should be used in respect to the solution used to impregnate the sampling filters.

1.9.3. Chemical characterization of the total elemental content

The main analytical complication in the determination of metals in the particulate matter is related to the simultaneous presence of many different elements at different concentration ranges. A suitable technique should be therefore multielemental and show a large range of linear calibration (two or three orders of magnitude). In addition, as the low-volume samplers collect small amounts of particulate, more attention has to be paid to the choice of analytical conditions in order to ensure the proper sensitivity and detection limits also when trace metals has to be determined on a small mass of sample. A wide variety of techniques has been developed in these years, that are either non destructive (Xu et al. 1997; Einax et al. 1994), to be applied directly on the solid sample, or requiring a previous dissolution step by digestion treatment (Schmeling and Klockow 1997; Serrano et al. 1996).

Most used non destruction techniques are the X Ray Fluorescence (XRF) and the Proton Induced X ray Emission (PIXE). The XRF technique allows both qualitative and quantitative elemental determinations and is based on the principle by which a material is irradiated by an X ray source giving on its turn X rays emission, that is giving "fluorescence". X-rays are energetic enough to expel tightly held electrons from the inner orbitals of the atom, producing its ion. The removal of an electron in this way makes the electronic structure of the atom unstable, and electrons in higher orbitals "fall" into the lower orbital to fill the hole. In falling, energy is released in the form of X radiation. The PIXE technique is based on a similar principle as for XRF by measuring the X rays emissions of the atoms. In this case, differently from XRF, the atoms are energetically excited by proton irradiation, coming from an ion accelerator instead that by an X-rays tube, with the main advantage of smaller background noise of the PIXE spectrum. These techniques have the disadvantage of high limit of detections compared to those of the destructive ones. In fact they can be used to determine the "macro-elements" such as Al, Si, Fe, K, Ca, whose concentration in the atmosphere is in the order of $\mu g\ m^{-3}$.

The analysis of the elemental content by previous dissolution of the solid sample (destructive techniques) allows to choice between all the traditional instrumental techniques for the elemental determinations, such as the flame atomic absorption (F-AAS) or graphite furnace atomic absorption (GF-AAS) spectrometry and the inductively coupled plasma (ICP) emission spectrometry. Besides the lower detection limits, techniques based on plasma sources, particularly ICP-OES and ICP-MS, are usually characterized by wider linearity ranges of concentration, giving relevant advantages in the case of the analysis of many different elements with concentrations varying between different orders of magnitude, like in the case of airborne particulate samples. The inductively coupled

plasma mass spectrometry (ICP-MS) was definitely chosen (EMEP/CCC 1997) to be the reference technique for metals analysis within EMEP.

The ICP techniques are usually used to determine the trace elements such as As, Ba, Cd, Pb, Cr, Zn, etc., whose concentration is in the order few of ng m^3 depending on the emission source types. These techniques require the complete dissolution of the sample, that can be done by treating it with acid mixtures at hot temperature (Schmeling and Klockow**,**1997; Tschopel et al. 1980; Dreetz and Lund, 1992). Heating can be performed by conduction (hot plate) or by microwave irradiation in open or closed vessels. Microwave digestion using closed vessels is the most used method as it requires less time to dissolve the sample.

One of the most important problem in the elemental analysis of PM is the lack of standard procedures, so that there is no comparability among data obtained by applying different sampling methods or analytical determinations. Nowadays, only Pb, Cd, As and Ni are regulated by standard procedure. In the UNI EN 14902 standard all the procedures to sample and determine these metals in PM_{10} can be found.

1.10 References

Abbas Z, Steenari B M, Lindqvist O (2001), Waste Management, 21:725-739.

Allegrini I, De Santis F, Di Palo V, Febo A, Perrino C, Possanzini M Liberti A (1987), Science of Total Environment, 67: 1-16.

Ames R B, Malm W C (2001), Atmospheric Environment, 35: 905-916.

Aust A E, Ball J C, Hu A A, Lighty J S, Smith K R, Straccia A M, Veranth J M, Young W C (2002), Research Report Health Effects Institute, 110:1-65.

Barone T L, Lall A A, Zhu Y, Sheldon R Y, Friedlander K (2006), Journal of Nanoparticle Research, 8: 669–680.

Barry R G, Chorley R J (1992), Atmosphere, Weather & Climate, 6th ed. Routledge, London.

Behera S N, Sharma M (2010), Science of the Total Environment, 408: 3569–3575.

Bidleman (1988), Environmental Science e Technology, 22: 361-367.

CEN (1998). Air Quality. Determination of the PM_{10} fraction of suspended particulate matter – Reference method and field test procedure to demonstrate reference equivalence of measurement methods. Brussel (EN12341).

CEN (2005). Ambient air quality. Standard gravimetric measurement method for the determination of the PM2,5 mass fraction of suspended particulate matter (EN 14907).

Cheng Y H, Tsai C J(1997), Journal of Aerosol Science, 28: 1553-1567.

Chester R and Statham P. J (1988), Geochimica et Cosmochimica Acta, 52: 2433.

Claes M, Gysels K, Van Grieken R, Inorganic Composition of Atmospheric Aerosols in: Harrison R M, Van Grieken R E (1999), Atmospheric Particles Vol 5.

Di Menno Di Bucchianico A, Catrambone M, Perrino C, Passariello B, Quaresima S (2002), *La valutazione del materiale particellare alla luce del DM 2/4/2002,* Marina di Carrara 11/10/2002, *Eventi di trasporto di sabbie sahariane nell'Italia centrale.*

D.lgs 155/2012 Recepimento Direttiva 2008/50/CE, relativa alla qualità dell'ambiente e per un aria più pulita in Europa.

D.lgs 261/2002 Regolamento recante le direttive tecniche per la valutazione preliminare della qualita' dell'aria ambiente, i criteri per l'elaborazione del piano e dei programmi di cui agli articoli 8 e 9 del decreto legislativo 4 agosto 1999, n. 351.

D.lgs 60/2002 Recepimento della direttiva 1999/30/CE concernente i valori limite di qualità dell'aria ambiente per il biossido di zolfo, il biossido di azoto, gli ossidi di azoto, le particelle e il piombo e

della direttiva 2000/69/CE relativa ai valori limite di qualità aria ambiente per il benzene ed il monossido di carbonio.

Dreetz C D and Lund W (1992), Analytica Chimica Acta, 262:299.

EC (1997). Working Group on Particles. Position Paper on Ambient Air Pollution by Particulate Matter. http://europa.eu.int/comm.

EC (2004b). CAFE Working Group on Particulate Matter. Position Paper on Particulate Matter. http://europa.eu.int/comm; Chapter **2**.

EC (2004c). CAFE Working Group on Particulate Matter. Position Paper on Particulate Matter. http://europa.eu.int/comm; Chapter **3**.

EC (2004e). CAFE Working Group on Particulate Matter. Position Paper on Particulate Matter. http://europa.eu.int/comm; Chapter **10.**

Einax J, Geib S and Michaelis W (1994), Fresenius Journal Anaytical Chemistry 350 (10-11): 614-619.

EMEP/CCC (1996) (revised 2001) NILU-Norwegian Institute for Air Research: EMEP Manual for Sampling and Chemical Analysis – EMEP/CCC-Report 1/95NILU ref. O-7726.

EMEP/CCC (1997). EMEP-WMO workshop on strategies for monitoring of regional air pollution in relation to the need within EMEP, GAW and other international bodies. Aspenäs, Sweden, 2-4 June 1997. Kjeller, Norwegian Institute for Air Research (EMEP/CCC-Report 10/97).

EPA (1997) Reference Method for the Determination of Particulate Matter as PM_{10} in the Atmosphere. *Federal Registrer*, *62*, No 138, Appendix M to part 50.

EPA (1999). Particulate Matter ($PM_{2.5}$) Speciation Guidance (available at: http://www.epa.gov/ttn/amtic/files/ambient/pm25/).

EPA (1999). Particulate Matter ($PM_{2.5}$) Speciation Guidance (available at: http://www.epa.gov/ttn/amtic/files/ambient/pm25/).

Ferm, M (1979), Atmosferic Environment, 13:1385-1393.

Gelencsér A, Hoffer A, Molnár A, Krivácsy Z,. Kiss G, Mészáros E (2000), Atmospheric Environment , 34:823-831.

Goodarzi F, Huggins F E (2001), Journal of Environmental Monitoring, 3:1-6.

Gundel L A, Lee V C,. Mahanama K R R, Stevens R K, Daisey J M (1995), Atmospheric Environment, 29: 1719-1733.

Harrison R M, Stedman J, Derwent D (2008), Atmospheric Environment, 42(3): 603–606.

Heintzenberg J and Winkler P (1991), Fresenius Journal Analytical Chemistry 340:540-543.

Hering S V, Friedlander S K, Collins J J, Rchards L W (1979), Environmental Science and Techology, 13:184-188.

Hlavay J, Polyák K and Weisz M (2001), Journal of Environmental Monitoring, 3:74-80.

Hwang I and Hopke P K (2007), Atmospheric Environment, 4: 506–518.

Jennings S. G (1999), *Wet Processes Affecting Atmospheric Aeroso*l in: Harrison R M and van Grieken R E *Atmospheric Particles,– IUPAC Series on Analytical and Physical Chemistry of Environmental Systems*, Vol. 5 – John Wiley & Sons, England.

John W (2001) Size Distribution Characteristics Of Aerosols in: Paul A. Baron, Klaus Willeke Aerosol Measurement – Wiley InterScience New York.

Tidblad J, Kucera V, Materials Damage in: Fenger J, Hertel O, Palmgren U (1998), Urban Air Pollution - European Aspects, Kluwer Academic Publishers.

Kleeman M J, Cass G R (1998), Atmosferic Environment, 32:2803-2816.

Kong S, Han B, Bai Z, Chen L, Shi J, Xu Z (2010), Science of the Total Environment, 408(20): 4681–4694.

Losno R, Bergametti G and Buat-Menard P (1988), Geophysical Research Letter 25A:1389.

Manahan (2000), Chimica dell'ambiente, Editor: L Zoccolillo, Chapter 10, PICCIN.

Mark D (1999), *Atmospheric Aerosol Sampling* in:. Harrison R M and. Van Grieken R E, *Atmospheric Particles* Vol 5.

Moore J W, Ramamoorthy S (1994), *Heavy Metals in Natural Waters*, Springer-Verlag, New York.

Morselli L (1991), *Deposizioni Acide. I Precursori. L'interazione Con L'ambiente E I Materiali*, Maggioli Editor.

Pacyna J M (1999), *Source Inventories for Atmospheric Trace Metals* in: Harrison R M and Van Grieken R E, *Atmospheric Particles*, Vol 5.

Perrino C, Pietrodangelo A, Febo A (2001), Atmospheric Environment 35:5235–5244.

Perrino C, Catrambone M, Pietrodangelo A, (2008),Environment International 34:621–628.

Phongphiphat A, Ryu C, Finney K N, Sharifi V N, Swithenbank J (2011), Journal of Hazardous Materials, 186:218–226.

Polyak K, Hlavay J and Weisz M (2001), *Journal Of Environmental Monitoring*, 3:74-80.

Puxbaum H (1991), *Metal Compounds In The Atmosphere* in: Merian E (Edr), *Metals And Their Compounds In The Environment*, pp 257-286.

Querol X, Salvador P, Sanchez de la Campa A (2003), D.G. Environmental Quality and Evaluation, pp 424. (In Spanish with English summary)

Schmeling M and Klockow D (1997), Analytica Chimica Acta, 346:121.

Schurath U and Naumann K H (1998), Pure and applied chemistry, 70(7):1353-1361.

Serrano E, Beceiro E, Lopez P, Prada D (1996), *Quimica Analitica*, 15:38.

Sickles J, Shadwick D (2008), Atmospheric environment, 42: 2062–2073.

Tsai C J, Perng S N (1998), Atmospheric environment, 32:1605–1613.

Tschopel P, Kotz L, Schulz W, Veber M, Tolg G (1980), Fresenius Journal Analytical. Chemistry, 302:1.

UNI EN 14902:2005. Qualità dell aria ambiente - Metodo normalizzato per la misurazione di Pb, Cd, As e Ni nella frazione PM10 del particolato in sospensione

Whitby K (1978), Atmospheric Environment, 12:155.

Wittmaack K, Keck L (2004), Atmospheric environment, 38: 5205–5215.

Xu L, Bulatov V, Gridin V V, Schechter I (1997), Anaytica. Chemistry, 69:2103.

Zannetti P, Computational mechanics Publications (1990), Van Nostrand Reinhold, New York.

Chapter 2- Determination of water content in particulate matter

2.1 Introduction

As previously said in the Abstract section, one of the main objective of this research project was the determination of the water content in Particulate Matter samples.

Water is present in the atmosphere as vapor, whose concentration is very variable and depends on the temperature, and liquid in the form of clouds, rain and fog. Most of the atmospheric particles are able to interacts with water undergoing changes of their original physical and chemical features. Particularly this interaction affects particles' size distribution (Swietlicki et al.,1999), optical properties and residence time in the atmosphere (Sloane and Wolfe, 1985; Pilinis et al.,1995; Kreidenweis et al., 2001). Moreover, it is well known that high values of relative humidity (RH) favor the occurrence of acid-base reactions leading to the formation of secondary inorganic salts, widely discussed in the first chapter. (Baek et al., 2004; Squizzato et al., 2012). Inorganic salts are hygroscopic and can act as cloud condensation nuclei (CCN), which favor the formation of clouds and fogs. If the hygroscopic nuclei are numerous, water vapor rapidly condenses on them, leading to an increase in rainfalls over the cities due to the particulate air pollution (Lutgens and Tarbuck, 2004).

Finally, from the point of view of PM sampling, the amount of adsorbed water affects the solid-vapor equilibria of the secondary ammonium salts collected on the filters, a mechanism that is among the main responsible for sampling artifacts (Vecchi et al., 2009). Although in most cases the artifact is negative (loss of NH_4NO_3 due to release of NH_3 and HNO_3) (Chow et al., 2005; Yuc et al., 2006; Pathaket al., 2009), in the presence of very high humidity values it becomes positive, as the formation of particulate NH_4NO_3 from gaseous NH_3 and HNO_3 is favored (Gysel et al., 2007; Khlystov et al., 2009; Hu et al., 2011).

However, at present, the mechanism behind these equilibria is not completely known and a key role could be the study of the effect of humidity on the particles' distribution between solid and gaseous phase.

Of interest is also the contribution of water to the mass concentration of PM. The presence of considerable amounts of water in PM samples, in fact, causes an increase of PM mass concentration that might be responsible for the exceedances of the limit standards. It is worth noting that the knowledge of this contribution may be of interest also for a correct evaluation of the PM health effects: water is harmless, but it may cause a relevant variation of the aerodynamic diameter of the

particles and thus of their ability to penetrate into the respiratory system. Moreover, in many papers attempting PM mass closure, the unidentified mass (difference between gravimetric determination and reconstruction from the single chemical analyses) is generally attributed to the presence of water and/or to the difficulty in determining an adequate conversion factors to calculate organic matter (OM) from the measurement of organic carbon (OC) (Balasubramanian et al., 2003; Harrison et al., 2003; Tsyro, 2005; Almeida et al., 2006; Sasaki and Sakamoto, 2006; Perrino et al., 2007; Perrino et al., 2009; Perrone et al., 2012). This aspect will be widely discussed in Chapter 3.

Water can exist within the PM as bound or not-bonded water: the first is chemically bound to the crystalline structure of the inorganic salt. The only species present in atmospheric aerosols containing this kind of water is the Na_2SO_4. The not-bonded water is the water which condenses on the aerosol particles when the relative humidity atmospheric (RH) increases. All the inorganic salts are characterized by a *deliquescence relative humidity* point (DRH) which represents the atmospheric humidity above which the salt absorbs water up to form a saturated aqueous solution (Hanel, 1976). At relative humidity values lower than the DRH point, the salt is present in the solid phase; exceeding this value, water increasingly condenses on the particle to maintain the thermodynamic equilibrium. If, however, after exceeding the DRH value the relative humidity decreases, the not-bonded water begins to evaporate and reaching downhill the DRH point, the solution keeps supersaturated and the re-crystallization of the salt does not occur. For example, the DRH point for NH_4NO_3 is 60% and when the humidity decreases, the solid does not crystallize until it reaches values below 10% (Dassios and Pandis, 1999). Another example is given by the behavior of the $(NH_4)_2SO_4$ which has a DRH of 80%, while re-crystallization occurs at RH below 30% (Ansari and Pandis, 1999).

Many papers in literature relate to the study of the interaction between water and atmospheric particles: in 1996 Yang e Cotton theoretically demonstrated that there is a relation between the relative humidity and the capability of a dry particle to absorb water. In 2011 Hu et al. studied the effects of RH on the size and hygroscopicity of NH_4Cl and NH_4NO_3. It was found that the evaporation of NH_4Cl is promoted by increasing the RH values and a similar trend was also observed for NH_4NO_3 particles less than 50 nm. The proposed mechanism suggests that, by increasing the RH, the equilibrium (1) is altered, converting $NH_3(g)$ e $HX(g)$ in NH_3*nH_2O e $HX*nH_2O$ (X is given by Cl^- or NO_3^-), making the evaporation of NH_4X (s) faster.

$$NH_4X\ (s) \rightleftharpoons NH_3(g) + HX(g) \qquad (1)$$

In spite of the relevant role played by water in the study of atmospheric PM, a quantitative determination of adsorbed water was attempted only in a few papers. Water content was generally determined by indirect methods, consisting of the differential determination of particle dimension (Dick et al., 2000; Hu et al., 2001; Rees et al., 2004; Stanier et al., 2004; Kitamori et al., 2009) or collected mass amount (Speer et al., 1997; Speer et al., 2003) before and after the exposure to controlled RH conditions. These studies showed that water may constitute up to 20–30% of the total PM mass and indicated a dependence of the water uptake on the dimension and chemical composition of the particles. Water adsorption resulted to be relevant for fine particles, characterized by high surface area, and for particles containing water-soluble inorganic salts, mainly ammonium sulphate (Speer et al., 1997; Stanier et al., 2004; Kitamori et al., 2009), and hygroscopic organic species such as dicarboxylic acids (Ansari and Pandis, 2000; Dick et al., 2000; Decesari et al., 2001; Speer et al., 2003). In most of these papers the instruments used to carry out the analysis are some particular analyzers, the *Dry-Ambient Aerosol Size Spectrometers* (DAASSs) or *Humidified Tandem Differential Mobility Analyzers* (H-TDMAs). These devices are very expensive and quite complex to run and to manage and also the analysis are carried out only on not-sampled aerosol. Moreover, these differential techniques evaluate only the amount of surface-adsorbed water and are not able to give information about further contributions due to structurally-bound water.

To our knowledge, only two papers reporting a direct analytical determination of water on sampled PM by the Karl-Fisher method have been published up to now (Ohta et al., 1998; Tsai et al., 2005). The first one is based on the thermal desorption of water at 150°C from Teflon filters sampled for two weeks; the results showed that a percentage of the total $PM_{2.0}$ mass ranging from 0.4% to 3.2% could be attributed to the crystallization water of $(NH_4)_2SO_4$, NH_4NO_3 and NaCl. In the second paper, the water contained on quartz filters conditioned at 60% RH was extracted by using anhydrous methyl alcohol; in these conditions water resulted to be the individual component at highest concentration (about 30% of the total PM mass). In spite of the different operative conditions employed in these two studies, these results demonstrate that the Karl Fisher technique is suitable for determining water in PM samples; the described methods, however, are not appropriate for a routine use in intensive monitoring campaigns because of too high detection limits (Ohta et al., 1998) and/or method complexity (Tsai et al., 2005).

2.3 Aim of the work

The idea to determine water in PM came from a preliminary study carried out during my graduation thesis, concerning the thermal behavior of the atmospheric semi-volatile compounds. The thermogravimetric analysis (TG) of the reference material NIST 1649a pointed out two well-defined weight losses in the range 80°-120°C and 150°-180°C (as shown in figure 2.1), which could not be attribute to both inorganic and organic compounds. We assigned then those losses to particle-bound water. Moreover, the wider loss in the range 225°C-310°C was due to the release of several organic and inorganic specie with a possible contribution of crystallization water, in agreement with the results obtained by Matuschek et al., 2004. However, the quantitative determination of water by thermogravimetric techniques was not possible due to the presence of other volatile species, which, although present at much lower quantities than those of water, can cause interference in the analysis. Furthermore, the use of TG in PM real samples has been seriously compromised by the presence of the sampling membrane, which has a mass much greater than the sampled dust.

These findings, published in 2012 by Atmospheric Environment (Perrino et al. 2012) suggested that the thermoanalytical techniques can be a suitable support for the determination of the water in PM. Therefore, the purpose of this work was to optimize and validate a method sufficiently sensitive for the qualitative and quantitative determination of water in real samples, easily applicable to routine field campaigns. As described above, water determination can be useful to interpret the sampling artifacts (one of the main causes of error in the assessment of air quality) and to perform the PM mass reconstruction, without the "a priori" assumption that the missing part is water.

The employed device was a coulometric Karl Fischer (KF), able to analyze samples with a low water content (10 pg-10 mg).

The method is based on the use of a thermal ramp for the selective desorption of different water contributions, retained by the sample with different strength. This was possible thanks to the software flexibility that allowed to set different temperature of desorption. Preliminary application of the method to PM real samples was also performed in order to investigate the dependence of the water content from the PM chemical composition.

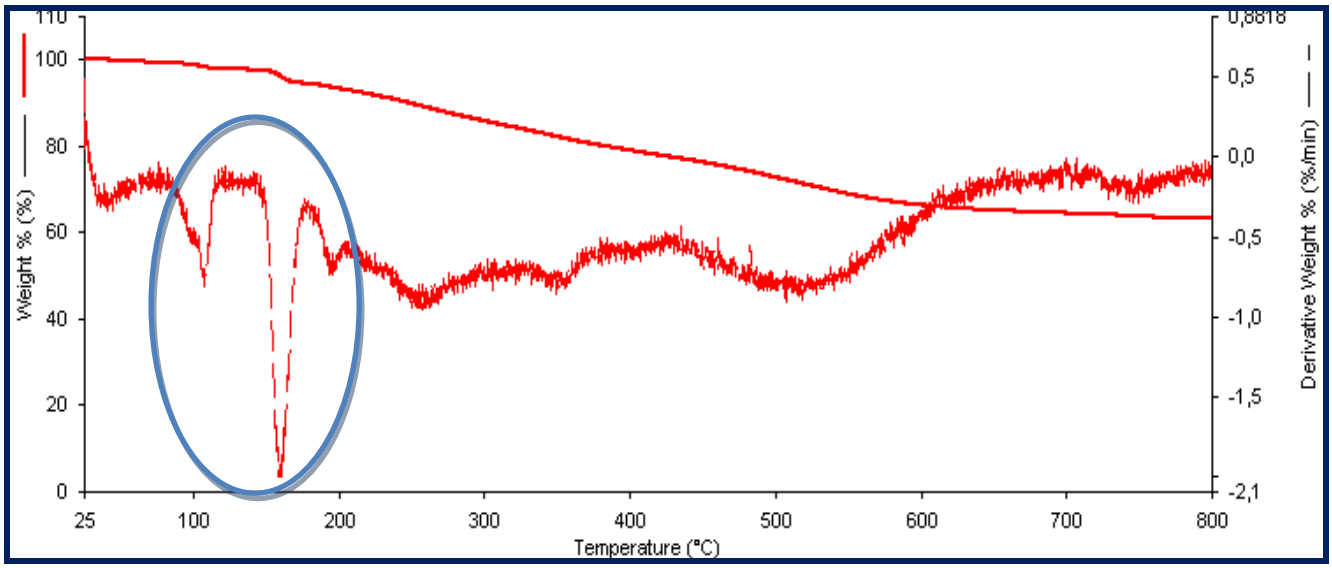

Fig. 2.1: TG and derivative curve of a sample of NIST1649a(4 mg), scan from 25°C to 800°C, nitrogen atmosphere; the blue circle indicates the two losses in weight attributable to water (Perrino et al., 2012).

2.3 Experimental

2.3.1 Materials and devices

- Reference material NIST 1649a (Urban Particulate Matter);
- HYDRANAL Water Standard KF-Oven 220°C–230°C (HYD; Fluka Analytical) , containing 5.55±0.05% of water;
- Water Standard Oven 1%, (WSO; ACS Merck KGaA), containing and l.0±0.03% water, respectively;
- SiO_2, Al_2O_3, NH_4HSO_4, NH_4Cl, NH_4NO_3, $(NH_4)_2SO_4$, lactose, fructose, sucrose, levoglucosan, tartaric acid, citric acid, succinic acid, oxalic acid, phenylalanine, analytical grade (ACS Merck KGaA);
- Saharan dust, road dust, soot from vehicular exhaust, skin, bacteria, moulds, pollens, taken directly from the environment and analyzed without any pretreatment;
- Filters Teflon ® Omnipore, 0.45 µm porosity, 25 mm diameter;
- Quartz filters, 1 µm pore size, diameter 47 mm, Pall Corporation;
- Molecular sieves, 0.3 nm pore size, Metrohm Italy;

- Glass vials, 6 ml, Metrohm Italy;
- Silicone caps with aluminum septum, height 7.4 mm, 20.7 mm external diameter, Metrohm Italy;
- Manual gripper to close the vials, Metrohm Italy;
- Polyethylene bag, AtmosBag, Sigma-Aldrich.
- Analytical balance GIBERTINI Elettronoca E505 (0.01 mg sensitivity);
- Analytical balance GIBERTINI Elettronica 60 (0.1 mg sensitivity);
- Universal stove, used as a dryer or sterilizer, DAS 40000, 40 liters, Inter® continental;
- 874 831 Oven Sample Processor with coulometric Karl Fischer titrator, Metrohm Italy.

2.3.2 Vials and samples pre-treatment

Before each measurement sample vials were kept in the oven at 250°C for 12 h, then placed in a desiccator and transferred inside an AtmosBag filled with Argon dried by using molecular sieves. Samples were weighted by using an analytical balance (sensitivity 0.01 mg) and put inside the AtmosBag, where they were inserted into the vials, as shown in figure 2.2.

2.3.3 *PM_{10} sampling*

Twenty pairs of equivalent real PM_{10} samples were collected during the period November-December 2011 in three different geographical areas. The location in Rome (Central Italy,41°54'03.69''N, 12°30'44.93''E) was a traffic site, about 50 meter from the nearest road (8 pairs of samples); the location in Ferrara (Po valley, Northern Italy, 44°50'55.44''N,11°33'40.96''E) was an industrial site, about 5 km from the city center and 1 km from the nearest industrial plant (10 pairs); the location in Tel Aviv (Israel, 32°06'54.16''N,34°48'16.74''E) was the roof of the Tel Aviv University (2pairs).

Daily PM_{10} samples were collected on 47 mm diameter PTFE membranes, 1 μm pore size (PALL Corporation, USA) by means of dual-channel samplers (HYDRA Dual Sampler, FAI Instruments, Fontenuova, Rome, I) equipped with two independent PM_{10} sampling heads compliant with EN 12341. At Rome and Tel Aviv the two channels were operated at the flow rate of 2.3 m^3h^{-1}. At Ferrara, which is characterized by very high relative humidity, the sampling heads were modified in order to reduce the flow rate to 1.15 m^3h^{-1} and to avoid clogging of the sampling membranes. An additional collection of six parallel samples was carried during the period 14–20 December 2011 at the Ferrara site, by using three HYDRA Dual Samplers placed side-by-side. These samples were

used to evaluate the effect of sample conservation. Teflon filters were allowed to equilibrate for two days at 20°C and 50 % RH before weighting according to EN 12341 (CEN 1998). After sampling, filters were placed in Petri dishes and stored at 5°C. Different procedures were used to evaluate the effect of storage conditions. Before the analysis all samples were re-equilibrated and re-weighted and the plastic rings of the filters were cut off by using a steel scalpel.

Fig. 2.2: Polyethylene bag filled with Argon.

2.3.4 Karl-Fischer analysis

Karl-Fisher (KF) is a well-established analytical technique developed in the first half of the XX century (Fisher, 1935). It is based on the quantitative red-ox reaction between water and I_2,

$$\mathbf{H_2O + I_2 + SO_2 + CH_3OH + 3RN \rightarrow (RNH)SO_4CH_3 + 2(RNH)I} \quad \mathbf{(2)}$$

where iodine is reduced to iodide and sulfur dioxide is oxidized to sulphate, RN indicate a base that usually is pyridine. The KF method is usually applied in alimentary an pharmaceutical fields, the advantages of using this method are:

- Highly specificity and precision (the absolute amount of moisture can be determined without a working curve, in the case of coulometric titration);
- It covers a wide range of concentration;
- It takes short times of execution;
- The method can be used with small amount (few mg) of solid, liquid and gaseous samples.

In the coulometric version of the technique, I_2 is electrochemically generated inside a cell containing a specific solution (methanol, pyridine and sulphur dioxide). The total amount of water inside the cell is determined by measuring the total electric charge needed to generate I_2. Iodine generation stops when the end point of the titration is reached. The end point is indicated voltammetrically by the drastic lowering of the voltage difference between the wires of a double Pt electrode. The water amount is calculated by the software using the Faraday's low, $m = (M\ Q)/(z\ F)$, where m is the water mass, M is the molecular weight, Q is the charge in time, z is the number of the exchanged electrons, F is the electrochemical equivalent (1F=96485 Coulomb/mol). With this relation the generated I_2 amount is calculated, that is equal to the water amount as the stoichiometry ratio between water and iodine in the reaction (2) is 1:1.
In this study we used a 831 KF Coulometer (Metrohm AG,Herisau, CH) equipped with an oven (874 Oven Sample Processor; Metrohm), showed in figure 2.3.

Fig. 2.3: 874 Oven sample processor con 831 KF coulometer, Metrohm Italia.

The samples are inserted into glass vials and placed inside the oven; water released when heating the sample is transferred to the measurement cell by a carrier gas and measured (figure 2.4).

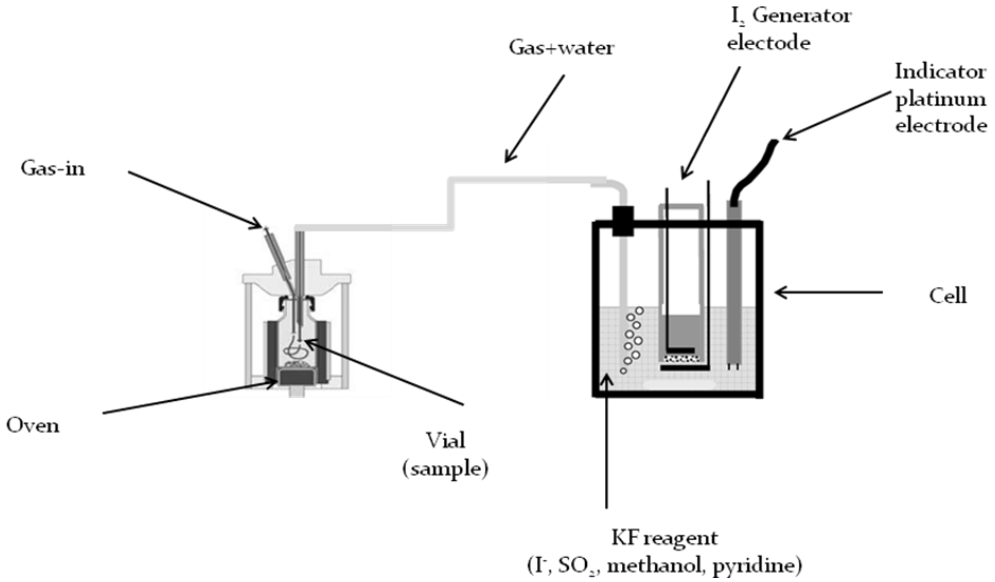

Fig.2.4: Schematic picture of the oven and the titration cell.

Karl Fisher reagent (100 mL) was used in the titration cell. For transferring the sample from the oven to the measurement cell we used ambient air at the flow rate of 20 mL min^{-1}, previously filtered and dried by using molecular sieves. To avoid clogging of the carrier gas transfer line due to the condensation of species desorbed from PM (e.g.: ammonium salts), the lines of the titration cell and the needle entering the vials were accurately cleaned every day.

This instrumental configuration implies the presence of a signal drift, being unfeasible to eliminate at all the water contained in the system (mainly in the carrier gas). In these conditions, the end point is reached when the drift value returns to its initial value, and the instrument software calculates the amount of desorbed water by subtracting the contribution due to the baseline drift from the final water amount; the baseline drift contribution is calculated by extrapolating its initial value to the end of the analysis. In the next session all the needed changes of the parameters aimed to the reduction of the drift contribution will be described.

2.4 Method optimization and validation

The following results have been already published by Atmospheric Chemistry and Physics Discussion journal (Canepari et al., 2013).

As previously discussed, the instrument used in this study was equipped with a temperature-programmable oven that allows the setting of tailor-made heating ramps. This instrumental feature was necessary to obtain the selective desorption of different water contributes. However, the use of

heating ramps required to perform some modifications to the default settings of the instrument software. As previously outlined, the instrument is equipped with an automatic system that identifies the end point of the titration according to the return of the baseline drift to its initial value. When using a thermal ramp, it is necessary to exclude the end point identification, as each return of the drift to the initial value indicates the separation of a different water contribution. As a consequence, the minimum value of the voltage difference between the indicator platinum electrodes was set at 30 mV, the limit value of the drift was set at 1 μg min^{-1} and the total duration of the analysis (extraction time) was fixed at 3000s, in a way that the determination was never stopped by the reaching of the end point. Moreover, in our case, the use of the thermal ramp caused the increase of the analytical time with a consequent increase of the drift contribution to the final water amount, which becomes comparable with the amount of water in the PM samples.

Also, the drift value is variable, and the influence of this variability on the repeatability of the analytical results increases with the duration of the analysis. In our conditions, the intra-day and inter-day variations were 0.05 μg min^{-1} and 0.9 μg min^{-1} respectively (calculated as 10 replicate analyses of the operative blank). To reduce the effect of the drift variability as much as possible, the measurement of the operative blank (empty vial) was carried out every two samples, and the KF curve of each sample (water vs. time) was obtained by subtracting the blank value to each point of the graph. In figure 2.5 an example of KF analysis performed on the reference material NIST1649a before and after the blank curve subtraction is reported. This process allows a direct reading of the water amount on the y-axes of the graph; also, this method allows a direct subtraction of the water contribution due to the air inside the vial, adsorbed on the vial walls and contained in the plastic vial cap.

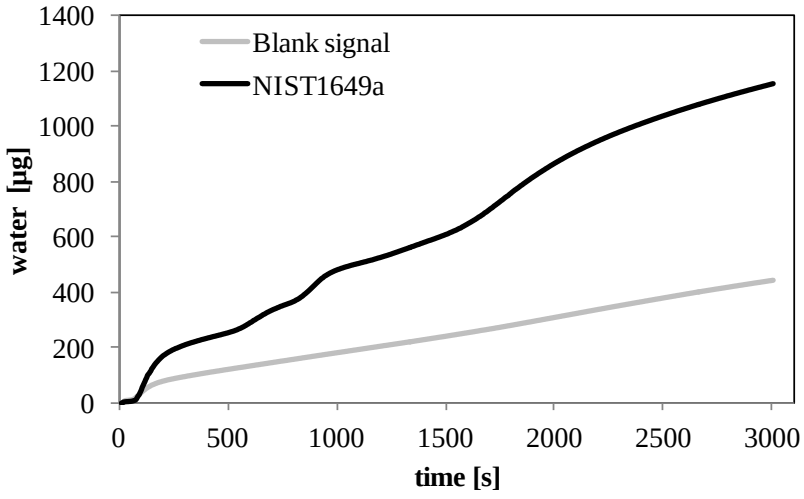

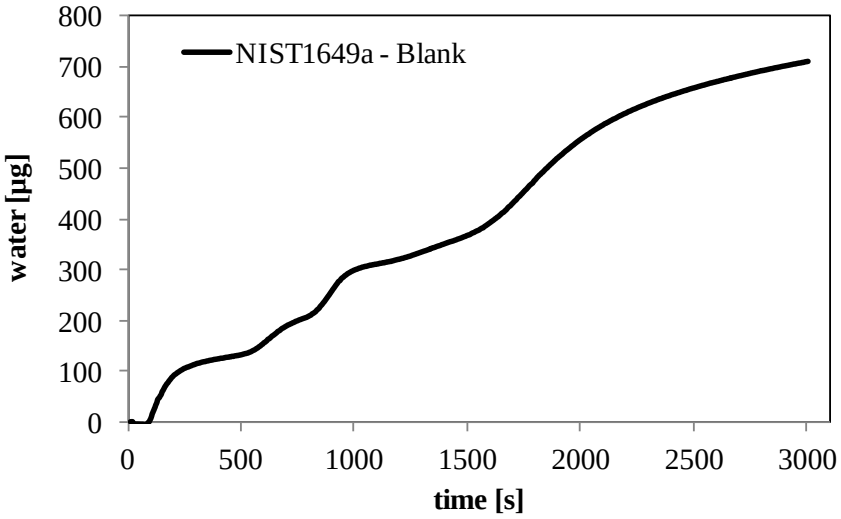

Fig. 2.5: Karl-Fisher analysis of the reference material NIST1649a. Upper panel: original sample signal and blank signal. Lower panel: sample signal after blank subtraction.

2.4.1 LODs and LOQs calculations

As previously mentioned, the presence of secondary reactions, the penetration of atmospheric water inside the cell and the humidity of the carrier gas led to a continuous consumption of iodine during the conditioning time, causing the presence of a variable drift during the analysis. This drift significantly influence both the LOD (Limit of Detection) and the LOQ (Limit of Quantification).

LOD and LOQ values are often calculated following IUPAC (International Union of Pure and Applied Chemistry) indications, considering the average value of the operating blank and its standard deviation. The LOD represents the smallest concentration which can be detected with reasonable certainty by a given analytical procedure and is evaluated as the average value of the operative blank plus three times the standard deviation, obtained from an adequate number of measurements. The LOQ instead represents the smallest concentration of a certain analyte in a sample that can be quantitatively determined with an acceptable level of precision and accuracy, and is calculated as the average value of the operative blank plus ten times the standard deviation.

In our case, the calculation of LOD and LOQ following the IUPAC directions would lead to excessively high values due to the inevitable presence of the drift and the relatively long analytical time due to the use of the programmed temperature. Hence, we use only the drift variability not considering the average value of blanks. In this way, LOD and LOQwere calculated as three times and ten times the standard deviation of the blank (10 replicates). For a typical intra-day variability

we obtained the following results we obtained respectively a LOD = 7 µg and a LOQ = 25 µg, absolutely compatible with the application of the method to real samples.

2.4.2 The thermal ramp

The method was optimized by using the Reference Material NIST1649a (National Standard Institute of Technology – USA), consisting of urban atmospheric particulate matter. Although its water content is not certified and it show some differences with respect to real PM_{10} samples (Canepari et al., 2006 a,b), this material makes it possible to perform the optimization phases on a rather representative homogeneous material.

The first optimization phase concerned the heating ramp and was aimed to obtain a satisfactory separation of the different water contributions to atmospheric PM. To this purpose, we referred to the previous work carried out in our laboratory, already mentioned in 2.2 section, trying to simulate the same linear thermal ramp used by TG (figure 2.1) . Figure 2.6 shows some examples of thermal ramp (left panels) and KF curves obtained when applying the ramp to NIST 1649a (right panels). The total amount of water was 100±6 g Kg^{-1}, irrespective of the selected ramp. It is noteworthy that the analytical results obtained by the analysis of the reference material are reported on a dry mass basis. According to the information provided by certificate, this material contains a residual moisture equal to 1.23 ± 0.07% , with a confidence level of 95%. The amount of measured water on the NIST 1649a by KF method is approx. 6-7%, much higher than those initially present, due to the presence in the sample of hydrophilic compounds.

The curve profile strongly depends on the thermal ramp, as shown by the drift graph (grey lines in fig. 2.6). When the heating temperature is constant, the operational mode generally used in this type of instruments, we obtain only one signal which is relative to the total water amount (Fig. 2.6, upper panels).

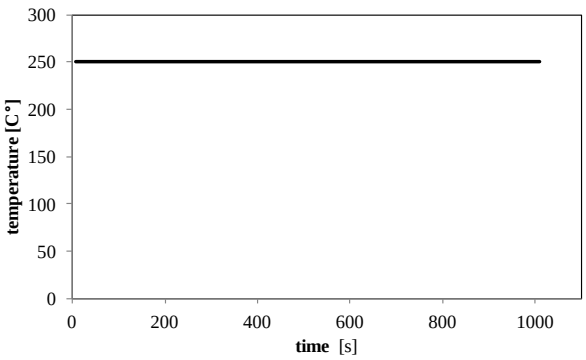

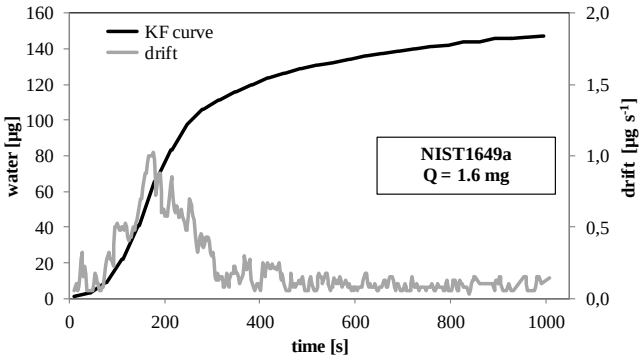

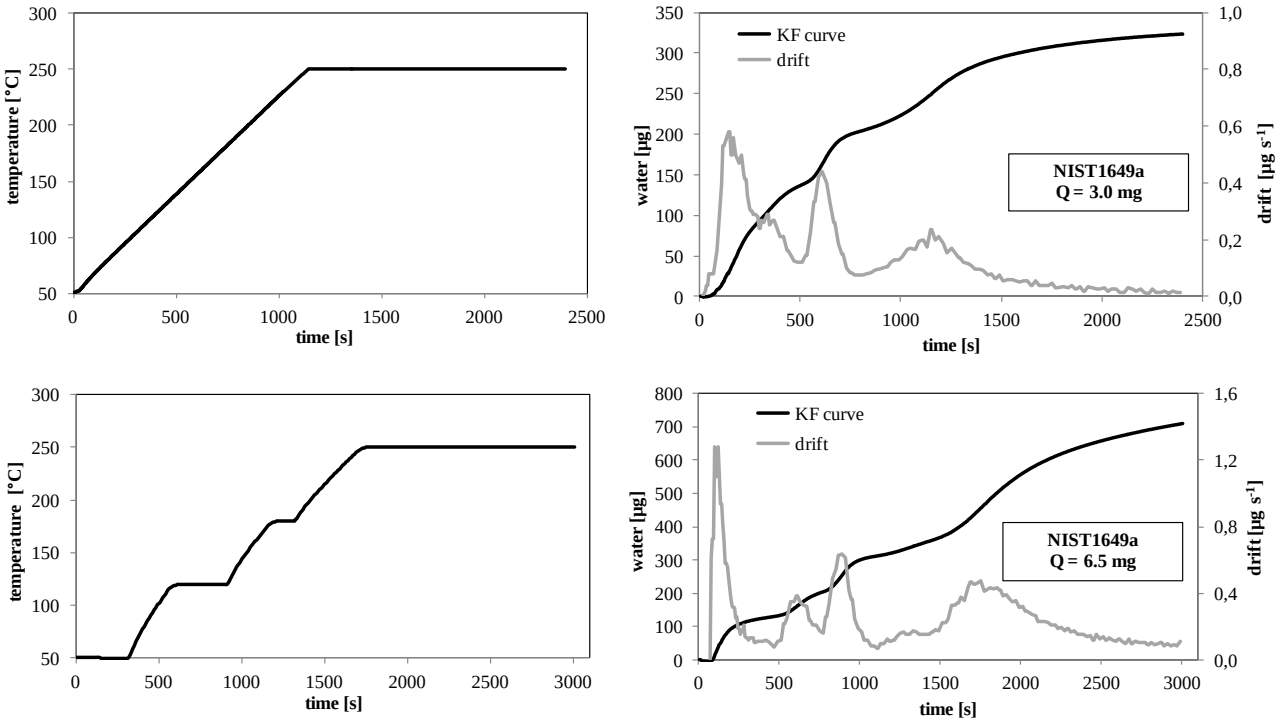

Fig. 2.6: Different thermal ramps (left panels) and resulting Karl-Fisher curves (right panels) for the analysis of Reference Material NIST1649a.

The use of a linear thermal ramp (50°C-250°C, 10°C/min, 250°C-20mins) allows the differentiation of several water contributions that are released from the sample at increasing temperatures (Figure 2.6 middle panels). In these conditions, however, the contributions are insufficiently separated. It is worth noted that this is properly the linear ramp used in the previous works concerning the TG analysis (Perrino et al., 2012). Although the results obtained by KF and TG are qualitatively similar, the separation of the water contributions by the KF method is lower, probably because of a higher thermal inertia in the heat transfer from the oven to the sample.

The lower panels of Fig. 2.6 reports the optimized thermal ramp, obtained by a trial and error procedure, that was used to perform all subsequent analyses (5 min at 50°C, from 50°C to 120°C at 14°C min^{-1}, 5 min at 120°C, from 120°C to 180°C at 12°C min^{-1}, 2 min at 180°C, from 180°C to 250°C at 14°C min^{-1}, 20 min at 250°C). In these conditions, we obtained a significant improvement in the analytical resolution, and a profile very similar to that obtained by TG. The first peak in the drift graph, which had not been detected by the TG analysis, identifies water that can be desorbed at low temperature (50°C), probably due to moisture weakly adsorbed on the particles. The following three peaks (in the range 400-700 s, 700-1100 s, 1100-2300 s) are in very good agreement with the results of the previous TG analysis and confirm the presence of different water contributions, bound to atmospheric particles with different strength.

2.4.3 Recoveries of the method

To calculate the exactness, we used two standard materials HYDRANAL Water Standard (HYD) and Water Standard Oven (WSO) containing different amounts and qualities of water. Figure 2.7 reports the KF curves and the drift graphs of the two certified materials. HYD (upper graph) shows only one water contribution, desorbing over 200°C, that is due to crystallization water.

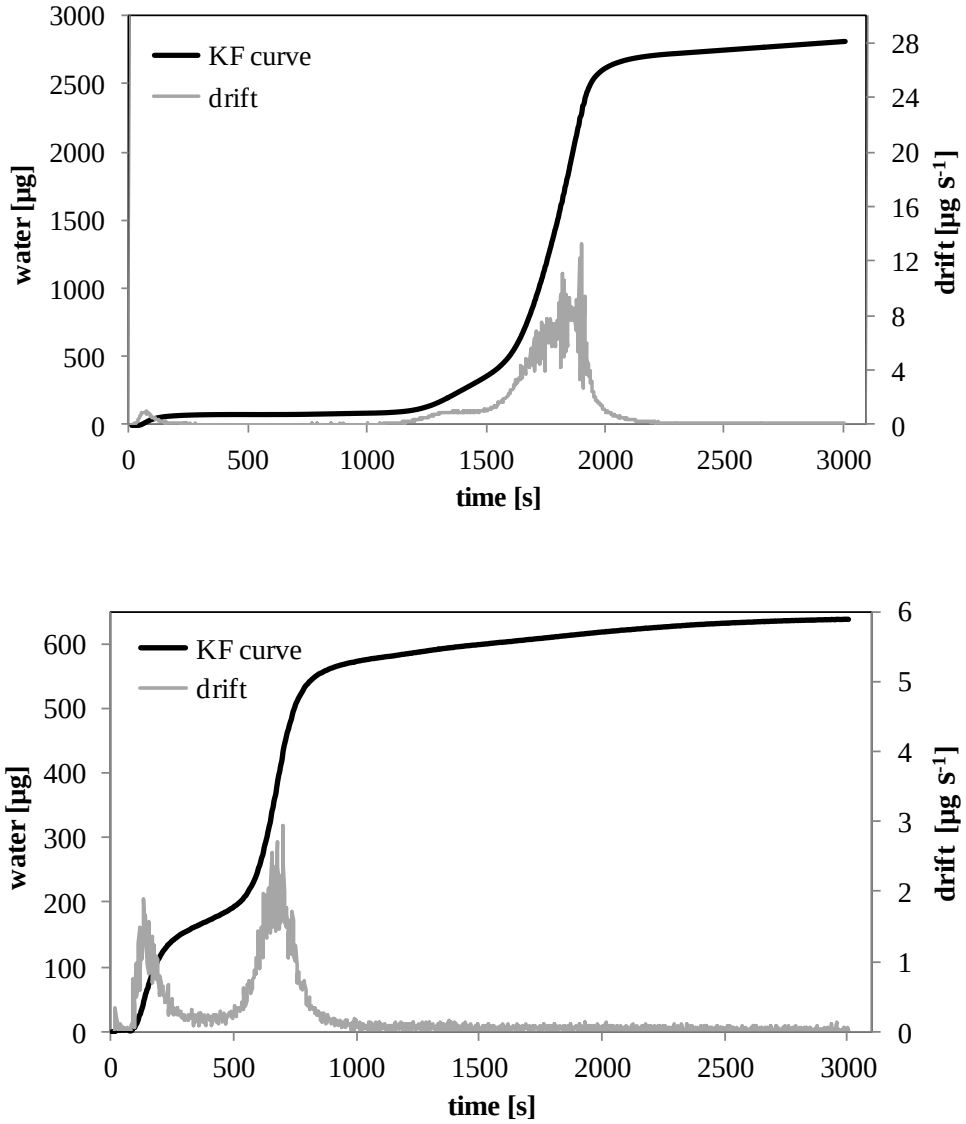

Fig. 2.7: Karl-Fisher curves of about 50 mg of standard materials HYD (upper panel) and WSO (lower panel).

WSO (figure 2.7, lower graph) shows two different contributions: the first one, weakly retained, is released at the beginning of the analytical run at about 50 °C, the second one is released in the range 500-800 s, at the temperature of about 120°C.

Table 2.1 shows the recovery of different amounts of the two standard materials. We did not consider amounts lower than 5 mg in order to avoid the introduction of a high uncertainty contribution due to the gravimetric determination and transfer of very small sample amounts. In all cases the recovery was close to 100%, while the repeatability was better for HYD (high amounts: about 3%; low amounts: about 6%) than for WSO (high amounts: about 9%; low amounts: about 11%), probably because of the lower stability of the water contained in WSO.

Tab.2.1: Recovery of water from standard materials HYDRANAL (HYD) and Water Standard Oven (WSO). N=10

		Certified µg	**Measured µg**	**Recovery %**
HYD	Low (5 mg)	278±3	272±15	98±6
	High (50 mg)	2775±25	2817± 67	102±3
WSO	Low (10 mg)	100±3	101±8	101±11
	High (50 mg)	500±15	497±28	99±9

A further validation phase concerned the recovery from silica and alumina, which are among the hydrophilic species contained in PM. These compounds are thermally stable and available on the market at high purity level; it is thus possible to carry out a gravimetric determination of the water that is desorbed when heating in oven (105 °C for 24 hours). We also tested the molecular sieves used to dry the carrier gas of the KF (silicate with inorganic binder), in order to verify the influence of the material porosity on the profile of the KF curve. The KF curves obtained for these materials are shown in Figure 2.8. All the materials show a contribution in the range 0-500 s, probably due to moisture weakly adsorbed on the particles; the following part of the curves, instead, are quite different. The curve of silica (upper graph) shows only a further single contribution in the range

500–1000 s. Molecular sieves (middle graph) show a very similar behavior in the first part of the curve; with respect to silica, however, molecular sieves release a relevant amount of water also in the second part of the analysis (1000–1500 s), likely due to the release of water adsorbed inside pores. Alumina shows the same profile in the range 500 - 1000 s (lower graph), but also two other more retained contributions, not completely separated, between 1000 and 2300 s, probably due to the presence of active sites of different strength.

Table 2.2 reports the recovery values for these materials. Also in this case the method shows good performance, with recoveries higher than 95% and repeatability around 6%.

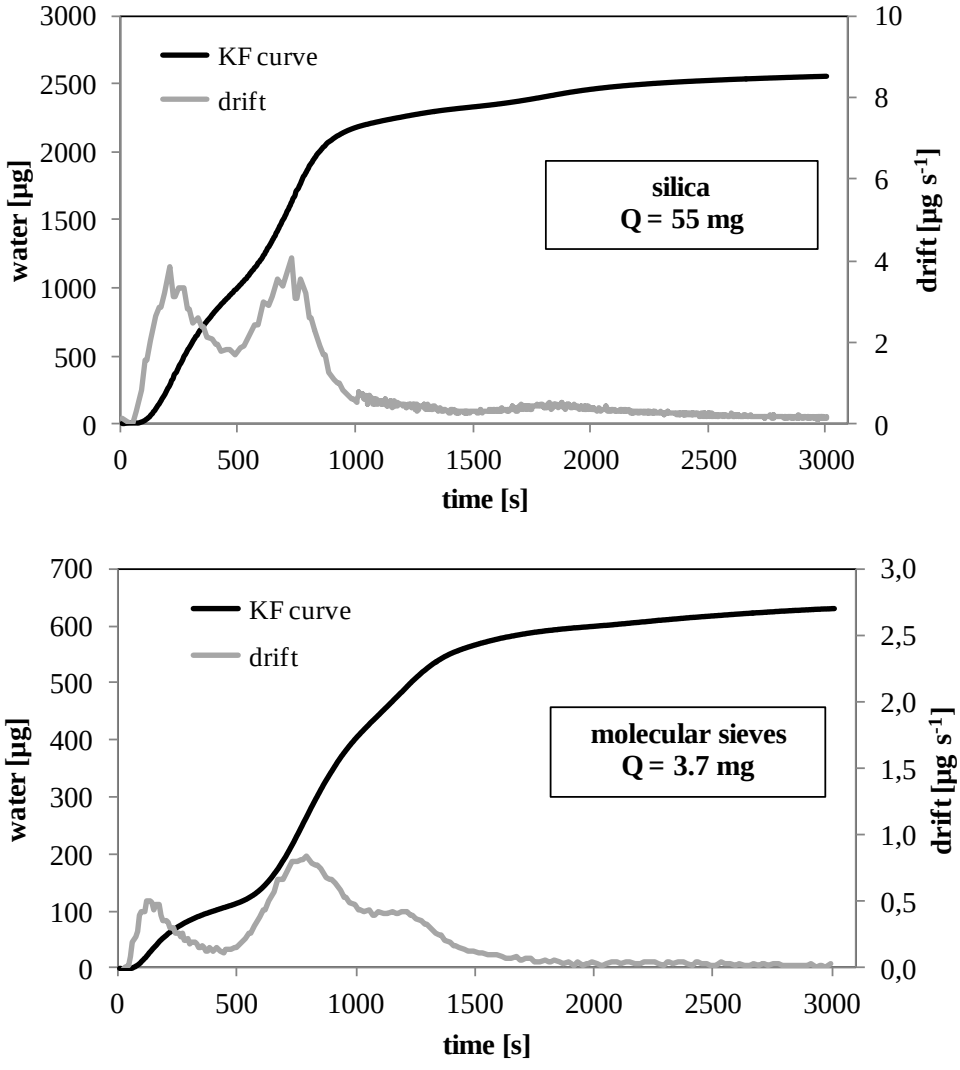

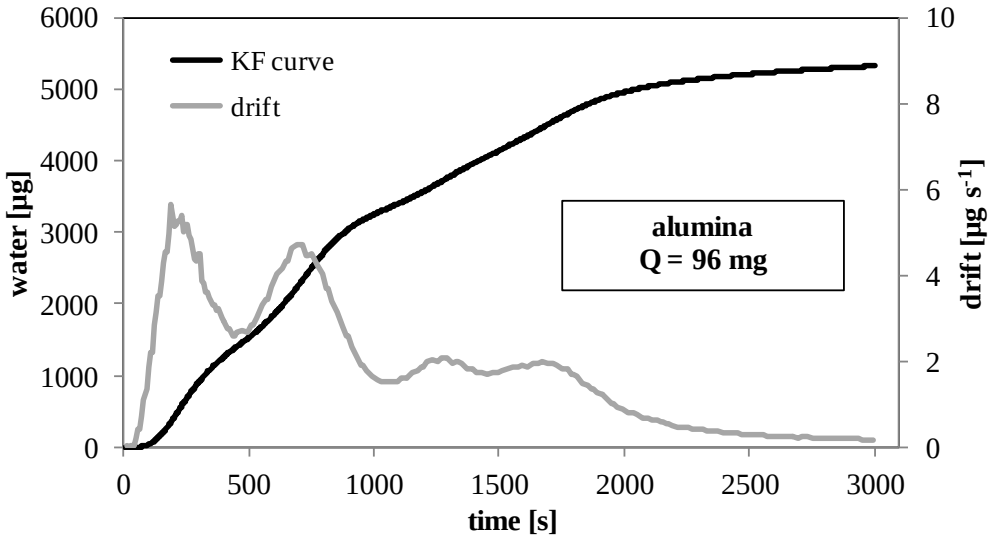

Fig. 2.9. Karl-Fisher curves of silica (upper panel), molecular sieves (middle panel) and alumina (lower panel).

Results reported in Table 2.2 refer to very variable sample amounts (5-100 mg) and to measured water amounts in the range 0.3– 7.0mg. The shape of the curves and the recovery values do not depend on the sample weight, indicating robustness and wide linearity range of the proposed method.

Tab. 2.2: Comparison of gravimetric and Karl Fisher determination of the water content, N=10.

	Water content g Kg^{-1}		**Recovery %**
	Gravimetry	Karl Fisher	
SiO_2	46±1	45±3	98±9
Molecular sieves	165±4	167±6	101±6
Al_2O_3	50±2	48±2	96±8

2.4.4 Interferences

KF method suffers from the interference of some classes of compounds, both organic and inorganic (EPA Method 9000, 2007). If side reactions occur the titration may fail to reach the end point or a huge amount of KF reagent can be consumed, leading to errors in the water determination. Positive errors can be due to the interfering compounds, such as Fe(III) and Cu(II) salts, which react directly with I_2, behaving like water. Also positive errors can be due to organic compounds such as aldehydes and ketones which interfere with the methanol contained in the KF reagent, by producing water. Some of these interfering compounds are likely found in PM samples. Given the huge number of organic and inorganic species present in the PM, many of which are not yet known, it is not possible to study in a rigorous way the interference of the individual classes. However most of these species are not able to interfere in analytical techniques based on heating, due to their very low vapour pressure (levoglucosan, glucose, fructose, sucrose) (Chow et al., 2007). As far as carbonyl compounds are concerned, the species that reach high atmospheric concentration are mostly in the vapor phase (Levart and Veber, 2001). Some Authors highlight the presence of some semi-volatile ketones (n-alcan-2-ones and o-Hydrocarbons Polycyclic Aromatics) (Schnelle-Kreis et al., 2005, 2007), but the atmospheric concentration of these species is usually very low (a few tenths of ng m^{-3} for 6,10,14-trimethylpentadecan-2-one, the most abundant species) and their possible interference is well below the quantification limit of the method. Another possible analytical artifact might derive from the formation of water during the heating of hydroxyl compounds (Pavlath and Gregorski, 1985). Also in this case, the atmospheric concentration of these species is generally too low to be responsible for an appreciable artifact (Moreira dos Santos et al., 2002).

The possible positive interference of iodine reduction reaction due to ammonia ($NH_3 + 3I_2 \rightarrow NI_3 + 3HI$) is also highlighted in the EPA Method 9000 (2007). In the temperature range of the proposed KF method, ammonia is released from secondary ammonium salts, particularly the ammonium nitrate which constitute a relevant fraction of atmospheric PM

Previously studies carried out in our laboratory show that the thermal decomposition of the ammonium nitrate is complete at 250°C. The ammonium chloride, generally present in the PM in rather low concentrations (1-2% of total mass) has a thermal behavior very similar to ammonium nitrate, while the release of ammonia from ammonium sulfate (which may be present at high concentrations in some geographical areas) occurs at higher temperatures (Perrino et al., 2012).

Most of the possible interference from ammonia should then be caused by the decomposition of ammonium nitrate.

To verify this hypothesis, the method was applied to pure NH_4NO_3, $(NH_4)_2SO_4$ and NH_4Cl salts. Obtained results are reported in figure 2.9 and table 2.3.

It can be observed in all the salts, with the exception of chloride, the presence of a signal after 1000s for the bisulfate and above 1500s for nitrate and sulfate. The correspondent temperature ranges respectively 120-180°C and 180-250°C. It should be noted that these temperature ranges are compatible with the release of ammonia due only to the ammonium nitrate dissociation.

The results shown in table 2.3, also show that the signal KF obtained corresponds to 17% for the bisulfate (which hardly present in the samples of PM, at least in western areas), approx. 9% for sulphate, less than 2% for nitrate and less than 1% for chloride. Since all these salts are hygroscopic, a part of the signal is surely due to water (especially for sulphate and bisulphate salts).

To quantify the interference of ammonia we considered NH_4Cl, that is the species that yields the lowest signal.

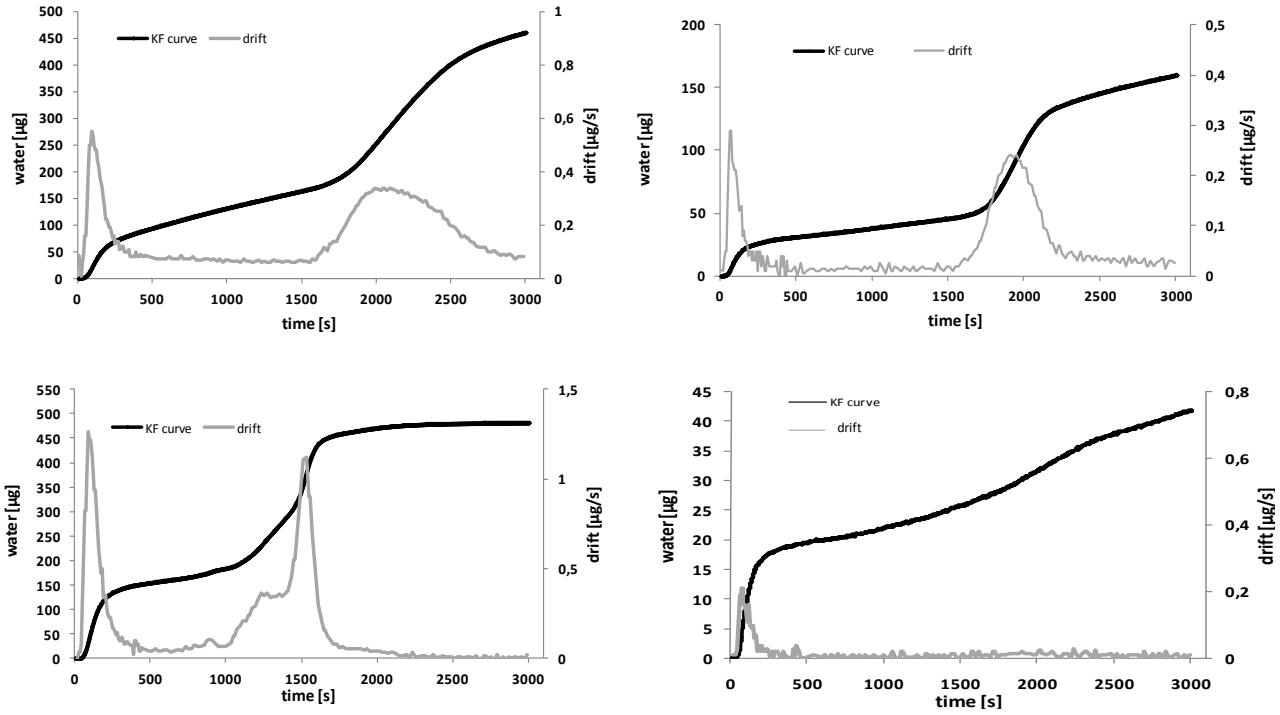

Fig.2.9: KF water profile and drift obtained for ammonium sulphate (approx. 3 mg), ammonium nitrate (approx. 10 mg) and ammonium chloride (approx. 5 mg).

Table2.3: Percentage of water and standard deviation of the ammonium salts, N=6.

	NH_4NO_3	NH_4HSO_4	$(NH_4)_2SO_4$	NH_4Cl
H_2O ± SD (%)	1.6 ±0.1%	16 ±1.4%	8.5±0.4%	0.9±0.1%

Considering that all the ammonia content of the salt is transferred in the cell, we obtain a maximum signal equivalent to a water amount of 0.9% of the salt weight.

Considering a total ammonium amount on the sampled filter as high as 500 µg (very high values, corresponding to an ammonia concentration of about 10 µg m^{-3} for 24-h samplings at the flow rate of 2.3 m^3 h^{-1}) even if the measured signal were totally attributed to interfering ammonia (anhydrous salt) we would obtain a signal equivalent to only 14 µg of water (0.9% of 500 µg multiplied by the molecular weight of ammonium chloride and divided by the molecular weight of ammonium). We can thus conclude that ammonia interference, if present, would in any case be negligible.

2.4.5 Application to real samples

Some preliminary tests addressed the analysis of the most common sampling media and the effect of the sampled filters conservation procedure on the water content. Figure 2.10 shows the KF analysis carried out on Teflon and quartz not-sampled filters.

The profile of KF curves from the analysis of quartz fiber filters resembles the profile of molecular sieves, in agreement with the common siliceous composition. Blank filter values, as expectable, were quite high (about 1400µg of water per filter). The profile of teflon filters, instead, was indistinguishable from the operative blank (vial), both before and after conditioning at 50% Relative Humidity (RH), in agreement with their hydrophobic characteristics. Teflon filters were thus considered as suitable media for PM sampling aimed at water content determination.

The influence of the sample conservation procedure was studied by analyzing six groups of six equivalent PM_{10} samples sampled side-by-side. One filter of each group was removed from the sampler immediately after the end of the sampling, conditioned at 20°C and 50% R.H. for 48 hours and then analyzed. The other five filters were left inside the unloader box of the sampler until the end of the last sampling day. A second element of each group was directly conditioned and analyzed, while other three filters were placed inside Petri dishes, sealed with parafilm and kept for

three months at ambient temperature, 5°C or -18°C, respectively. The last element of each group was kept for six months at 5°C, before being conditioned and analyzed.

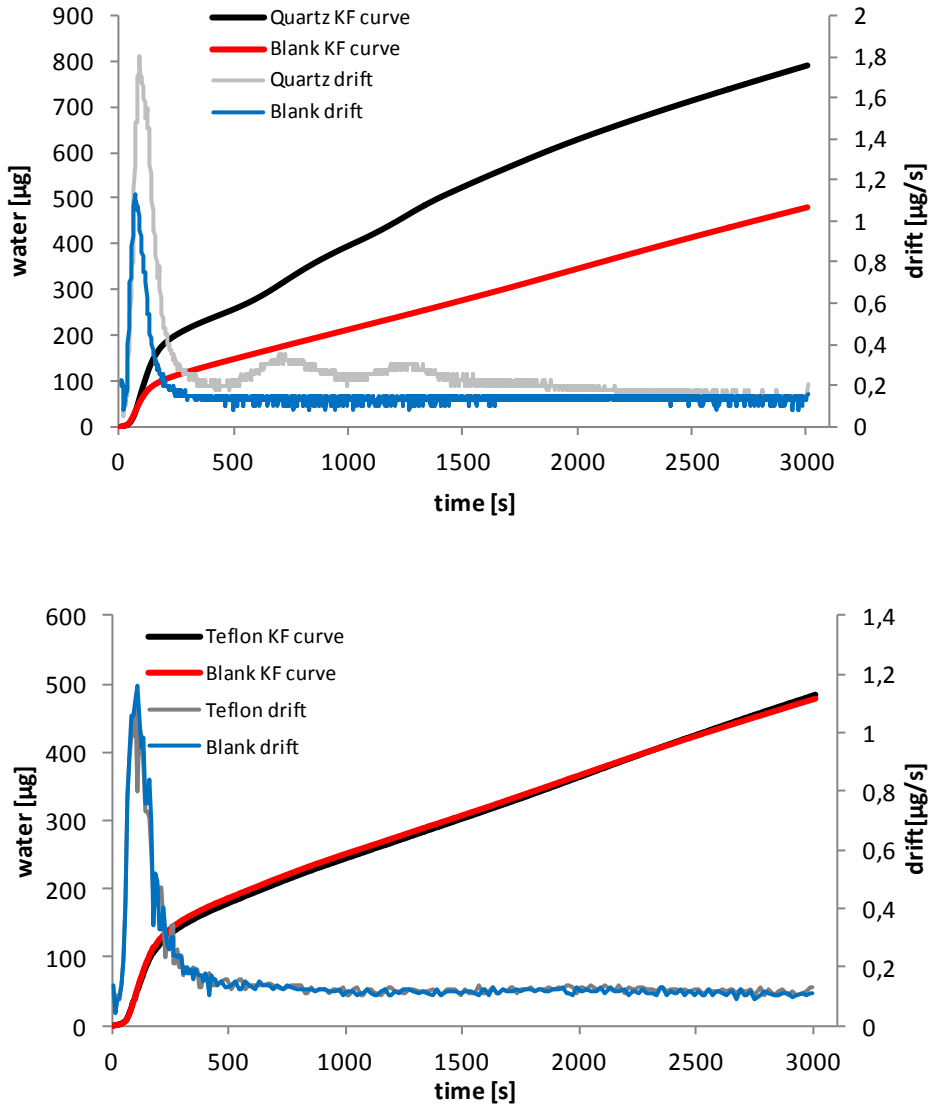

Fig.2.10: KF curve and drift of Quartz (upper panel) and teflon (lower panel) not-sampled filters compared with the analysis of the operative blank.

No significant differences were observed among the six profiles of each group of samples; the analytical repeatability was about 10%, indicating a good stability of the water retained by the particles. Storage temperature was then set at 5°C.

The validation of the method on real samples was completed by analyzing 20 pairs of PM_{10} samples collected at very different locations: a traffic site in Rome (A), an industrial site in Ferrara (Po Valley, (Northern Italy) (B), a urban site in Tel Aviv (Israel) (C) as shown in figure 2.11.

Fig. 2.11: Map of the three sampling sites. Rome (A), Ferrara (B), Tel Aviv (C).

The collected amount of dust was variable (range: 0.5–2.9 mg); the wide differences in the emission sources and meteo-climatic conditions at these three sites should also assure a variety in the chemical composition of the collected dust.

The repeatability on PM_{10} samples was calculated as follows, according to EN 14902 (2005),:

$$r_{rel} = \frac{r}{\overline{X}} * 100 \quad ; \quad r = \sqrt{\frac{\sum_{i=1}^{N} (m_{iA} - m_{iB})^2}{2N}} \quad ; \quad \overline{X} = \frac{\sum_{i=1}^{N} (m_{iA} + m_{iB})}{2N}$$

where m_{iA} and m_{iB} are the water amount determined on each component of the filter pair, and N is the total number of PM_{10} sample pairs (N=20). The obtained value (r_{rel}= 10.2%) was satisfactory and consistent with the repeatability values determined for NIST 1649a and for pure materials.

Figure 2.12 shows the scatter plot of the results obtained from each filter pair. The regression parameters (slope: 0.98; intercept: 0.15 µg m^{-3}; Pearson's coefficient: 0.96) confirm the good analytical performance of the method also when applied to real samples.

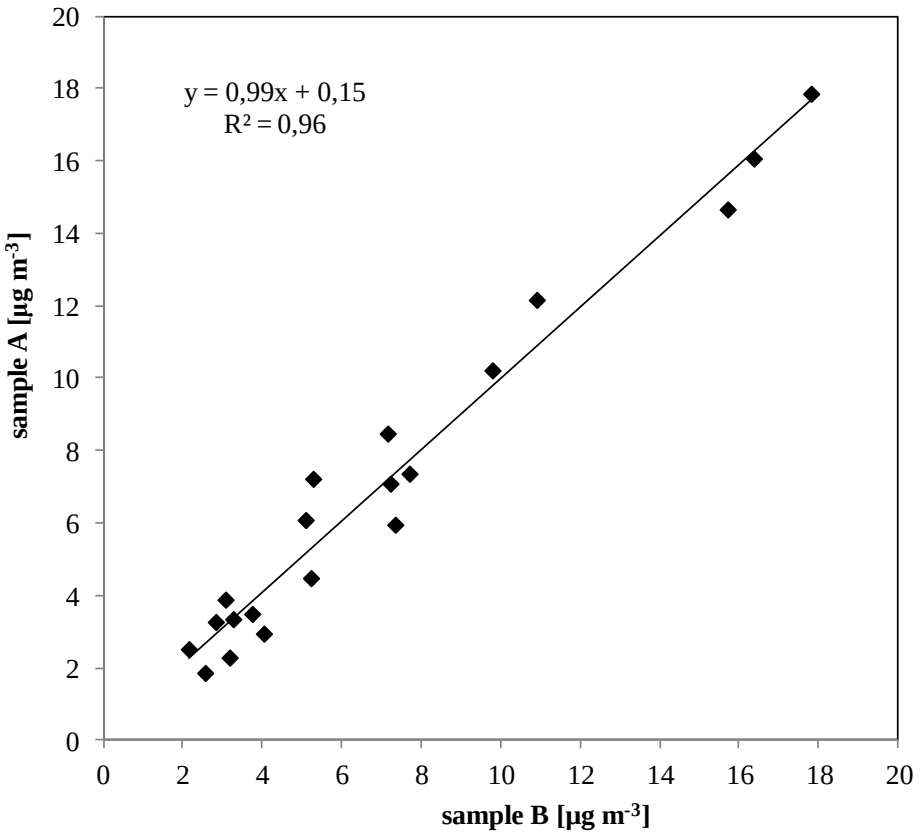

Fig. 2.12: Scatter plot of the water content of PM_{10} samples collected side-by-side (20 pairs).

The water content of our samples was very variable and reached remarkably high values, especially in Ferrara and Tel Aviv. In general, water constituted about 3-4% of the total PM mass of the samples collected in Rome, while in Ferrara and in Tel Aviv we obtained percentages over 10%, with a contribution of more than 20 µg m^{-3} to the environmental concentration of PM_{10}. This means that water content could greatly influence the overcoming of the PM standard limits and a correct evaluation of this contribution could lead to some revisions in the PM standard requirements, above all in areas where the particular weather conditions cause the presence of high concentration of atmospheric water.

Figure 2.13 shows some examples of the KF curves obtained from pairs of samples collected at the three sites.

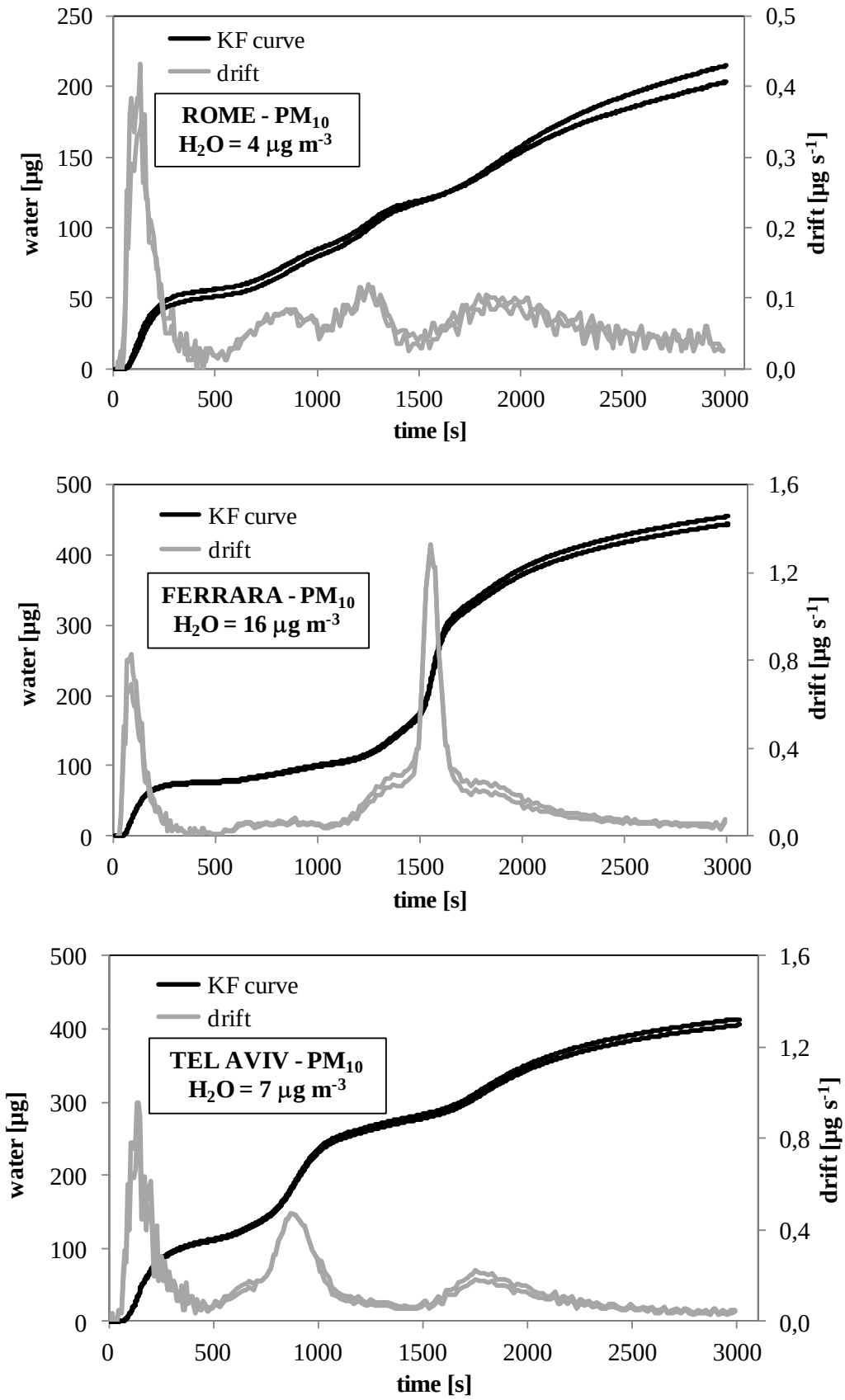

Fig.2.13: Examples of the Karl-Fisher curves of PM_{10} paired samples collected side-by-side at the three sites.

The KF profiles of the two elements of each pair are alike; the three examples, however, show very different profiles. The first water contribution, in the range 0-500 s, is due to weakly adsorbed moisture and is contained in all samples; the amounts are in the range 50-150 µg. From 500s on, the profiles become characteristics of the sampling site, with small inter-day variations. The release of water from the samples collected in Rome occurs in many steps, during the whole analytical run. The samples collected in Ferrara show a sharp signal at about 1500s, superimposed to a broader signal in the interval 1000-2000s. Tel Aviv samples show, instead, two well-defined contributions, in the range 700-1100s and after 1500s.

Since these differences are very probably due to a different chemical composition of PM at the three sites, we carried out some exploratory qualitative analyses of some hydrophilic components of PM, such as inorganic compounds, dicarboxylic acids, sugars, biological materials. We also analyzed soot, sand and road dust samples. Some of these (alumina, silica, molecular sieves and ammonium salts) have been already discussed in the sections 2.4.3 and 2.4.4.

Carbohydrates and dicarboxylic acids (figure 2.14 upper and lower panels) present a simple water profile with a relevant water contribution in the range 1500-2500 s, corresponding to temperatures greater than 200°C, due to the crystallization water, besides to the first contribution in the range 0-500 that is present in every compounds and is due to the humidity adsorbed on the solid powder. This is the case of tartaric acid, succinic acid, citric acid, saccarose and glucose. Only the oxalic acid show a single contribution in the range 0-500s much higher than the other compounds. Conversely more complex is the water profile of the biological materials (figure 2.14 middle panel) and soot, road dust and Saharan sand, which show more contributions at different times and characterized by different shapes. This is due to their complex structure in which water is retained with different strengths.

Water profiles obtained in the PM_{10} samples have been then compared with the profiles of the hydrophilic compounds. The most interesting results are reported in fig 2.15. The profiles of soot (sampled inside the exhaust silencer of a diesel car) and of road dust (sampled at the kerbside of a high-density traffic road) were very similar to the profile of PM_{10} sampled in Rome, in agreement with the relevance of the primary traffic emission and the crustal component associated with the traffic resuspension, which represent approx. 50% of the PM composition in this area (Canepari et al., 2009; Perrino et al., 2009) (fig.2.15 upper panels). Water contained in secondary salts and in some carbohydrates and dicarboxylic acids is detected mainly in the range 1000 – 2000 s. It is likely

that the curve obtained by analyzing the samples collected in Ferrara is due to water associated to these compounds.

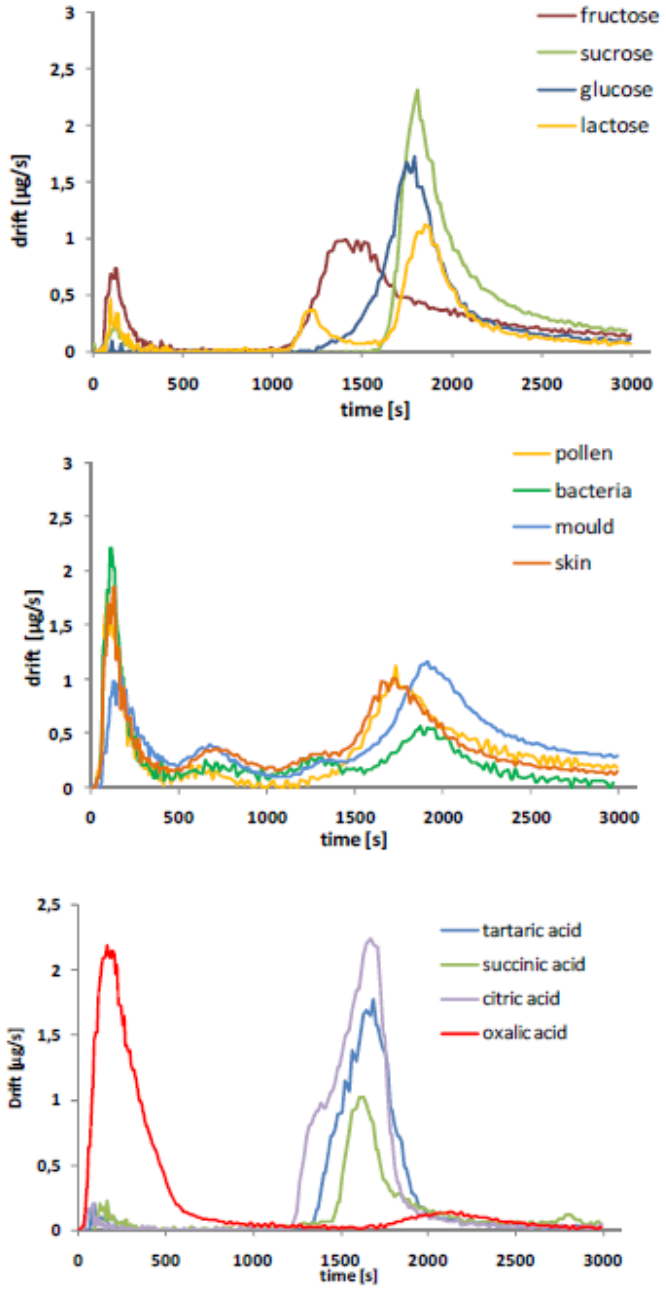

Fig 2.14: Qualitative KF drift profiles of some sugars (upper panel), biological materials (middle panel) and dicarboxylic acids (lower panel).

In the area of Ferrara, in fact, particularly during the winter, the formation of organic and inorganic secondary species is favored by the occurrence of frequent and long-lasting atmospheric stability conditions (Matta et al., 2003), contributing to more than 70% of PM composition (fig.2.15, middle panels).

Saharan dust (collected at Erfoud, Morocco) in agreement with its composition, shows a profile close to those of SiO_2 and Al_2O_3, with a sharp contribution between 700 and 1100 s.

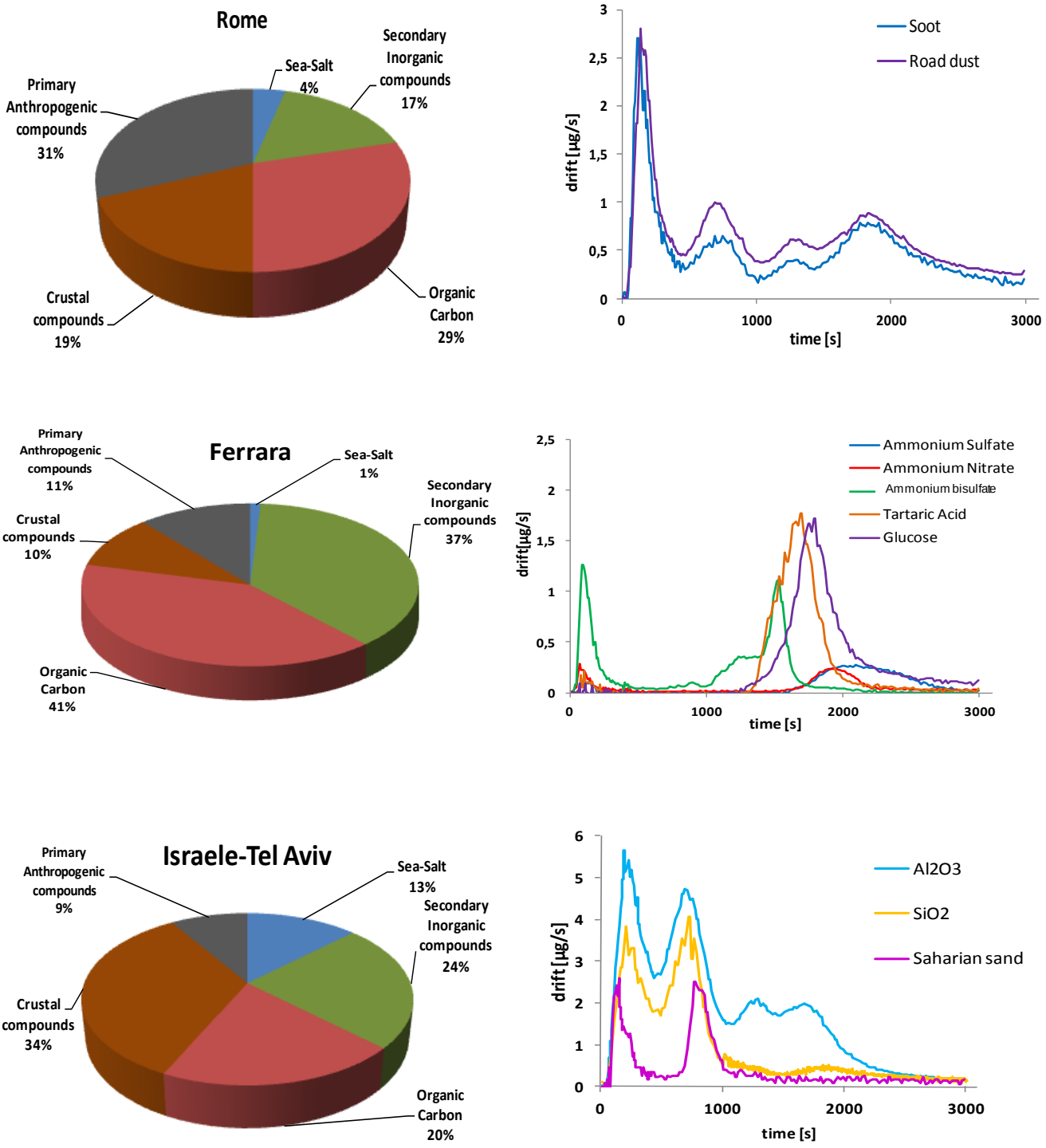

Fig.2.15: Left panels: average PM_{10} composition in the three sampling sites. Right panels: drift profiles of some single hydrophilic components of PM.

This contribution is very similar to one of the contributions detected in the filters collected in Tel Aviv, where the dust intrusions from the nearby desert are very frequent (Ganor, 1994) and the crustal component represents more than 30% of the PM composition (fig.2.15 lower panels). It is worth noting that the last contribution in these filters resembles the road dust and soot profile, as expected for an urban site.

2.5 Conclusions

The described method, employing a coulometric Karl Fisher systems, allows the direct water determination in atmospheric particulate matter. The optimization and validation show good analytical performance, reaching very low LODs and LOQs values, allowing then to measure with a good reliability the concentrations present in the PM samples. Also this method does not require any filter pre-treatment and is suitable to the application in routine field studies. The preliminary application to a series of PM_{10} samples collected in different geographical areas, showed that the water content of PM samples is variable and can reach values over 20 $\mu g\ m^{-3}$. Such an amount of water constitutes a relevant fraction of the total mass of PM and may seriously affect the exceedance of the regulatory concentration limit values. Finally, the use of a thermal ramp for the desorption allows the separation of different water contributions that are bound to atmospheric particles with different strength. The profile of the curve resulted to be characteristic of the sampling site suggesting that the amount and variety of water is likely linked to the chemical characteristics of the dust.

2.6 References

Almeida S M, Pio C A, Freitas M C, Reis M A, Trancoso M A (2006), Science of the Total Environment, 368:663–674.

Ansari A and Pandis S N (1999), Atmospheric Environment, 31:745-757.

Ansari A S and Pandis S N (2000), Environmental Science and Technology, 34:71-77.

Baek B H, Aneja V P, Tong Q, (2004), Environmental Pollution, 129:89–98.

Balasubramanian R, Qian W B, Decesari S, Facchini M C, Fuzzi S (2003), Journal of. Geophysical Research, 108:4523-4539.

Canepari S, Farao C, Marconi E, Giovannelli C, Perrino C (2013), Atmospheric Chemistry and Physic, 13: 1193–1202.

Chow J C, Watson J G, Lowenthal D H (2005), Journal of Air & Waste Management Association, 55, 1158–1168.

Chow J C, Yu J Z, Watson J G, Hang Ho S S, Bohannan T L, Hays M D, Fung K K (2007), Journal of Environmental Science and Health., Part A, 42:1521–1541.

Dassios K G and Pandis S N, (1999), Atmospheric Environment, 33:2993-3003.

Decesari S, Facchini M C, Matta E, Lettini F, Mircea M, Fuzzi S, Tagliavini E, Putaud J P (2001), Atmospheric Environment, 35:3691-3699.

Dick W D, Saxena P, McMurry P H (2002), Journal of Geophysical Research, 105:1471–1479.

EN 14902:2005 Ambient air quality—standard method for the measurement of Pb, Cd, As and Ni in the PM10 fraction of suspended particulate matter, 2005.

EN12341 (1998): Air Quality. Determination of the PM10 fraction of suspended particulate matter – Reference method and field test procedure to demonstrate reference equivalence of measurement methods. Brussels.

EPA Method 9000 (2007): Determination of water in waste materials by Karl Fischer titration.

Fisher K (1935), Chemistry 48 (26):394-396.

Ganor E (1994) , Atmospheric Environment, 28: 2867-2871.

Gysel M, Crosier J, Topping D O, Whitehead J D, Bower K N, Cubison M J, Williams P I, Flynn M J, McFiggans G B, Coe H, (2007), Atmospheric Chemistry and Physic, 7:6131-6144.

Hanel G, (1976), Advances in Geophysics, 19:73-188.

Hu D, Chen J, Ye X, Li L, Yang X, (2011), Atmospheric Environment, 45:2349-2355.

Khlystov A, Lin M, Bolch M A, Ma Y (2009), Atmospheric Environment, 43:364–370.

Kitamori Y, Mochida M, Kawamura K. (2009), Atmospheric Environment, 43:3416-3423.

Kreidenweis S M, Remer L A, Bruintjes R, Dubovik O (2001), Journal of Geophysical Research, 106, 4831–4844.

Levart A and Veber M (2001), Chemosphere, 44: 701-708.

Lutgens F K and Tarbuck E J, (2004) The Atmosphere: An Introduction to Meteorology, Prentice Hall, Upper Saddle River, New Jersey.

Matta E, Facchini M C, Decesari S, Mircea M, Cavalli F, Fuzzi S, Putaud, J P, Dell'Acqua A, (2003), Atmospheric Chemistry and Physic, 3:623–637.

Matuschek G, Saritas Y, Karg E, Schroeppel A, (2004), Journal of Thermal Analysis and Calorimetry,78:575- 586.

Moreira dos Santos C Y, de Almeida Azevedo D, Radler de Aquino Neto F (2002), Atmospheric Environment, 36:3009-3019.

Ohta S, Hori M, Yamagata S, Murao N (1998), Atmospheric Environment, 32:1021–1025.

Pathak R K., Wu W S, Wang T (1985), Journal of Analytical and Applied Pyrolysis, 8:41-48.

Perrino C, Canepari S, Cardarelli E, Catrambone M, Sargolini T (2007), Environmental Monitoring Assessment, 128:133–15.

Perrino C, Canepari S, Catrambone M, Dalla Torre S, Rantica E, Sargolini T, (2009), Atmospehric Environment, 43:4766–4779.

Perrino C, Marconi E, Tofful L, Farao C, Materazzi S, Canepari S (2012), Atmospheric Environment, 54: 36-43.

Perrone M G, Larsen B R, Ferrero L, Sangiorgi G, De Gennaro G, Udisti R, Zangrando R, Gambaro A, Bolzacchini E (2012), Science of the Total Environment, 414:343–355.

Pilinis C, Pandis S N, Seinfeld J H (1995), Journal of Geophysiacal Research, 100:18739–18754.

Rees S L, Robinson A L, Khlystov A, Stanier C O, Pandis S N (2004), Atmospheric Environment, 38:3305-331.

Sasaki K and Sakamoto K (2006), Water Air and Soil Pollution, 171:29–47.

Schnelle-Kreis J, Sklorz M, Peters A, Cyrys J, Zimmermann R (2005), Atmospheric Environment, 39:7702–7714.

Schnelle-Kreis J, Sklorz M, Orasche J, Stolzel M, Peters A, Zimmermann R (2007), Environmental Science and Technology 4:3821-3828.

Sloane C S and Wolfe G T (1997), Aerosol Science and Technology, 27:50–67.

Speer R E, Edney E O, Kleindienst T E (2003), Journal of Aerosol Science, 34:63–77.

Squizzato S, Masiol M, Brunelli A, Pistollato S, Tarabotti E, Rampazzo G, Pavoni B, (2012), Atmospheric Chemistry and Physic Discussion, 12:16377–16406.

Stanier C, Khlystov A, Chan W R, Mandiro M, Pandis S N (2004), Aerosol Science and Technology, 38:215-228.

Swietlicki E, Zhou J, Berg O H, Martinsson B G, Frank G, Cederfelt S, Dusek U, Berner A, Birmili W, Wiedensohler A, Yuskiewicz B, Bower K N (1999), Atmospheric Research, 50:205-240.

Tsai Y I and Kuo S C (2005), Atmospheric Environment, 39:4827-4839.

Tsyro S. G (2001), Atmospheric Chemistry and Physic, 5:515–532.

Vecchi R, Valli G, Fermo P, D'Alessandro A, Piazzalunga A, Bernardoni V (2009), Atmospheric Environment, 43:1713–1720.

Yang S and Cotton W R (1996), American Metereorological Society, 35:2261-2269.

Yuc X Y, Lee T, Ayres B, Kreidenweis S M, Malm W, Collett Jr J L (2006), Atmospheric Environment, 40:4797–4807.

Chapter 3- Water contribution to particulate matter mass closure

In this section the Karl-Fisher method has been applied to atmospheric particulate matter sampled in different geographic areas characterized by different environmental conditions, in order to highlight its contribution on the PM mass reconstruction by chemical analysis.

3.1 Mass closure and macro-sources calculation

As mentioned in the previous paragraphs water sampled together with the atmospheric particles can largely affect the reconstruction of the PM mass.

Mass closure is the correspondence between the mass concentration of PM and the sum of the single chemical analyses. It is based on the simple chemical analyses of the PM macro-components which can be then grouped into five main PM macro-sources: crustal matter, marine aerosol, secondary inorganic compounds, combustion products (vehicular emissions) and organics (Perrino et al., 2013a). Micro- components (such as trace elements), because of their low abundance in the PM, are generally considered negligible in the mass balance calculation. Afterwords, the algorithms used to calculate these macro-sources are reported:

- ***crustal matter*** contribution is calculated by adding the concentration of elements generally associated with mineral dust (Al, Si, Fe and the insoluble fractions of Na, K, Mg and Ca, calculated as the difference between the XRF and the Ion Chromatography determinations) and carbonate, calculated from calcium and magnesium determined by Ion Chromatography. A correction factor for oxygen had to be applied for the macro-elements in order to consider them as metal oxides (Chan et al., 1997; Marcazzan et al., 2001).

$$\textbf{Crustal matter} = 1.89\ Al + 2.14\ Si + 1.42\ Fe + 1.35\ Na_{insoluble} + 1.2\ K_{insoluble} + 1.67\ Mg_{insoluble} + 1.4\ Ca_{insoluble} + CO_3^{2-} \quad (1)$$

$$CO_3^{2-} = 2.5\ Mg^{2+} + 1.5\ Ca^{2+} \quad (2)$$

- ***Marine aerosol*** contribution is calculated from the sum of the concentrations of soluble sodium and chloride, determined by Ion Chromatography, multiplied by 1.176 in order to take into account of minor sea water components (sulphate, magnesium, calcium, potassium).

- ***Secondary inorganic components*** are calculated by adding the non-sea-salt sulphate, nitrate and ammonium concentrations.

- ***Combustion products*** (Vehicular emission) are calculated by adding elemental carbon to the same amount multiplied by 1.1 (primary organic carbon), in order to take into account organic species that condense from the exhaust gases and coat the surface of elemental carbon particles (Castro et al., 1999).

  Combustion products = EC+ 1.1 EC (3)

- ***Organics*** are calculated by multiplying the non-primary organic carbon by a factor α taking into account the atoms other than C present in the organic molecules.. It includes primary OC coming from biomass combustion and biogenic aerosol and secondary organic compounds. α can be assume values from set to 1.6 for urban sites to 2.2 for rural, as suggested in Turpin and Lim (2001) and Viidanoja *et al.* (2002)

  Organics= α OC – (1.1 EC) (4)

It must take into account that the empiric factor α used to convert the OC in Organic Matter (αOC) is influenced by the spatial and temporal variability of the C-contain compounds' concentrations. Therefore it represents one of the main source of uncertainty in the reconstruction of the PM mass. However this problem is inherent to the particle nature and then difficult to solve. For this reason it needs to reduce any other error source that may affect the mass closure calculation.

The determination of the ionic species is not particularly difficult and it is carried out on a routinely basis. The ion chromatography is the analytical method, since it is simple and economic and able to determine all the anions and cations required by the Italian D.lgs 155/2010 described in first chapter (paragraph 1.7).

Much more complex is the determination of EC and OC deposited on the filters. The most used method for the determination of the carbonaceous material is the thermo-optical analysis, implemented by the instrumentation developed and produced by Sunset Laboratory, which is currently the most widely used in Europe (Birch and Cary, 1996). The aerosol sampled on a quartz filter is subjected to two successive stages of analysis. During the first stage the filter is heated under an inert atmosphere (helium), between 550 and 900° C, to release the organic compounds. A

part of it, however, undergoes a process of pyrolysis. In the second stage, the furnace is cooled and then heated again in an oxidizing atmosphere (in the carrier gas is added to 5-10% oxygen) up to 800-900° C. In this phase are released from the filter elemental carbon and pyrolytic carbon (PyC) produced in the previous step. All species released from the filter during the two stages of analysis are in contact with an oxidizing agent (manganese dioxide) and oxidized to CO_2, which is subsequently reduced to methane, the CH_4 concentration is then determined by a flame ionization detector. For a correct determination of the pyrolitic carbon, a laser, which continuously determines the reflectance or transmittance of the filter portion subjected to analysis, is used. The transmittance or reflectance of the filter varies depending on the pyrolitic carbon formation. The determination of the amount of EC which is necessary to bring the transmittance or the reflectance to an initial value makes possible the correction. However, it should be noted that the results of thermo-optical analysis are subject to various uncertainties. The main problems that occur in discriminating OC and EC are due to the pyrolytic carbon evaluation and to the identification of an optimal thermal protocol (times and temperatures of the different steps of heating) (Bae et al., 2009).

The reconstruction of the PM mass by chemical analysis is not always complete, mainly due to the large number of sources, the high spatial variability of the contributions and the occurrence of particular weather conditions. Despite of the analytical techniques used are highly sensitive, not always the sum of the obtained values matches the total mass obtained by gravimetry. For example, during periods characterized by high atmospheric stability, a significant increase in the concentration of PM secondary, especially ammonium nitrate is registered (Vecchi et al., 2004; Perrino et al., 2008). At the same time an increase in the mass of PM considered "unknown" is observed. In circumstances of PM_{10} concentrations around 100 $\mu g\ m^{-3}$, the percentage of ammonium nitrate can grow up to 30-35% of the total mass, while the unknown fraction can reach value up to 20%.

A study conducted by our research group showing the mass balance closure performed on samples collected at three different geographical areas is reported as example (Perrino et al., 2013b), (figure 3.1). The graphs show a clear discrepancy between the sum of the chemical analysis and the mass determination at Montelibretti site, while at the other two cases there is a good agreement between the obtained results. In particular, at the peri-urban site the reconstructed mass by chemical analysis is 20% lower than the gravimetric measurement. This occurs between 20 and 30 June 2006 when a transport event of Saharan sand has been registered in central Italy.

Therefore two particular meteorological situations that fail the mass closure can occur: long periods of high atmospheric stability and transport of desert sand. In the first case the PM appears rich in

secondary components, while in the second it is rich in crustal species such as sand. The common feature of these two class of compounds is their hygroscopicity, suggesting that the water bound or adsorbed on the PM particles plays a very important role.

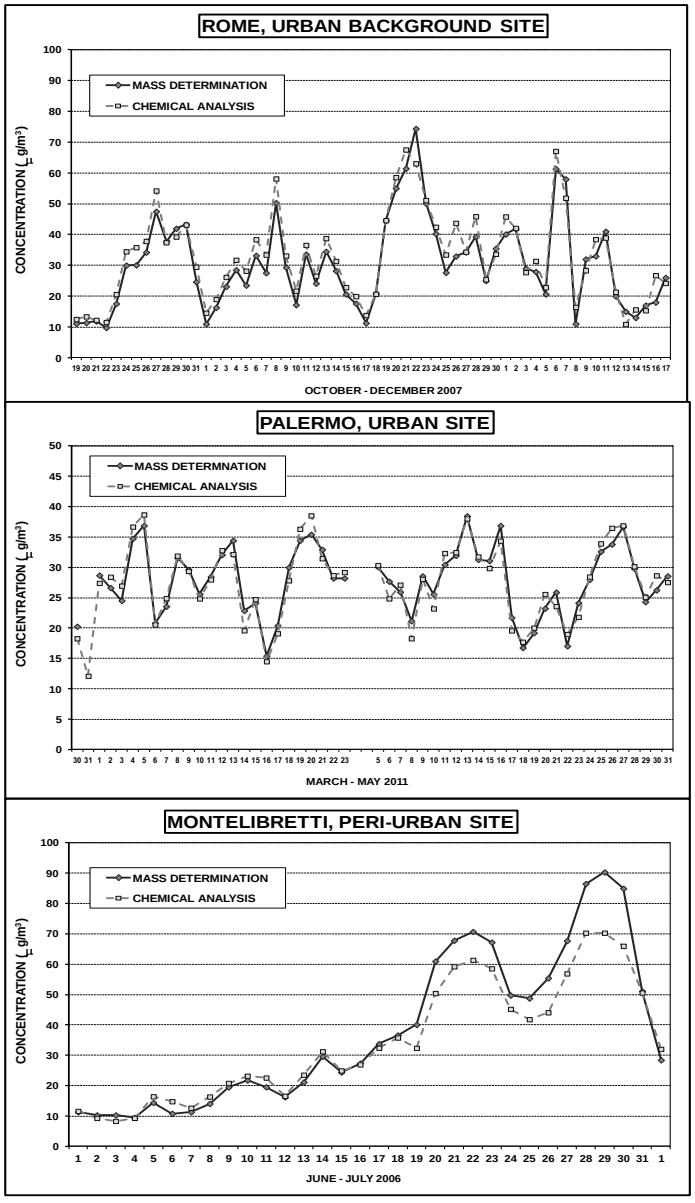

Fig. 3.1: mass balance comparison among PM_{10} samples collected in three different sites: Rome (urban background site), Palermo (urban site), Montelibretti (peri-urban site).

It is interesting also to note that the above described phenomenon is not as noticeable when investigations are carried out on quartz fiber filters. The different behavior of quartz and Teflon can be explained by their different ability to interact with atmospheric moisture. In fact, the hydrophilic

nature of the quartz facilitates the transfer of water molecules from the PM to the filter, from which they can evaporate during the sampling phase (Perrino et al., 2013b).

3.2 Aim of the work

The strength of this work lies in the development of a valid method that ensures high reliability in the PM mass reconstruction. As already discussed in the introduction of this work, one of the reason of the mass reconstruction failure is the uncertainty of the empirical factor used to multiply the OC content in the calculation of the Organics macro-source. Unfortunately, this problem strongly depends on the high variability of the matrix and thus difficult to solve. Moreover, the greater discrepancies between the mass concentration and the sum of the chemical analysis are observed in samples collected in areas characterized by special climatic conditions, e.g. the Po Valley, where the relative humidity is consistently higher than in other regions, or areas in which transport events of sand from the nearby desert occur. To achieve a complete mass closure is then necessary to minimize the uncertainty of each component's measurement, through an analytical quality control of the data, and verify the nature of the "unknown" component. The explained considerations gave rise to the idea that it was useful to integrate the water contribution in the chemical analysis used in the PM mass reconstruction. Therefore, after the optimization and the validation widely discussed in Chapter 2, the KF method was applied to measure water content in atmospheric PM samples collected in geographical areas, characterized by different meteorological situations. The results of these investigations have fully satisfied our assumptions, as it can be seen from the next reported results.

3.3 Experimental

3.3.1 PM sampling

PM_{10} samples used in this phase of the work were collected at three different sites:

- the peri-urban site of Montelibretti, about 25 km from Rome, Italy, during the period April 3-6, 2012
- the residential site of Cassana, close to the city of Ferrara in the Po Valley, during the period January-February 2012. This area is particularly problematic for the atmospheric

monitoring, because of it is characterized by climatic and weather conditions that often lead to the intensive foggy phenomena favoring the accumulation of the secondary species.

- at a residential area of La Spezia, near to a school and to the sea, during the period July 2012.

PM_{10} has been collected by means of an automatic system for simultaneous sampling on two different channels (HYDRA Dual Samplers, FAI-Instruments, Fonte Nuova, Rome, Italy). The instrument was configured with a single head of PM_{10} for each channel, in accordance with the standard EN 12341, operating at a flow rate of 2.3 m^3h^{-1} for 24 hours. Two teflon membranes were employed (47 mm in diameter, 1 µm porosity, Pall Co., MI-USA), one of which was used for the analysis of the inorganic macro components by X-ray fluorescence and ion chromatography, and the other has been employed for the water analysis. A third quartz filter (47 mm in diameter, Pallflex) was employed to collect PM_{10}, aimed to the analysis of the elemental and organic carbon by thermo-optical technique. Quartz filters were heated at 400°C for 8 hours before the sampling in order to remove the organic impurities. Teflon filters were conditioned for 48 hours in a controlled atmosphere at 50 ± 5% RH and 20± 1°C (CE 1998). This conditioning has been carried before and after the sampling phase. PM mass concentration has been gravimetrically determined by means of an analytical balance (0.001µg sensitivity) placed in the same environment used for conditioning. In addition size-segregated samples were collected at by means of a 10-stage MOUDI cascade impactors (mod. 110, MSP Co., MN-USA) at Cassana (Ferrara) site.

3.3.2 Chemical analysis

To carry out the PM mass closure the main PM components have to be chemically determined. In this work water analysis and trace elements analysis have been performed in our laboratory, while the other chemical analysis (macro elements, ions, EC and OC) were performed at the Atmospheric Pollution Institute of CNR (Montelibretti, Rome).

The simultaneous sampling of PM on teflon and quartz filters allowed the chemical determination of several components. Quartz filter were analyzed for their elemental carbon and organic carbon content (EC/OC) by means of a thermo-optical analyzer (OCEC Carbon Aerosol Analyzer, Sunset Laboratory, OR-U.S.A.), by following the procedure described in the 3.2 paragraph. Teflon filters were analyzed by following the procedure reported in figure 3.2. This analytical procedure has been previously optimized and validated in our laboratory by evaluating the recovery percentages and the

repeatability on both certified material (NIST1648) and real samples (Canepari et al., 2006 a,b; Canepari et al., 2009).

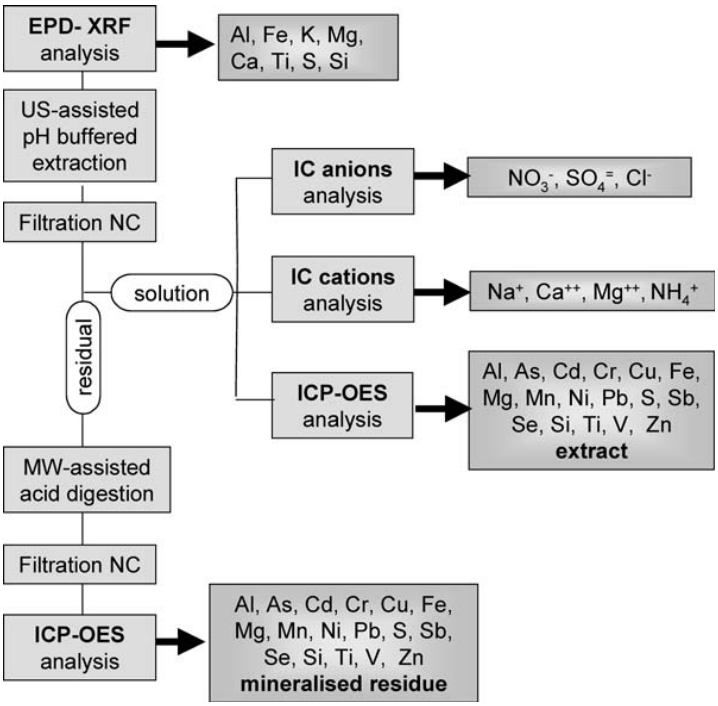

Fig.3.2: Sequence of the chemical analysis performed on Teflon filters.

Briefly, macro-elements Al, Fe, K, Mg, Ca, Ti, S and Si were analyzed by energy-dispersive X-Ray fluorescence (EPD-XRF, X-Lab 2000, SPECTRO). Then each filter was extracted in an acetate buffer solution using an ultrasonic bath. The solution was divided in two aliquots, one analyzed for anions (Cl^-, NO_3^-, SO_4^{2-}) and cations (Na^+, NH_4^+, Mg^{2+}, Ca^{2+}) using Ion Chromatography (DX 100, DIONEX Co., CA-USA) and the other analyzed for the extractable fraction of the elements (Al, As, Cd, Cu, Fe, Mg, Mn, Ni, Pb, Sb, S, Si, Ti, V, Zn) using inductively coupled plasma with optical (ICP-OES) and mass spectrometer detection (ICP-MS) (Bruker 820, equipped with a reaction cell, CRI, and a 400 µl min^{-1} MicroMist nebulizer). The choice of the extracting solution was driven by the intention to increase the selectivity of elements as PM source tracers but also to estimate the environmental mobility and bio-accessible fraction of toxic elements (Canepari et al. 2010).

The residual teflon filter was digested in a mix of HNO_3 and H_2O_2 (2:1) using a microwave oven (Milestone Ethos Touch Control with HPR 1000/6S rotor) and the mineralized fraction was then analyzed by ICP-OES and ICP-MS for its insoluble elemental content. The use of both ICP-OES and ICP-MS allowed the analysis of a larger number of elements. According to the results of the

previous studies, we quantified Fe, Cu, Mn and S by ICP-OES and the others elements with ICP-MS.

Matrix-matched standard solutions were used for calibration; Y was used as internal standard; the collision reaction interface (CRI) was activated for As, Se, Fe and V determination.

This overall procedure allows the determination of macro-elements (including Al and Si, which show a low recovery after the acid digestion), soluble inorganic ions and the extracted and residual fractions of micro- and trace- elements on individual 24-h filters; furthermore the determination of the same element with different analytical techniques (e.g. Fe, Mg, S) makes it possible to check the quality control of the determinations by means of an inter-techinique comparison(Canepari et al. 2009b).

3.3.3 Data quality control

As previously discussed, the PM mass balance relies of some algorithms and the uncertainty related to each of them has an impact on the uncertainty of the final result. Moreover, very often PM sample is unique and the quality of the data obtained cannot be compared with the certificate materials , as the latter have different characteristics compared to real samples (Canepari et al., 2006 a).

The initial stage of reconstruction of the PM mass consists of an X-ray fluorescence (XRF) analysis to determine the total content of Al, Ca, Mg, Fe, K, Mn, Si, S, Ti, as shown schematically in figure 3.2. This technique is highly accurate, non-destructive and provides good quantitative data, but the instrument calibration is not easy. The instrument is provided with a factory calibration performed on pure salts. Indeed, the elements present in the PM are in a chemical form different from that of the pure salts thus their response will necessarily be different. It is necessary to validate a method to guarantee the data quality based on an external calibration of the instrument. The samples are initially read with the XRF and then analyzed by ICP-OES. The data obtained from the latter analysis are used for the XRF calibration. As regards the ICP-OES analysis, to ensure the complete solubility of each element (especially Al, Si, and Ti, which form very stable compounds)the samples are mineralized in a mixture of HNO_3 and HF according to the procedure described by Betinelli et al. (2000). The correlation between XRF and ICP-OES data is expressed by the linear equation XRF = a * ICP + b (the intercept is generally equal to 0) and a slope different from 1 is due to calibration errors. The observation of this correlation is useful to correct the XRF calibration.

A further confirmation of the quality of the analytical results, is given by a procedure previously developed in our laboratory. This procedure is based on a inter-technique comparison by using the same parameters determined by different analytical techniques. This allows the quality control of each sample and to check the method step by step, from the sampling to the analysis, identifying the weak points, giving the sources of uncertainty. The inter-technique comparison is able to correlate the individual contributions of the measurement uncertainty to the analytical technique used for the determination (XRF, IC anions, cations IC, ICP-OES) or to the operating phases of the sample preparation (ultrasonic extraction, filtration, dilutions, acid digestion) (Williams et al., 2000). The instrumental error, coming from the calibration, the instrumental drift and systems to introduce the samples, can be easily controlled by using the internal standards and the control charts.

Once identified the species determined by at least two technique is therefore possible to employ them as analyte-tracers for tracking the introduction of operating errors. The data obtained from the two techniques are then subjected to a linear regression. The goodness of the analytical data can be appreciated if the Pearson coefficient is greater than 0.9, the slope value is next to the unit and intercepts close to 0. The analytical quality control of the data is a long and laborious procedure but absolutely necessary to obtain correct results, especially with complex matrices such as particulate matter.

3.4 Results obtained on PM_{10} samples collected at Montelibretti

Part of this work focused on the characterization of the air composition with relative mass balance closure at the peri-urban area of Montelibretti, between April 3rd and 6th 2012. This area is generally characterized by a moderate air quality, but sporadically, some anomalies can be recorded that lead to PM concentrations exceeding the standard limits. In this particular case these anomalies have been highlighted through the water analysis, as shown in Figure 3.3. The water profiles are characterized by discrete inter-day variability. Particularly, the graph related to April 5th shows a very pronounced peak in the range 500-1200s, circled in red. Table 3.1 summarizes the results of the Karl-Fisher analysis compared to the mass concentration of PM_{10} measured at Montelibretti and at Corso Francia, a traffic station in Rome.

On April 5th PM mass concentrations was particularly high and exceeding the standard limit of 50 μg $m^{-3.}$ Moreover, the mass concentrations at the two sites were approximately equal, while in the other days it was higher at Corso Francia, in agreement with the greater contribution from vehicular traffic. This information was then integrated with those provided by the PM composition, which on

April 5th presents some differences compared to the average values (figure 3.4). On that date, in fact, there was a significant increase in the crustal fraction, which exceeded 50% of the total mass. A similar situation could not be due to the analytical errors, and led to the association of these trends with an increase of the sand component in the particulate, probably coming from the Sahara desert. These episodes are not unusual along the area of Montelibretti and are also often recorded in Sicily and in Israel, due to their geographical position. The deserts of Algeria, Morocco, Libya and Tunisia are, in fact, responsible for the annual transport of approx. 80-120 million tons of sand in Europe. Because of the intense convective activity of the atmosphere characterizing this area, the sand can be easily rise up to the high troposphere, where it can travel very long distances (Gobbi et al., 2007).

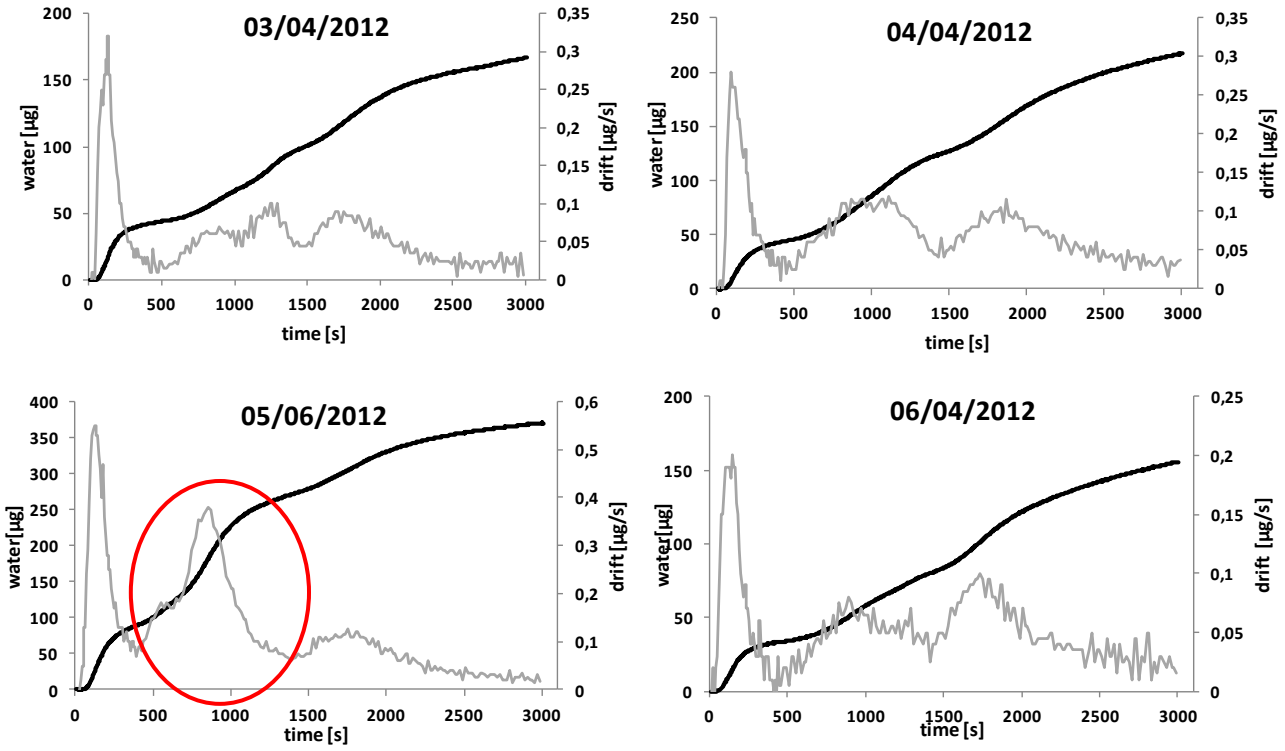

Fig. 3.3: KF curve and drift of PM_{10} samples collected at Montelibretti during the period 3-6 April 2012.

Tab.3.1: Water analysis results and PM_{10} mass concentration at Montelibretti and Corso Francia.

Date	Conc. (µg m^{-3}) Montelibretti	Conc. (µg m^{-3}) Corso Francia	H_2O tot (µg)	H_2O (µg m^{-3})
03/04/2012	25	38	166	3
04/04/2012	42	47	217	4
05/04/2012	**65**	**60**	**370**	**7**
06/04/2012	26	33	155	3

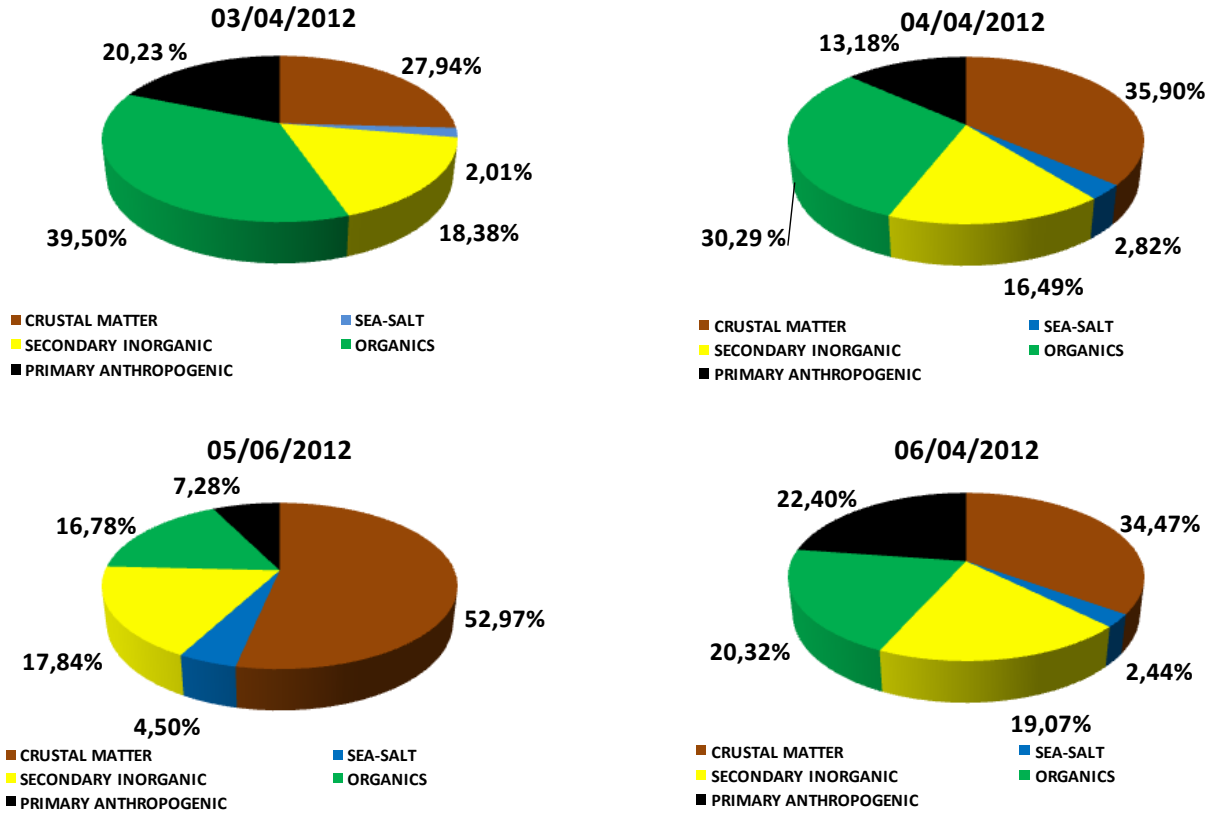

Fig. 3.4: daily PM_{10} chemical composition.

The current PM legislation (D.lgs 155/2010), however, allows to deduct the pollution events due to natural origin if the real nature of these kind of episodes is proved.

One of the most used tools to prove this kind of events is the meteorological model (HYSPLIT), that allows to reconstruct the origin of the air masses by means of the back trajectories. Figure 3.5 shows how effectively the air masses arrived at Montelibretti on April 5th originated from North Africa (green line).

Furthermore, figure 3.6 shows the comparison between water analysis on April 5th and water profile obtained by analyzing silica, alumina and Saharan sand. The profiles are very similar and show the same contribution of water between 500 and 1200s. This result provides a further confirmation of the advection of desert sand at the sampling site and clearly indicates that the KF curve profile is highly correlated to the chemical composition of the sample, thus providing a useful support to the study of the transport events.

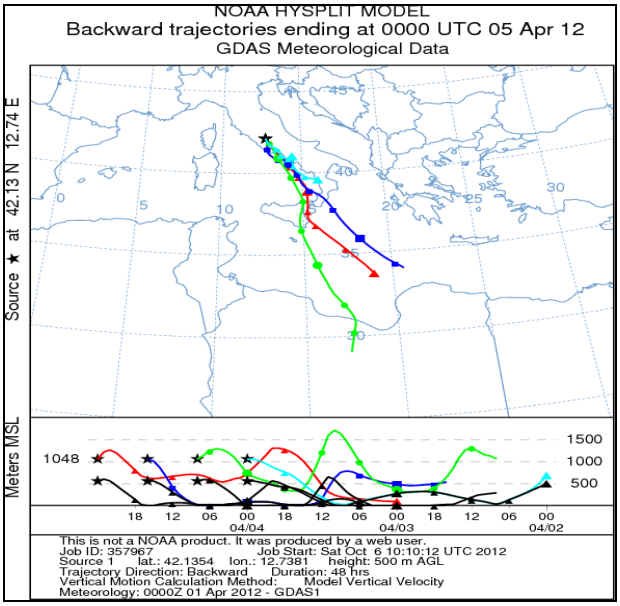

Fig 3.5:Air mass back-trajectories related to the Saharan event. (www.arl.noaa.gov/HYSPLIT.php).

The presence of a net peak in the alumina, silica and sand is justified by their hygroscopic nature. At higher temperatures some differences can be observed, due to the presence of water bonded to the particles with greater strength.

Figure 3.7 shows the mass balance closure and the PM macro sources calculated on Montelibrettis' samples.

The difference between the PM concentration measured by gravimetry and the calculated one on the basis of chemical analysis is emphasized on April 5th in which the "unknown" fraction is 6.7 µg m^{-3} compared to the average 3.4 µg m^{-3}.

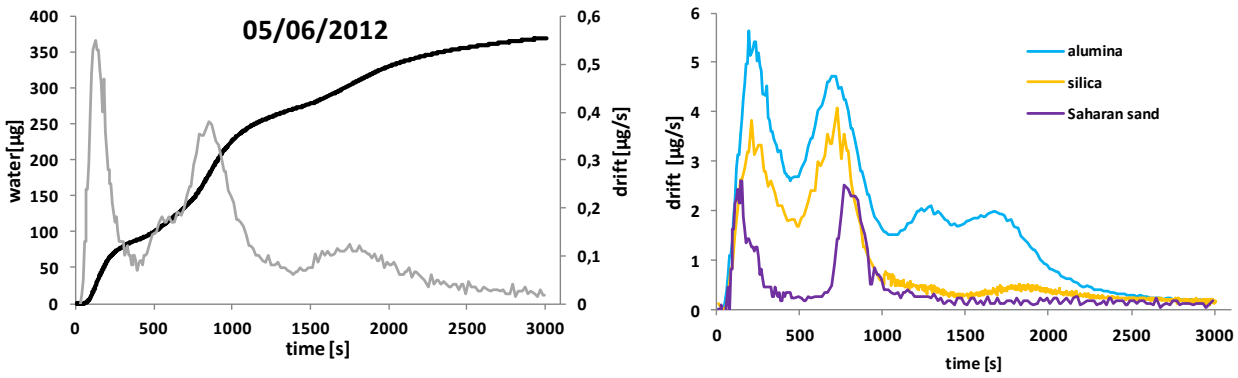

Fig. 3.6: Comparison between water analysis of April 5th and water profile obtained on silica, alumina and saharan sand.

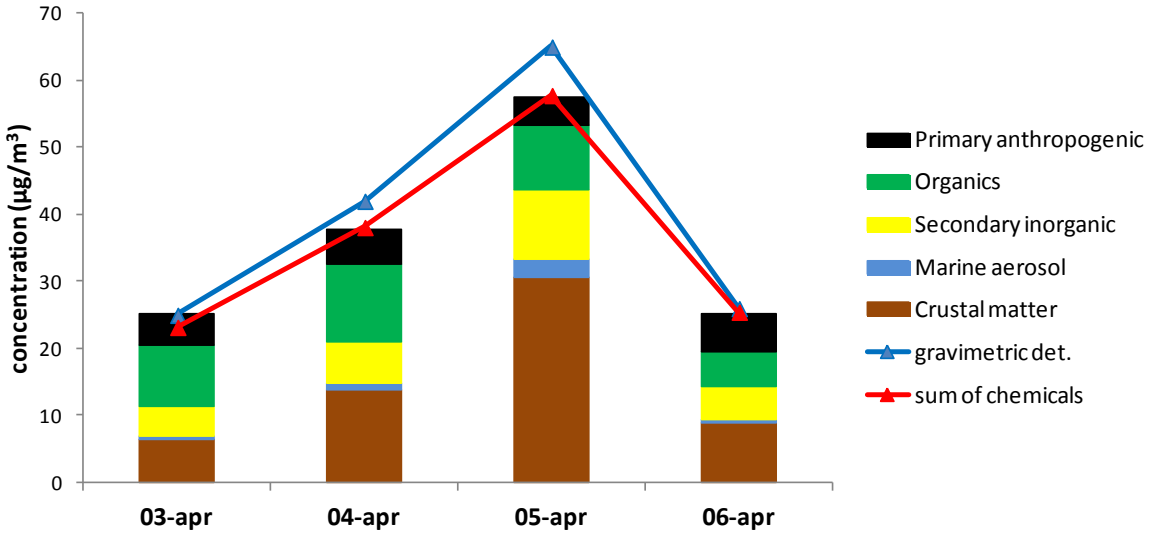

Fig.3.7: Differences between the PM mass concentration measured by gravimetric and the sum of the chemical analysis at Montelibretti.

By adding the water contribution it was possible to fill this gap and therefore to complete the mass closure, as shown in figure 3.8.

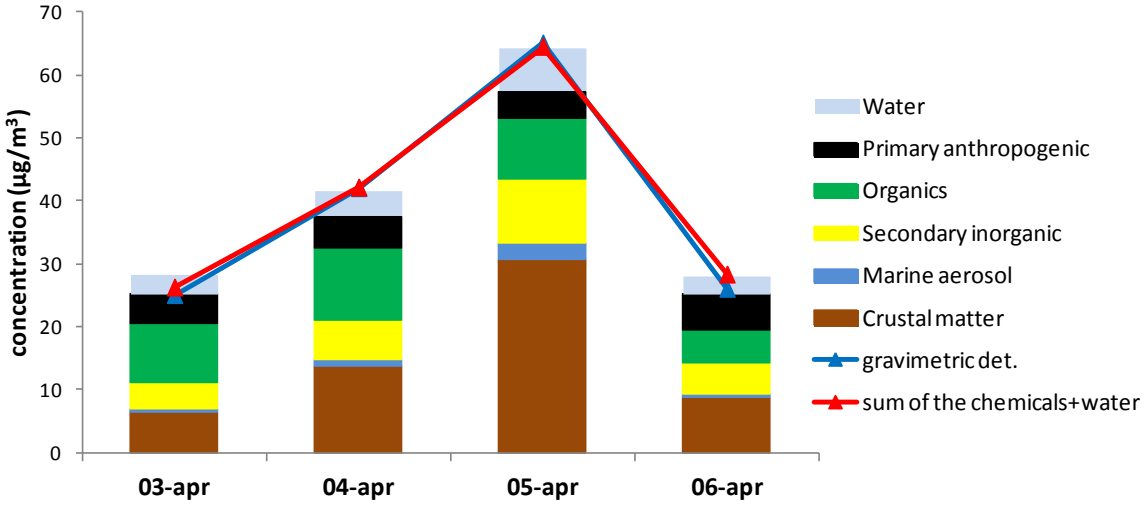

Fig.3.8: PM mass balance obtained by adding the water contribution to the chemical analysis at Montelibretti.

This graph clearly shows that it was possible to reconstruct almost the totality of the mass, indicating that each stage of the procedure has been carried out in an optimal manner, providing thus a really negligible uncertainty. As mentioned several times, the uncertainty associated with the empirical factor used to multiply the OC is considered a major source of error. Its significant variability is attributed to a very heterogeneous composition of the organic fraction as a function of the location where sampling is carried out. In this specific case it is appropriate to note that the organic fraction accounts for a small contribution , and therefore, any error in the measurement of this conversion factor would be irrelevant to the final error. The crustal matter, however, appears to be the predominant source, since the sand transport events lead to an increase of Si and Al terrigenous-rich substances.

3.5 Results obtained on PM_{10} samples collected at Ferrara

The Po Valley is an extensive geographical area characterized by particular climatic conditions, such as poor mixing of the air and poor ventilation which lead to the accumulation of the atmospheric pollutants. This situation get worse by the persistence of a high relative humidity which acts as a promoter of the condensation and, therefore, the retention of the pollutants. This is due to its geomorphological structure, as it is situated among high mountains opened only on the eastern side, which partially obstruct the winds and favor the accumulation of high humidity in the

air. Furthermore this region is highly populated and industrialized and Ferrara is the major area of industrial development and one of the first petrochemical sites in Italy (Perrino et al., 2013a). These features make the Po Valley one of the most polluted areas in Europe (see fig. 3.9) and the fourth area most polluted in the world.

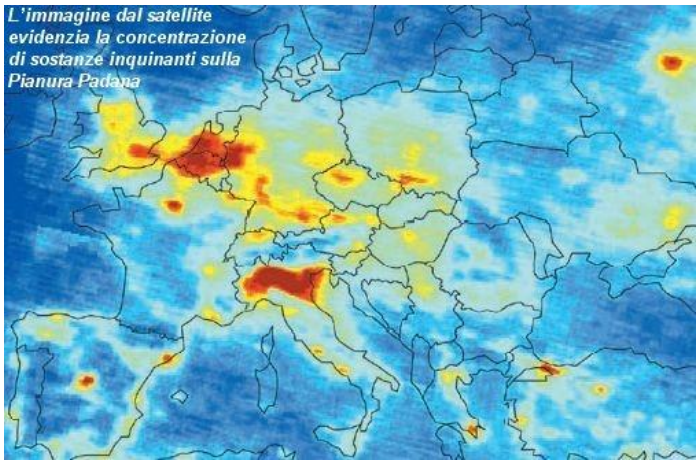

Fig.3.9: satellite view of Europe; the red areas represent the most polluted zones.

For these reasons, since the second half of the 70s, the legislature set the obligation to carry out intensive monitoring campaigns twice a year. The monitoring network of Ferrara is appropriated for cities with less than 500000 inhabitants, which require at least six urban stations. Figures 3.10 shows the top view of Cassana station where the samples analyzed in this step of the work were collected.

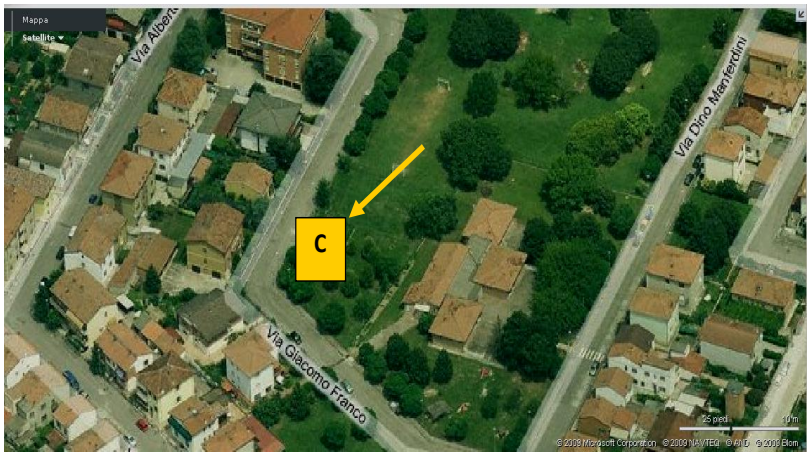

Fig.3.10: top view of Cassana sampling site.

The Cassana station provides valuable information about air pollution, since it is a residential area where is necessary to reduce the environmental impact. PM_{10} samples collected from January 12th to February 29th 2012 were analyzed and the respective KF graphics are shown in Figure 3.11, while water content is reported in table 3.2. It has to be noted that the LOQ value was calculated on the total method (as described in Chapter 2), while values reported in table 3.2 were simply calculated by subtracting the water amount provided by the instrument at the considered temporal ranges. For this reason water contents lower than the LOQ were considered as good.

At first a substantial inter-days variability can be noticed even if the curve trend of some days are very similar. In particular, the water content released in the range 1450- 1600 s is of course the most variable, showing very high values on February 17-19th and very low values on January 26th, and from January 29th to February 4th. Even the water content released in the range 1600- 3000s is quite significant, but it shows a lower variability.

Regarding the profile shape, it is noted that in some days only one contribution predominates, while in others there is the co-presence of various contributions. In the first case the curve assumes a shape similar to a sigmoid, while in the second it appears flatter and equally distributed along all the temporal range. Finally, by examining the total water content for each day we can certainly conclude that it was particularly high on January 23th and February 17-19th, in which the water concentration was approaching the PM_{10} limit, while it reached the lower value on February 28th. Water concentration tends to increase in the days in which the PM concentration is higher, as shown in figure 3.12. This could be due to the presence of a constant percentage of water in the dusts or could indicate an active role of water in the increase of concentration.

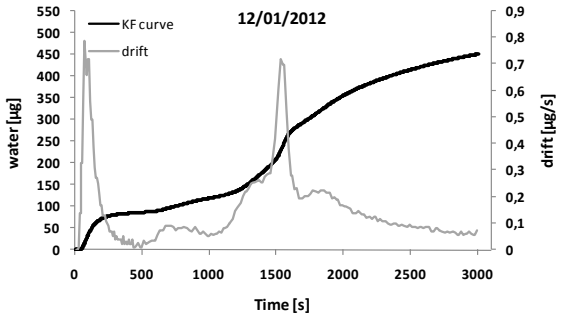
12/01/2012
KF curve
drift
water [µg]
drift [µg/s]
Time [s]

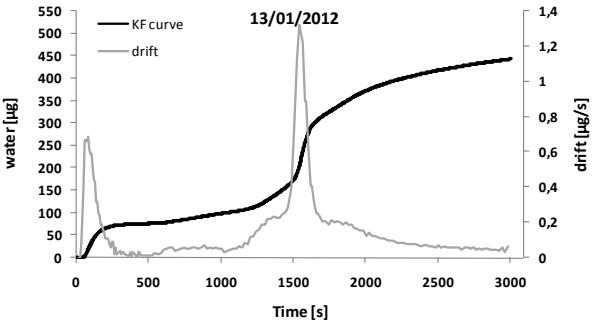
13/01/2012
KF curve
drift
water [µg]
drift [µg/s]
Time [s]

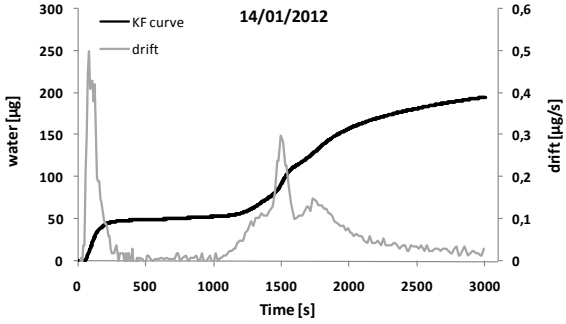
14/01/2012
KF curve
drift
water [µg]
drift [µg/s]
Time [s]

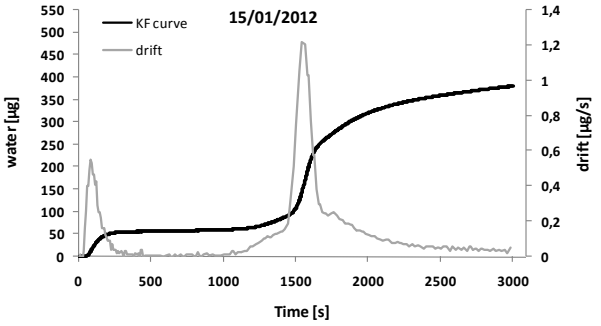
15/01/2012
KF curve
drift
water [µg]
drift [µg/s]
Time [s]

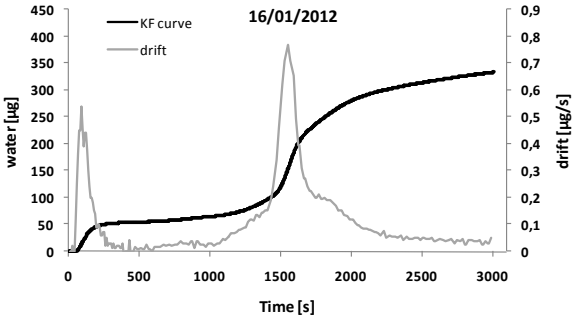
16/01/2012
KF curve
drift
water [µg]
drift [µg/s]
Time [s]

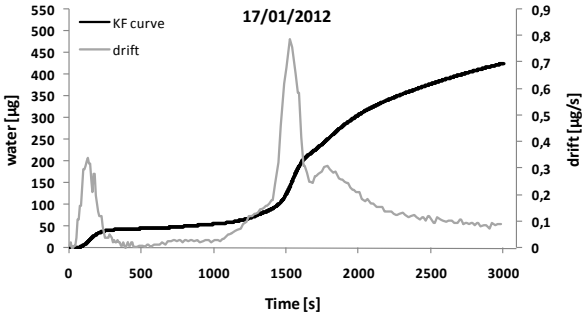
17/01/2012
KF curve
drift
water [µg]
drift [µg/s]
Time [s]

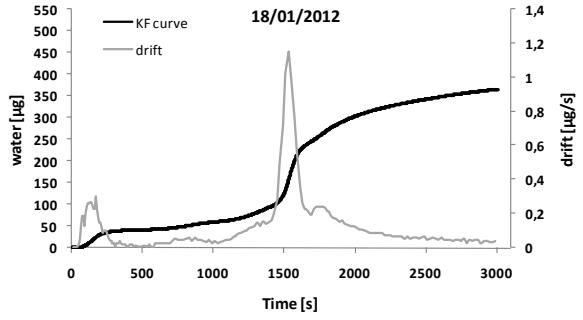
18/01/2012
KF curve
drift
water [µg]
drift [µg/s]
Time [s]

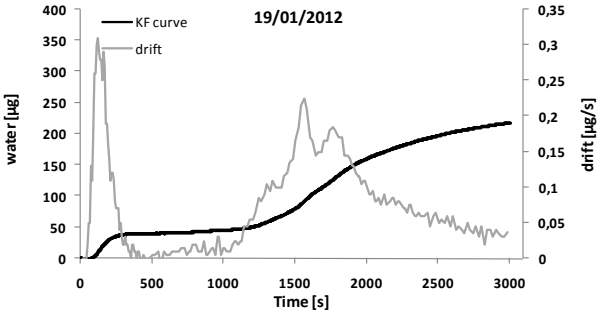
19/01/2012
KF curve
drift
water [µg]
drift [µg/s]
Time [s]

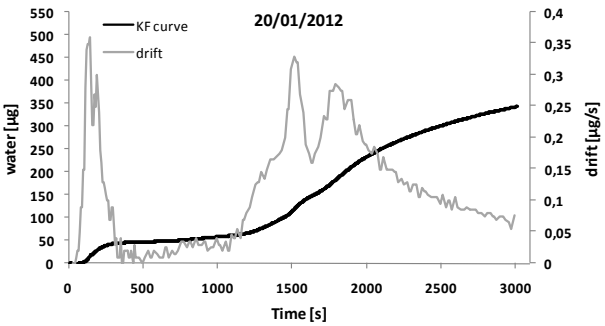
20/01/2012
KF curve
drift
water [µg]
drift [µg/s]
Time [s]

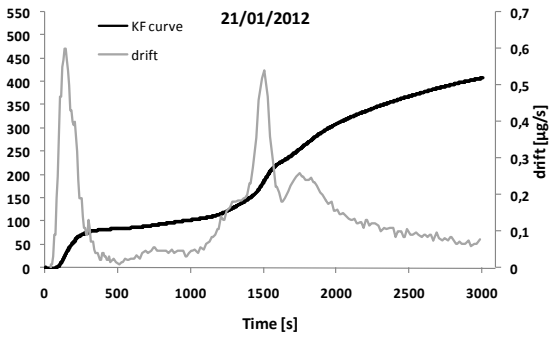
21/01/2012
KF curve
drift
water [µg]
drift [µg/s]
Time [s]

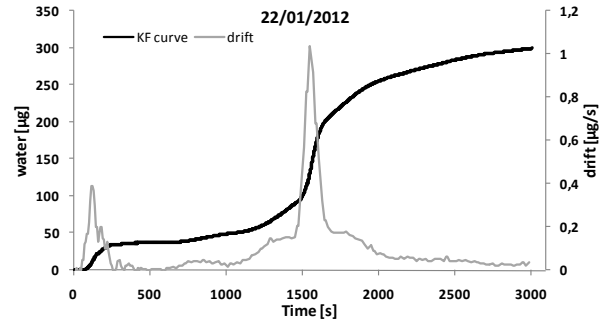
22/01/2012
KF curve
drift
water [µg]
drift [µg/s]
Time [s]

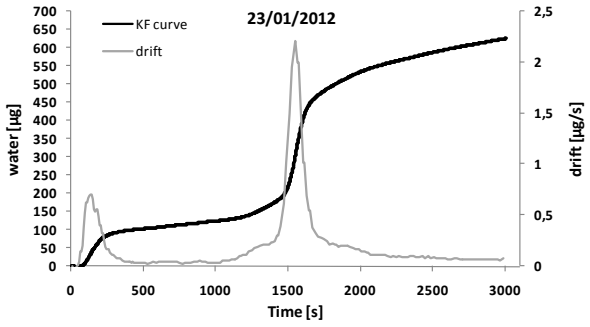
23/01/2012
KF curve
drift
water [µg]
drift [µg/s]
Time [s]

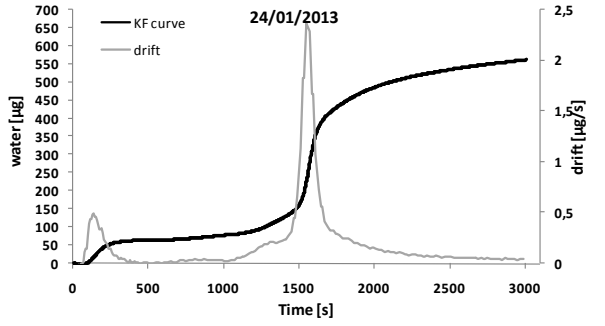
24/01/2013
KF curve
drift
water [µg]
drift [µg/s]
Time [s]

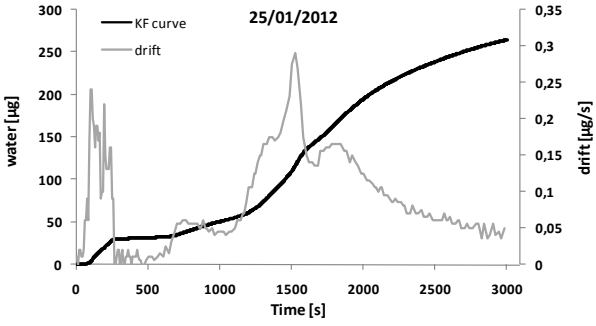
25/01/2012
KF curve
drift
water [µg]
drift [µg/s]
Time [s]

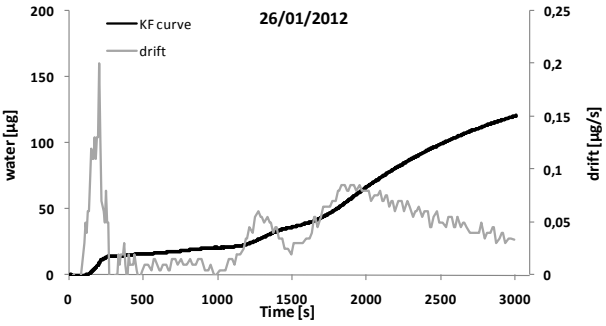
26/01/2012
KF curve
drift
water [µg]
drift [µg/s]
Time [s]

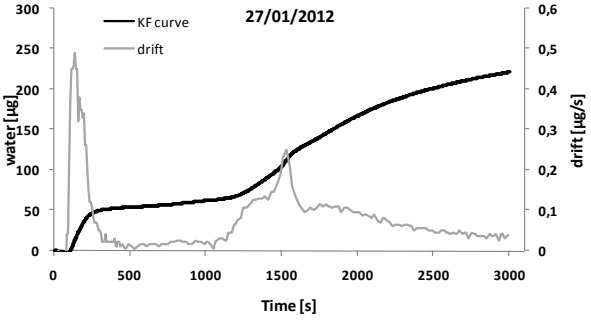
27/01/2012
KF curve
drift
water [µg]
drift [µg/s]
Time [s]

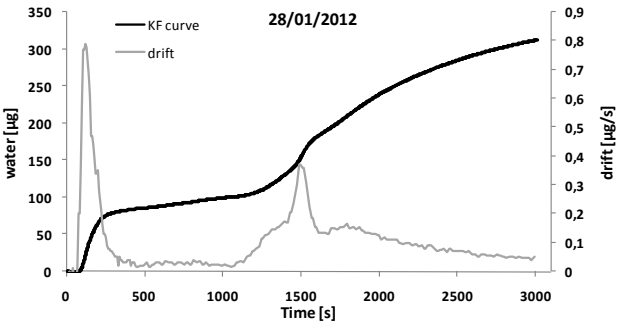
28/01/2012
KF curve
drift
water [µg]
drift [µg/s]
Time [s]

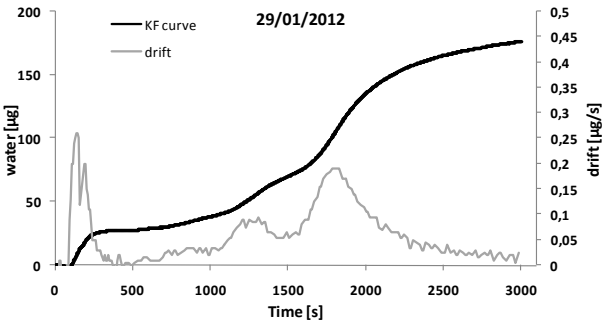
29/01/2012
KF curve
drift
water [µg]
drift [µg/s]
Time [s]

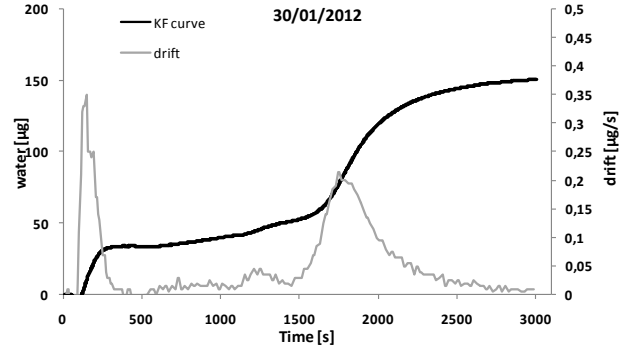
30/01/2012
KF curve
drift
water [µg]
drift [µg/s]
Time [s]

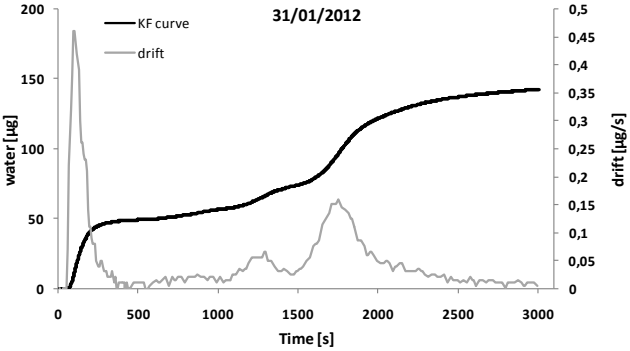
31/01/2012
KF curve
drift
water [µg]
drift [µg/s]
Time [s]

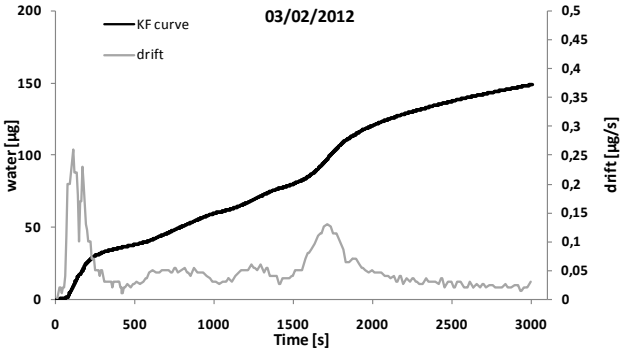
03/02/2012
KF curve
drift
water [µg]
drift [µg/s]
Time [s]

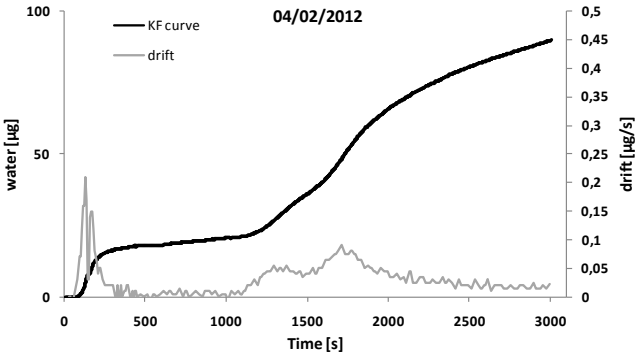
04/02/2012
KF curve
drift
water [µg]
drift [µg/s]
Time [s]

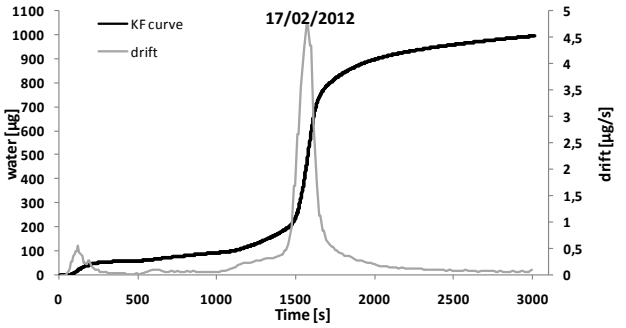
17/02/2012
KF curve
drift
water [µg]
drift [µg/s]
Time [s]

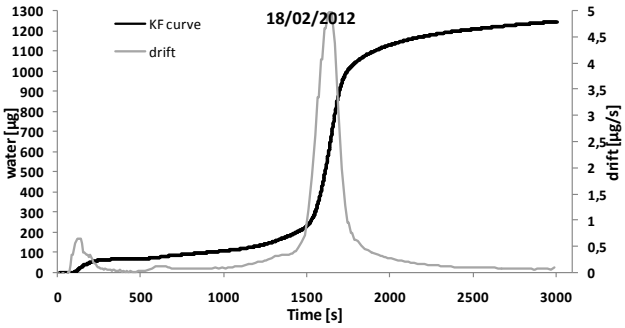
18/02/2012
KF curve
drift
water [µg]
drift [µg/s]
Time [s]

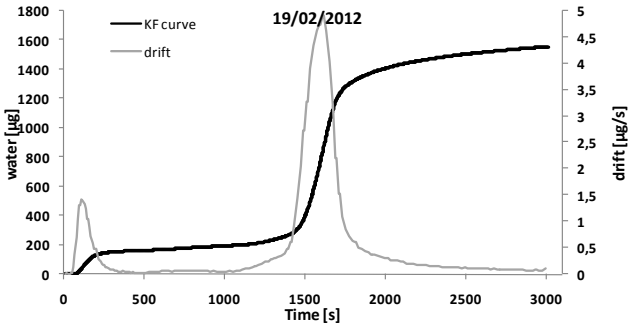
19/02/2012
KF curve
drift
water [µg]
drift [µg/s]
Time [s]

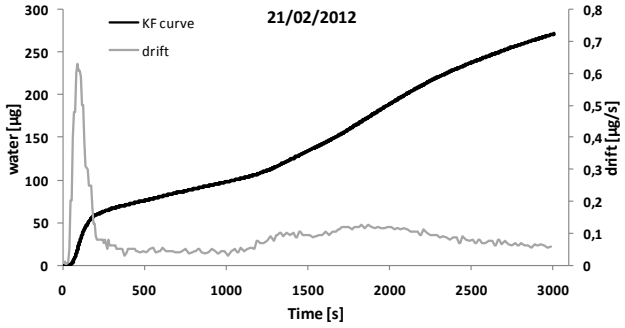
21/02/2012
KF curve
drift
water [µg]
drift [µg/s]
Time [s]

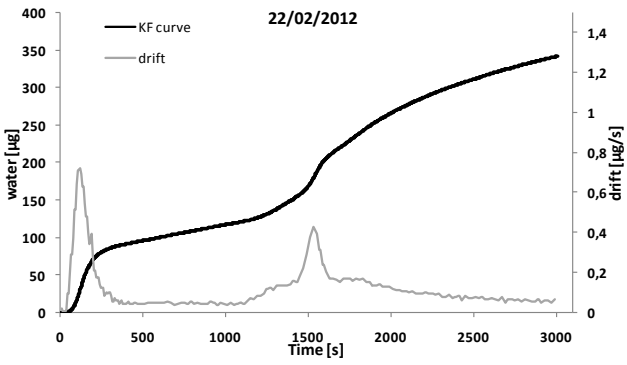
22/02/2012
KF curve
drift
water [µg]
drift [µg/s]
Time [s]

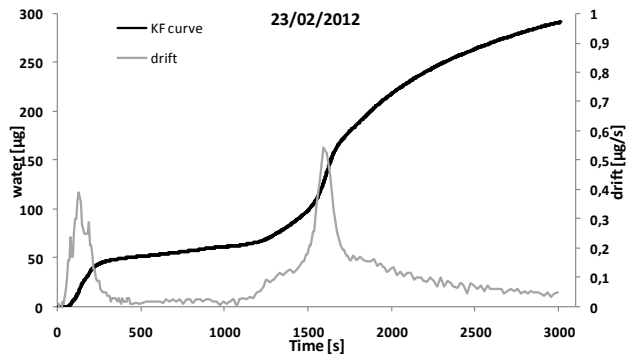
23/02/2012
KF curve
drift
water [µg]
drift [µg/s]
Time [s]

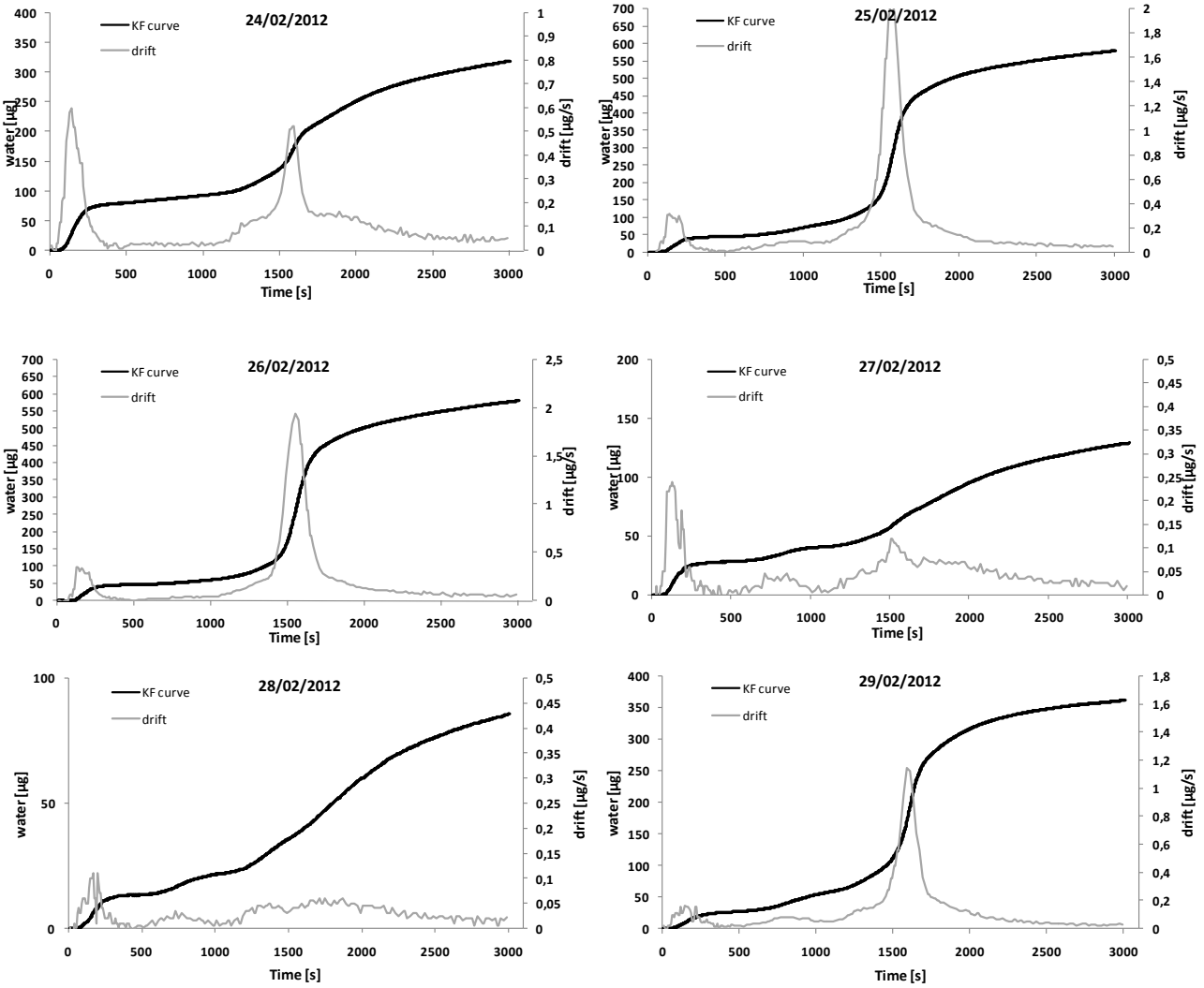

Fig.3.11: Water analysis of Ferrara samples.

Tab.3.3:Water concentration (µg m^{-3}),total water content and water content in each contribution (calculated by subtracting the water amount given by the instrument at the considered times) for the Ferrara samples.

Date	H_2O tot (µg)	Conc.H_2O tot (µg m^{-3})	0-500 s (µg)	500-1000 s (µg)	1000-1450 s (µg)	1450-1600 s (µg)	1600-3000 s (µg)
12/01/12	452	12	86	33	74	76	182
13/01/12	444	15	76	22	58	115	173
14/01/12	195	7	50	4	28	32	82
15/01/12	381	10	57	4	32	116	173

16/01/12	334	9	55	10	39	84	146
17/01/12	426	12	45	11	45	92	234
18/01/12	366	10	42	18	44	115	148
19/01/12	218	6	40	5	28	26	120
20/01/12	343	9	46	12	44	40	201
21/01/12	408	11	84	18	57	58	186
22/01/12	300	8	37	12	40	89	121
23/01/12	626	17	103	21	63	210	228
24/01/12	562	15	64	14	62	200	222
25/01/12	265	7	32	19	48	36	131
26//01/12	121	3	16	5	14	4	82
27/01/12	222	6	54	8	34	29	97
28/01/12	313	9	85	14	40	42	131
29/01/12	176	5	28	11	29	9	100
30/01/12	151	4	33	6	11	6	97
31/01/12	142	4	49	7	16	6	64
3/02/12	149	4	38	22	19	7	64
4/02/12	90	3	18	3	13	6	50
17/02/12	996	29	59	37	106	659	136
18/02/12	1248	34	71	38	96	873	170
19/02/12	1555	43	163	31	116	1043	206
21/02/12	272	7	76	22	31	42	101
22/02/12	342	9	95	22	40	46	139

23/02/12	291	8	52	10	30	41	159
24/02/12	320	9	81	13	36	47	145
25/02/12	580	16	45	26	68	342	99
26/02/12	582	16	47	14	69	348	104
27/02/12	129	4	28	12	13	15	62
28/02/12	86	2	13	9	12	20	32
29/02/12	361	10	27	27	44	197	66

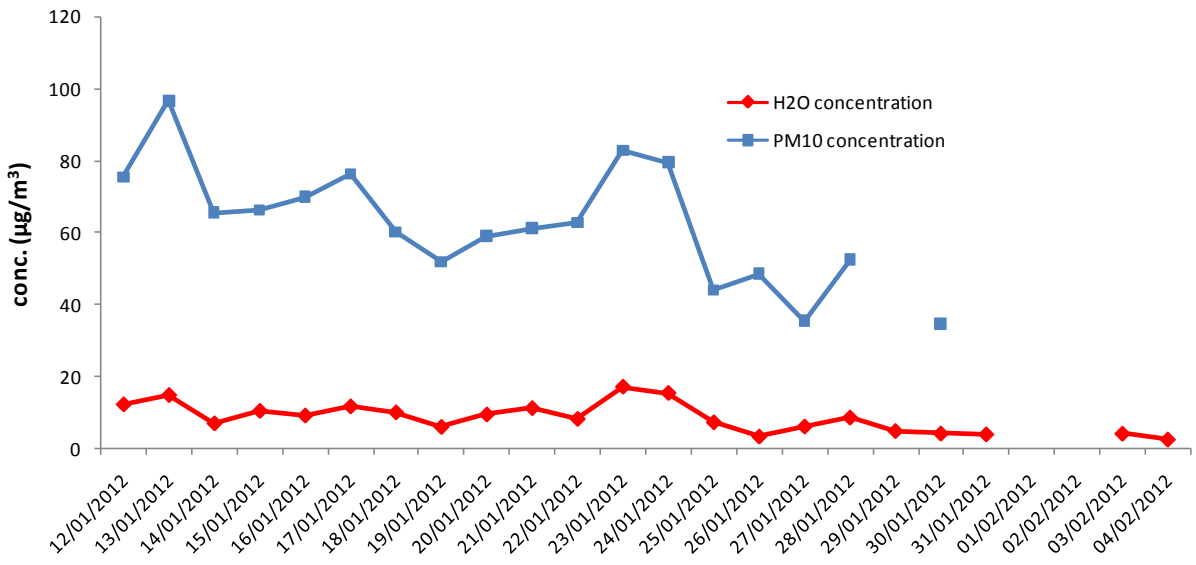

Fig.3.12: comparison between water concentration (blue line) and PM_{10} concentration (red line) trends in the Ferrara samples.

It is also interesting to note that the concentration of water contained in PM seems to have a very important role on the performances of the different materials used as support in the sampling phase. In a recent study, carried out by our research group, it was shown that, under particular climatic conditions, PM_{10} concentrations measured on teflon filters were significantly higher than those measured at the same place and at the same time using quartz membranes. This observation could

not be explained by the known effects of the support sampling on the solid-vapor equilibria, considered the main responsible for the different performance of the teflon and quartz membranes. In fact, many studies show that the displacement of these equilibria leads to sample larger masses on quartz filters. In that work, we showed how the differences between the two values are particularly evident under high humidity conditions and it is therefore assumed that water adsorbed on the power plays an active role.

Figure 3.13 shows a comparison between the PM_{10} concentrations measured on both quartz and teflon filters during the monitoring period under study. The graph shows that PM concentration is much higher on teflon filters, especially in the most polluted days. Moreover the difference between the two concentrations corresponds to the amount of water present in the filters: the sum between the concentrations measured on quartz and the water content is coincident with the total concentration measured on teflon filters. Although we need of further investigations, it seems reasonable to assume that the quartz filter, being hydrophilic, is able to adsorb the water contained in the PM particles, allowing the achievement of a dynamic equilibrium with the support.

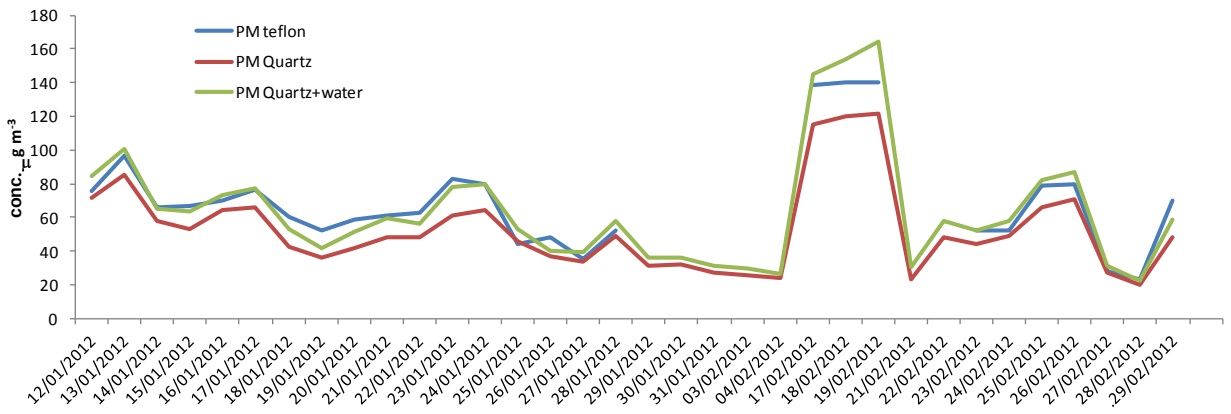

Fig.3.13: temporal trend of PM_{10} concentration measured on Teflon (blue line), quartz (red line) and sum of the concentration measured on quartz and water content (green line).

Hereafter the results of the mass closure obtained for this monitoring campaign are reported. As previously described in the preliminary application of the KF method to real samples (paragraph 2.4.5) the chemical composition of the powders collected in the Po Valley is very different from Central Italy. The main components are, in this case, the secondary inorganic and organic compounds, both of natural and anthropogenic origin.

In figure 3.14 the mass closure of the monitoring period and the daily trend of the PM macro-sources are reported, both excluding (fig. 3.14 a) and including (fig. 3.14 b) the water content.

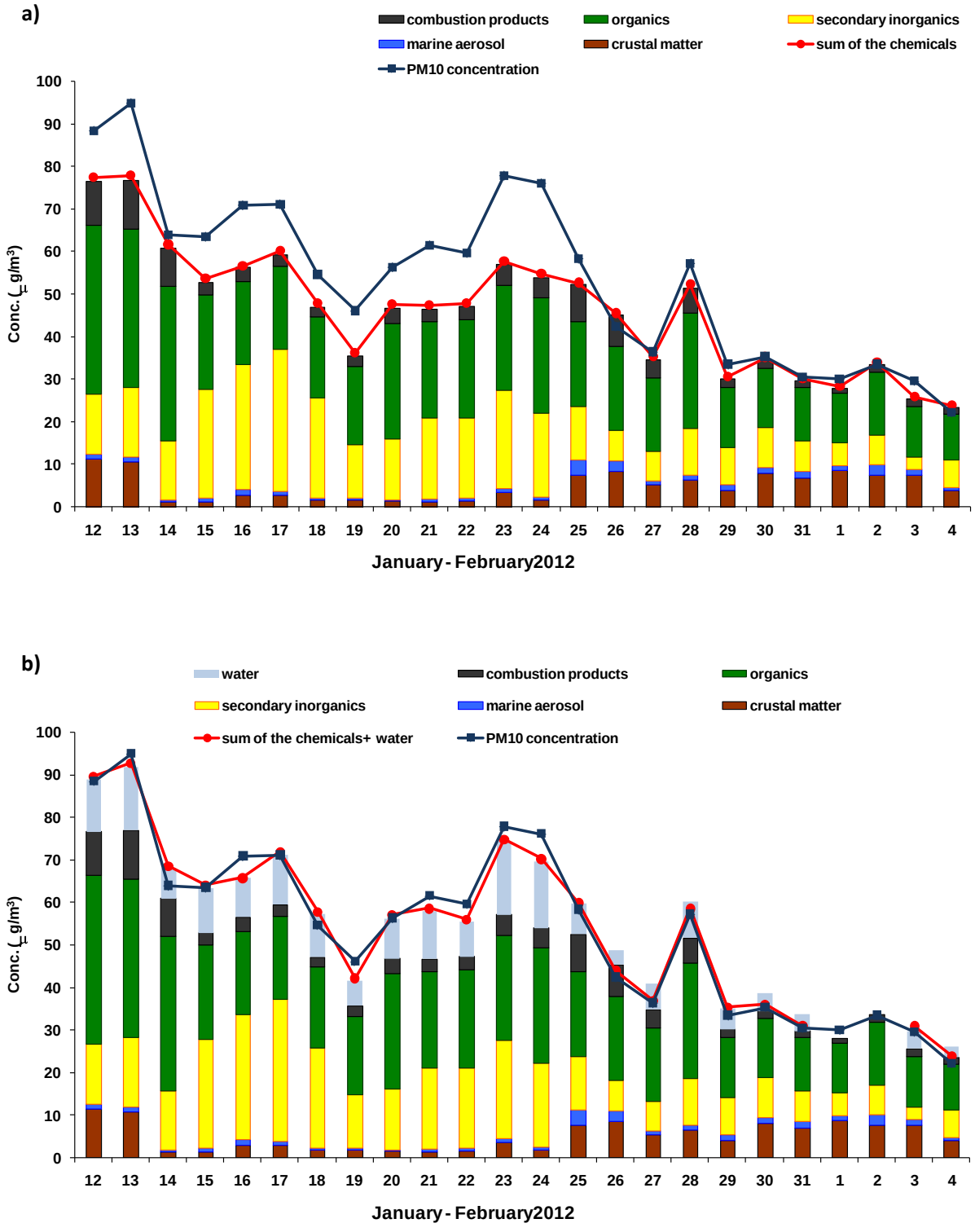

Fig 3.14: Mass balance and PM macro-sources at Ferrara, a) not including water analysys, b) including water analysis.

In the first case only 70% of the PM mass was reconstructed. Conversely, including the water content up to 99% of the total mass can be obtained. The main differences between PM_{10} concentration and the sum of the chemical analysis can be seen during the first days of January, in which water concentration reached values up to 20 μg m^{-3}, while in last days of the campaign the water concentrations values were low (3-4 μg m^{-3}).

To interpret these results it is also necessary to consider the weather conditions during the sampling period. Figure 3.15 shows the main meteorological parameters (relative humidity and wind speed) and the trend of the natural radioactivity, which indicates the lower atmosphere mixing properties. This latter is given by the measurement of the radon gas emitted from the ground at a rate that can assumed to be constant on the temporal and spatial scale of the observations (a few weeks, several kilometers) and its only transformation is the radioactive decay. As discussed in Chapter 1, radon concentration increases when the atmospheric mixing is slow and decreases in situations of efficient atmospheric mixing. Usually, during the cold periods the diurnal pattern of natural radioactivity is, mostly, no longer apparent. In the area of the Po Valley (Figure 3.15 middle panel) winter is very often characterized by very weak atmospheric mixing, which corresponds to constantly high radioactivity values. In these conditions, the worse PM pollution episodes occur when many consecutive days are characterized by high daytime *and* nighttime radioactivity values.

By looking at the atmospheric parameters it has been possible to subdivide the monitoring period in two phases, characterized by different climatic and weather conditions. The first phase, January 12–25th (January 25th has to be considered a day of transition, in which the conditions described below have changed), was characterized by very high humidity, low wind intensity (1-3 m/s) and day/night atmospheric stability. The second phase can be identified from January 26th to February 4th. From January 25th the relative humidity values sharply decreased, the wind speed significantly increased and the lower values of the natural radioactivity showed a typical condition of the advection periods. The conditions observed during the first period and the prevalence in the PM composition of secondary inorganic and organic species indicate that water was easily adsorbed on the hydrophilic particles. This is confirmed by the KF curve profiles that are very similar to those observed for the ammonium salts. Conversely the weather condition registered during the second period favored the abatement of the secondary inorganic and organic species and the increase of the crustal particles. This led to a decrease in water percentages (3-4%) and to a change in the water profile which is very similar to that observed for the particles coming from resuspension phenomena. It can be concluded that the interaction of water with the atmospheric particles strongly related to both their chemical composition and climatic conditions.

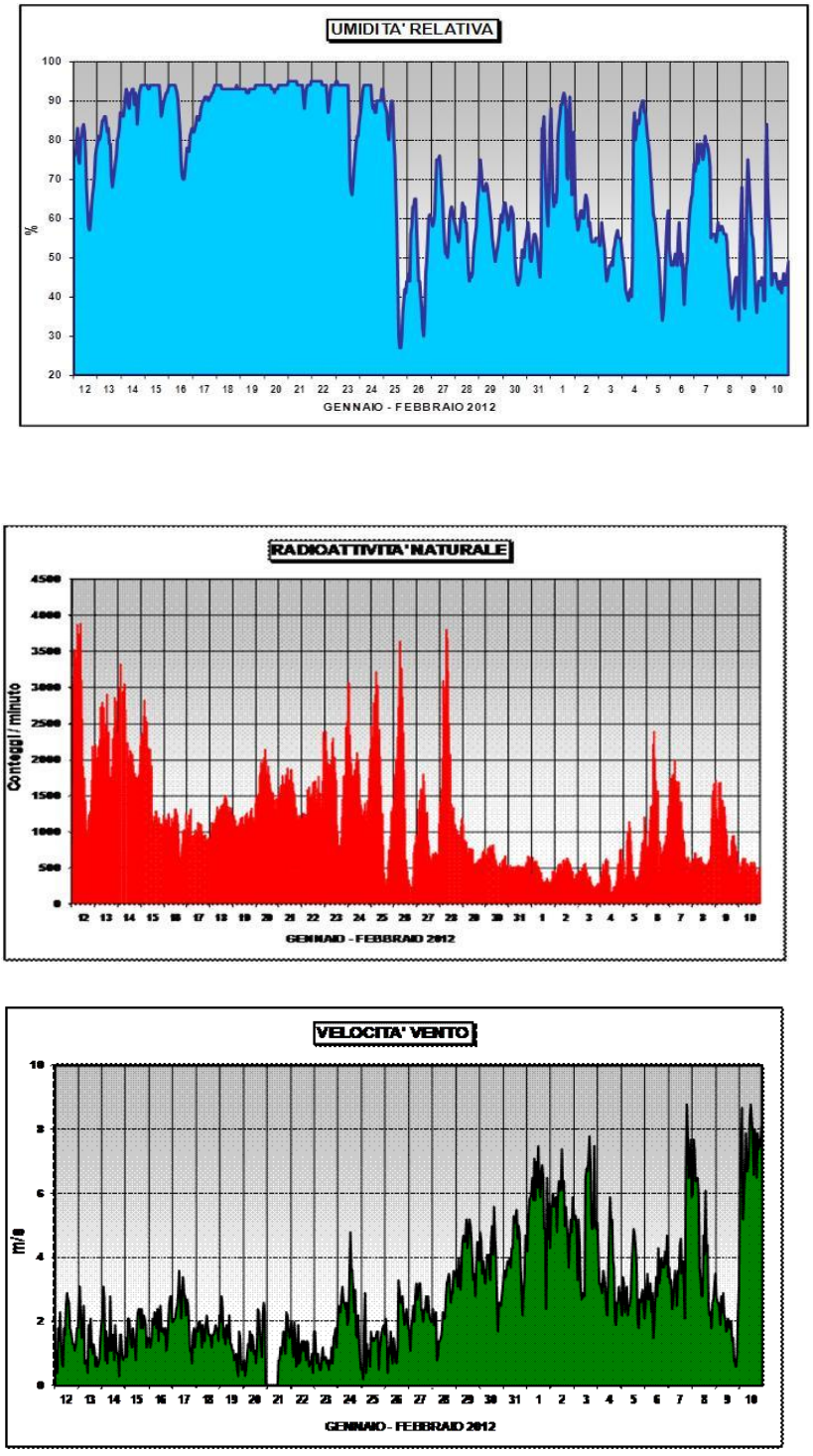

Fig.3.15: Relative humidity (upper panel), natural radioactivity (middle panel), wind speed (lower panel) trends during the monitoring campaign.

At the same site of Cassana, as previously mentioned, the atmospheric particles have been collected also by means of a multistage impactor. This device provides the particles' separation based on their

inertial properties, each stage is arranged in cascade to obtain information about different aerodynamic diameters.

The knowledge of the particles' size distribution can provide more information about their nature: in fact, the particles produced by combustion processes and the secondary particles formed in the atmosphere typically have aerodynamic diameters less than 1 µm, while particles coming from abrasive mechanisms and the natural components (sands of the Sahara, marine aerosols) have diameters greater than 1 µm. In figures 3.16 and 3.17 are shown, respectively, the KF curves and drifts of the water analysis relative to the 11 stages, following from Sf to S0.

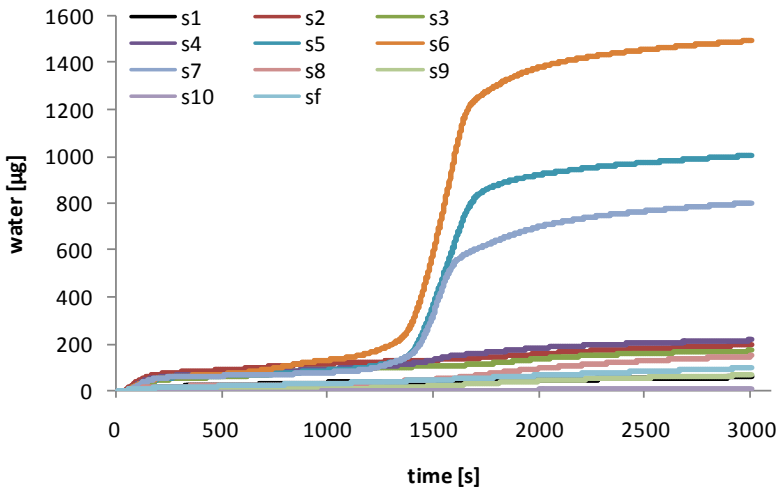

Fig.3.16: KF curve obtained from the water analysis on each cascade impactor stage.

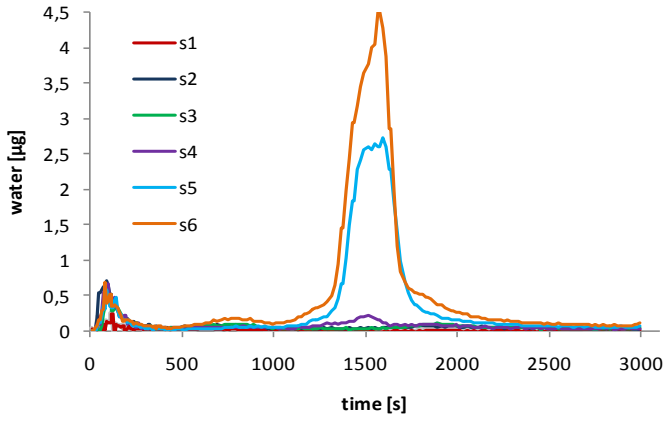

Fig.3.17: Drift curve of water analysis on some of the cascade impactor stages.

In table 3.4 the water amount for each size range is reported.

Tab.2.6: Water content (µg) in every impactor stage.

Stage	Size range (µm)	H_2O tot (µg)
sf	<0.056	96
s0	0.056-0.10	<LOQ
s9	0.10-0.18	64
s8	0.18-0.32	146
s7	0.32-0.56	802
s6	0.56-1.00	1496
s5	1.00-1.80	1005
s4	1.80-3.20	215
s3	3.20-5.60	170
s2	5.60-10.00	194
s1	10.00-18.00	57
s0	>18.00	50

The results show the interdependence between the particle size and the amount of water, highlighting that the fine particles (0.3 to 1.8 µm) are the most hygroscopic (0.8-1.0 mg of water). These particles are responsible for the peak observed in the range 1500-1800, similar to the secondary ammonium salts. There is also a small water contribution from particles with size distribution ranging between 3 and 10 µm (about 200 µg of water), but the KF curves are definitely different. These curve are characterized by the presence of a low and crushed peak between 500 and 1000s, which is indicative of the dust of crustal origin. In this size range there is also a water contribution around 2000s, probably associated with the presence of bio-aerosols (see figure 2.15,

middle panel). As an example in figure 3.18 the KF curve and drift relative to a fine and a coarse stage were reported.

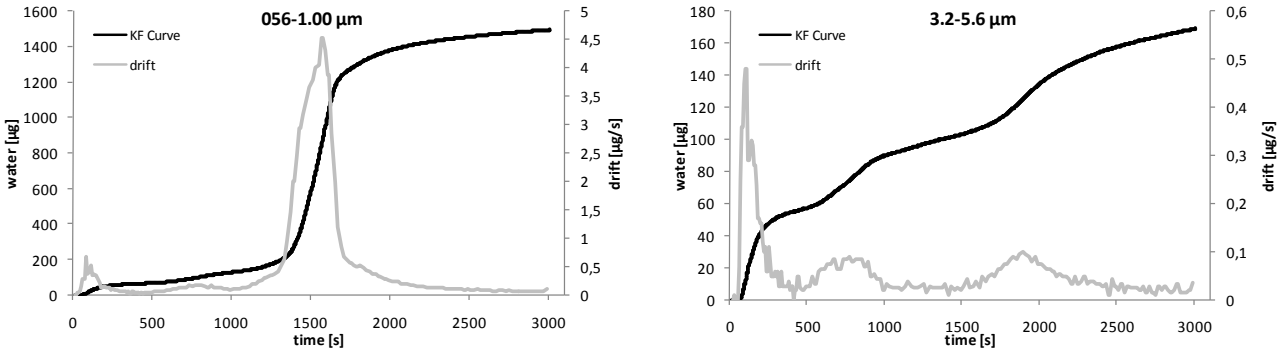

Fig. 3.18: KF curve and drift of the water analysis on the size stages 0.56-1.00µg and 3.2-5.6 µg.

Finally it is also interesting to point out that the water profile obtained for the 1.8-3.2 (figure 3.19) µm is compatible with the overlap of the two profiles relative to *coarse* and *fine* particles. This stage of the impactor collects particles belonging both to the fine and the coarse modes, due to the not-perfect dimensional separation performed by these sampling systems. This observation can be a further confirmation of the good performances of the method even for evaluating the different types of water present on integral samples.

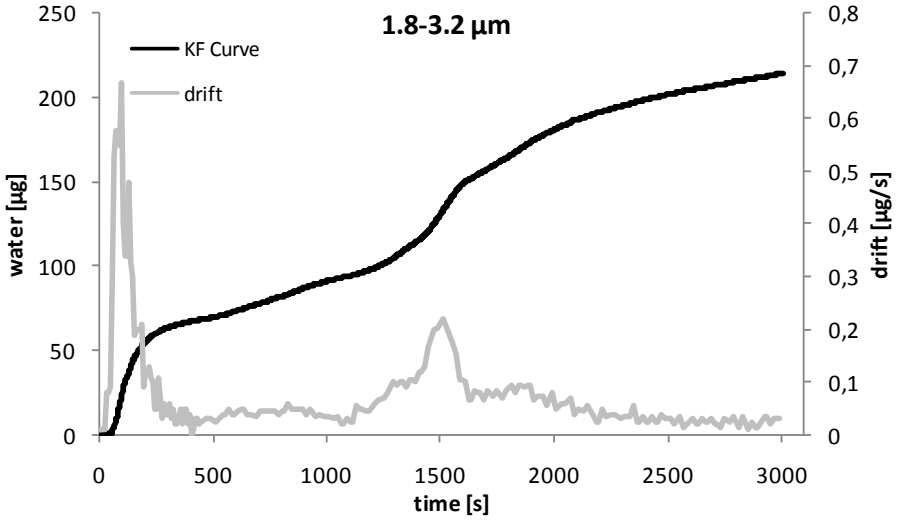

Fig.3.19: KF curve and drift of the 1.8-3.2 µm stage.

Moreover, by looking at both the left and the right panels in figure 3.20, the water size distribution follows the PM size distribution, indicating that much more PM is sampled then more water is detected and, once again, the hygroscopicity of the particles appears mainly due to the fine fraction of PM.

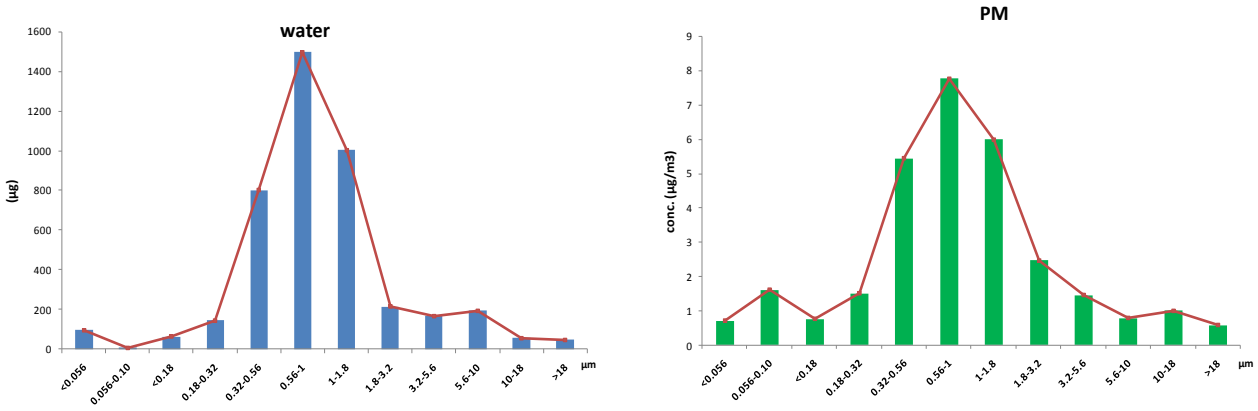

Fig. 3.20: left panel: water size-distribution (µg), right panel: PM distribution size-distribution (µg m^{-3}) at Ferrara.

The interpretation of these results must always be accompanied by an evaluation of the particles'concentration. Of course, if the particles which adsorb more water are less abundant in the sample, the content of water in that dimensional range would be lower. For this reason, the data obtained were normalized to the concentration of the PM collected in each stage.

The principle of the sampling by a multistage impactor is to collect particles of different sizes on different impact surfaces. The particles collected in each stage have then the same dimensional characteristics but are not necessarily homogeneously distributed on the membrane. For this reason, it is not possible to realize the XRF and EC/OC analysis on these samples. These two analytical techniques, in fact, require a small area of the sample, but if this is not representative, there is a systematic error that denies the possibility of performing a mass balance. However it was possible to carry out ionic analysis, such as Ca^{2+}, Mg^{2+}, NH_4^+, Na^+, SO_4^{2-}, NO_3^- and Cl^-. The results confirm the prevalence of secondary ionic species such as nitrate, sulfate and ammonium in the air of Ferrara (shown in figure 3.21), and their distribution is very similar to the water distribution confirming that the fine particles are the most hygroscopic.

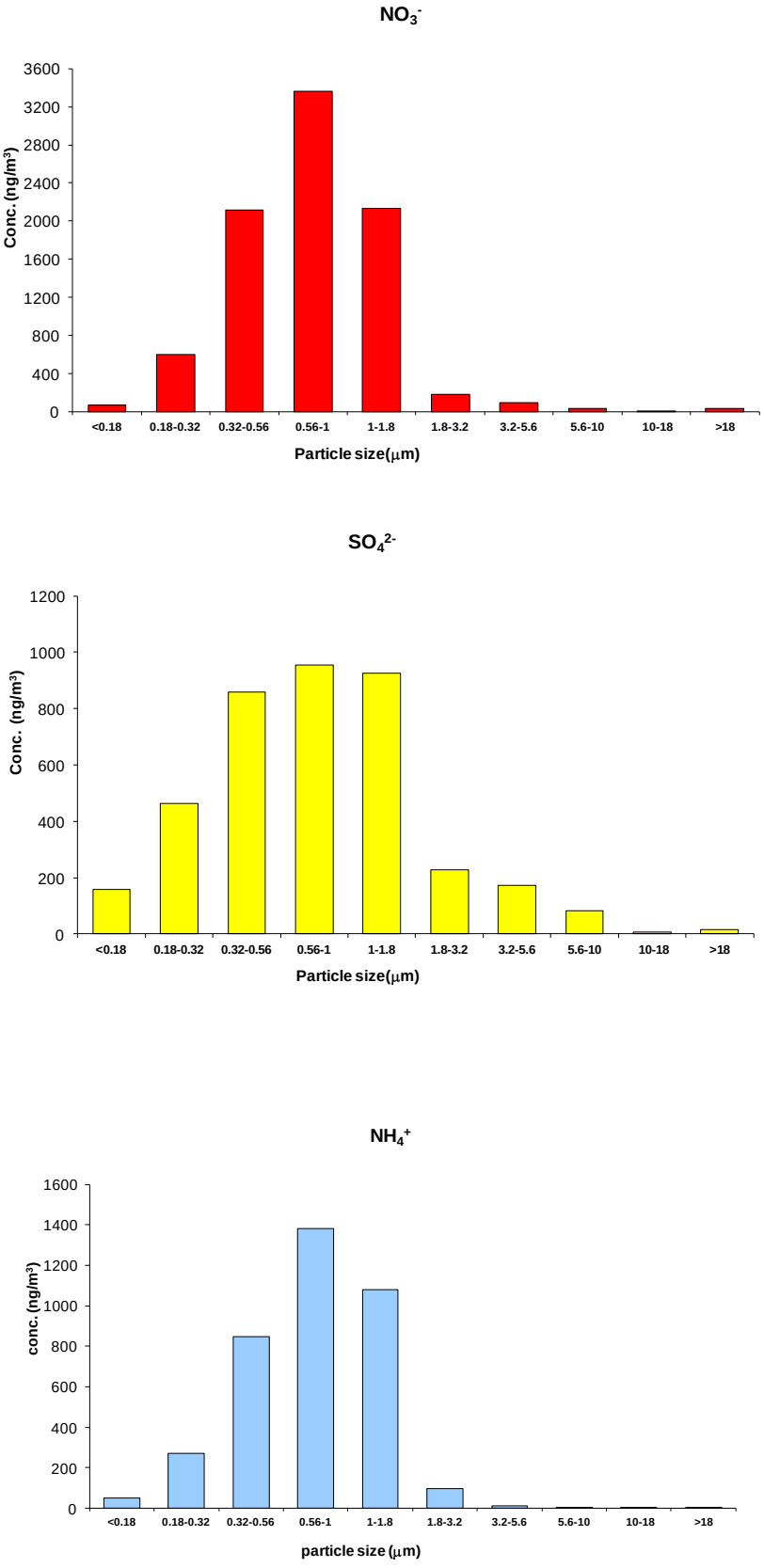

Fig.3.21: Size distribution of nitrate, sulphate and ammonium at Ferrara

3.6 Results obtained on PM_{10} samples collected at La Spezia

The last application regarding the PM mass reconstruction with the integration of the water analysis is related to PM_{10} collected in La Spezia at an urban site located close to the sea. Figure 3.22 shows a top view of the sampling site. The study was aimed to a qualitative and quantitative characterization of the PM composition in a coastal area.

Fig.3.22: Top view of the sampling site at La Spezia.

The PM composition in this area is usually dominated by the presence of marine aerosol which is rich in inorganic salts such as chlorides, iodides and sulphates accounting for an high percentage of the total mass and forming the coarse fraction. These compounds are released into the atmosphere by the explosion of air bubbles produced by the sea waves. Recent studies about the ocean water have, however, testified that the fine fraction progressively increases and contains insoluble organic species (Facchini et al., 2007) .

Figure 3.23 shows the graphs of the KF analysis carried out on PM_{10} samples collected from July 4^{th} to 17^{th} 2012. The trends of the KF curves and drifts show a moderate inter-day variability.

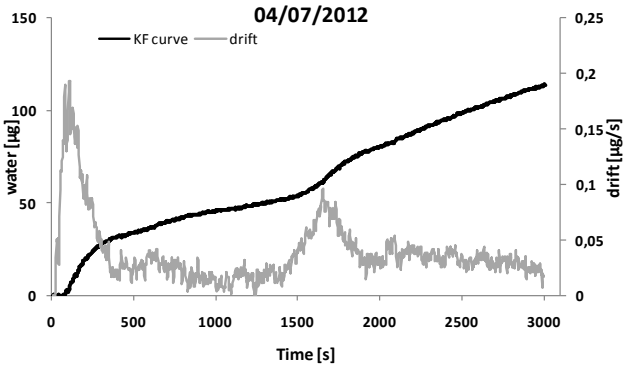
04/07/2012
KF curve
drift
water [µg]
drift [µg/s]
Time [s]

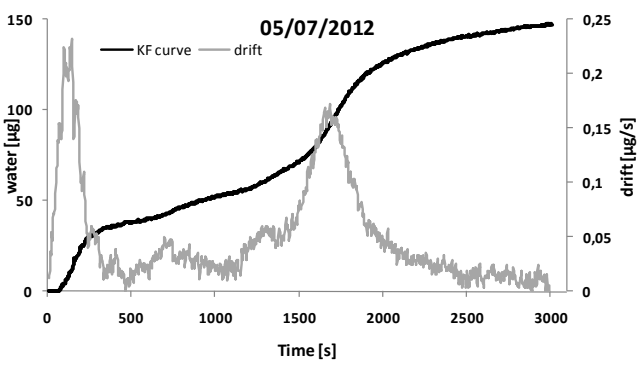
05/07/2012
KF curve
drift
water [µg]
drift [µg/s]
Time [s]

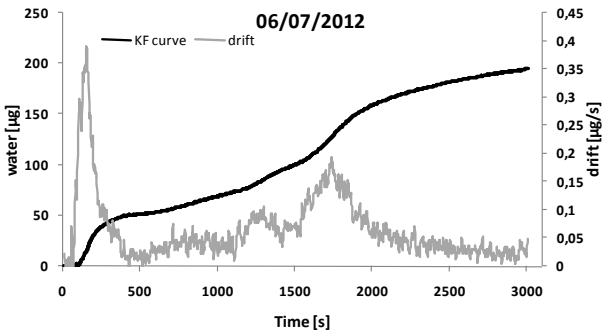
06/07/2012
KF curve
drift
water [µg]
drift [µg/s]
Time [s]

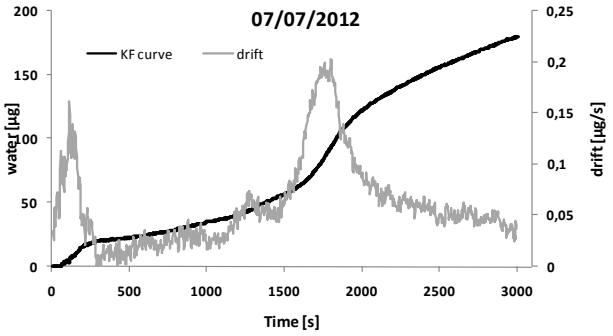
07/07/2012
KF curve
drift
water [µg]
drift [µg/s]
Time [s]

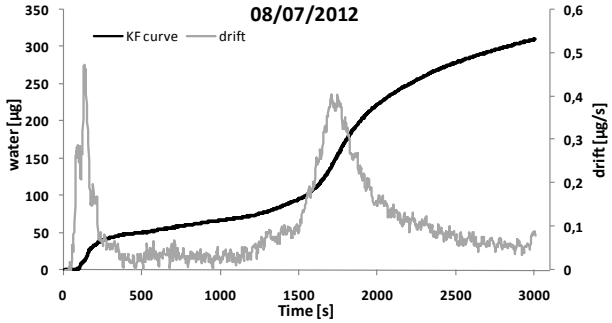
08/07/2012
KF curve
drift
water [µg]
drift [µg/s]
Time [s]

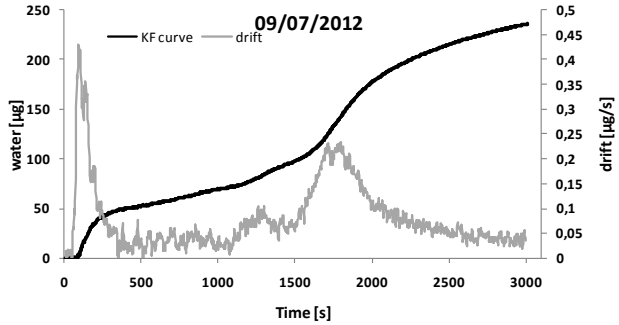
09/07/2012
KF curve
drift
water [µg]
drift [µg/s]
Time [s]

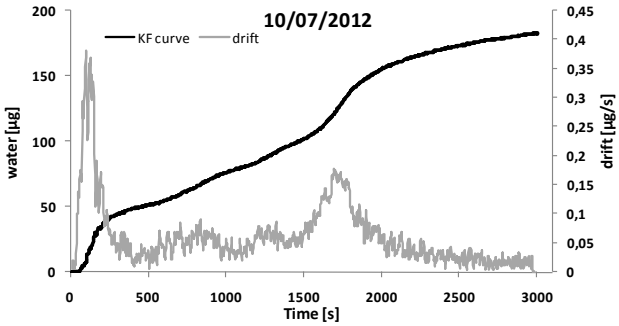
10/07/2012
KF curve
drift
water [µg]
drift [µg/s]
Time [s]

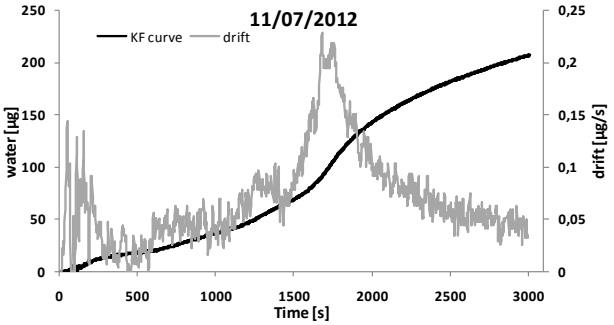
11/07/2012
KF curve
drift
water [µg]
drift [µg/s]
Time [s]

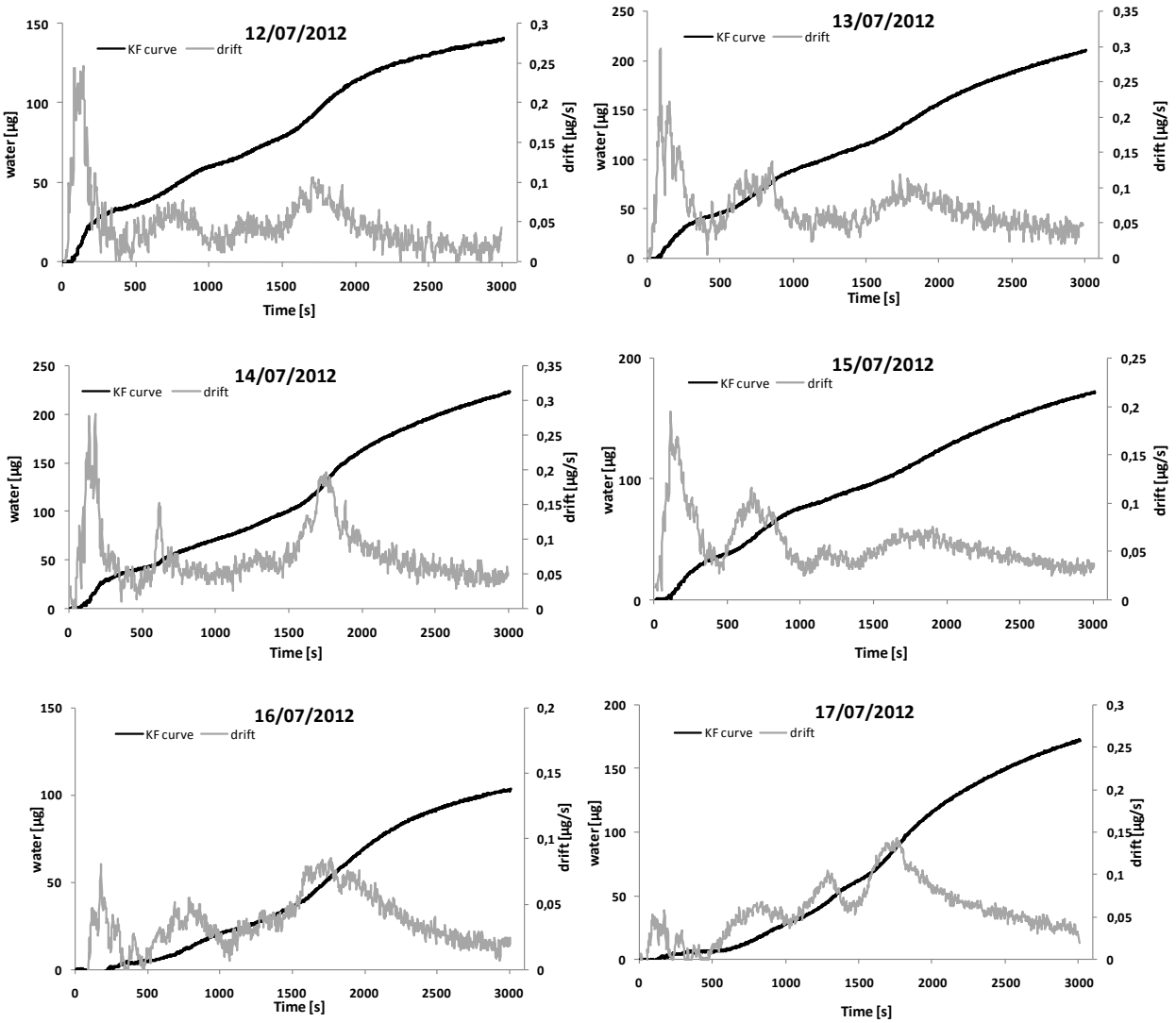

Fig.3.23: KF curves and drifts obtained by analyzing La Spezia samples.

However two types of water can be identified: the first provides a peak between 500 and 1000s which had already been isolated in the samples of Montelibretti in the absence of sand transport events, probably due to inorganic species such as silica and alumina. The second contribution provides a peak in the range 1500- 2000 s referred to the hygroscopic inorganic salts. Table 3.4 shows the water concentration and the different contributions determined on the samples.

Tab.3.4: Water concentration (µg m^{-3}) and water amount (µg) for each contribution shown by the drift profiles in the La Spezia Samples (the latter are calculated by subtracting the water amount provided by the instrument at the considered times).

Date	Conc. H_2O (µg m^{-3})	H_2O tot (µg)	0-500 s (µg)	500-1000 s (µg)	1000-1450 s (µg)
04/07/2012	3	114	34	11	53
05/07/2012	3	147	38	15	88
06/07/2012	3	195	51	18	113
07/07/2012	3	180	22	13	121
08/07/2012	6	311	50	17	212
09/07/2012	4	236	52	18	146
10/07/2012	3	182	51	25	97
11/07/2012	4	207	18	18	145
12/07/2012	3	141	36	25	70
13/07/2012	4	210	45	44	99
14/07/2012	4	223	41	30	127
15/07/2012	3	172	38	38	77
16/07/2012	2	103	11	21	71
17/07/2012	3	172	22	28	122

At first we can noticed that the water concentrations are much lower than those registered in Ferrara all along the monitored period and are comparable to the Montelibretti concentrations registered in absence of transport events.

The highest amount of water associated with the PM particles was found the July 8th (311 µg corresponding to a concentration of 6 µg m^{-3}). It is interesting to point out that the KF profile on that date is very similar to those obtained in the Ferrara samples, which had been attributed to the secondary inorganic compounds. These findings are rather unexpected. In fact before to carry out these analysis it was reasonable to assume that the samples collected at a coastal area were mainly characterized by the presence of aerosols marine rich in sodium chloride.

On July 16th the lowest water concentration was recorded (2 µg m^{-3}). Also in this case there was a curious analogy between a decrease of the concentration and the water profile change, more similar to the road dust.

The mass balance and the PM macro-sources trends is reported in figure 3.24, both including (fig. 3.24 a) and not-including (fig. 3.24 b) water analysis.

Looking at this graphs we can surely point out at first that the differences between the gravimetric PM_{10} mass determination and the sum of the chemical analysis are lower than those observed at Cassana (average value for La Spezia is 3 µg m^{-3} while at Cassana the average value was 8 µg m^{-3}). This leads to the conclusion that in this particular application the water content did not influence the PM mass closure, even if by adding the water content an improvement in the mass reconstruction can be clearly noticed (fig. 3.23 b).

Moreover the daily composition of the macro-sources confirm what was observed from the water profiles. Indeed, on July 8th besides an higher water concentration there was also registered an increase of the secondary inorganic concentration, while on July 16th the secondary inorganics decrease and the PM composition was dominated by crustal matter and organics. Finally on July 15th, which shows the maximum value of aerosol marine concentration, did not point an increase in the water concentration.

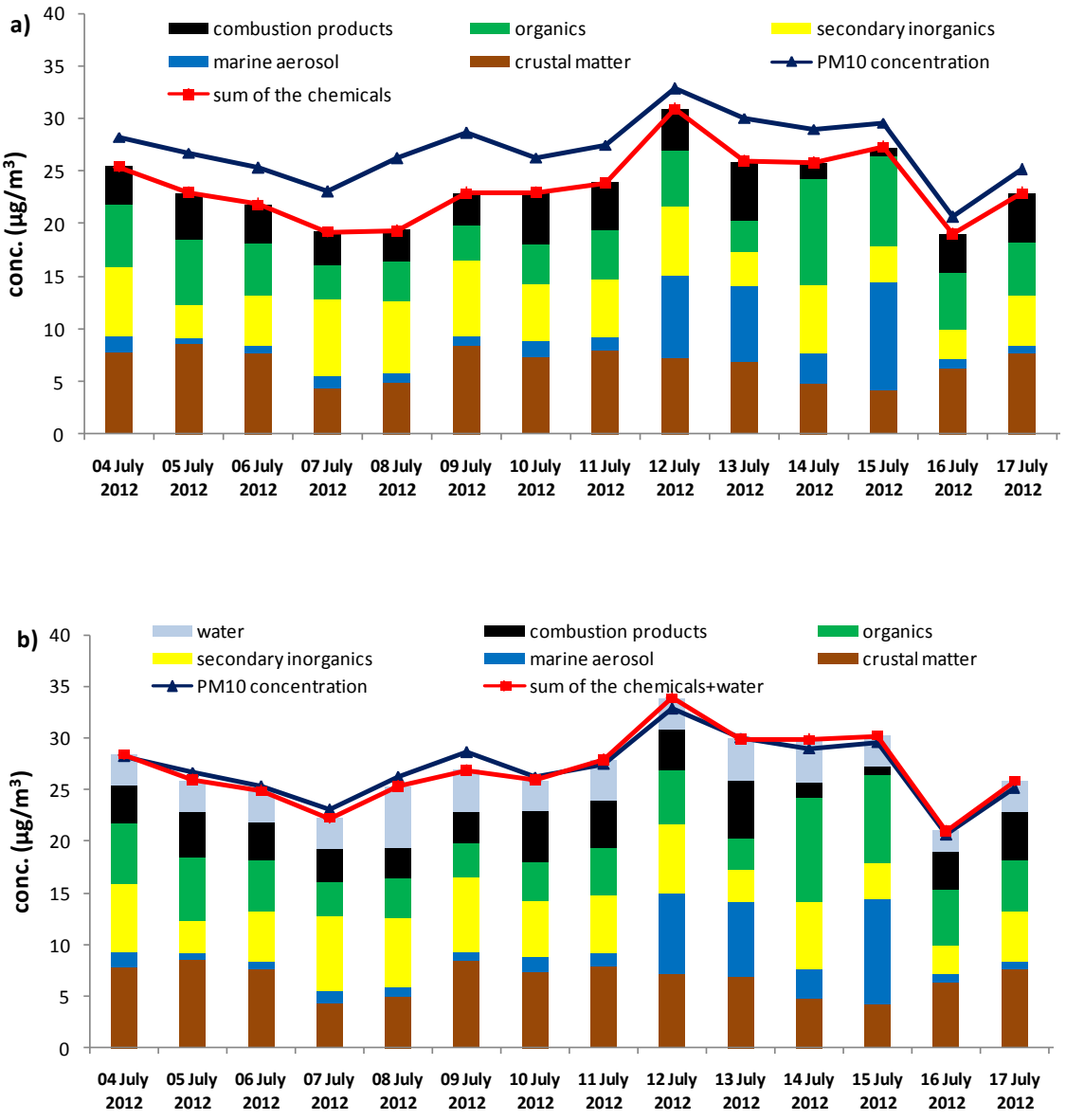

Fig.3.24: Mass balance at La Spezia, a)excluding the water analysis, b) including water analysis.

Therefore in these samples, being representative of a coastal area, the water amount turns out to be small and in any case associated to the secondary inorganic species rather than to the marine aerosol components. Also the average PM_{10} average composition, reported in figure 3.25, shows amazingly higher percentage of crustal matter, organic and secondary inorganic compounds rather than of marine aerosol.

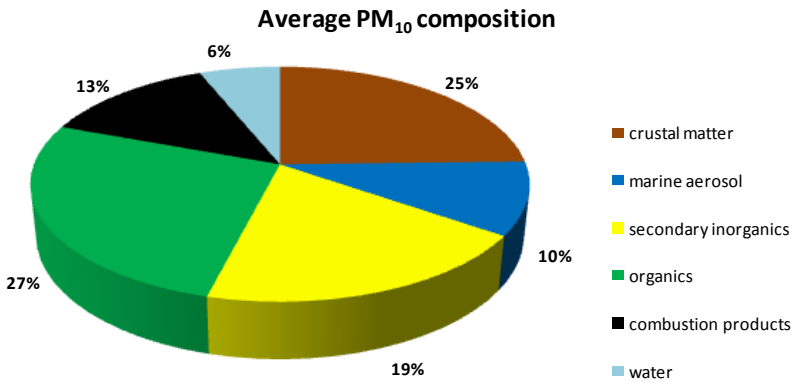

Fig.3.25: Average PM_{10} composition during the monitored period at La Spezia.

These results provide a valid support to the conclusion that the inorganic salts such as sodium, calcium or magnesium chlorides, which constitute the marine aerosol, are not as hygroscopic as the inorganic salts of secondary origin (ammonium sulphate and nitrate). As already said, this result is rather unexpected, but it must be highlighted that the sampling phase was carried out in the summer season and the high temperatures may have partially caused the water evaporation from the PM particles. To this purpose, our research group is planning to carry out a monitoring campaign at the same site in winter.

Regarding the Air Quality Framework we can conclude that this coastal area is characterized by a low air pollution, with the maximum PM_{10} concentration reaching 32 µg m^{-3}, values well below the air quality standard limits. Only a small part of this concentration can be attributed to water, which then does not represent a great contribution to the mass closure and does not influence the overcoming of the standard limits.

The usefulness of these studies is reflected in the ability to assess the environmental impact caused by the different transport phenomena of the natural materials : in fact, the transport of marine salts, which took place on July 12th, 13th, 15th, were not responsible for the overcoming of the PM_{10} regulatory limits, while the opposite result was obtained at Montelibretti on April 5th 2012, in which the transport of Saharan sands has widely contributed to the raising of PM_{10} concentration above 50 µg m^{-3}.

3.7 Conclusions

Pondering on the results obtained by this research plan it is certainly possible to conclude that the developed method is highly suitable to complete the PM mass balance. The integration of the water content in the procedure to evaluate the PM chemical composition has produced high-quality data detected for a large number of analytical samples. And it is also reasonable to assume that the goodness and the applicability of this method is independent from the spatial and temporal variability that characterizes the air quality monitoring network.

This research work allowed to identify with water one of the constituent of the atmospheric particulate, until now unknown, improving the knowledge about the particles 'composition. The amount of water, mainly associated to the *fine* particles can reach up to 20 % of the sampled mass, value that cannot certainly be considered negligible. From a qualitative point of view, the possibility to attribute the water fraction to the different components can help the study about the toxicological properties, allows to better characterize the impact of particulate matter on human health. Also the measurement of the water concentration can be useful to assess the reason of the limit standard overcoming.

As discussed in different points of the work, the objective of this research was to define a rather accurate PM composition in order to identify the occurrence of transport phenomena of natural materials which impacts on the increase of PM_{10} concentration. The results point out by this work led to the consideration that the transport events of sand from the Saharan Africa have a much more significant environmental impact than the transport of marine aerosols.

These encouraging results can be helpful to find an agreement between the State and the community, aimed to ensure a sustainable development.

3.8 References

Bae M, Schauer J, Turner J, Hopke P, Science of the Total Environment 2009, 407, 5176–5183.

Bettinelli M, Beone G M, Spezia S, Baffi C (2000), Analytica Chimiqua Acta, 424:89–296.

Birch M E, Cary R A, (1996), Aerosol Science and Technology, 25, 221–241.

Canepari S, Cardarelli E, Giuliano A, Pietrodangelo A (2006a), Talanta, 69: 581–587.

Canepari S, Cardarelli E, Pietrodangelo A, Strincone M (2006b), Talanta, 69: 588–595.

Canepari S, Pietrodangelo A, Perrino C, Astolfi M L, Marzo M L (2009), Atmospheric Environment 43, 4754–4765.

Canepari S, Astolfi ML, Moretti S, Curini R (2010), Talanta, 82:834–844.

Castro L M, Pio C A, Harrison R M, Smith D J T (1999), Atmospheric Environment, 33: 2771-2781.

Chan Y C, Simpson R W, McTainsh G H, Vowles P D (1997), Atmospheric Environment, 31: 3773–3785.

D.lgs 155/2012 Recepimento Direttiva 2008/50/CE, relativa alla qualità dell'ambiente e per un aria più pulita in Europa.

Facchini M C, Fuzzi S, Mircea M, Istituto di Scienze dell'Atmosfera e del Clima, CNR, Bologna, Italia. (http://www.dta.cnr.it/dmdocuments/pubblicazioni/volume_clima).

Gobbi G P, Barnaba F, Ammannato L (2007), Atmospheric Environment, 41(2): 261-275.

Marcazzan G M, Vaccaro S, Valli G ,Vecchi R (2001), Atmopheric Environment,35: 4639–4650.

Perrino C, Catrambone M and Pietrodangelo A (2008), Environmental International, 34: 621–628.

Perrino C, Catrambone M, Dalla Torre S, Rantica E, Sargolini T, Canepari S (2013a), Environmental Science and. Pollution Reasearch, DOI 10.10077/s11356-013-2067-1.

Perrino C, Canepari S, Catrambone M (2013b), Aerosol and Air Quality Research. 13: 137-147.

Turpin B J, Lim H (2001), Aerosol Science and Technology, 35: 602–610.

Vecchi R, Marcazzan G, Valli G, Ceriani M and Antoniazzi C (2004), Atmospheric Environment, 38:4437–4446.

Viidanoja J, Sillanpää M, Laakia J, Kerminen V M, Hillamo R, Aarnio P, Koskentalo T (2002), Atmospheric Enviroment, 36: 3183-3193.

Williams A, Ellison S L R, Roesslein M (2000) (Eds.), EURACHEM/CITAC Guide Quantifying Uncertainty in Analytical Measurement, 2nd ed. (English).

Chapter 4- High-time resolution sampling and analysis of inorganic ions in particulate Matter

4.1 Introduction

Every parameter related to the variability of the atmospheric pollutants' concentrations, including the PM, undergoes changes during short-time intervals (few minutes or some hours).

This variation depends on the amount of the emitted pollutants, the distance from the sources, the physical condition of the medium in which they are dispersed and their formation processes that can affect both the mass and the volume of air in which this mass is present. The following equation explains what has just been said. It expresses the variation of the concentration C of a generic pollutant *i* with time *t*,

$$\frac{\partial C_i}{\partial t} = \alpha \left[\Phi_i(t)\right] - \beta \left\{C_i\right\} Adv + \sum F_i - \sum R_i - D_S$$

in which are taken into account both the factors affecting the mass and the volume. Factors affecting the mass are the primary emission- expressed by the source emission flow ([Φ_i *(t)*])-, the chemical-physical transformation and chemical removal processes- expressed respectively by F_i and R_i- and the deposition- expressed by D_s. Volume variations are due to the advective phenomena expressed by *Adv* and the convective phenomena expressed by α and $\beta\{C_i\}$, which take into account respectively the stability conditions of the surface layer and the mixing processes.

Given the complexity of the atmospheric processes responsible of these changes, a detailed interpretation of the relationship among the intensity of the sources, the formation processes and the meteo-climatic conditions requires sufficiently high temporal resolution measurements (Kidwell and Ondov,2004a).

As already discussed in the first chapter, PM samples are typically collected during 24 hours (Bukowiecki et al., 2005). These periods are much longer than those in which the changes of the emission sources and the weather conditions occur (Kidwell and Ondov, 2001). However, sometimes it is not easy to perform high-time resolution sampling. For example, regarding the denuder sampling technique (described in paragraph 1.6.4), aimed to sample the inorganic species without artifacts, the ability to increase the temporal resolution of the measurements is hampered by some operative factors. If we want to follow the evolution of the inorganic species every hour for

24 hours, we have to dispose of 24 denuder lines and an operator replacing the line every 60 minutes. Obviously this is not possible for routinely analysis even because the monitoring campaigns can last for weeks or months.

For these reasons, in recent years new sampling and analysis methods aimed to provide dataset with high temporal resolution have been developed. These techniques are grouped into physical and chemical methods. For the first category we shall consider the optical particle counters, while for the second category we will focus our attention on three systems, the Semi-continuous Element in Aerosol Sampler (SEAS), the Aerosol Mass Spectrometer (AMS) and the Particle Into Liquid Sampler (PILS). The latter is object of this section of the work.

4.1.1 Particle optical-counters

The optical particle counters (OPC) is an instrument which allows to count in real time the number of the particles by classifying them according to their size (in general, particles with a diameter greater than 0.05 μm). These devices are made up of a collimated source (a laser) that illuminates the volume in which the air flows.

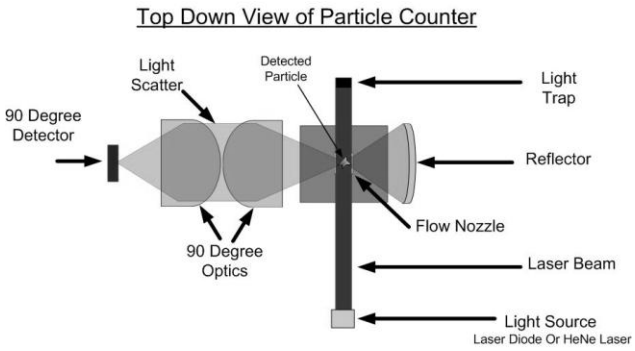

Fig. 4.1: scheme of a particle-optical counter.

A photodetector, positioned at 90 degrees in respect to the axis of the laser beam, measures the light scattered of every single particles by refraction, reflection and diffraction (Figure 4.1). They can determine simultaneously both the number and the size of the particles by measuring respectively the number and the intensity of the pulses reaching the detector.

The intensity of the diffracted light in the various directions depends on the shape and size of the particles but not on their composition.

This method has the advantage of providing an immediate measure of the number of particles present in the air in a given time and, since does not require a membrane, it can perform a continuous measurement. Then it allows to evaluate the temporal evolution of the particle size distributions. It should however be considered that it is not possible to determine the proper shape of the particle; the measure will be related only to the *optical equivalent diameter* that is the diameter of a spherical particle having the same optical behavior of the particle in question, which then spreads the light in the same way. This fact is very important when comparing dimensional data from different measurement techniques: it is not absolutely likely that the optical diameter corresponds to the actual diameter of the particle. It has been demonstrated that the particle shapes are far from a sphere and the particles' surfaces often show a high roughness. Also, these devices calculate the mass concentration by giving a unit density to each particle. Actually, the density cannot be considered equal to 1 and constant for every particle so that very often the mass concentration value is quite different from the real one. Finally, the particles are counted per unit of volume. It has to be noted that the fine particle are much more numerous than the coarse ones, but they contribute much less to the total PM mass. Consequently, the optical-particle counters are very sensitive to the fine dust and very little sensitive to the coarse particles.

4.1.2 Semi-continuous Element in Aerosol Sampler (SEAS)

The SEAS device allows to obtain aqueous solutions from PM particles whit specific dimensions, by means of a specific cyclone that is located at the top of the instrument.

It is substantially constituted by an aerosol concentrator coupled to an automated system for collecting samples collection into the vials (figure 4.2). By means of a peristaltic pump, deionized water is send to an heated chamber (100°C) so as to generate water vapor. The water vapor meets and reacts with the particles contained in the sampled air flow, producing the particle growth. A cooling system (up to 0.5°C) is placed after the heated chamber, leading to the condensation of the vapor and consequently to the formation of the sample solution. Then the solution is conveyed to the collection vials through a system of impactors. Two impactors can be distinguished: the first impactor, *virtual*, reduces the intake flow (can be up to 190 L/min); the second impactor, *real*, guides the solution to the collection vials. An opening, in the proximity of the virtual impactor, connects the pump at the inlet of the air flow and aspires all those species (mostly gas atmospheric) that do not have the strength to reach the impactor. It was observed that with this system particles from 0.08 μm in diameter with a temporal resolution of up to 30 minutes may be sampled (Kidwell

and Ondov, 2004b). To ensure a high aspiration flow the instrument generally works with a very powerful pump. This has two drawbacks:

1. The pump vibrations can damage the instrument;
2. The instrument needs of high amounts of power to work, so for field studies powerful energy generators are needed, difficult to transport and expensive (Pancras et al., 2005).

For these reasons it has been developed a more compact and easily transportable instrument, which operates at a lowest flow (about 16 L/min), but, compared to SEAS, it is affected by lower analytical sensitivity due to the lower flow sampling.

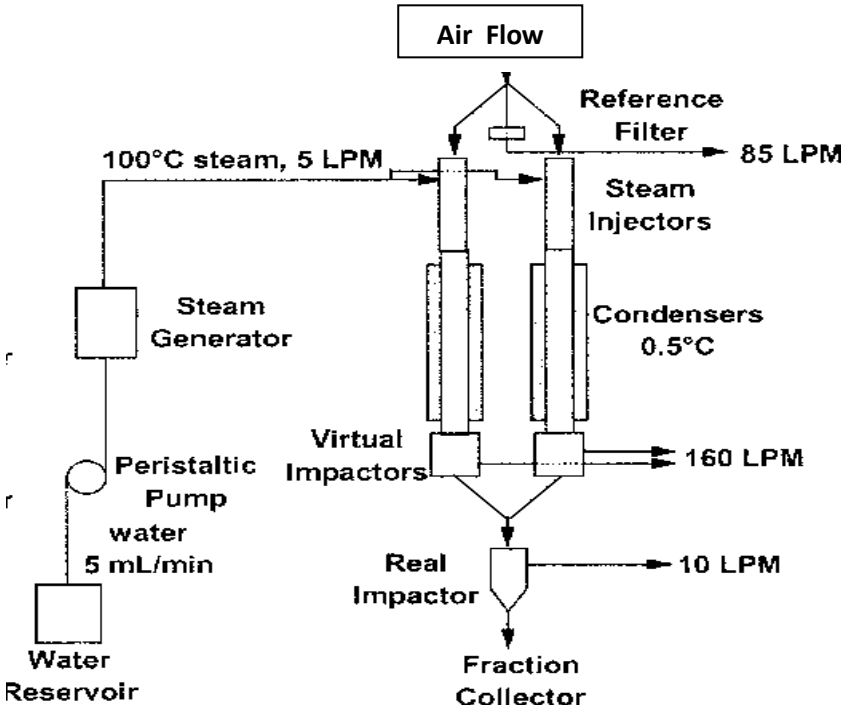

Fig.4.2: schematic representation of a SEAS.

4.1.3 Aerosol Mass Spectrometer (AMS)

The AMS is an instrument able to measure the size and chemical composition of the PM volatile and semi-volatile components with high temporal resolution (up to 1-10 seconds) (Jayne et al., 2000). It is a combination of a mass spectrometer with an atmospheric particulate sampler (Figure 4.3).

The particles, whose diameter has been selected by a cyclone, are forced to enter into an orifice (critical orifice) under the action of an aspiration pump. They are then sent in an aerodynamic lenses system. This latter consists of a series of circular discs (separated by a distance of a few cm)

which have a central hole. The diameter of the holes varies from the first (inlet hole) to the latter (outlet hole) of about 2-4 mm.

The particles and gases undergo a series of expansions and convergences. While the gas can easily diverge so that they are removed, the particles deviate by less and are gradually focused. The last lens generates a supersonic expansion which produces an acceleration of the particles. The particles acquire a velocity dependent on their aerodynamic diameter. Smaller particles are more accelerated while the larger particles, because of the greater inertia, acquire a lower speed.

At the bottom of the lens system a particle separation based on their size occurs. A chopper, which is a rotating disc having two slots, selects the particles' beam to enter in a flight chamber (ToF) When the chopper is open all the particles can pass through, while when it is closed all the particles are blocked. By calculating the time spent by the particles to pass through the flight chamber, the aerodynamic diameter can be known.

After the flight chamber, the particles go through a heated plate (up to 800° C) where is the vaporization of non-refractory species and their ionization by electron impact. Therefore, only the organic species and most of the nitrate and sulphate salts are detected.

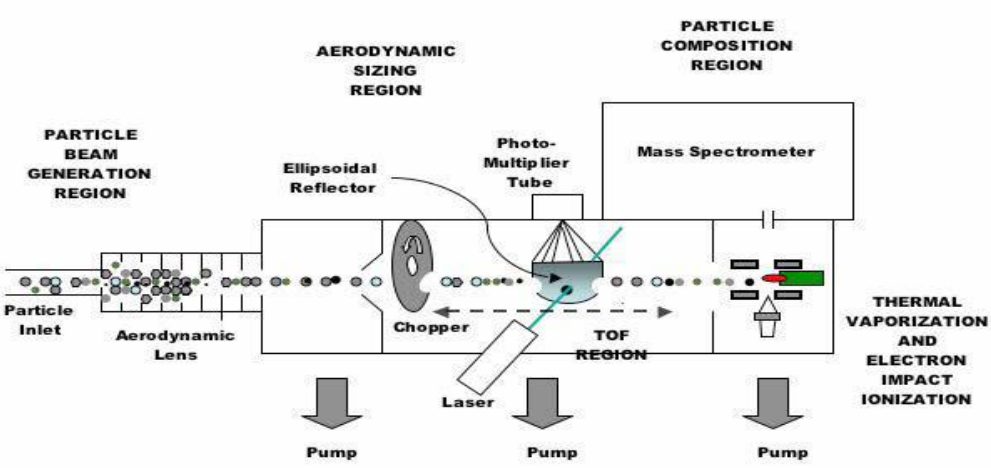

Fig.4.3: Schematic representation of an AM.

All the ionized species are finally send to a mass spectrometer which performs the chemical analysis, giving the chemical composition of every particle.

This instrument can transported by mobile unit but it is very expensive and also only experienced operators can handle the huge amount of provided data.

4.1.4 Particle Into Liquid Sampler (PILS)

The basic working principle of the PILS (Weber et al., 2001) is similar to the SEAS (described in section 4.1.2). It allows to obtain samples of particulate (with selected diameter) in aqueous solutions, with high temporal resolution. Several versions of this instrument have been proposed and the one used in the present work is the most recent. In general, the complete system consists of three main components:

1. A zone of particle growth.
2. A zone of particle impact and collection of the solution.
3. A zone of direct connection to the instrument used for the analysis (in our case the ion chromatograph, IC).

The first two points will described in the present paragraph, leaving the discussion of the last component in the following sections.

As it can be observed in Figure 4.4, the sampler consists of a vapor generator placed perpendicularly at the inlet of the sampled air flow, a central cylinder which acts as a growth chamber and finally an impact structure (enlarged area of Figure 4.4) where the particles impact and are successively collected. The vapor, which is obtained by heating deionized water through a system of electrical resistances, meets the flow of sampled air (inlet by a vacuum pump at about 15 L/min) at the beginning of the conical structure. This happens for two reasons: to avoid the high temperature of the vapor can change the structure and composition of the particulate and to ensure that it works in oversaturation conditions. Oversaturated vapor is the vapor in a condition of unstable equilibrium, at a temperature lower than that would cause its condensation, but that does not condense because the condensation nuclei are absent (Weber et al., 2001). The conical structure, in fact, favors the expansion of the vapor flow, so that it cools. Moreover the walls of the cone favor the condensation of the excess vapor that is sent to a drain (Douglas et al., 2003).

We must also point out that in order to maintain constant the supersaturated environment the heating temperature must be constant and then a thermocouples system checks the temperature value.

The sampled particulate instead, besides favoring the condensation (it is our condensation nucleus), move along the growth chamber up to the impact surface by an inertial push. The impact plate is made of quartz, which is continually "washed" by the collection solution. To make homogeneous the whole impact surface, a steel grid is applied around the quartz plate.

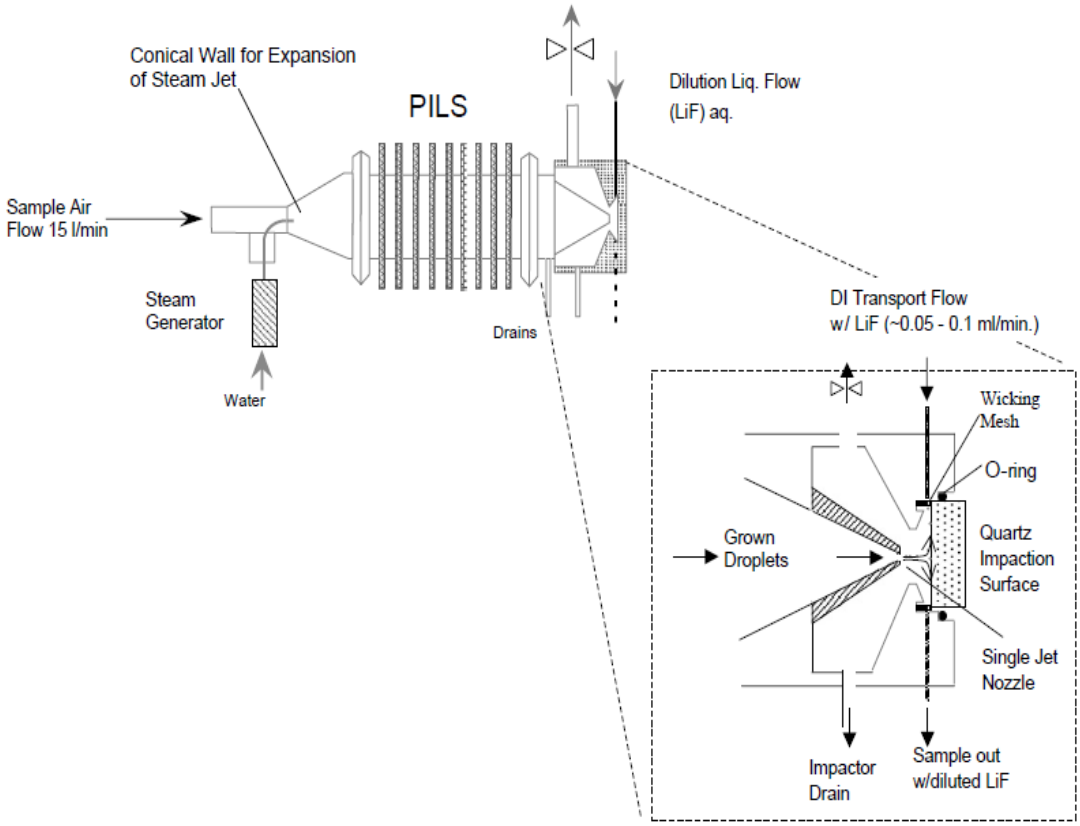

Fig.4.4: Schematic representation of a PILS.

4.2 Aim of the work

This work concerned the sampling and analysis of inorganic ions in the PM, with high temporal resolution. To this purpose, we used the sampler PILS (previously described) coupled with two ion chromatographs placed in parallel, in order to study simultaneously both cations (Na^+, K^+, NH_4^+, Mg^{2+}, Ca^{2+}) and anions (Cl^-, NO_2^-, NO_3^-, SO_4^{2-}).

This type of system is relatively recent, the first works in the literature refer to the early 2000's, and to date the instrument is still under development and validation. The first problem affecting this kind of devices is the achievement of detection limits that are sufficiently low to allow the real-time analysis even in low polluted environments. The PILS works in fact at relatively low flow rates (15 L/min) and, as previously mentioned, operates a significant dilution of the sample due to both the growth phase and the use of the washing solution on the impact plate (Timonen et al., 2010). For this reason, it is often impossible to make a comparison with the reference method (line denuders).

The second problem concerns the temporal coverage of the obtained data. In the usual employment of the system, the collected solutions are continuously sent to the chromatographic loop. Then, the

fraction analyzed by chromatography consist only in the portion of the sample present within the loop at the time of the injection into the column while, during the elution from the column the sample coming from the PILS is directed towards the drain. In standard conditions, with a loop of 200 µL, only the sample collected in about 1 minute is introduced and analyzed by the system. The results are usually considered as representative for the whole duration of the chromatographic run, thus reducing the representativeness of the information.

To this purpose the aim of the present work was to test the method PILS-IC, by introducing a preconcentration system, to reduce the detection limits and at the same time to maintain the temporal continuity of the sampling-analysis phases. After the optimization phase and the validation of the preconcentration system, the analyzer has been used and tested during an intensive monitoring campaign carried out at the Arnaldo Liberti station, located inside the area of the National Research Council of Montelibretti (Rome). This monitoring campaign was under the European Program EMEP (European Monitoring Environment program), which produces regular reports on emissions, concentrations and depositions of the air pollutants, on the relevance of the long-range transport flows and on the overcoming of the standard limits. Moreover the comparison of the results obtained from PILS with those relating to several different techniques, such as the AMS and the denuders, made possible to achieve the full validation of the proposed method.

4.3 Experimental

4.3.1 Materials and devices

H_2O high purity level, obtained by a deionizer Elga LabWater Purelab Plus;

HNO_3 65% Suprapur (Merck KGaA);

Na_2CO_3 (Merck KGaA);

$NaHCO_3$ (Merck KGaA);

Standard solutions (1000ppm) of Na^+, K^+, NH_4^+, Mg^{2+}, Ca^{2+},Cl^-, NO_2^-, NO_3^-, SO_4^{2-} (Sigma-Aldrich);

LiBr (Sigma-Aldrich);

"Spectroquant® Ammonium-Test" (Merck KGaA);

Standard solution (1000 ppm) of Y used as internal standard for ICP-OES analysis, (Sigma-Aldrich);

Methansulfonic acid (Carlo Erba).

Particle Into Liquid Sampler (Metrohm);

Chromatograph 761 Compact IC (Metrhom);

Spettrofotometer UV-VIS, Cary 50 Scan (Varian);

Ion Chromatograph Dionex, ICS-1000;

Ion Cromatograph, Dionex DX-120;

ICP-OES,Varian Vista-MPX;

Analytical balance GIBERTINI EUROPE 60 (0.1 mg sensitivity);

Peristaltic pump WATSON-MARLOW 205S;

All the solutions were taken by micropipettes GILSON previously calibrated, results are reported in table 4.1;

Guard column for anions ION-PAC AG12A;

Guard column for cations ION-PAC CG12A.

Table 4.1: average and standard deviation values (µL) obtained after the micropipettes calibration.

Micropipette 50 µL	**Micropipette 100 µL**	**Micropipette 200 µL**	**Micropipette 500 µL**	**Micropipette 1000 µL**
Mean 50.87	Mean 99.76	Mean 200. 80	Mean 499.99	Mean 1036.70
sd 2.26	sd 1.02	sd 1.06	sd 11.76	sd 56.91
rsd % 4.45	rsd % 1.03	rsd % 0.53	rsd % 2.35	rsd % 5.45

All the glass containers were deeply washed with deionized water, to ensure the maximum cleaning since the low concentration values of the samples.

4.3.2 Chemical analysis

The optimization tests, carried out in our laboratory, involved the use of three analytical techniques: ion chromatography (IC), UV-VIS spectrophotometry and inductively coupled plasma with optical detection (ICP-OES).

Ion chromatography

The anions determination was performed by an anion exchange chromatography with suppression system cartridge and electric conductivity detector (761 Compact IC, Metrhom). Table 4.2 shows the operating conditions at which the analyses were carried out and the type of column used.

The species of interest were: Cl^-, NO_2^-, Br^-, NO_3^-, SO_4^{2-}. In these conditions we obtain a full separation of the ions in about 10 minutes. For calibration standard solution of 50, 100, 500 and 1000 ppb were employed. The correlation coefficient (R^2) of the calibration curves obtained are reported in Table 4.3. Limits of detection (0.1 µg for Cl^- and Br^-; 0.2 µg for NO_2^-, NO_3^- and SO_4^{2-}) were evaluated from six operative blanks by applying the IUPAC method.

Tab. 4.2.: Ion chromatography operative parameters

Column	Metrosep A Supp 4
Guard column	Metrosep A Supp 4/5 Guard
Suppression system	Cation Exchange cartridge, rigeneration with H_2SO_4 $5.6*10^{-2}$ M
Eluent	Na_2CO_3 2.4 mM/$NaHCO_3$ 2.0 mM (5% acetone)
Flow rate	Isocratic 1.2 mL/min

Tab.4.3:Retention time (min) and correlation coefficient of the detected anions.

Anions	**Cl^-**	**NO_2^-**	**Br^-**	**NO_3^-**	**SO_4^-**
Retention time(min)	3.9	4.4	5.3	5.8	9.4
R^2	0.9930	0.9998	0.9998	0.9886	0.9994

UV-VIS spectrophotometry

The ammonium analysis was performed by the Spectroquant ® Ammonium-Test and the reading was made with the UV-VIS spectrophotometer set at a wavelength of 690 nm . The test involves the use of three different derivatizing reagents: at 4-13 pH conditions there is the transformation of ammonia in monocloroammina, which form a colored derivative with thymol blue indophenol. Following the instructions in the tests, it was verified the absence of species present in concentration such that they could cause interference against derivatizing reagents. To construct the

calibration curve ammonium solution of 60, 120, 250 and 500 ppb were used, obviously treated with the same reagents of the Spectroquant Test. Limits of detection (0.01 µg) was evaluated from six operative blanks by applying the IUPAC method.

ICP-OES analysis.

The analysis of Na, Li , K, Mg, and Ca was carried out using the ICP-OES Varian Vista-MPX, because of the absence of a cationic chromatograph in our laboratory. The calibration curve was obtained using standard solution of 2, 4, 9 ppb for the lithium and of 20,50 and 100 ppb for the other elements. Yttrium 100 ppb was used as internal standard to control the plasma fluctuations and the spray processes. All the standard solution were prepared in the same matrix of the samples. Because the cations analyzed were extracted from the preconcentration system with dilute methanesulfonic acid (eluent used in the system PILS-IC),some preliminary tests to rule out the interference in the plasma by the organic matrix have been carried out. From these tests it was decided to treat the sample with a solution of HNO_3: H_2O 1:4.

Denuder lines

The denuder lines used during the monitoring campaign are summarized in figure 4.5.

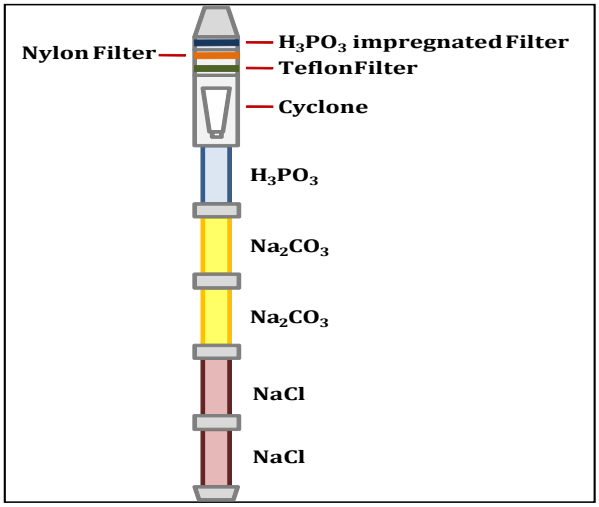

Fig. 4.5: schematic representation of the denuder user in this study

The assembly involves two elements coated by NaCl (0.05% NaCl in a solution of ethanol: water 9:1) for the simultaneous collection of hydrochloric acid (HCl) and nitric acid (HNO_3), followed by two denuders coated with sodium carbonate (1% Na_2CO_3+1% glycerol in a solution of

ethanol/water 1:1) for the simultaneous collection of sulfur dioxide (SO_2) and nitrous acid (HONO). A fifth denuder coated with a solution of phosphorous acid (1% H_3PO_3 in a solution of ethanol/water 9:1) for the specific collection of ammonia. After the coated elements a cyclone with 2.5 µm diameter cut-off and a series of filter packs were placed. The filter pack consisted a Teflon filter (1 µm pore diameter) a nylon filter (1 µm pore diameter) and a filter paper with phosphorous acid, to collect the possible ammonia evolving from the PM collected on the teflon filter. Sampling flow rate and cut-off size of the cyclone were, respectively, 15 L/min and 2.5 µm.

After the sampling phase these filters were extracted in an aqueous solution and the extracted solution was analyzed by IC. These denuder were assembled and analyzed at the CNR laboratories.

4.4 Results and discussion

4.4.1 System assembly

The schematic picture of the PILS used in this study and assembled inside the CNR laboratory is reported in figure 4.6.

At the top of the system two annular denuders in series and a cyclone with a cut-off of 2.5 µm were set up (figure 4.7a). The use of denuders was necessary to block the gaseous species HNO_3 and NH_3 and avoid the interference of these species; for this reason the reagents used to coat the denuders were, respectively, Na_2CO_3 and H_3PO_3. Instead we chose to work with a cut of 2.5µm because the other techniques used in the monitoring campaign (denuders with filter pack and AMS), used to control the system PILS, operated in this mode. A copper tube was used for the air sampling, since this material is not electrostatic, and its walls are physically and chemically inert towards the species to be analyzed (figure 4.7b).

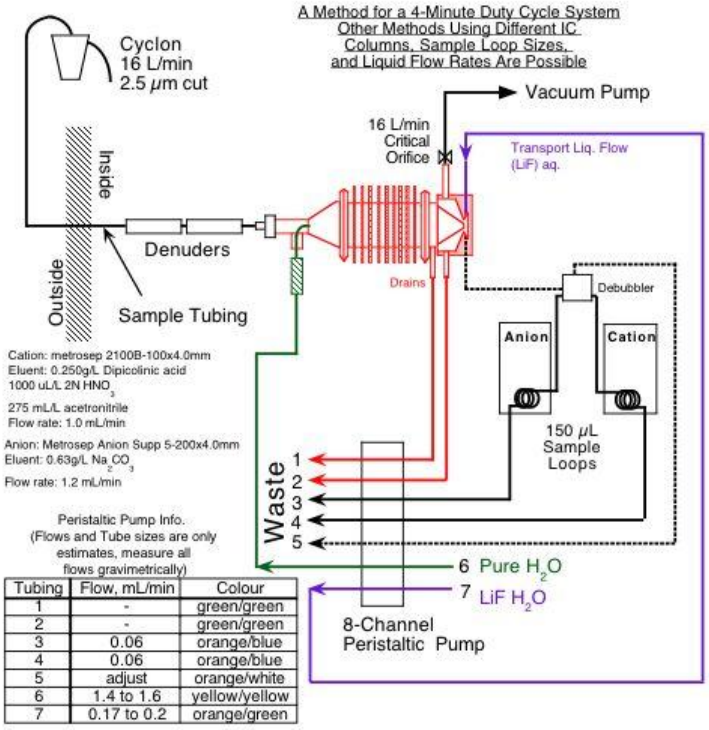

Fig.4.6: schematic PILS assembled in this study.


a)

b)

Figura 4.7: a)annular denuder and cyclone, b) copper sampling tube.

Regarding the PILS, Figure 4.6 also shows schematically the assembly of the hydraulic system. The tubes used are in tygon, of variable diameter and the flow was managed through a single peristaltic pump, equipped with eight channels at a speed of 24 RPM. In Table 4.4 are reported the workflows of the different tubes, distinguished by a different color. The green arrow indicates the transport of the deionized water to the vapor generator, whose task was already discussed in the introduction. In purple we have the transport of the washing solution. In our case this is constituted by a solution of lithium bromide (internal standard method) at a concentration of 50 ppb which has remained constant during the whole campaign. In red we have two drains: the first is aimed to collect the excess water condensed in the growth chamber and the second, located in the vicinity of the impact plate, has the function to not accumulate the washing solution in the impact chamber avoiding phenomena of dilution. In black, finally, we have two tubes connecting physically the sampler to the measuring instruments (chromatographs Dionex ICS-1000 for the anions and Dionex DX-120 for cations, figure 4.8a), and a third tube, called *degassing tube*, which has the task of to not get any air bubbles into the instruments. The degassing system is constituted by a quartz capillary with a shape of "T", oriented perpendicularly to the arrival direction of the solution, so that from the above side the air is eliminated while the degassed sample passes to the underside (figure 4.8b).

Tab. 4.4: Tube types and flows for the PILS system

PILS function	**Tube type**	**Flow (mL/min)**	**Reference to fig. 3.5**
Trasport evaporatio H_2O	Gray/gray (g/g)	1.5	Green
Drain evaporation H_2O	Yellow/yellow (y/y)	0.9	Red
Trasport washing solution	Orange/yellow (o/y)	0.8	Purple
Drain impact plate	Yellow/yellow (y/y)	0.8	Red
Degassing tube	Orange/yellow (o/y)	0.3	Black
Anion analysis tube	Orange/yellow (o/y)	0.3	Black
Cation analysis tube	Orange/yellow (o/y)	0.2	Black

4.4.2 Connection to the ion chromatographs

The connection to the chromatographs and their operation is a fundamental part of this work, so that it was appropriate to dedicate a separated paragraph to a topic that might seem obvious. As previously mentioned, to avoid problems of sensitivity, we operated in such a way as to concentrate the ions on a support, with the consequent need to modify the used devices. In a normal ion chromatograph, the injection of the sample through a syringe or an autosampler takes place by means of a control valve (typically a 6-way valve) integrated by a known volume capillary (loop). So at first the loop is loading (load operation, fig.4.9a), then by rotating the valve the sample is sent to the column (inject operation, fig. 4.9b).

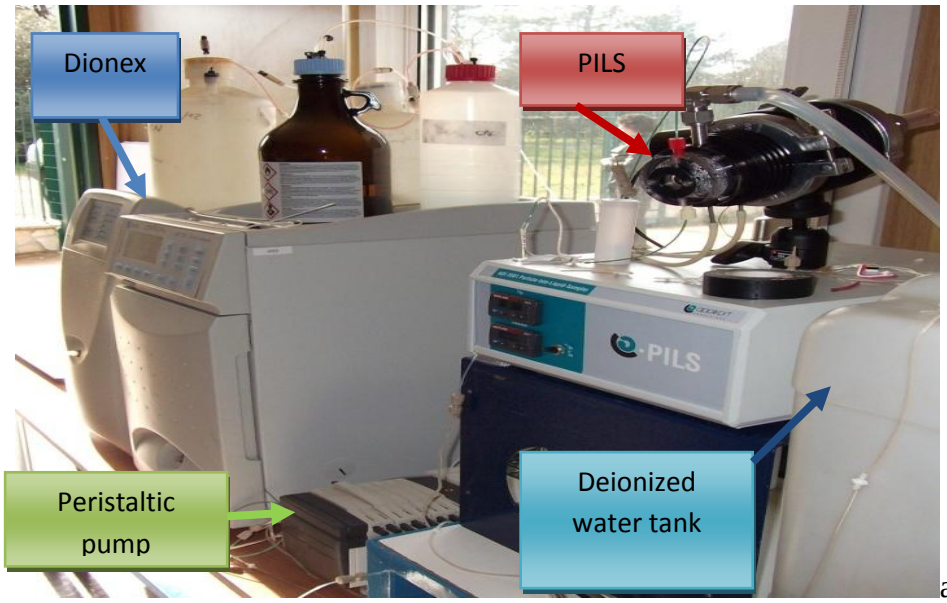

a)

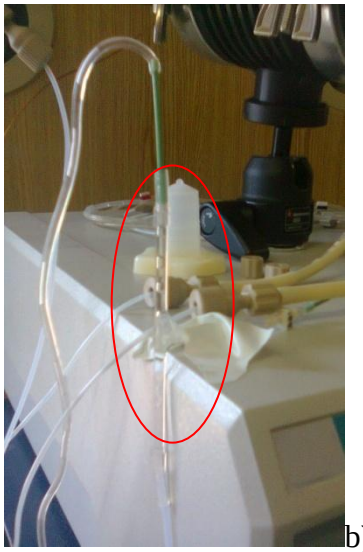
b)

Figura 4.8: a) PILS-Dionex , b) degassing system.

a) 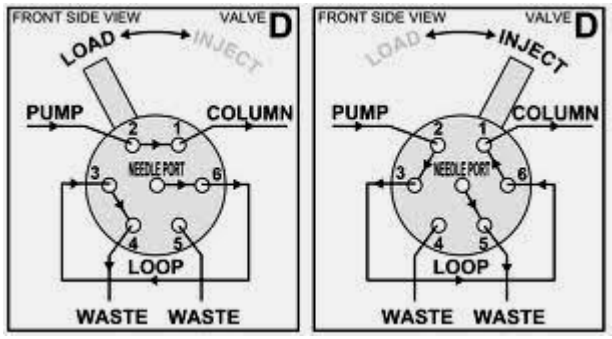

b)

Figura 4.9: 6-way valve a) load phase, b) inject phase.

In our case, the tubes coming out from the impact plate of the PILS were connected to the 6-way valve. Also we disconnected the loop from the valve and placed a pre-column cartridge, which has the task of blocking the ions coming from the PILS (figure 4.10). In this way during the load phase the cartdrige locks the ions, while during the inject phase the eluent solution enters the guard column and brings the ions inside the chromatograph. We should highlight that, in the guard column, the flow of the solution coming from the PILS is opposite to the in-column injection flow (backflush mode) to facilitate the removal of the blocked ions. For anion analysis we used the guard column ION-PAC AG12A, while for the cations the ION-PAC CG12A. The eluent phases were: methansulfonic acid (0.1 M) for the cations, and a mixture of Na_2CO_3 (0.5 M) / $NaHCO_3$ (0.5 M) for anions. The columns used were: the ION-PAC AS12A for the anions and ION-PAC CS12A for the cations. The species of interest were able to accumulate for a certain sampling time (pre-concentration), and then enter directly into the column. It should also be noted that besides the gain of analytical sensitivity, it was possible, during the acquisition of the chromatogram, to set the valve on the load phase, in order to accumulate what in the "normal" mode would definitely lost. The only losses have occurred during the injection, since during the injection phase the guard column is crossed by the eluent solution.

During the monitoring campaign, we set the duration of the load phase for 12 minutes and the injection phase for 3 minutes. The system worked continuously for 24 hours, for about two weeks (from January 29th to February 11th 2013). This was possible with the support of the Chromeleon software, which automatically set the load and inject phases and also allows to check the analysis in real-time.

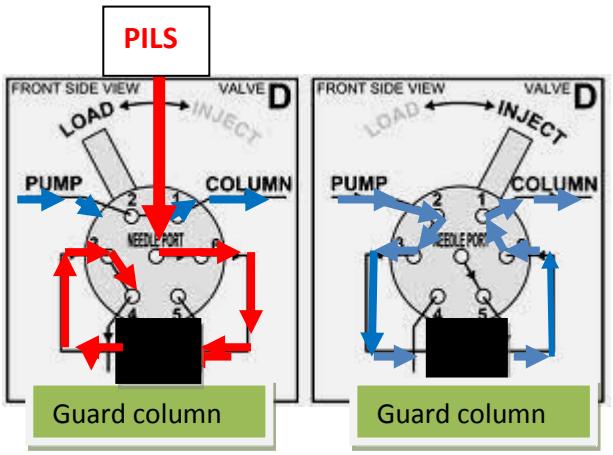

Figura 4.10: injection scheme including the guard column in the 6-way valve.

4.4.3 Optimization tests

Before to use the system Dionex-preconcentrator, a number of tests aimed both to check the guard column performances and to optimize all the procedures to follow during the monitoring campaign were carried out. These tests were performed both on-line and off-line with the Dionex.

Off-line tests.

Off-line mode tests were performed by using solutions of known concentration introduced into the guard columns by means of a peristaltic pump. As regards the recovery the blocked species the have been treated with the same eluent phases used in Dionex in backflush mode. The obtained samples were analyzed by ICP-OES (cations, excluding the NH_4^+), IC (anions) and UV-VIS spectrophotometry (NH_4^+), as described in the experimental section.

BREAKTHROUGH VOLUME

These tests involved the use of two standard solutions for cations and anions. The first consists of 100 ppb of Na^+, NH_4^+, K^+, Mg^{2+} and Ca^{2+} and 7.5 ppb of Li^+, while the second consists of 100 ppb of Cl^-, NO_2^-, NO_3^- and SO_4^{2-}, and 93 ppb of Br^-. These quantities were chosen because they correspond to the higher standard concentrations used for the calibration of the instruments. The standard solutions, were introduced into the guard columns and they were collected in fraction of 5 mL to be analyzed. Results obtained for the cations were reported in figure 4.11. The less retained

species appeared to be the lithium, which around 25 mL of solution reachedthe breakthrough volume. Sodium appeared in the collected solutions at around 50 mL, while ammonium and potassium respectively after 70 and 85 mL were no longer retained. Calcium and magnesium did not appear in the collected fraction even after the passage of 225 mL of solution, resulting in the most retained species. This result was expected, as the employed guard columns are functionally similar to the columns used in the chromatographic analysis of these cations. This explains also why the release of the species has the same order as the chromatographic elution.

Results obtained for the anions are shown in figure 4.12. Also in this case the order of the guard column saturation follows the order of the chromatographic elution. In particular, around 30 mL, 65mL and 125mL the peaks related respectively to chloride, nitrite and bromide were recorded. Nitrate and sulfate, however, have not reached the volume of breakthrough even after the passage of about 300 mL of solution.

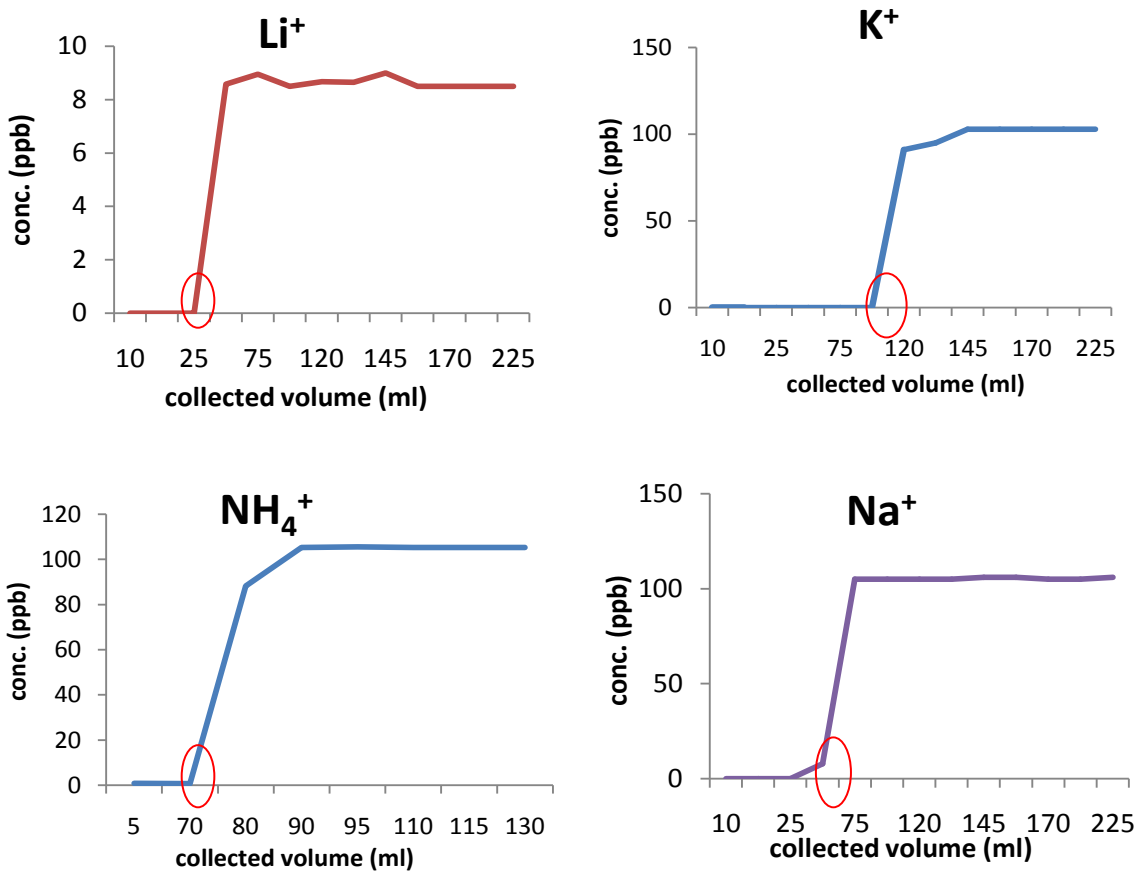

Fig. 4.11: Breakthrough tests for cations.

These tests proved the high load capacity of the guard columns and considering the amount usually found in the atmosphere, we can say that there is no risk to have saturation phenomena resulting in the analyte losses. To give an example, taking the nitrite as reference, up to 65 mL of a 100 ppb solution do not have breakthrough phenomena. This means that 6.5 µg of nitrite are present in the column, a very high amount compared to those obtainable by using the system PILS-IC in preconcentration mode.

Further verification was performed by placing two cartridges in series and by passing a volume twice than that used in the analytical system, to verify the absence of the analytes in the second cartridge.

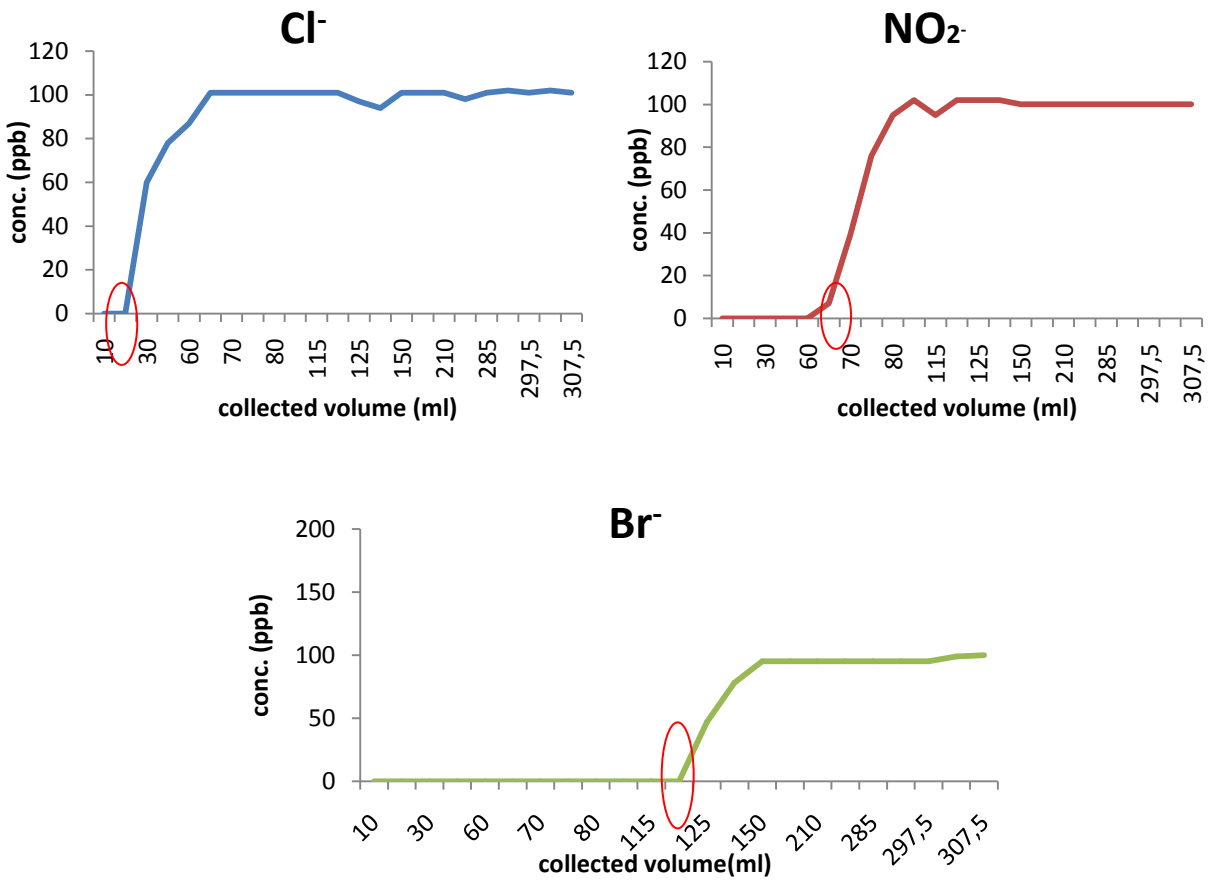

Fig.4.12: Breakthrough tests for anions.

RECOVERY TESTS

To perform this test the same standard solutions of the breakthrough test were used. The species were accumulated for 12 minutes in the guard columns. The volume was collected and quantified by weighing. Then the cartridges were eluted in backflush mode with 1 mL of the Dionex eluent phases, and the resulting solutions were collected and analyzed. Knowing the title and the volume of the solution used, we calculated the theoretical amount of the inorganic species blocked. While by the analysis of the recovered solutions the experimental value was obtained. The ratio between the experimental and the theoretical gave the value of the recovery for each species (Table 4.5).

Tab 4.5: Recovery and standard deviation values (%) of the preconcentration cartridges (N=6).

	Cl^-	NO_2^-	Br^-	NO_3^-	SO_4^{2-}	Li^+	Na^+	K^+	NH_4^+	Mg^{2+}	Ca^{2+}
R±SD(%)	101±6	97±4	99±2	100±2	96±3	95±1	98±2	96±6	101±3	99±3	97±5

On-line tests

On-line mode tests were performed by connecting the guard columns to the 6-way valve. Through these tests it has been possible to solve the different problems arisen during the planning phase of the work. The main doubts were due to the behavior of these guard columns, as they were used for a purpose other than for which they were designed.

EVALUATION OF THE LOAD AND INJECT TIMES

In the previous section we described the sampling and analysis times. To optimize these times two points were considered. First of all to have data with a high temporal resolution the sampling and analysis phases have to be temporally closest as possible. Secondly the necessity to send into the column all the species blocked in the load phase. As regards the first point, we considered that the last species to be eluted have a retention times around 10-11 minutes and then to have the complete chromatogram we could not fall below this limit. As regards the second point, we must remember that during the inject the solution coming from the PILS is lost. So on one hand we have the need to minimize this time and on the other hand we must be sure to analyze all the blocked species.
To assess this time we made a simple test: we loaded the pre-column with a standard solution containing all the ions and, before giving inject, we disconnected the chromatography column,

creating a direct connection of the guard column to the detector. Since there was not a chromatographic separation, all the ions arrived simultaneously to the detector, giving a single peak. The inject time was then chosen on the basis of the peak width.

The Figure 4.13a refers to the anions. From the enlarged imagine on the right it can be seen that the conductivity returns to the baseline value after 2 minutes, so that this time is sufficient to send the all the species in the column. Figure 4.13b refers to the cations. In this case the time required to "clean up" the cartridge is equal to 3 minutes.

From these results we decided the time scale used during the monitoring campaign: 12 minutes to conclude the chromatographic run and 3 minutes to injected all in column.

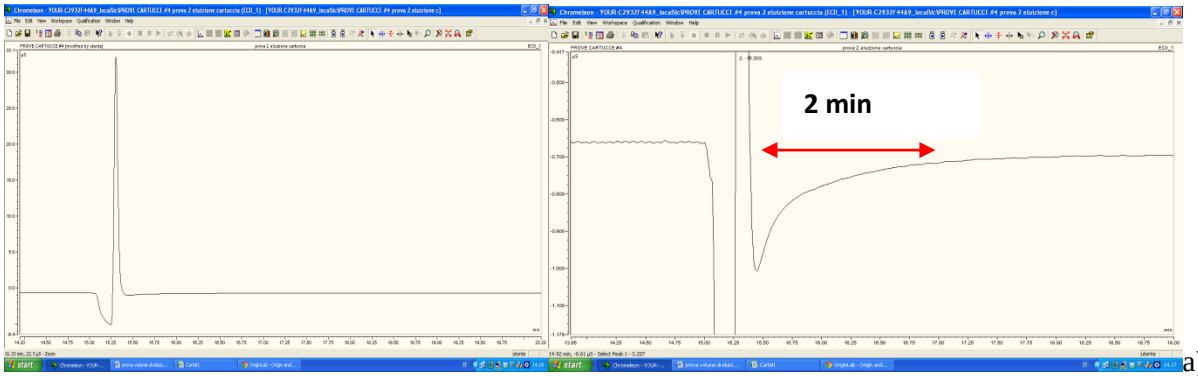

a)

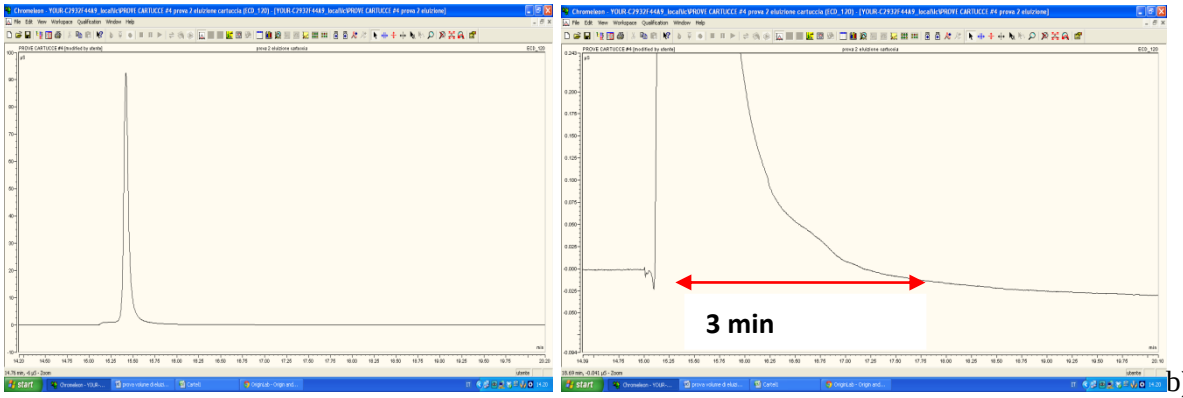

b)

Figura 4.13: Results of the injection times, a)anions and b)cations.

CALIBRATION OF THE SYSTEM.

Even for a simple operation such as the calibration, it was necessary to perform some tests. Calibration can be performed both with or without the connection of the pre-concentration cartridge to the chromatographic system. To assess the differences between the two methods, we operated in

both the ways and compared the results. The mode with the system of pre-concentration was performed by using three standard solutions, both for cations and anions, of 25, 50 and 100 ppb. For each solution 3 replications were performed. We applied the program of 12 minutes of load and 3 minutes inject, collecting the output volumes that were then quantified by weighing. Even with the loop mode (without pre-concentration column) 3 standard solutions of the species were used and 3 replications were done. To prepare these solutions, the amount (μg) of each species used in the test with cartridge inserted into the valve were calculated (knowing the volume and concentrations of the standard solutions). Subsequently, based on the volume of the loop (25μL), the final standards were prepared (for the anions 3.2, 6.4 and 12.8 ppm, while for the cations 2.6, 5.2 and 10.4 ppm), to send the same amounts of ions into the column. Comparison were than done on the bases of the areas' values.

The response linearity was satisfactory in both the modes, with linear regression coefficients greater than 0.9. However, from the values obtained, the areas corresponding to the injected quantities are different depending on the injection mode. In particular there is a general increase of the areas in the tests carried out using the loop. The differences cannot be attributed to a low recovery of the species from the pre-concentration cartridge, since the recovery tests showed values exceeding 95%. It is likely that these differences are attributable to the low linearity of the conductivity detector and to the chromatographic peak broadening due to the use of the cartridge. This aspect, not yet understood, deserves further study, but led us to perform the calibration of the chromatograph using the pre-concentration system.

MEMORY EFFECT AND RECOVERY TESTS

It was verified the occurrence of memory effect phenomena, i.e. it was assessed if the analysis of consecutive samples could be considered independent or the results were influenced by the previous determination. The test was conducted in two phases. The first involved the analysis of a standard solution with the same program used during the campaign monitoring. In the second instead we simulated the load phase for 12 minutes (disconnecting the peristaltic pump) and then the inject phase involved the unloading cartridge.

The chromatograms obtained from these tests can be seen in figure 4.14. The first image refers to the cations, and we can see a profile without peaks. In the second image, referring to the anions, we notice the presence of two peaks, not particularly pronounced. Therefore, the retention time of the first peak does not correspond to the studied species. Instead the second peak is close to the position

assigned to the chlorides, but we must emphasize that it is extremely less pronounced, to be confused with the background noise and comparable to the blank value. We can conclude that in the described conditions, this system does not suffer from memory effect.

Additional recovery tests were carried, in which known amounts of standard solutions were injected into the chromatograph in back flushing mode. These tests confirmed the values obtained in the off-line system and also constituted a confirmation of the adopted calibration mode.

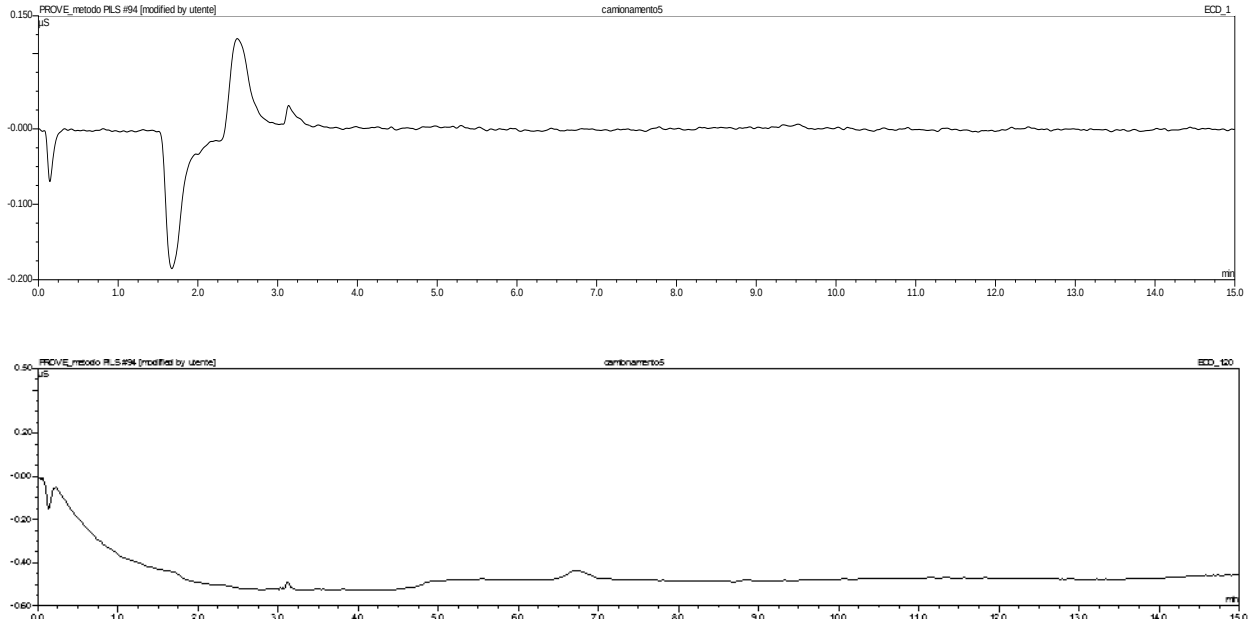

Fig.4.14:Tests to evaluate the memory effect on cations (upper panel) and anions (lower panel).

4.4.4 LODs and LOQs

The PILS-IC system is quite complex from the analytical point of view. The stage of sampling and analysis cannot be separately considered. We assessed the LOD and the LOQ of the method with the entire system in the working phase. In practice we replaced the denuders with the filters which are normally used for the 24 hours sampling. In this way both the particles and the volatile species were blocked before entering the PILS. So, what reached the instruments and analyzed, was considered our operative blank. LODs and LOQs values were calculated by following the IUPAC definitions (IUPAC,1997):

LOD = Xb + 3sb

LOQ = Xb + 10sb

Where Xb is the mean value of the single species found in the blank and sb its standard deviation. In our case, we performed 6 blanks and the results are reported in table 4.7.

Nitrite and nitrate were not detected in the blank, so we proceeded differently. We analyzed standard solutions in descending concentration, up to obtain a signal equal to 3 and 10 times the background noise, conventionally accepted as indicators of LOD and LOQ.

Tab.4.7: LODs and LOQs values (N=6) calculated with the pre-concentration system.

	µg m^{-3}			**µg m^{-3}**	
Anions	**LOD**	**LOQ**	**Cations**	**LOD**	**LOQ**
Cl^-	0.01	0.02	**Na^+**	0.01	0.01
NO_2^-	0.001	0.002	**NH_4^+**	0.007	0.01
NO_3^-	0.003	0.005	**K^+**	0.005	0.007
SO_4^{2-}	0.02	0.04	**Mg^{2+}**	0.01	0.02
			Ca^{2+}	0.02	0.04

Analogous tests were carried out to evaluate LOD and LOQ without cartridge. In these tests a loop of 100 µL was used and the operating procedures were identical to those previously described. For the quantitative was employed the calibration curve obtained with the loop of 25 µL.

The results obtained are shown in table 4.8. The blank values in this case were quantifiable only for Na^+ and Cl^-, which the LOD and LOQ are slightly higher than those obtained with the preconcentration due to a lower repeatability of measurements. For all the other analytes, the balnk was not quantifiable and the values of LOD and LOQ were determined on the basis of the calibration curve, using the procedure previously described for NO_2^- and NO_3^-. As can be observed, the values obtained are much higher (10 to 15 times), confirming the improvement obtained by using the pre-concentration system.

Tab.4.8: LODs and LOQs (N=6) values calculated without the pre-concentration system.

	µg m^{-3}			**µg m^{-3}**	
Anions	**LOD**	**LOQ**	**Cations**	**LOD**	**LOQ**
Cl^-	0.02	0.04	**Na^+**	0.02	0.03
NO_2^-	0.01	0.03	**NH_4^+**	0.1	0.1
NO_3^-	0.05	0.07	**K^+**	0.07	0.1

SO_4^{2-}	0.2	0.6	Mg^{2+}	0.1	0.3
			Ca^{2+}	0.3	0.6

4.4.5 Calculation of the atmospheric concentrations

Before to discuss the results obtained from the monitoring campaign, we need to specify the mode in which the data provided by the two chromatographs were processed. In the classic use of PILS, there are two ways to use the instrument: with or without the internal standard in the washing solution.

In the first case, the calculation of the ion concentration is given by the following formula:

$$[C_a] = [C_L] * q_{in} * R / Q_a \quad (4.1)$$

where:

Ca is the concentration of the species in the ambient air (in µg m^{-3}), C_L is the concentration of the species in the sample liquid (µg/L) coming from the impact plat, q_{in} is the internal standard flow calculated at the entrance of the impact plate (ml/min), R is the ratio between the internal standard concentration at the entrance and at the exit of the impact plate. This factor takes into account the dilution of the sample due to the water condensation. *Qa* is the flow of the sampled air (L/min).

In the second case, instead, the formula to be applied is the following:

$$[C_a] = [C_L] * q_{smp} / Q_a \quad (4.2)$$

where:

Ca is the concentration of the species in the ambient air (in µg m^{-3}), C_L is the concentration of the species in the sample liquid (µg/L) coming from the impact plat, q_{smp} is the flow of the liquid sample at the entrance of the chromatograph (ml/min), Qa is the flow of the sampled air (L/min). Operating in the second mode brings to obvious difficulties. First of all the exit flow from the PILS must be continuously measured, and this necessarily involves the interruption of the analysis. Furthermore, in a system with two devices connected in series, as in our case, the use of an internal standard is useful to understand how the PILS output solution is distributed between the two chromatographs.

We then operated in the first mode using lithium bromide as the internal standard. Despite this choice, the related formula cannot be used in our work. In fact there are two terms in equation 4.1, C_L and *R*, that in a pre-concentration system cannot be detected, so we operated in terms of amount of substance (µg or ng).

The calculation in μg m^{-3}occurred in two phases. In the first we correlate the obtained areas with the mass. In fact, during the calibration of the instruments, we collected the standards' volume passed through the cartridge and quantified it by weighing. Knowing the volume and the concentration of the standard, we calculated the mass (ng) and we constructed the calibration curves in ng. A summary table with the results obtained for all the species is reported (Table 4.9).

In the second phase, we calculated the concentration of the ions in the environment. To do this we have taken into account that the values provided by the instruments, are related to the fraction of solution that has reached the single chromatograph. To get the total result, we obtained the theoretical value of the areas of the internal standard at the entrance of the PILS. Subsequently, from the ratio between the areas of the internal standard obtained in the analysis phase and the theoretical one, we obtained the multiplicative factor to apply to all the analyzed species. Finally, dividing these amount by the pump flow (14.65 L/min), we obtained the values in μg m^{-3}.

Tab.4.9: Correlation coefficient values (R^2) obtained from the calibration curves of the ions.

Cations	R^2	Anions	R^2
Li^+	0.99	Cl^-	0.99
Na^+	0.99	NO_2^-	0.99
NH_4^+	0.92	Br^-	0.99
K^+	0.99	NO_3^-	0.99
Mg^{2+}	0.98	SO_4^{2-}	0.99
Ca^{2+}	0.98		

4.4 Application of the PILS-IC system to a monitoring campaign

The final phase of the work focused on the application of the optimized system to an intensive monitoring campaign. The monitoring was carried out at the CNR Institute of Montelibretti (Rome). This station consists of several buildings, inside which it is possible to assemble different instruments and samplers. The image in figure 4.15 shows the cabin assigned to the PILS–analysis.

Fig. 4.15:Picture of the working station.

The monitoring campaign started on January 29th, 2013 and ended on February 11th, 2013. In this period we measured the main meteorological parameters (wind speed and direction, precipitation, pressure, relative humidity, etc). Also the natural radioactivity was measured to know the height of the mixed layer. During this period other techniques have been used to support the PILS-IC. In particular, from 20:00 of January 29th to 17:00 of February 1st, the comparison was made with a system of denuders with three-hourly resolution . Throughout the campaign, also the AMS system remained active so that we could make further comparisons. These comparisons can be useful to provide additional information on the robustness of the validated method. However it should be noted that, to date, there is no system enough reliable to be considered as a reference method for the validation. The denuder lines represents the effective system to determine the inorganic species of the PM without being affected by the artifacts due to the solid - vapor equilibria. However these systems are typically used with a temporal resolution of 24 hours, due to the high values of the blanks and excessive analytical times. The AMS, which allows a high-time resolution monitoring (5 min), can measure only a few species (ammonium nitrate and sulphate) and does not allow a quantitative measure, because the system calibration is complex. The calibration phase of the AMS, in fact, requires the generation of aerosol by nebulizing a solution of ammonium nitrate. The "known" amount used for the calibration is estimated through a counter device placed in series to the nebulizer.

4.4.1 PILS-denuder data comparison

Because of a lack of a reference standard, PILS data were compared with those obtained by other techniques. A first comparison is done with data obtained by the denuder system sampling.

As already mentioned, the temporal resolution of denuders was three hours so that the PILS data were averaged over this time. The comparison was not performed with all the ions determined by PILS because some of them (Na^+, Mg^{2+} +, Ca^{2+} +, K^+, NO_2^-) are not detectable with the three-hourly sampling denuder (<LOQ). In Figure 4.16 the temporal trend of the species analyzed by both the techniques are reported. The lack of PILS data in some sections was not related to detection limit problem, but to a failure of the software managing the chromatographs. Although the comparison was made for a short time only, some important conclusions can be pointed out. Qualitatively, the concentrations follow rather faithfully the same trend for all the analyzed species. From the quantitative point of view there are some discrepancies, more marked for Cl^- and NH_4^+. This is likely due to the high blank values registered in the back-up filters of the denuders. These values are variable and fairly close to the measured values, resulting in an increase of the repeatability uncertainty which is reflected in the inter-comparison technique. As previously discussed, the PILS, thanks to the optimized pre-concentration system, reached LOD and LOQ values sufficiently low to allow a good repeatability of the measurements during the whole campaign. This comparison does not allow to verify the data quality of PILS, but it is necessary to assess the equivalence of the measured concentration levels. Correlations tests and recovery percentage on the data obtained with the two systems (Tables 4.10 and 4.11 respectively) were performed.

A good correlation, pointed out from the R^2 values, is found for chloride, nitrate and sulfate, while, as expected, ammonium does not show a satisfactory agreement between the techniques. It may however be noticed that the slope values, which represent the coherence of the two techniques from the quantitative point of view, are in all the cases quite close to unity. Values lower than unity are obtained only for chloride, due to the denuder measurements affected by high blank values and to a partial dragging of NaCl used to impregnate the denuder up to the filter. Results of table 4.11 show that the average recoveries are good enough for all the ions, although the standard deviation is quite high, probably due to the low data repeatability of the denuder lines.

4.4.2 PILS-AMS data comparison

In this section the comparison between PILS and AMS data will be discussed. The AMS is able to analyze only not-refractory species, which are characterized, after the ionization, by a specific value

of the ratio m/z. For this reason, the comparison has been done only for NH_4^+, NO_3^- and SO_4^{2-}. The data of the AMS were averaged over 15 minutes, since the AMS had a temporal resolution of 5 minutes. Trends of the species are reported in figure 4.17.

The concentration trends are in good agreement throughout the whole monitoring campaign. This confirms the qualitative excellent results provided by the PILS. From the quantitative point of view, however, we found in this case substantial differences, in agreement with the difficulties occurred during the AMS calibration. To highlight the dual nature of the results, also in this case tests of correlation were performed. The results are reported in table 4.12.

In this type of comparison, as already seen, the slope value indicates the quantitative agreement between measurements carried out with different techniques. In our case all the found values deviate much from the optimal value (1), and then there was a problem in at least one of the two techniques. Good results, however, have found for R^2 value. This indicates that the two techniques well agree qualitatively. Ammonium deviate from the linearity at high concentrations, probably due to the lack of linearity in response typical of the IC analysis with suppression system. In fact in this work we have chosen to calibrate the instrument at concentration levels typically found in 24-hours sampled filters. Increasing the temporal resolution some very high concentrated peaks occurred, which led some values outside the range of linearity. Clearly this problem can be solved by adopting a calibration curve or a combination of calibration curves in different concentration ranges.

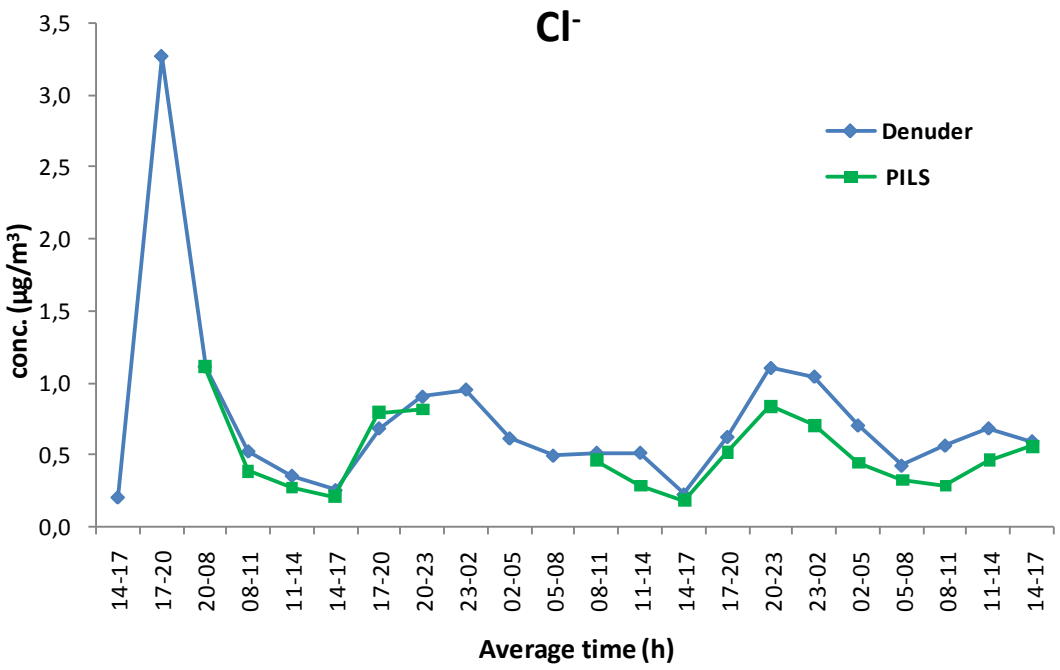

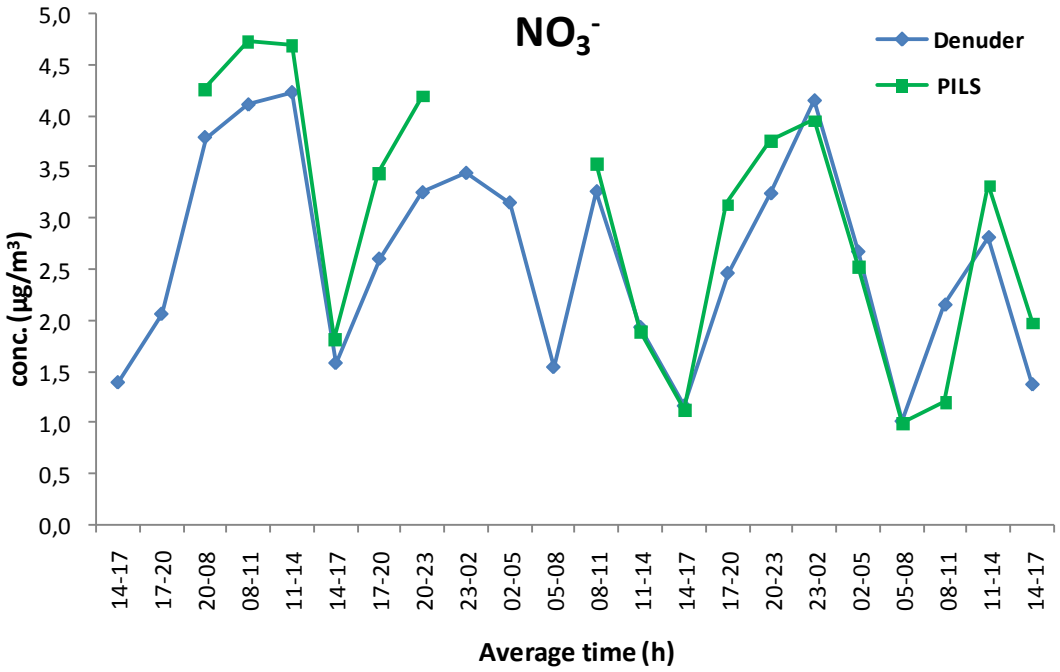
NO3-
Denuder
PILS
conc. (µg/m³)
5,0
4,5
4,0
3,5
3,0
2,5
2,0
1,5
1,0
0,5
0,0
14-17
17-20
20-08
08-11
11-14
14-17
17-20
20-23
23-02
02-05
05-08
08-11
11-14
14-17
17-20
20-23
23-02
02-05
05-08
08-11
11-14
14-17
Average time (h)

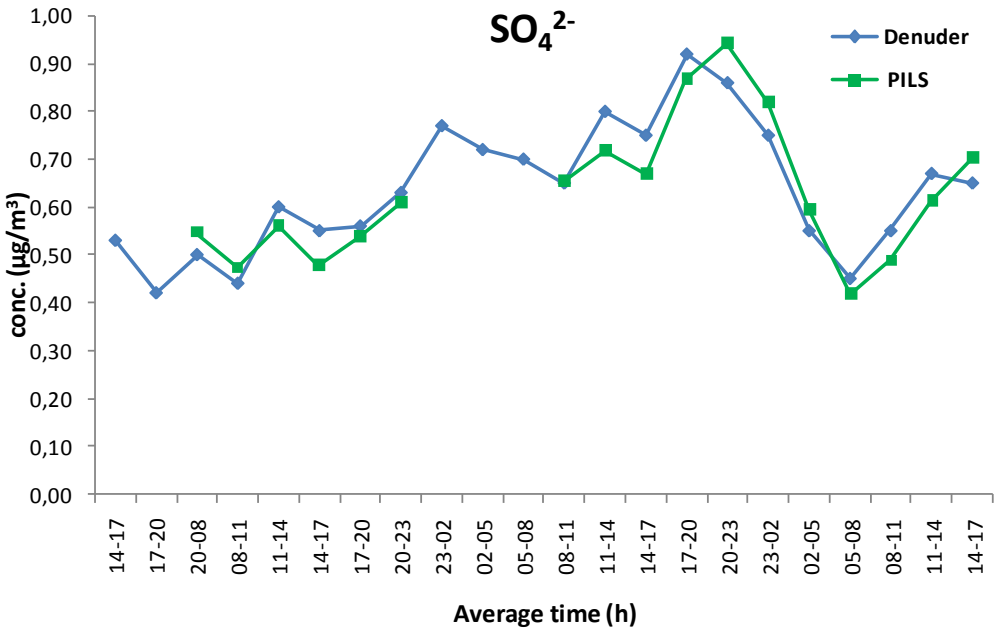
SO4 2-
Denuder
PILS
conc. (µg/m³)
1,00
0,90
0,80
0,70
0,60
0,50
0,40
0,30
0,20
0,10
0,00
14-17
17-20
20-08
08-11
11-14
14-17
17-20
20-23
23-02
02-05
05-08
08-11
11-14
14-17
17-20
20-23
23-02
02-05
05-08
08-11
11-14
14-17
Average time (h)

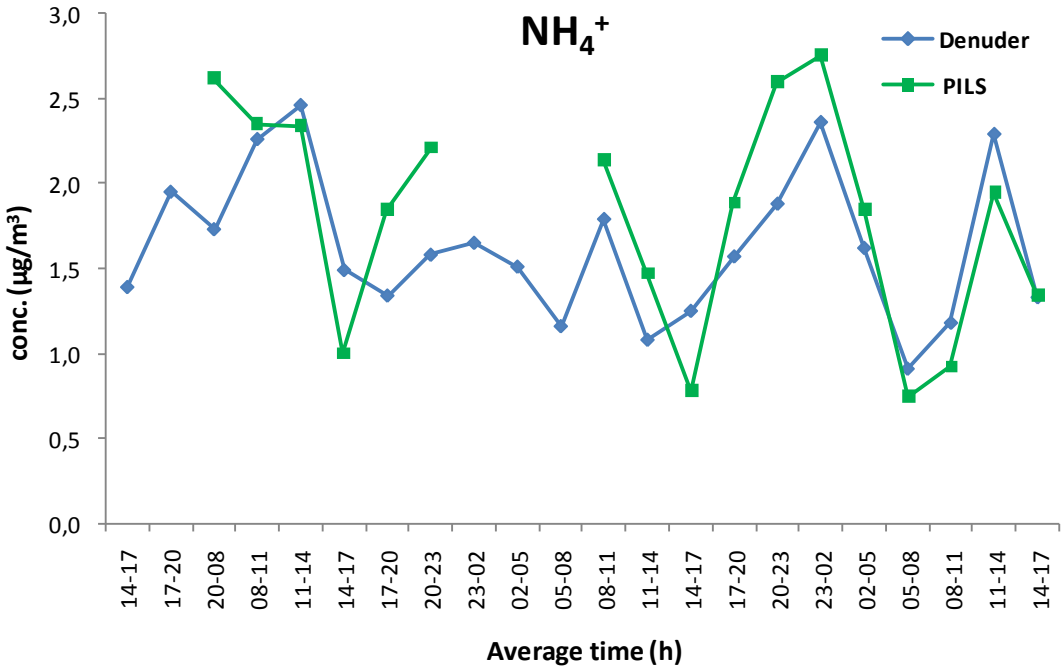

Fig.4.16: Comparison between PILS and denuder data for Cl^-, NO_3^-, SO_4^{2-}, NH_4^+.

Tab. 4.10: PILS-denuder correlation values.

Ion	Equation	R^2
Cl^-	y=0.87x-0.05	0.81
NO_3^-	y=1.19x-0.08	0.87
SO_4^{2-}	y=0.97x+0.01	0.85
NH_4^+	y=1.10x-0.01	0.60

Tab.4.11: PILS-Denuder recoveries values and SD (%).

	Recovery%			
Temporal range (h)	**Cl^-**	**NO_3^-**	**SO_4^{2-}**	**NH_4^+**
20-08	101	112	58	152
08-11	74	115	59	104
11-14	76	111	80	95
14-17	82	114	102	67
17-20	116	132	83	138

20-23	90	129	77	140
08-11	89	108	81	119
11-14	55	98	67	136
14-17	80	96	82	63
17-20	82	127	82	120
20-23	76	116	82	138
23-02	67	95	65	117
02-05	63	95	87	114
05-08	76	97	93	82
08-11	50	56	114	78
11-14	67	118	128	85
14-17	94	143	135	101
Average R%	**79**	**110**	**98**	**109**
SD	**17**	**20**	**8**	**27**

Tab. 4.12: PILS-AMS correlation values.

Ion	**Equation**	**R^2**
NO_3^-	y=2.7x-0.07	0.91
SO_4^{2-}	y=2.9x-0.08	0.85
NH_4^+	y=4.1x+0.2	0.92

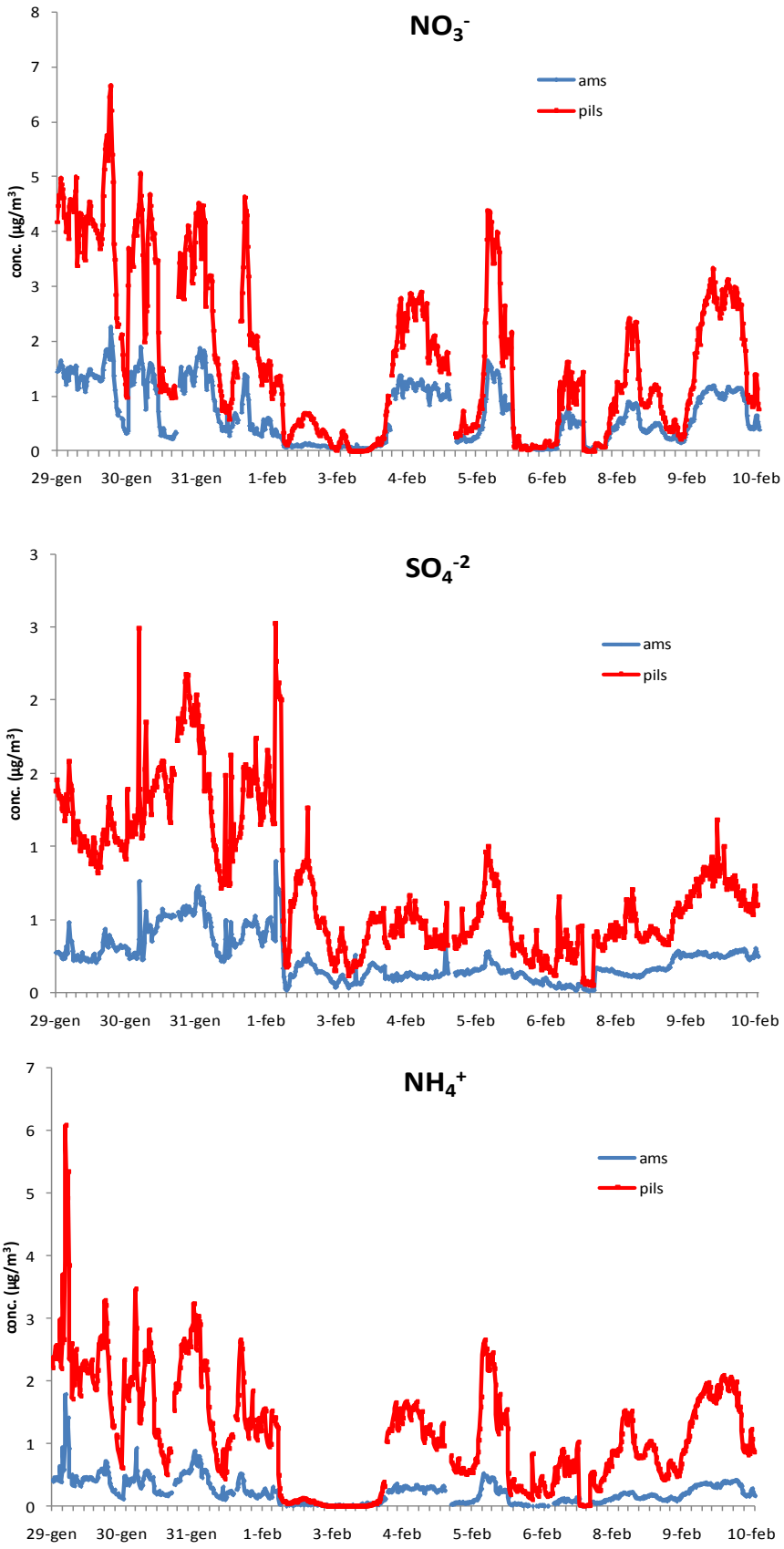

Fig. 4.17: Qualitative comparison between PILS and AMS data for NO_3^-, SO_4^{2-}, NH_4^+.

4.4.3 Monitoring campaign results

Final results about the monitoring campaign have not yet been obtained and discussed. In fact, the measurements performed by the optimized method described in this work, are only a small part of a larger and articulated monitoring project. To interpret the obtained data a comparison whit the meteo-climatic parameters is necessary, particularly with the natural radioactivity. Preliminary results can be shown and discussed to point out the fundamental concepts in studying the atmospheric pollution. The wide importance of the high time resolution sampling can be better understood giving a look to the figure 4.18.

All images refer to the same sampling period, the upper panel shows the 24-hours sampling (performed by the denuder). The middle panel shows a temporal resolution of 3-hours, up to reach a resolution of 15 minutes, obtained by the system PILS-IC (lower panel). In the first panel only three concentration levels relative to three days considered can be known, providing no more information about the quantities distributed throughout the day. The three hours resolution provides slightly more complete information but it fails, for example, to distinguish the day/night variability. The information supplied by PILS (every 15 minutes) is instead definitely more comprehensive. Observed maxima and minima points cannot be detected by other sampling procedures, so it is possible to know some possible immission sources, always considering the mixing properties of the lower atmosphere. It should be noted that the observed variability is not the result of a background noise, but it represents the actual changes in concentrations over a very short time scales. This is confirmed by comparison with the AMS measurements which have the same qualitative trend. The interpretation of these rapid changes is not easy, but it can provide useful information about the processes of formation of the secondary species and about the spatial modulation of the monitored concentrations. A first key to the interpretation consists of comparing the obtained data with the natural radioactivity in the same sampling period. The radioactivity data have 1-hour time resolution (figure 4.19). We can see that they are extremely variable, and this is another reason why it is necessary to get high temporal resolution data. The maximum values indicate atmospheric stability due to the absence of mixing phenomena, while the lower values indicate the occurrence of convective phenomena.

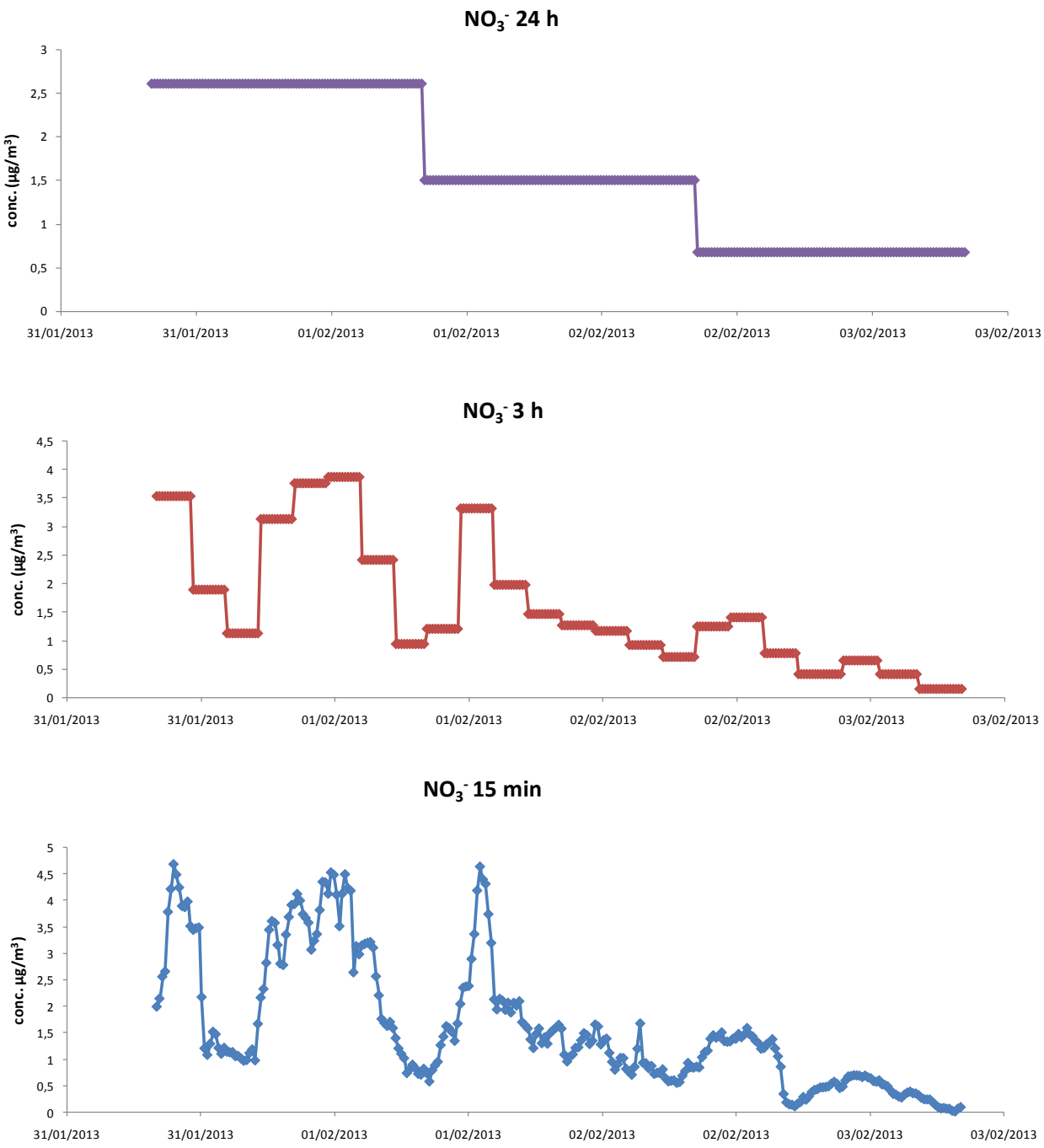

Fig. 4.18: Different temporal resolution obtained for NO_3^-.

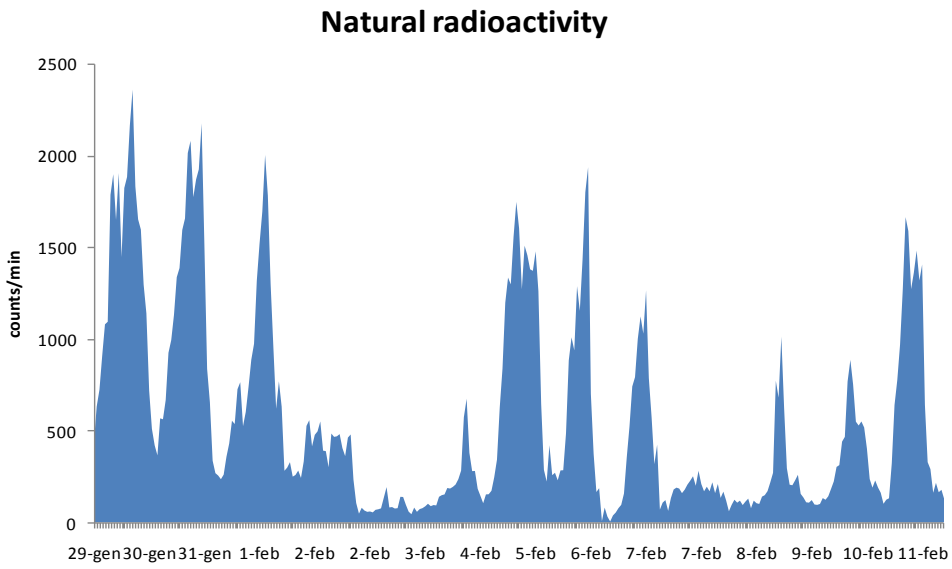

Fig.4.19: Natural radioactivity trend during the monitored period.

As already mentioned, the study is not yet complete and final. However some first considerations can be done by looking at the following graphs (figure 4.20) showing the measured ions with PILS-IC and comparing them with the natural radioactivity trends (figure 4.19). This comparison has only a qualitative scope, because the temporal resolution of both the measurements is different (15 mins for ions vs 1 hours for natural radioactivity). Looking at both the trends two different situations can be observed. In the first one (till February 4th) the ion and the natural radioactivity concentrations follow opposite trends. In particular, in correspondence of the minimum radioactivity values, maximum peaks for Cl^-, Na^+, Mg^{2+} and SO_4^{2-} were registered around February 3rd (signed by red arrows). This is due to an emission event (local sources or transport phenomena), the nature of which can be assumed on the basis of the involved species, and confirmed through the meteorological parameters. Indeed, species such as Cl^-, Na^+ and Mg^{2+}, are now recognized to be tracers of the marine aerosol source, while the sulphate is linked to pollution phenomena. These hypotheses are confirmed by comparison with the results obtained from the model Hysplit. This model, as widely discussed in Chapter 2, is able to reconstruct the origin and the path of the air masses which have affected a particular area, starting from meteorological parameters.

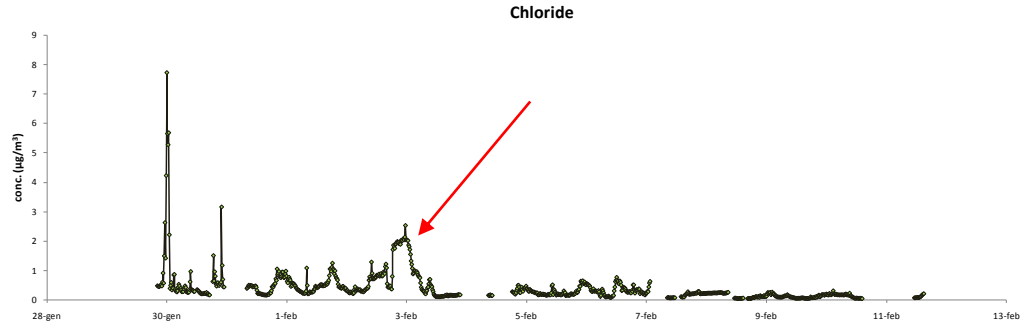
Chloride
conc. (µg/m³)
0
1
2
3
4
5
6
7
8
9
28-gen
30-gen
1-feb
3-feb
5-feb
7-feb
9-feb
11-feb
13-feb

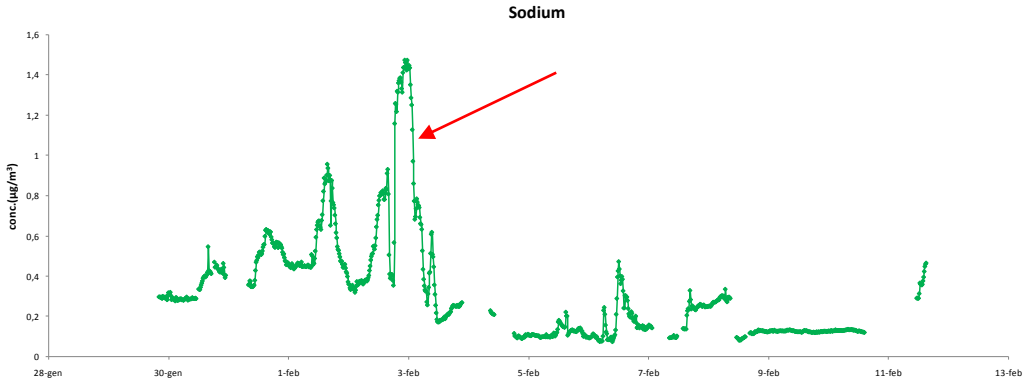
Sodium
conc.(µg/m³)
0
0,2
0,4
0,6
0,8
1
1,2
1,4
1,6
28-gen
30-gen
1-feb
3-feb
5-feb
7-feb
9-feb
11-feb
13-feb

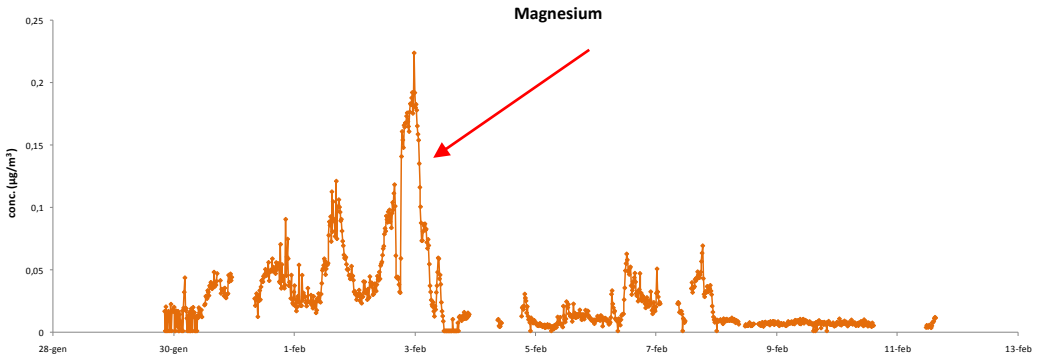
Magnesium
conc. (µg/m³)
0
0,05
0,1
0,15
0,2
0,25
28-gen
30-gen
1-feb
3-feb
5-feb
7-feb
9-feb
11-feb
13-feb

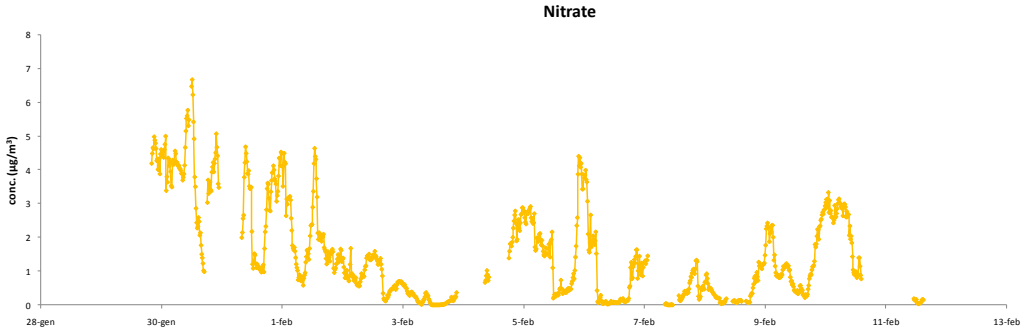
Nitrate
conc. (µg/m³)
0
1
2
3
4
5
6
7
8
28-gen
30-gen
1-feb
3-feb
5-feb
7-feb
9-feb
11-feb
13-feb

Nitrito

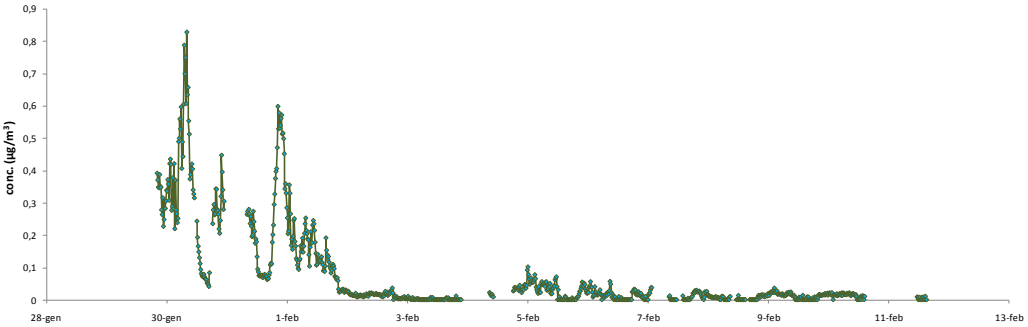

Sulphate

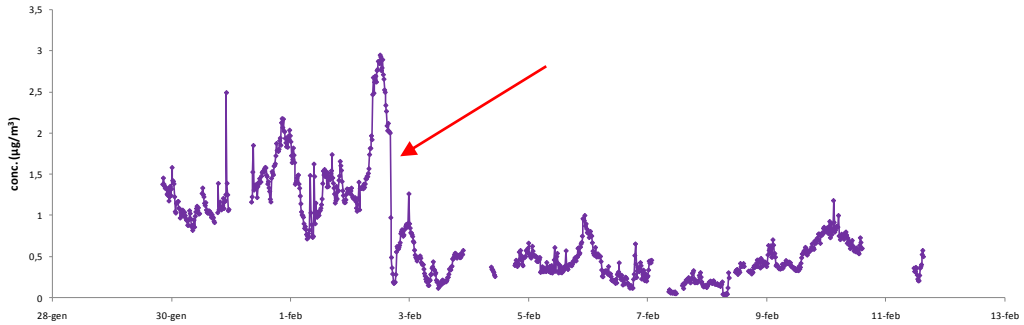

Calcium

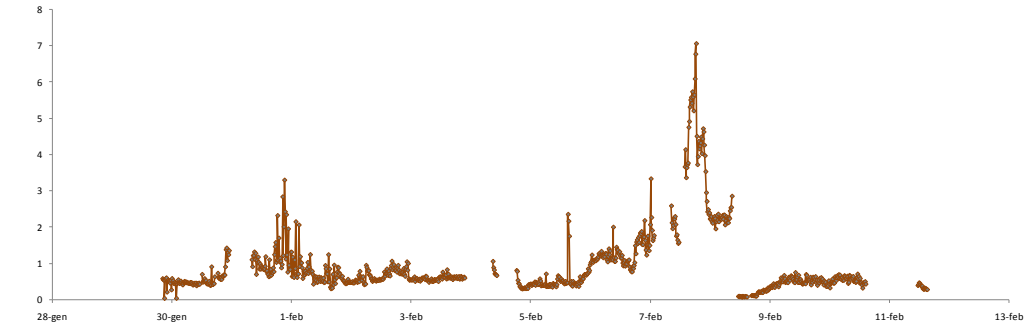

Ammonium

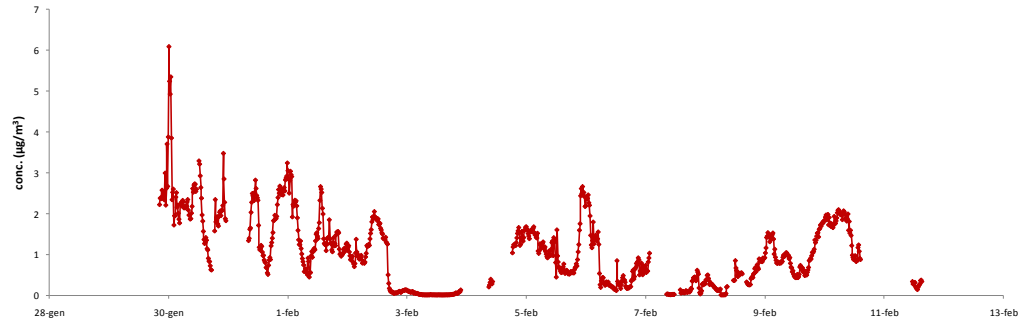

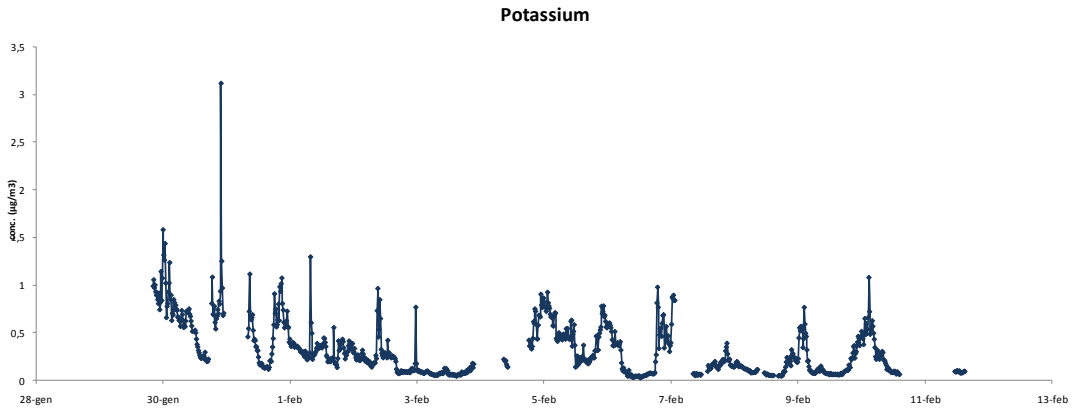

Fig.4.20: Ionic concentration trends from Janaury 30th to February 11th.

In figure 4.21 results obtained by Hysplit for the period February 2nd -3thare shown, in particular the circled area refers to February 3rd. The air mass on that date came from the Balkan area (known to be affected by anthropogenic pollution) and flew over the Adriatic Sea. Therefore this caused, most likely, the high concentration only for Cl^-, Na^+ and Mg^{2+} and SO_4^{2-}.

In the second part of the campaign, February 5-11th, however the trends of concentrations and radioactivity evolved in a quite similar way. Thus, the maximum and minimum observed are due to changes in the lower atmosphere, which alter the background levels of the various species.

Instead species such as NO_3^- and NH_4^+ follow the natural radioactivity trend for all the monitored period. In fact the formation of the secondary NH_4NO_3 is favored during the high stability period and its concentration is higher, as the gaseous species have more time to react; while during the advective period the salt concentration is lower.

To deepen these first assumptions, more specific correlations between the ionic species were done, trying to interpret the chemical form in which they were present in the atmosphere at the sampling time.

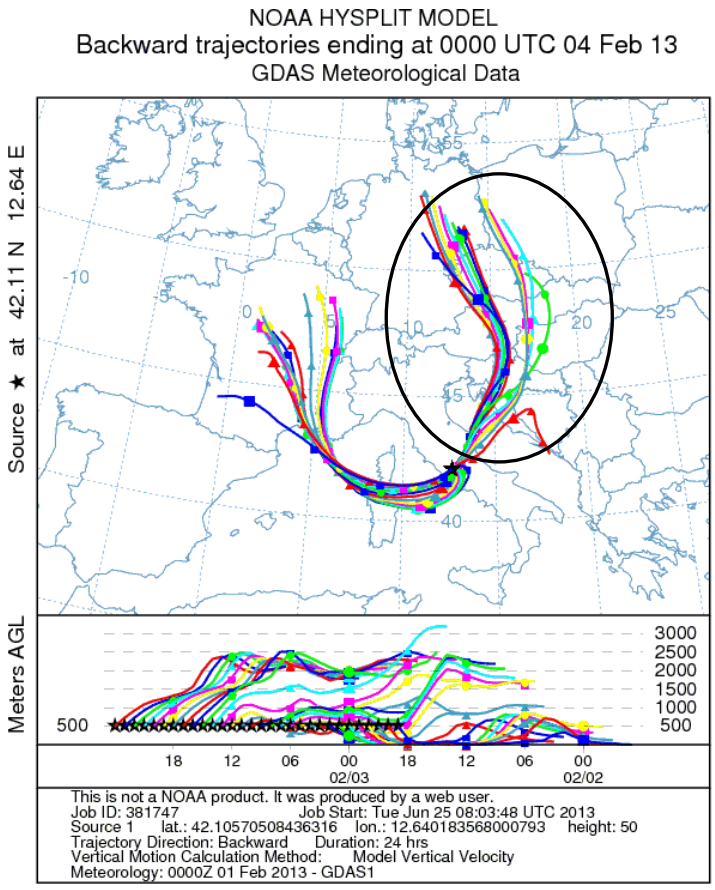

Fig.4.21: Hysplit air mass back-trajectories on February 2nd-3rd.

Correlations among Cl^-, Na^+ and Mg^{2+}

Qualitative comparison among these three ions are reported in figure 4.22. The three species perfectly follow the same trend in the periods highlighted with red boxes. As already discussed an advective phenomenon characterized by high speed winds (4 m/s) was registered during February 1st-4th. Chloride, sodium, and magnesium are tracers of the marine aerosol and since Italy is surrounded by the sea very often long-distance transports occur, as certainly happened in this case. The period highlighted in the second box shows a second transport event, coinciding with the rising wind during the night of February 6th, coming from the same directions of the first recorded event.

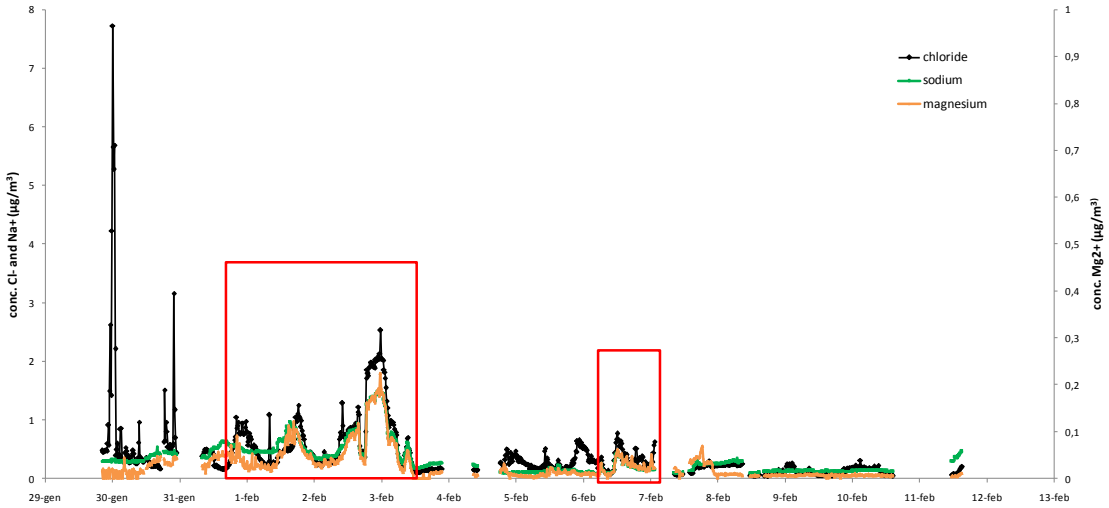

4.22: Overlap of Cl^-, Na^+ and Mg^{2+} trends.

Correlation among NH_4^+ and NO_3^-

Among the secondary species, the ammonium nitrate is the most present in Italy, depending on the type of pollutant emissions in our area. Less frequent are high concentrations of ammonium sulphate, usually linked to transport phenomena from Eastern Europe. Then in Italy the nitrate should be well correlated to the ammonium trend. By looking at Figure 4.23 ammonium nitrate was present for the whole monitoring campaign, except at midnight on January 30th, and during some hours of the night on February 8th (blue arrows in Figure 4.23), in which there are two ammonium peaks not correlated to the nitrate. We can observe a third strange peak of ammonium (blue box in Figure 4.23), where the nitrate concentration increases but not perfectly follows the trend of ammonia. The ammonium nitrate probably was not the only salt present in the atmosphere in that moment. Referring to the previous study on the natural radioactivity we can say that in addition to the classic build-up during the atmospheric stability (from January 30th to February 2nd), there may have been some transport phenomena or local emissions, that because of the favorable conditions, led to the formation of the secondary origin salts.

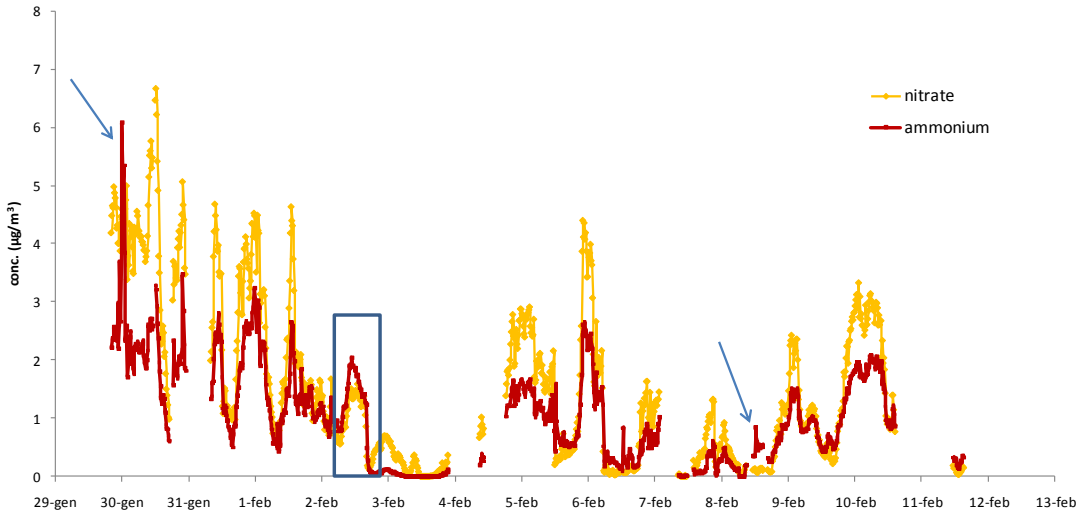

Fig.4.23: Overlaps of NH_4^+ and NO_3^- trends.

Correlation between NH_4^+ and SO_4^{2-}

The other important secondary species is the ammonium sulphate. Sulfate is mainly indicative of the presence of industrial and power plants that use coal combustion and diesel, of the harbor activities and a small part is released by the marine spray. In Italy, high concentrations of sulphate are absolutely atypical, therefore they are index of long-range transport events from Eastern Europe or Northern Africa.

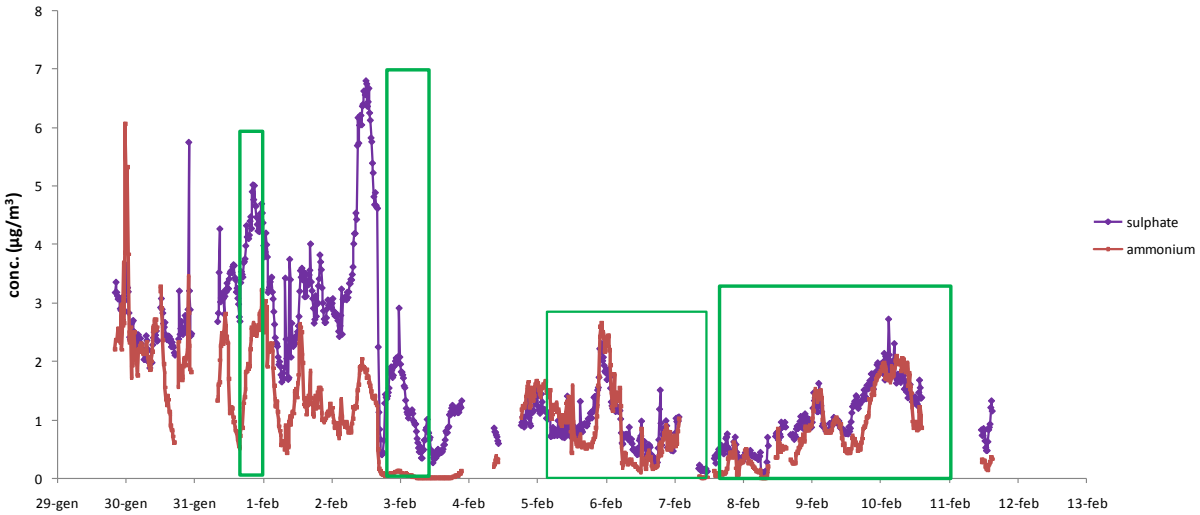

Fig. 4.24: Overlaps of SO_4^{2-} and NH_4^+ trends.

As we can see from Figure 4.24, the sulphate does not follow perfectly the ammonium trend, except for a few points that are the ones highlighted (green boxes in Figure 4.24).
Referring also to the natural radioactivity, the first peak is included in the period of stability, while the second peak occurred during an advective period confirming the hypothesis of long-distance transport. In the latter period of the campaign, the trends of ammonium and sulfate return to follow the radon, and the trends are very similar, confirming again that all the ammonia was present in the in the form of nitrate and in part also in the form of sulfate.

Correlation between NH_4^+ and Cl^-

Carefully observing the trend of ammonium, we recorded a first peak that will dissolve in a short time (figure 4.25). The high temporal resolution offered by our system PILS-IC has allowed to highlight one of the pollution events called *hot spots* (Allegrini et al., 2007). Looking at all the species, the only one correlated with that peak was found to be the chloride. So we detected the presence of ammonium chloride for a short time during the stability at the midnight of January 30th.

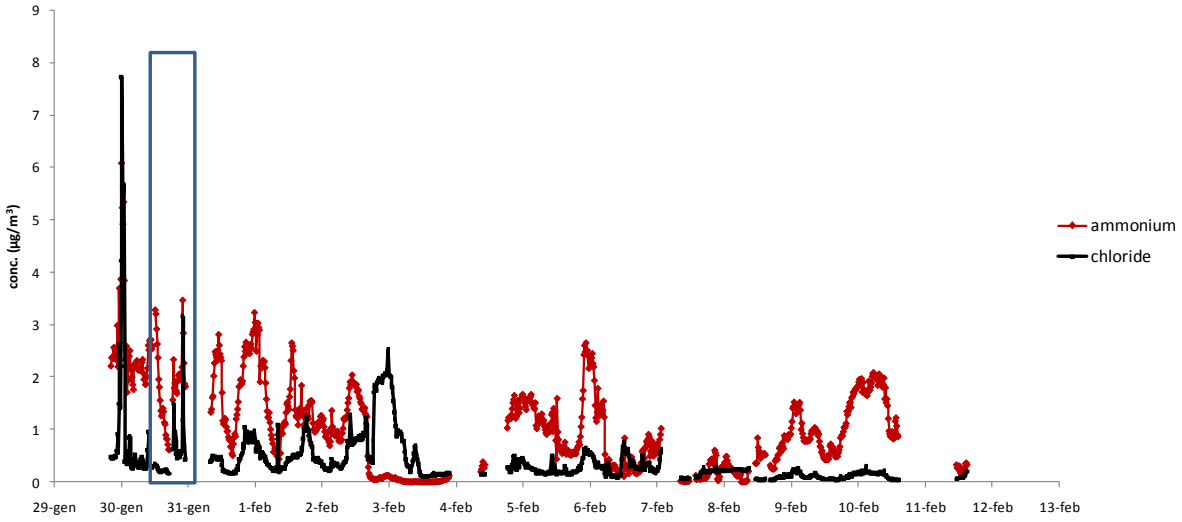

Fig.4.25: Overlaps of NH_4^+ and Cl^- trends.

Correlation between NH_4^+ and K^+

Surprisingly we have found a correlation between the ammonium and potassium trends, more or less for the entire campaign (figure 4.26). Both the ammonium and potassium are tracers of agricultural events, or of the fossil fuel and wood combustion. The area of Montelibretti, in which is situated the monitoring station of the National Research Council, is located in an open countryside and the sampling period occurred in the middle of winter. Consequently, the hypothesis on this correlation are entirely plausible.

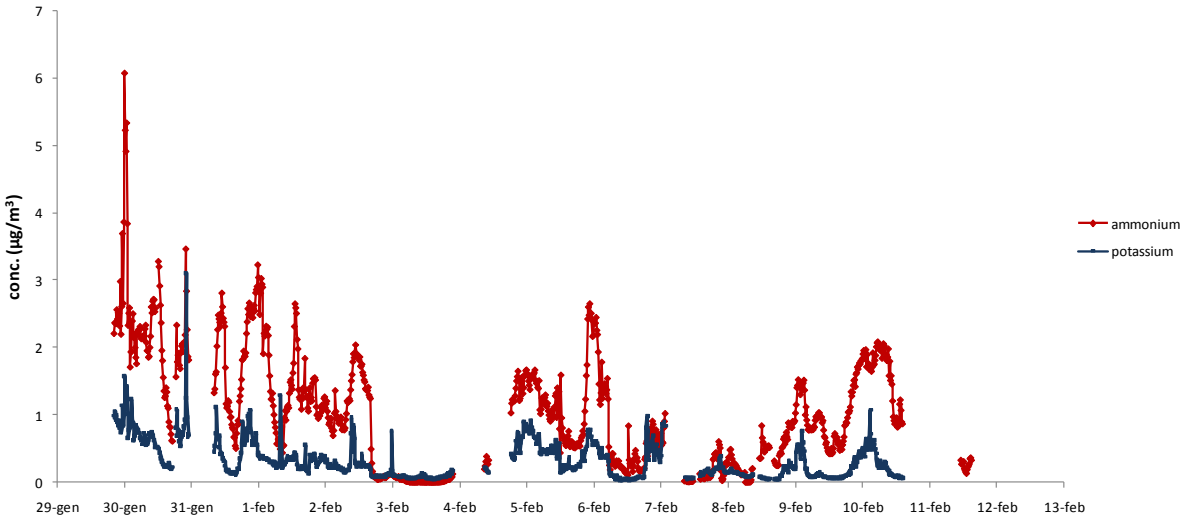

Fig.4.26: Overlaps of NH_4^+ and K^+ trends.

4.5 Conclusions

The system PILS in its basic use is affected by relatively high limits of quantification and this affects the purpose to sample PM with high-time resolution. In this context, however, the PILS-IC with the introduction of a pre-concentration system shows great potentialities. The system optimized in this work has allowed a significant improvement of the values of LOQ, which are essential to fully exploit the technique PILS. In fact, applying the LOQ related to an unmodified PILS–IC (with loop) and considering the data obtained from the monitoring campaign, we calculated that it would be lost about 65 % of the nitrite data, the 8% of nitrate and sulfate, 53% of

calcium, 18% of ammonium, 30% of potassium and virtually 100% of magnesium . The optimized system also allowed to continuously sample (for each hour of sampling only 12 minutes were lost with the inject operations), providing a qualitative response comparable to the AMS data and quantitatively comparable to three-hourly denuder data. Another great advantage is that the system is able to perform sampling and analysis at a distance of a few minutes, resulting in a high time saving for the operators. The system may be further improved in the future, especially as regards the calibration method and the number of measurable analytes. The present work has in fact laid the foundation to develop new methods for the high temporal resolution determinations in PM, for example, heavy metals coupling PILS with ICP-MS.

The application to an intensive monitoring campaign highlighted the importance of the availability of data at high temporal resolution in combination with meteorological parameters . In this study, in fact, we have shown how low resolution data, can hide some information that are potentially useful to identify the contributions of the various emission sources and to reconstruct the fate of the species dispersed into the atmosphere. Useful and detailed information about all the studied species were obtained, allowing the recognition of secondary species formation and the distinction of long-distance transport events that altered the average concentration of dust usually present in the our sampling zone.

We also experienced as the methods able to work at high temporal resolution, suffer from various problems, reduced to a minimum with the use of PILS. In the case of three-hourly denuders obvious problems of chemical type were encountered due to poor analytical reproducibility, but also operational, given the hard work required by the analysts. Also the AMS highlighted calibration problems, but it proved to be very reliable for semi-quantitative analysis of trace concentrations.

To conclude we can say that the results obtained through our system PILS-IC are quite satisfactory, and have fulfilled the expectations regarding the scope of this work.

4.6References

Allegrini I, De Santis F, Perrino C, Pietrodangelo A, Metodi innovativi per il monitoraggio dell'inquinamento atmosferico, SILVAE, Anno III – n°8, (2007).

Bukowiecki N, Hill M, Gehrig R, Zwicky C N, Lienemann P, Hegedus F, Falkenberg G, Weingartner E, Baltensperger U (2005) Environmental Science and Technology 39:5754-5762.

Douglas A Orsini D, Ma Y, Sullivan A, Sierau B, Baumann K, Weber R J (2003), Atmospheric Environment, 37:1243–1259.

IUPAC (1997), Pure and Applied Chemistry, 69:297-328 .

Jayne J T, Leard D C, Zhang X, Davidovits P, Smith K A, Kolb C E, Worsnop D R (2000), Aerosol Science and Technology, 33:49-70.

Kidwell C B and Ondov J M (2001), Aerosol Science and Technology, 35:596–601.

Kidwell C B, Ondov J M (2004a), Aerosol Science and Technology 38:205–218.

Kidwell C B and Ondov J M (2004b), Aerosol Science and Technology, 38:205–218.

Pancras J P, Ondov J M, Zeisler R (2005), Analytica Chimica Acta, 538:303–312.

Timonen H, Aurela M, Carbone S, Saarnio K, Saarikoski S, Makel T, Kulmala M, Kerminen V M, Worsnop D R, Hillamo R (2010), Atmospheric Measurement Techniques Discussions, 3:1063–1074.

Weber R J, Orsini D, Daun Y, Lee Y N, Klotz P J, Bretchek F (2001) Aerosol Science and Technology, 35:718-727.

Chapter 5- Sources of particulate matter: Traceability of the sources using elemental chemical fractionation

This part of the present project regarded a field study conducted in an industrial area of the Po Valley since 2008, aimed to the chemical characterization and to the identification of the emission source of PM in this area. This study was performed in collaboration with the research group headed by Doct. Cinzia Perrino of the Institute of Atmospheric Pollution (CNR). The identification of the main sources of atmospheric particulate matter (PM) is one of most demanding tasks in atmospheric pollution studies, given the high complexity of this matrix and the numerous sources that are involved in its emission processes, particularly in areas characterized by a high atmospheric pressure such as the Po Valley.

5.1 Introduction

Elements in PM are often used as tracers in source apportionment studies (in which ambiental concentrations are apportioned to likely sources), as some of them, or, more often, some combinations of them, can be considered as tracers of specific sources (Almeida et al. 2006; Viana et al. 2008; Gielt et al. 2010; Argyropoulos 2012, 2013). However, particularly in wide industrial areas, elements can be simultaneously released into the atmosphere by a number of different emission sources and this strongly reduces the reliability of source apportionment results.

In this context, improving the selectivity of the source tracers can constitute the key step to solve the apportionment problem. Furthermore, an enhanced selectivity of the source tracers can be strictly necessary in areas characterized by frequent and severe atmosphere stability episodes, where the vertical diffusion of pollutants is impaired and the horizontal diffusion and the aging of the air masses cause a more and more homogeneous mixing of the emission products.

A first way to enhance the traceability of some classes of emission sources is to perform a dimensional fractionation of PM. It is well known, in fact, that combustive sources release mainly particles with aerodynamic diameters (AD) lower than about 2.5 μm ($PM_{2.5}$; fine fraction) while mechanical-abrasive processes produce larger particles, with AD generally higher than 2.5 μm ($PM_{10-2.5}$; coarse particles) (Hueglin et al. 2005; Canepari et al. 2008; Li et al. 2013; Pant et al. 2013). Studying the elemental concentrations in the fine and coarse fraction of PM can thus give a first set of information about some characteristics of their sources.

Further improvements in the selectivity of elements as source tracers can be obtained by applying a chemical fractionation methodology based on their solubility (Fernandez Espinosa et al. 2002; Sillanpää et al. 2005; Al-Masri et al. 2006; Dutkiewicz et al. 2006; Sato et al. 2008; Canepari et al. 2008, 2009a, 2010). Elemental solubility, in fact, provides information about the chemical form in which the element is released and this, on its turn, may be typical of its emission source. Moreover, biogeochemical cycles, environmental and health effects are strongly related to the chemico-physical behavior of the chemical species in which the elements is contained (Harrison and Yin 2000; Cho et al. 2009; Barrett et al. 2012). In the case of toxic elements, a reliable identification of their atmospheric sources and bioaccessibility is even more important, as inhalation is one of the most relevant route of exposure to these pollutants (Marmur et al. 2006; Reche et al. 2012).

Although environmental studies reported in the scientific literature mostly concern the determination of total elemental concentration, in the last decades many different extracting procedures have been developed to study the solubility of elements and thus their environmental mobility and bioaccessible fraction (Dos Santos et al. 2009; Limbeck et al. 2012; Armiento et al. 2013; Mukhtar and Limbeck, 2013). However, only a few studies concern the application of these procedures to intensive monitoring campaigns and include the interpretation of the results on the basis of the meteorological situation and the local emission framework, as this kind of methodologies require a lot of work both to carry out the chemical analysis and to elaborate and interpret the obtained data(Voutsa and Samara 2002; Heal et al. 2005; Birmili et al. 2006; Qureshi et al. 2006; Sato et al. 2008; Canepari et al. 2009a).

In this part of the work the results of a 5-year monitoring study carried out in the area of Ferrara (Po Valley, Italy) were reported and discussed, concerning the concentration and solubility of micro- and trace- elements in atmospheric PM. As evidenced in Chapter 3, this area is characterized by a very complex background: frequent unfavorable meteo-climatic conditions during the cold season and many different anthropogenic PM sources concurrently cause frequent and severe atmospheric pollution events.

To these purposes, we applied the chemical fractionation methodology optimized in our laboratory, by analyzing twenty elements: As, Ba, Be, Cd, Co, Cu, Fe, Li, Mn, Pb, Ni, Rb, S, Sb, Se, Sn, Sr, Ti, Tl and V. Both the influence of the mixing properties of the lower atmosphere and the strength of PM sources on the seasonal variations of elemental concentration in PM were studied in deep. Moreover the seasonal differences of the size distribution and solubility of the elements and their selectivity as source tracer and availability to biological and environmental systems were evaluated and discussed.

5.2 Experimental

5.2.1 PM sampling

The area of the field study is located in the surroundings of Ferrara (Po Valley, Italy), already discussed in section 3.5 of Chapter 3). In particular the sampling area related to this study is influenced by several PM sources: the urban area, the highway A13 and a major industrial area containing a power plant, a urban waste incinerator and many small and medium size enterprises (SMEs), as shown in figure 5.1. The study was run from January 2008 to September 2012. Ten 1-month Special Observation Periods (SOPs) were carried out during the winter (January-February) and the spring-summer (May-June) of each year. During the first six SOPs (years 2008-2010) the measurements were performed at a residential site, located in the hamlet of Cassana, about 6 km from the centre of Ferrara. (site C; Google Earth coordinates: 44°50'54.95"N, 11°33'40.36"E) located at about 6 Km from the center of Ferrara and about 1 Km from the industrial area. During the last four SOPs (years 2011-2012) the study was extended to an industrial site (site A; 44°51'26.26"N, 11°33'36.90"E), close to the power plant, the waste incinerator and the SMEs and a rural site (site B: 44°49'31.53"N, 11°32'55.01"E) located as far as feasible from the main emission sources. Distances between the sites are: A-B: 3.7 km, A-C: 1 km; B-C: 2.8 km. From October 2011 to September 2012 the study included also additional measurements with a time coverage of 16 days/month at site C and of 8 days/month at sites A and B (extended monitoring, EM).

Mass concentration was measured daily at all three sites, by means of dual channel beta attenuation automatic monitors (SWAM 5a Dual Channel Monitor – FAI Instruments, Fonte Nuova, Rome - IT) configured with PM_{10} and $PM_{2.5}$ heads compliant with the EN 12341 (PM_{10}) and EN14907 ($PM_{2.5}$) standards. Samplers were equipped with teflon membrane filters (TEFLON, 47 mm, 2.0 micron pore size, PALL Life Sciences). Three additional dual channel samplers (HYDRA Dual Sampler, FAI Instruments, Fonte Nuova, Rome - IT) were placed at the three sites in order to collect daily PM_{10} and $PM_{2.5}$ samples also on quartz fibre filters (TISSUQUARTZ 2500QAT, 47 mm, PALL Life Sciences). During the same periods, the mixing properties of the lower atmosphere were evaluated at site C, on a 1-h hour time basis, by using an automated monitor of the natural radioactivity due to radon progeny (PBL Mixing Monitor, FAI Instruments, Fonte Nuova, Rome - IT).

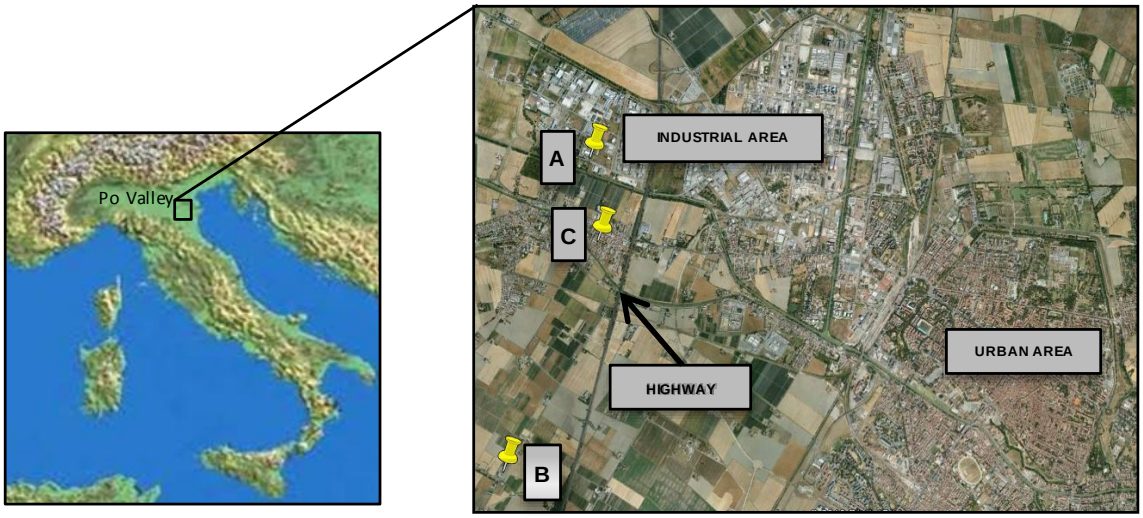

Fig.5.1: Map of the studied area showing the three sampling sites.

5.2.2 Chemical analysis

Chemical analysis to determine the PM composition are the same of those schematized in figure 3.2 and described in 3.3.2 section (Chapter 3).
Samples collected during the first six SOPs (2008-2010) and during the EM were only analyzed for the extracted and residual fractions of micro- and trace- elements.
Only micro and trace elements data were object of the first part of this work.

5.3 Results and discussion

The following results are being published by Environmental Science and Pollution Research (Canepari et al., 2013).

5.3.1 Total elemental concentration

Table 5.1 reports the mean values and variability (10°-90° percentile) of the elemental concentration in $PM_{2.5}$ and PM_{10} measured at the three sites during the EM (October 2011-September 2012); the detection limit (LOD) of each element in the extracted and residual fractions, calculated from operative blank values (6 replicates), is reported in the first two columns. On the whole, concentration values were comparable, or even lower, to those usually measured at peri-urban or background sites in the Mediterranean basin (Marcazzan et al. 2001; Rodrıguez et al. 2004; Marenco et al. 2006; Canepari et al. 2009a; Öztürk et al. 2009; Pey et al. 2009). This finding indicates that industrial emissions, whose strength is usually traced by these minor- and trace-

constituents, are not the main responsible for the high PM concentrations typically recorded in the study area. Moreover, concentrations at sites A, B and C were very similar, confirming the substantial homogeneity of the air masses in the studied area and the low contribution of local emissions even at sampling site A, placed in the proximity of the industrial area.

Figure 5.2 shows the monthly mean values of the total concentration of As, Cd, Ni and Pb in PM_{10} (sum of the extracted and residual fractions). Data show that higher concentrations were generally recorded during the cold season, due to the presence of additional PM sources and/or to the lower mixing of the atmosphere.

A similar behavior was observed for most of the other elements. Differences among sites were not significant, and mainly regarded concentrations at site C. During the EM the time coverage at this site was higher (16 days/month versus 8 days/month at sites A and B) and the observed differences may thus likely reflect the regular temporal variability of ambient air concentrations.

As, Cd, Ni and Pb concentration values were always well below the EU regulatory limits of 6ng m^{-3} for As, 5 ng m^{-3} for Cd, 20 ng $m^{-3}$for Ni (EU Directive 2004/107/CE) and 500 ng m^{-3} for Pb (EU 2008/50/CE), thus these elements do not constitute a critical factor in the air quality assessment in this area.

5.3.2 Chemical and dimensional distribution

As already evidenced in previous studies (Birmili et al. 2006; Canepari et al. 2008, 2010; Dos Santos et al. 2009), the combined use of chemical and dimensional fractionation significantly increases the selectivity of elements as source tracers. Each emission source is in fact responsible for the release of particles having a specific dimensional range and containing chemical species having a characteristic solubility. Generally, combustion and secondary formation processes produce particles in the fine fraction, while abrasive and mechanical processes are mostly responsible for the release of coarse particles (Li et al. 2013; Pant et al. 2013). Chemical fractionation makes it possible to further discern these contributions and single out sources that emit elements as soluble and as insoluble chemical species in each dimensional fraction.

Tab. 5.1:. Detection limits (LODs) in the extracted and residual fractions, mean elemental concentrations (sum of the extracted and residual fractions) and variability (10° ÷ 90° percentile) in PM_{10} and $PM_{2.5}$ at the three sites (October 2011 - September 2012)

	LOD		$PM_{2.5}$			PM_{10}		
	Extracted fraction (ng/m^3)	Residual fraction (ng/m^3)	Site A Industrial (ng/m^3)	Site B Rural (ng/m^3)	Site C Residential (ng/m^3)	Site A Industrial (ng/m^3)	Site B Rural (ng/m^3)	Site C Residential (ng/m^3)
As	0,01	0,01	0,88 *(0,32÷1,7)*	0,84 *(0,29÷1,7)*	0,92 *(0,41÷1,6)*	1,1 *(0,3÷2,0)*	1,0 *(0,4÷1,9)*	1,1 *(0,4÷2,0)*
Ba	0,003	0,01	1,8 *(0,8÷3,7)*	1,7 *(0,8÷3,5)*	1,9 *(1,1÷3,1)*	4,7 *(2,1÷10)*	4,5 *(1,9÷8,0)*	4,4 *(2,1÷7,6)*
Be	0,0001	0,0001	0,0022 *(<LOD÷0,0040)*	0,0024 *(<LOD÷0,0054)*	0,0026 *(<LOD÷0,0051)*	0,0072 *(0,0012÷0,018)*	0,0065 *(0,0016÷0,015)*	0,0071 *(0,0011÷0,015)*
Cd	0,001	0,001	0,27 *(0,05÷0,53)*	0,26 *(0,05÷0,49)*	0,29 *(0,05÷0,54)*	0,30 *(0,07÷0,59)*	0,29 *(0,05÷0,60)*	0,30 *(0,05÷0,65)*
Co	0,001	0,001	0,06 *(0,01÷0,12)*	0,06 *(0,01÷0,11)*	0,06 *(0,01÷0,12)*	0,12 *(0,02÷0,25)*	0,11 *(0,02÷0,21)*	0,10 *(0,02÷0,21)*
Cu	0,06	0,04	4,7 *(1,9÷9,6)*	4,7 *(2,1÷9,1)*	4,7 *(2,0÷8,9)*	10 *(4÷21)*	11 *(5÷18)*	10 *(4÷17)*
Fe	0,2	0,7	103 *(36÷187)*	102 *(30÷172)*	108 *(31÷195)*	303 *(101÷649)*	286 *(109÷547)*	277 *(118÷500)*
Li	0,0005	0,001	0,14 *(0,06÷0,24)*	0,13 *(0,03÷0,24)*	0,13 *(0,03÷0,24)*	0,25 *(0,10÷0,43)*	0,25 *(0,08÷0,48)*	0,25 *(0,09÷0,46)*
Mn	0,01	0,07	5,2 *(1,7÷11)*	4,9 *(1,5÷9,5)*	5,3 *(2,3÷10)*	9,7 *(5,0÷18)*	9,0 *(3,9÷17)*	9,4 *(4,6÷16)*
Ni	0,005	0,01	2,2 *(1,2÷3,5)*	2,2 *(1,1÷3,7)*	2,1 *(1,2÷3,4)*	2,7 *(1,5÷4,5)*	2,9 *(1,3÷4,5)*	2,5 *(1,3÷3,9)*
Pb	0,01	0,04	8,0 *(1,5÷20)*	7,7 *(1,5÷18)*	8,0 *(1,7÷18)*	9,4 *(1,9÷22)*	9,1 *(2,1÷20)*	8,8 *(2,2÷19)*
Rb	0,01	0,07	0,74 *(0,10÷1,7)*	0,76 *(0,16÷1,7)*	0,79 *(0,21÷1,8)*	1,0 *(0,4÷1,9)*	1,1 *(0,3÷2,0)*	1,1 *(0,4÷2,1)*
S	1	10	761 *(401÷1605)*	697 *(390÷1497)*	709 *(397÷1530)*	828 *(506÷1834)*	777 *(487÷1719)*	773 *(495÷1616)*
Sb	0,005	0,01	1,1 *(0,4÷2,0)*	1,0 *(0,4÷1,9)*	1,1 *(0,4÷2,0)*	1,6 *(0,6÷3,1)*	1,5 *(0,6÷2,8)*	1,5 *(0,6÷2,7)*
Se	0,004	0,01	1,1 *(0,3÷1,8)*	1,0 *(0,2÷2,1)*	1,1 *(0,3÷2,0)*	1,1 *(0,3÷1,9)*	1,2 *(0,2÷2,4)*	1,3 *(0,4÷2,2)*
Sn	0,001	0,04	1,7 *(0,4÷4,8)*	1,7 *(0,4÷4,5)*	1,8 *(0,4÷4,9)*	2,6 *(0,7÷6,4)*	2,5 *(0,8÷5,9)*	2,5 *(0,7÷5,3)*
Sr	0,001	0,01	0,82 *(0,13÷1,6)*	0,68 *(0,10÷1,2)*	0,72 *(0,12÷1,5)*	1,7 *(0,4÷3,2)*	1,6 *(0,3÷3,1)*	1,6 *(0,4÷2,9)*
Ti	0,005	0,01	1,2 *(0,6÷2,1)*	1,2 *(0,4÷2,6)*	1,3 *(0,4÷2,9)*	3,8 *(1,1÷7,5)*	3,6 *(1,1÷6,9)*	3,8 *(0,9÷7,3)*
Tl	0,0005	0,001	0,045 *(0,021÷0,083)*	0,045 *(0,013÷0,10)*	0,046 *(0,017÷0,096)*	0,054 *(0,016÷0,11)*	0,053 *(0,015÷0,10)*	0,051 *(0,016÷0,10)*
V	0,004	0,01	1,8 *(0,6÷3,5)*	1,9 *(0,6÷3,6)*	1,9 *(0,7÷3,5)*	2,3 *(0,9÷4,0)*	2,4 *(0,7÷4,5)*	2,4 *(0,8÷4,3)*

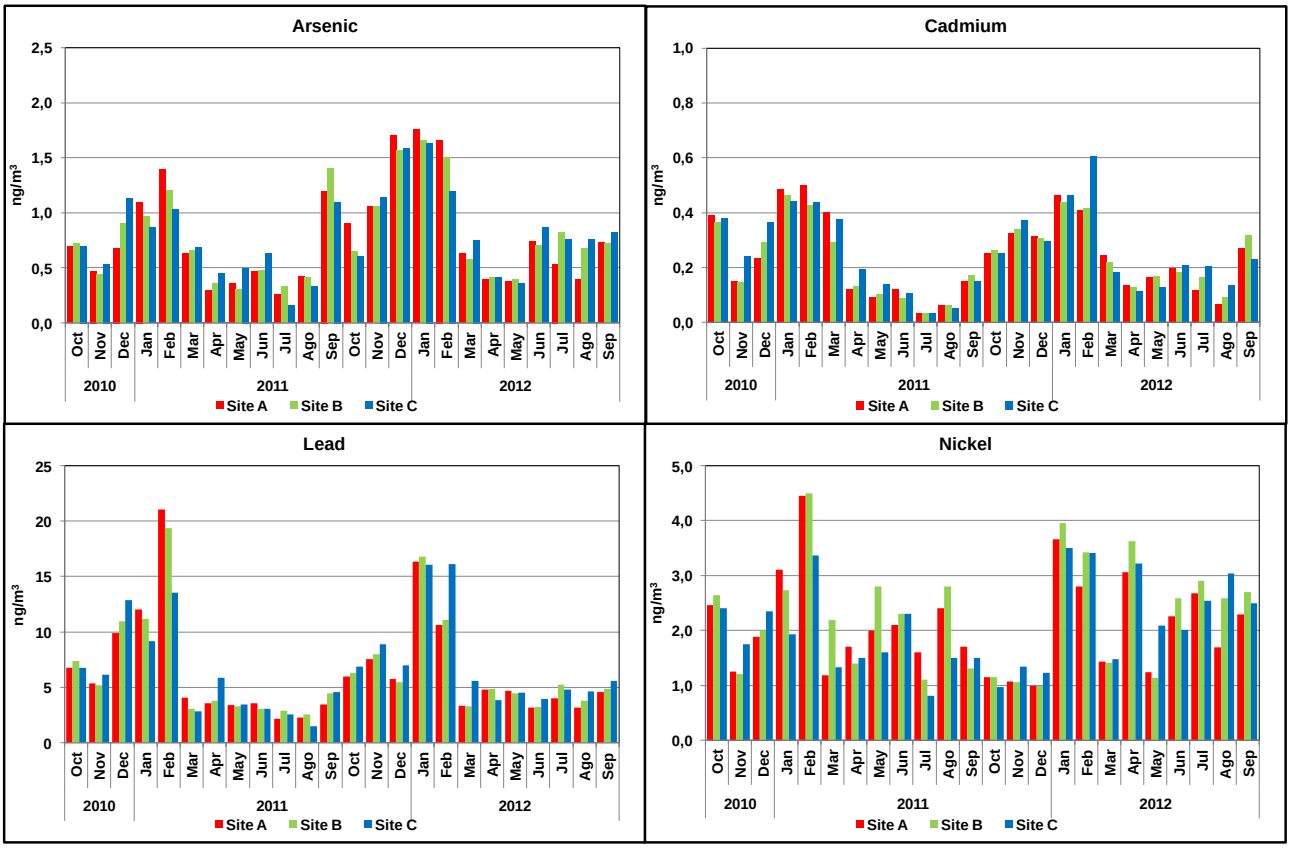

Fig.5.2: Monthly concentration of total As, Cd, Ni and Pb in PM_{10} at the three sites (time coverage: 16 days/month at site C; 8 days/month at sites A and B).

Furthermore, the use of an extraction procedure based on the elemental solubility also yields useful information for a rough estimate of the environmental mobility and bio-accessibility of the element. In this study, the total PM_{10} concentration of each element was split into four different portions: extractable and residual contribution to fine PM ($PM_{2.5}$), extractable and residual contribution to the coarse PM fraction, calculated by subtracting $PM_{2.5}$ from PM_{10}.

The results of this elaboration (mean values during the 2011-2012 EM) are shown in Figure 5.3. The chemical and dimensional distributions of all elements were very similar at the three sites, confirming the impressive homogeneity of the chemical composition of PM in the monitored area. Almost all the considered elements, which may be released in the atmosphere by different processes (Argyropoulos 2012, 2013), were distributed among the four fractions. Only sulphur was almost completely included in one fraction only (soluble, fine fraction) as it is mostly originated by secondary reactions in the atmosphere, thus in the form of soluble sulphates.

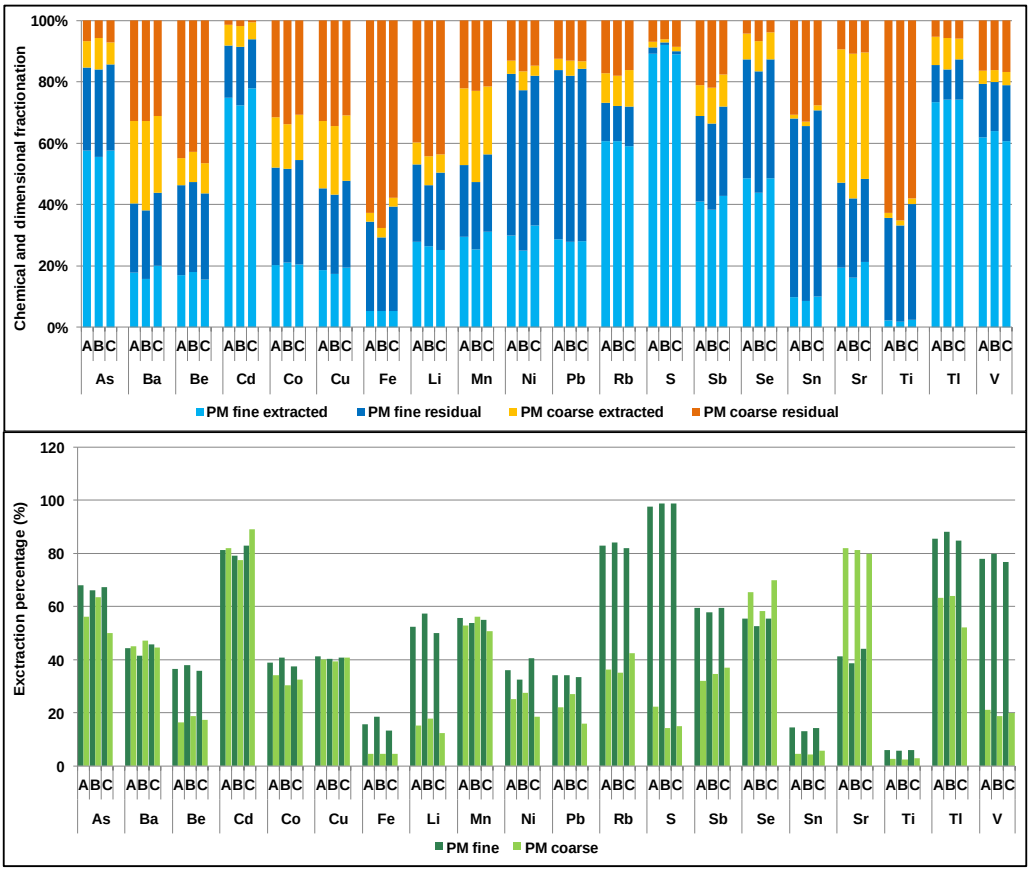

Fig. 5.3: Mean values (October 2011- September 2012) of the chemical and dimensional distribution of elemental concentrations (upper panel) and of the extraction percentage in the fine and coarse fraction of PM (lower panel) at the three sites.

The upper panel of Figure 5.3 shows that about 80% of the total concentration of As, Cd, Ni, Pb, Se, Tl and V and 60-70% of the total concentration of Sb and Sn was associated to fine particles; these elements were then released into the atmosphere mainly by combustion processes. Instead, 50-70% of the total concentration of Ba, Be, Co, Cu, Fe, Li, Mn, Sr and Ti was in the coarse fraction, indicating that these elements mostly derived from mechanical sources such as topsoil erosion and dust re-suspension. Furthermore, the data show that more than 60% of the total PM_{10} concentration of As, Cd, Rb, S, Sr, V and Tl was in the extracted fraction, and then associated to water-soluble chemical species; this fraction is expected to be easily mobilized from PM and transferred to environment and biological systems. On the contrary, the extracted fraction of Fe, Ti and Sn was very low (up to 10%) and these elements are then expected to exhibit a lower impact on environment and human health. All the other elements showed an extracted fraction between 20% (Be) and 60% (Mn, Sb, Se), being thus partially accessible to environmental and biological systems.

Element extraction percentages in the fine and coarse fractions of PM is shown in the lower panel of Figure 5.3. Differences are quite evident for some elements (Be, Li, Rb, V, S, Sb, Sr and, to a lower extent, Be, Co, Fe, Ni, Pb, Sn, Ti and Tl). For all of these, with the exception of Sr, the chemical species contained in the fine fraction were more soluble than those contained in the coarse fraction. Fine particles, produced by combustion or secondary processes, are then to be considered more hazardous than coarse particles not only for their small dimensions, that increase their capacity to penetrate deeply into the respiratory tract, and for their long residence-time in the atmosphere, but also because they contain more bio-accessible and mobile chemical species. Abrasive and mechanical processes, instead, produce coarse particles containing elemental species that are scarcely accessible to the environment (extraction percentages were lower than 40% for Be, Co, Cu, Fe, Li, Ni, Pb, S, Sb, Sn, Ti and V). Sr only shows a significant contribution of soluble species from a source of coarse particles, which accounted for about 40% of its total PM_{10} concentration.

It is worth noting that recent studies (Canepari et al. 2013) have shown that the bio-available fraction of elements determined by extraction procedures likely includes suspended solid NPs. This aspect merits to be further investigated, as the effect on human health of solid nanoparticles and soluble species might be substantially different (Oberdörster et al. 2001, 2005).

5.3.3 Seasonal variations

The availability of chemically and dimensionally fractionated data allows a detailed description of the seasonal variations of the elemental concentrations in PM. These variations may be originated by fluctuations in the strength of their sources and/or by differences in the mixing property of the atmosphere along the year. When the winter-to-summer variability is dominated by the atmospheric mixing, the elemental distribution among the four fractions is expected to remain roughly constant or to show small differences (i.e. due to variations in the deposition rate), while a change in the chemical and dimensional features of PM must be expected when a variation of the source emission context occurs.

Table 5.2 summarises the results obtained during the ten SOPs carried out at residential site C during the years 2008-2012 (summer and winter mean concentration values and their variability). On the whole, elemental concentration during the winter was higher than during the summer, in agreement with the general worsening of air quality observed in the Po Valley during the winter months (Vecchi et al 2004; Carbone et al. 2010, Perrino et al. 2013)

Winter-to-summer ratio (W/S) of the total PM_{10} concentration (sum of the four fractions) was higher than 3 for Cd, Rb and Pb and between 2 and 3 for As, Sb and Sn. W/S values higher than 1 were observed for Be, Ba, Co, Cu, Fe, Ni, Mn, S and Tl. Only for Ti, a concentration increase was observed during the summer period (W/S = 0.6); a few elements (Li, V, Se, Sr) did not show appreciable seasonal variations (W/S about 1). Variations were generally more pronounced in $PM_{2.5}$ than in PM_{10}: as an example, W/S values for Sn, Cu and Mn increased from 2.6, 1.6 and 1.5 (in PM_{10}) to 3.8, 2.4 and 2.8 (in $PM_{2.5}$), respectively. This is in agreement with the increased relative relevance of PM coarse sources, such as topsoil re-suspension and long-range transport of desert dust, during the summer.

Further information can be obtained by studying the seasonal variability of the four contributions to the concentration of each element, yielded by the dimensional and chemical fractionation. In order to facilitate the discussion of this complex subject, we report the results obtained for Cd, Pb and Li, which are illustrative of three different behaviours, in Figure 5.4 (colour codes as in Figure 5.3.+

Left panels show the average concentration measured in PM_{10} during the 10 SOPs, partitioned into the four contributions; right panels report the extraction percentage in the fine and the coarse fraction.

The upper panels in Figure 5.4 show that during both winter and summer periods Cd in PM_{10} was almost completely in the form of soluble chemical species contained in fine particles, and that its seasonal variability was dominated by the winter increase of this fine soluble fraction (W/S = 4.8). The extraction percentages in the fine and coarse fractions were similar, with no significant seasonal differences. These results indicate that the same main source(s) was active during both seasons, and that the seasonal variability was mainly due to meteo-climatic factors, even though the contribution of additional sources during the winter cannot be excluded. A similar behaviour is observed also for As and Tl, which show W/S ratios in the fine soluble fraction as high as 2.6 and 2.3, respectively.

Seasonal variability of Pb in PM_{10} (Figure 5.4,middle panels) was almost completely due to the marked winter increase in the concentration of insoluble chemical species contained in fine particles (W/S = 7.4). However, unlike Cd, As and Tl, winter and summer chemical and dimensional distribution were significantly different: extraction percentages in fine particles were much lower during the winter, while in coarse particles they were slightly higher.

Tab. 5.2:Mean winter and summer values and variability (10°÷90° percentile) of elemental concentration in the extracted and residual fraction of fine ($PM_{2.5}$) and coarse $PM_{10-2.5}$) particles (10 SOPs at site C).

	SUMMER				WINTER			
	PM fine		PM coarse		PM fine		PM coarse	
	extracted (ng/m^3)	residual (ng/m^3)	extracted (ng/m^3)	residual (ng/m^3)	extracted (ng/m^3)	residual (ng/m^3)	extracted (ng/m^3)	residual (ng/m^3)
As	0,34 *(0,10÷0,66)*	0,14 *(<LOD÷0,29)*	0,15 *(< LOD÷0,49)*	0,07 *(< LOD÷0,19)*	0,88 *(0,27÷1,7)*	0,26 *(< LOD÷0,62)*	0,15 *(< LOD÷0,37)*	0,09 *(< LOD÷0,22)*
Ba	0,54 *(0,19÷0,92)*	0,59 *(0,17÷0,93)*	1,1 *(0,3÷1,9)*	1,7 *(0,5÷2,9)*	0,86 *(0,31÷1,7)*	0,73 *(< LOD÷1,6)*	1,3 *(0,3÷2,6)*	1,9 *(0,2÷3,3)*
Be	0,0016 *(0,0003÷0,0032)*	0,0012 *(< LOD÷0,0035)*	0,0017 *(0,0004÷0,0033)*	0,0029 *(0,0001÷0,0059)*	0,0024 *(< LOD÷0,0062)*	0,0020 *(< LOD÷0,0043)*	0,0012 *(< LOD÷0,0025)*	0,0040 *(< LOD÷0,0079)*
Cd	0,12 *(0,02÷0,24)*	0,043 *(0,015÷0,069)*	0,022 *(< LOD÷0,038)*	0,001 *(< LOD÷0,029)*	0,58 *(0,16÷1,1)*	0,14 *(0,03÷0,30)*	0,048 *(< LOD÷0,16)*	0,017 *(< LOD÷0,053)*
Co	0,032 *(0,012÷0,062)*	0,051 *(0,011÷0,096)*	0,035 *(< LOD÷0,093)*	0,054 *(< LOD÷0,13)*	0,041 *(0,015÷0,083)*	0,052 *(0,007÷0,11)*	0,021 *(0,006÷0,039)*	0,039 *(0,007÷0,078)*
Cu	1,2 *(0,4÷2,0)*	1,5 *(0,7÷2,6)*	2,0 *(0,6÷3,6)*	3,3 *(1,4÷5,3)*	2,3 *(0,9÷3,9)*	4,2 *(1,1÷8,5)*	2,4 *(0,7÷4,3)*	4,7 *(0,5÷11)*
Fe	11 *(2÷20)*	45 *(12÷76)*	5,4 *(0,2÷9,1)*	127 *(55÷202)*	25 *(8÷44)*	84 *(30÷176)*	17 *(2÷36)*	130 *(32÷245)*
Li	0,021 *(0,008÷0,032)*	0,031 *(0,007÷0,063)*	0,013 *(< LOD÷0,035)*	0,075 *(0,014÷0,14)*	0,071 *(0,030÷0,12)*	0,012 *(< LOD÷0,024)*	0,016 *(0,001÷0,034)*	0,039 *(0,010÷0,078)*
Mn	1,3 *(0,6÷2,0)*	1,9 *(0,6÷1,8)*	2,4 *(1,0÷4,1)*	1,7 *(0,5÷2,9)*	3,4 *(1,1÷6,2)*	3,6 *(1,2÷6,6)*	2,0 *(0,6÷3,7)*	1,4 *(0,1÷3,2)*
Ni	0,89 *(0,28÷1,7)*	0,55 *(0,14÷1,0)*	0,65 *(< LOD÷1,8)*	0,46 *(0,04÷1,2)*	1,1 *(0,5÷1,9)*	2,1 *(0,8÷3,8)*	0,19 *(< LOD÷0,49)*	0,56 *(< LOD÷1,4)*
Pb	1,2 *(0,4÷2,1)*	1,1 *(0,4÷1,8)*	0,26 *(< LOD÷0,76)*	0,89 *(0,04÷2,07)*	4,1 *(1,1÷7,9)*	8,2 *(3,0÷15)*	2,5 *(0,01÷7,6)*	1,5 *(0,06÷2,5)*
Rb	0,15 *(0,05÷0,29)*	0,11 *(0,06÷0,16)*	0,03 *(< LOD÷0,07)*	0,23 *(0,08÷0,41)*	1,1 *(0,8÷1,4)*	0,16 *(0,11÷0,19)*	0,18 *(0,05÷0,29)*	0,13 *(0,07÷0,17)*
S	721 *(201÷1244)*	17 *(< LOD÷96)*	72 *(10÷119)*	19 *(< LOD÷54)*	1084 *(410÷1953)*	26 *(10÷63)*	64 *(26÷161)*	17 *(< LOD÷69)*
Sb	0,40 *(0,16÷0,65)*	0,22 *(0,10÷0,33)*	0,11 *(< LOD÷0,17)*	0,29 *(0,10÷0,52)*	1,0 *(0,3÷1,6)*	0,75 *(< LOD÷1,8)*	0,19 *(0,02÷0,38)*	0,48 *(0,03÷1,0)*
Se	0,40 *(0,15÷0,73)*	0,22 *(< LOD÷0,48)*	0,09 *(< LOD÷0,23)*	0,20 *(< LOD÷0,52)*	1,3 *(0,5÷2,3)*	0,45 *(0,16÷0,76)*	0,37 *(< LOD÷1,1)*	0,10 *(< LOD÷0,33)*
Sn	0,22 *(0,05÷0,45)*	0,38 *(0,16÷0,63)*	0,08 *(< LOD÷0,21)*	0,42 *(0,18÷0,66)*	0,49 *(0,12÷0,92)*	1,9 *(0,46÷3,8)*	0,15 *(< LOD÷0,37)*	0,83 *(0,13÷1,8)*
Sr	0,41 *(0,18÷0,73)*	0,35 *(< LOD÷0,65)*	0,99 *(0,26÷1,8)*	0,27 *(< LOD÷0,59)*	0,28 *(0,14÷0,45)*	0,46 *(0,13÷0,92)*	0,71 *(0,16÷1,5)*	0,21 *(< LOD÷0,47)*
Ti	0,07 *(0,02÷0,17)*	1,0 *(0,4÷1,7)*	0,12 *(< LOD÷0,33)*	2,6 *(0,6÷5,0)*	0,08 *(0,02÷0,15)*	0,48 *(< LOD÷0,95)*	0,08 *(< LOD÷0,21)*	1,4 *(0,3÷2,6)*
Tl	0,017 *(0,075÷0,027)*	0,009 *(< LOD÷0,023)*	0,004 *(< LOD÷0,009)*	0,001 *(< LOD÷0,005)*	0,039 *(0,014÷0,081)*	0,004 *(0,001÷0,021)*	0,003 *(< LOD÷0,013)*	0,002 *(< LOD÷0,007)*
V	1,4 *(0,22÷2,5)*	0,24 *(0,02÷0,54)*	0,17 *(< LOD÷0,49)*	0,28 *(0,03÷0,59)*	1,5 *(0,43÷2,9)*	0,30 *(0,05÷0,84)*	0,17 *(< LOD÷0,44)*	0,26 *(0,02÷0,52)*

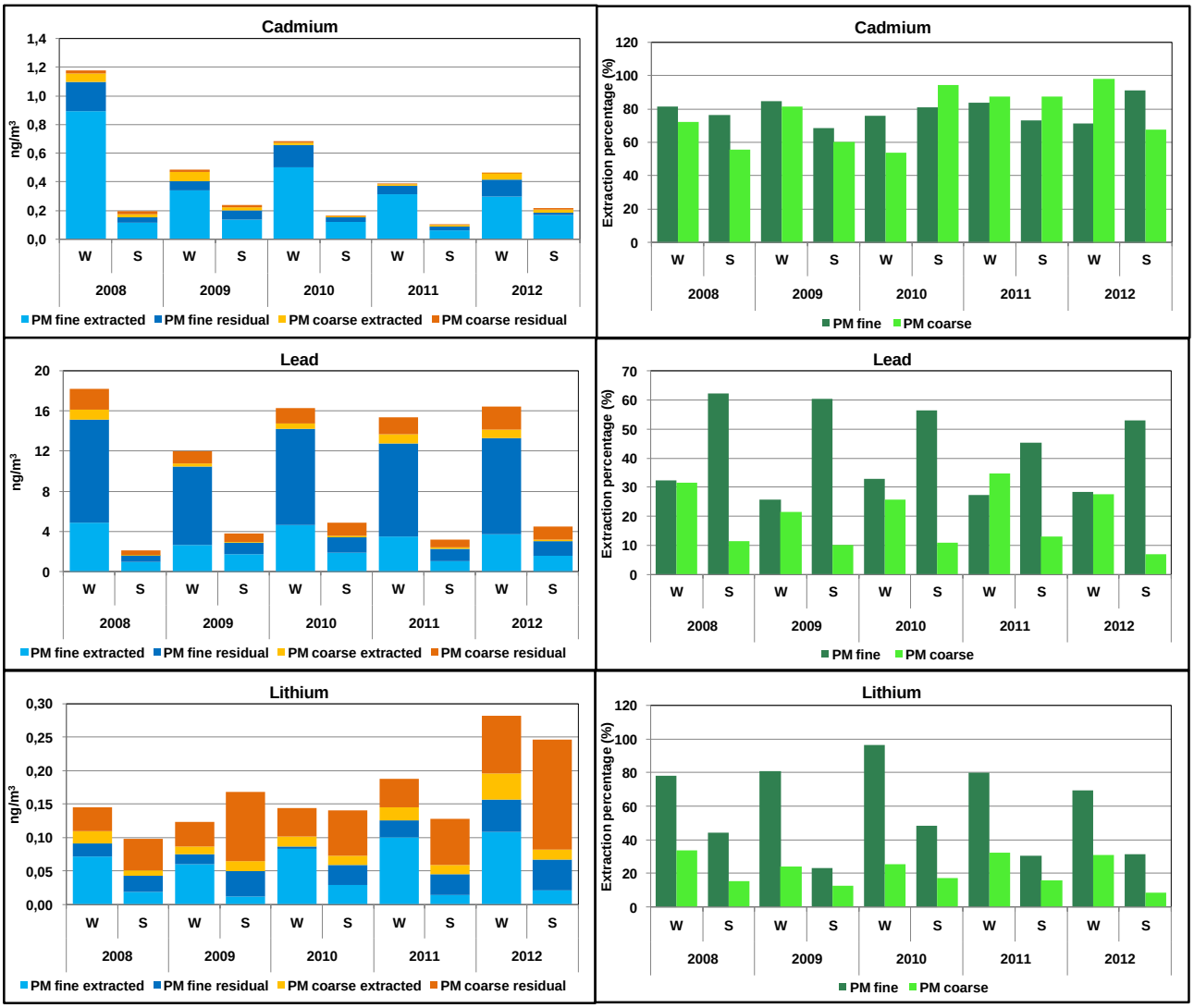

Fig.5.4: Average concentration of Cd, Pb and Li measured in PM_{10} during the 10 SOPs, partitioned into the four dimensional and solubility contributions (left panels); extraction percentage in the fine and coarse dimensional fraction (right panels).

These differences indicate a seasonal variations of the emission context. In particular, they reveal the presence of at least two winter sources of Pb: an intense source producing fine particles containing insoluble species and a weaker source releasing coarse particles containing soluble species. A similar behaviour was shown also by Sn and Ni, both characterized by the presence of at least one winter source of the fine, residual fraction (W/S as high as 5.0 and 3.8, respectively), and by Rb, whose winter additional contribution was in the fine, soluble fraction (W/S = 3.0).

The total concentration of Li in PM_{10} (Figure 5.4, lower panels) did not show a clear seasonal variability, however, relevant seasonal variations were observed in its chemical and dimensional

distributions. In this case, the soluble fine fraction showed the typical increase during the winter (W/S = 3.4), while the concentration of the residual coarse fraction was higher during the summer (W/S = 0.5); consequently, the extraction percentages in both the fine and coarse fractions were higher during the winter. It follows that the concentration of this element seems to have significant contributions from at least two different sources, having opposite seasonal variability. The first source, probably associated to combustion processes, was responsible for the release of fine particles containing soluble species; it accounted for more than 50% of the total Li concentration during the winter, but it was almost negligible during the summer. The second source, probably associated to natural contributions from local topsoil and from long-range transport of desert dust, was mainly responsible for the residual coarse fraction; its intensity increased during the summer. A similar framework of sources with different seasonal variability was observed also for Cu, Mn, Sb, Se, Co and Fe.

5.3.4 Daily variations

Atmospheric concentrations of the elements generally show wide daily variations, which are the result of many concurrent causes. Among these, variations in the intensity of manifold emission sources, the mixing properties of the atmosphere and the deposition rate, plus the additional occurrence of long-range transport of natural or anthropogenic dust. These factors have different effects upon the concentration of the individual chemical and dimensional fractions of each element. A detailed interpretation of all these factors for the twenty elements determined in this study would be excessively demanding. However, we will analyze some examples that extensively highlight the relationship among the tracer, the strength of its sources and the meteo-climatic situation.

Figure 5.5 reports the daily concentrations of Fe in the extracted and the residual fractions (upper and lower panel, respectively) during the SOP of June 2012; the contribution of coarse particles is depicted by the distance between PM_{10} and $PM_{2.5}$ values. Time pattern and dimensional distribution of the two chemical fractions were very different, clearly indicating that they traced different sources.

The residual fraction of Fe contained almost the entirety of this element and included a significant coarse contribution; it was presumably associated with non-exhaust vehicular emissions (re-suspension) and with soil dust of natural origin (Canepari et al. 2008, 2009a; Perrino et al. 2009). Due to the high deposition rate of coarse particles, PM_{10} concentration was more influenced by

local contributions, resulting in some differences among the patterns observed at the three sites. However, a spatially homogeneous peak is self-evident in coarse-residual Fe during the episode of desert dust transport occurred on June 19th-22nd , detected by the HYSPLIT model (Draxler and Rolph 2010), already discussd in Chapter 3. Long-range transport of desert dust episodes were more frequent during spring and summer, when they constitute an external source of coarse particles containing also soluble species of Sr, Co and Ba and insoluble species of Li, Ba, Li, Mn, Ti, Rb, Be.

The extracted fraction of Fe, instead, likely derived from one - or more - non-local industrial sources producing fine particles homogeneously distributed in the monitored area. Its contribution to the total Fe concentration was very low and this source(s) would have gone undetected when considering total Fe concentration only.

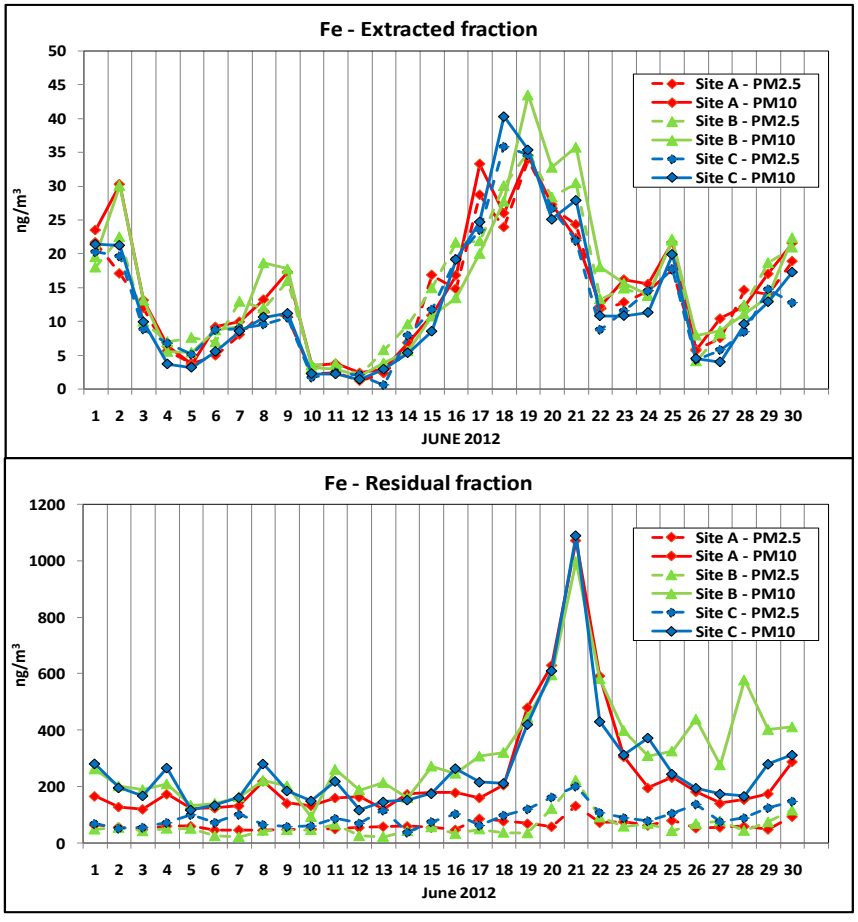

Fig. 5.5: Daily concentration of Fe in the extracted and the residual fraction during the SOP of May-June 2012.

By comparing the time pattern of the tracers with the mixing properties of the air masses, we can differentiate between constant and occasional sources. When the emission rate of any source is constant, in fact, the daily variability of its tracers is driven by atmospheric mixing variations. Instead, occasional local sources, as well as long-range transport of dust, cause concentration peaks that are independent from the mixing properties of the lower atmosphere. As described in Chapter 3 the mixing properties of the lower atmosphere can be followed by monitoring natural radioactivity due to the Radon decay products.

As an example, in Figure 5.6 the natural radioactivity pattern recorded during the SOP of January-February 2011 is compared with the daily concentrations of the extracted fractions of Pb (upper panel) and S (lower panel) in PM_{10}. The concentration of both tracers was spatially homogeneous and thus scarcely influenced by local sources (error bars indicate the standard deviation of the mean values among the three sites).

However, Pb concentration was clearly driven by the atmospheric mixing, while the concentration of soluble S was, in general, much less dependent on the height of the mixed layer. Going into details, an evident peak in S concentration was recorded on January 29th-31st, when the back-trajectories of the air masses, calculated by the HYSPLIT model, indicate advection from polluted areas of East Europe (Bosnia-Herzegovina and Croatia). The extracted-fine fraction of other elements (As, Li, Rb, Sb, Se, Tl, V) showed a concentration peak in the same period, indicating that they were most likely affected by the same long-range transport episode (Perrino et al. 2010). Similar episodes of polluted air masses transport from East Europe were quite recurring during the winter.

A time pattern very similar to Pb was shown by the extracted fraction of Mn, Li, Rb and Ni; for all of these, a constant emission rate is thus expected.

The upper panel of Figure 5.6 also shows that from January 13th to 19th-20th Pb concentration was lower than expected on the basis of the atmospheric mixing. The same behaviour, during the same days, was observed also for the mass concentration of PM and for most of the analysed macro- and micro- components. This very interesting period was characterized by a severe fog episode, evidenced by relative humidity (RH) values constantly higher than 90% and by very low intensity of the solar radiation. During fog episodes, very frequent in the Po Valley during the winter, water condensation generally causes a growth of hydrophilic particles, leading to an increase in their deposition rate (Svenningsson et al. 1992).

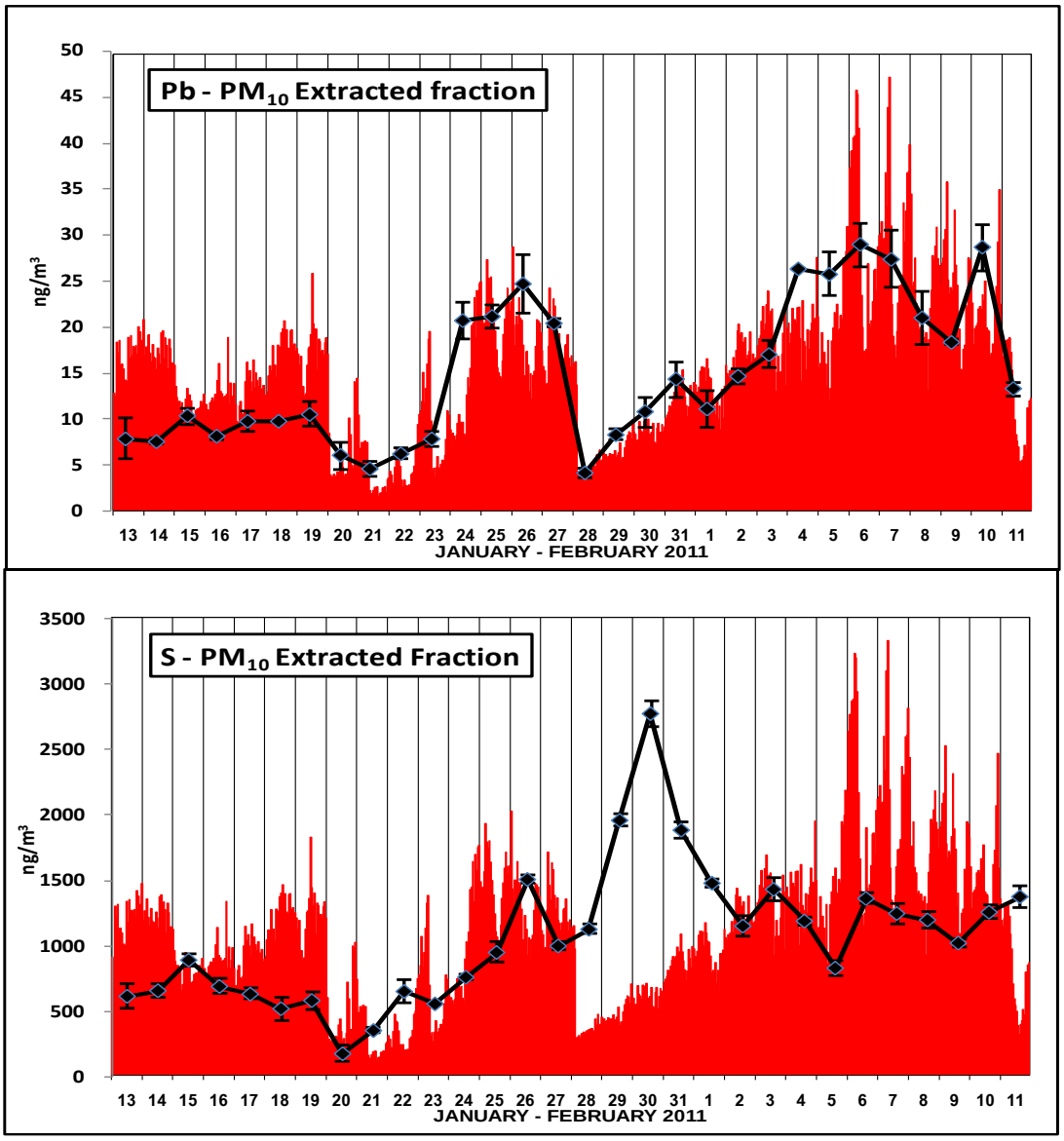

Fig. 5.6: Comparison between the daily pattern of natural radioactivity and of the extracted fraction of Pb (upper panel) and S (lower panel) in PM_{10} during the SOP of January-February 2012. Pb and S concentrations are reported as the mean value among the three sites; error bars indicate the standard deviation.

Moreover, their aerodynamic diameter (AD) can reach values higher than the cut-point of the sampling heads (2.5 and 10 µm). These two mechanisms were probably responsible for a considerable reduction in PM mass concentration during the first days of the SOP. Finally, Figure 5.7 shows that this particle growth also influenced the chemical and dimensional distribution of Pb, leading to a marked increase of its coarse relative contribution (mostly in the soluble, more hydrophyllic, fraction). This increase indicates that water condensation allowed some fine particles

to grow up to reach AD > 2.5 µm, moving from the fine to the coarse fraction, and possibly to reach even AD > 10 µm, being thus excluded also by the PM_{10} sampling head. The same behaviour was observed also for other elements containing a significant fine fraction (As, Cd, Ni, Rb, S, Sb, Se, Tl and V).

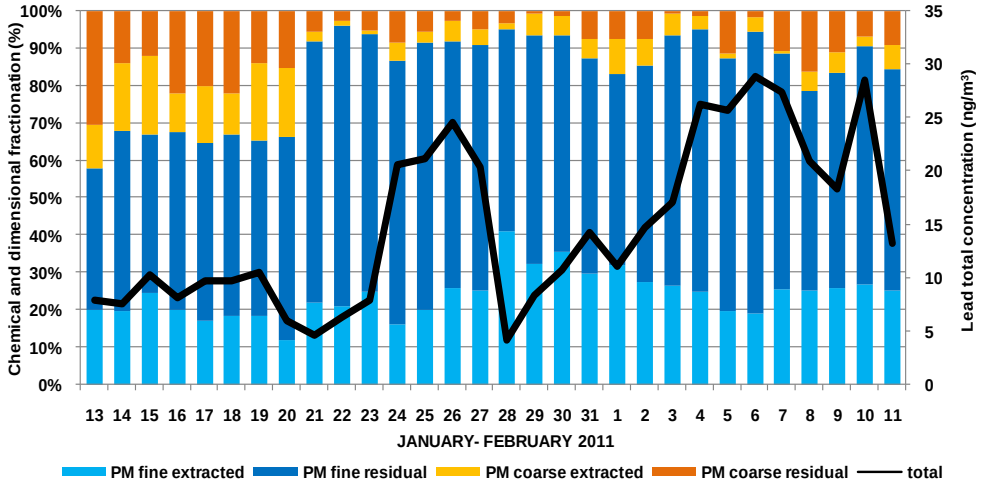

Fig. 5.7: Chemical-dimensional distribution and total concentration of Pb during the SOP of January-February 2012 .

During the fog period the concentration of elements typically present mainly in the coarse fraction (Ba, Be, Cu, Sr and Ti) was always very low, as coarse particles may easily reach AD values higher than 10 µm.

5.4 Conclusions

The results of the 5-year study described in this paper indicate that micro- and trace- elements do not constitute the main critical factor in the area of Ferrara (Po Valley, Italy) despite the presence of a high number of industrial sources and the frequent occurrence of severe pollution episodes that cause the exceedance of PM regulatory limits. However, the application of a chemical and dimensional fractionation procedure has shown that some of the toxic elements (As, Cd, Tl, V) are present mostly in fine particles and as soluble chemical species, being thus particularly accessible to environmental and biological systems. In many other cases (e.g.: Be, Li, Rb, V, Sb, Be, Sn), the elements are contained in both fine and coarse PM, but the fine fraction, mainly associated to

anthropogenic combustion processes, contains more soluble, and thus more bio-accessible, species than the coarse fraction. The very small variations in the concentration, chemical distribution and dimensional distribution of elements among the three sampling sites indicate a low contribution of local emissions, even in the proximity of the industrial area.

Seasonal variability was mainly driven by the poor atmospheric mixing occurring during the winter season. However, the concentration of some elements (Pb, Sn, Li, Rb and Ni) was also influenced by the presence of additional winter sources. Further studies are necessary to obtain a positive identification of this source(s), which could be tentatively identified as domestic heating.

Increase in the concentration of some other elements was due to the long-range transport of natural dust from North Africa, more frequent during the warm season (Sr, Co, Ba, Li, Ba, Li, Mn, Ti, Rb, Be), and of anthropogenic polluted air masses from East Europe, recurring during the winter (As, Li, Rb, Sb, Se, Tl, V). Fog episodes caused both the occasional lowering in the concentration of most elements and a significant variation in their dimensional distribution. The additional knowledge obtained by applying this chemical fractionation procedure to large sets of data will be helpful in further data analysis, carried out by using statistical tools as will be described in the second part of this study.

5.5 References

Al-Masri MS, Al-Kharfan K, Al-Shamali K (2006), Atmospheric Environment, 40:753–761.

Almeida SM, Pio CA, Freitas MC, Reis MA, Trancoso MA (2006), Atmospheric Environment, 40:2058–2067.

Argyropoulos G, Manoli E, Kouras A, Samara C (2012), Science of the Total Environment, 432:12–22.

Argyropoulos G, Grigoratos Th, Voutsinas M, Samara C (2013), Environmental Science and Pollution Research, (DOI 10.1007/s11356-013-1721-y).

Armiento G, Inglessis M, Mazziotti, Tagliani S, Montereali MR, Nardi E, Palleschi S, Piga L, Sacco F, Silvestroni L, Gianfagna A (2013), Periodico di Mineralogia, 82:199–216.

Barrett PM, Resing JA, Buck NJ, Buck CS, Landing WM, Measures CI (2012), Marine Chemistry, 142–144:41–53.

Birmili W, Allen AG, Bary F, Harrison RM (2006), Environmental Science and Technology, 40:1144–1153.

Canepari S, Cardarelli E, Giuliano A, Pietrodangelo A (2006a), Talanta, 69:581–587.

Canepari S, Cardarelli E, Pietrodangelo A, Strincone M (2006b), Talanta, 69:588–595.

Canepari S, Perrino C, Olivieri F, Astolfi ML (2008), Atmospheric Environment, 42:8161–817.

Canepari S, Pietrodangelo A, Perrino C, Astolfi ML, Marzo ML (2009a), Atmospheric Environment, 43:4754–4765.

Canepari S, Perrino C, Astolfi ML, Catrambone M, Perret D (2009b), Talanta, 77:1821–1829.

Canepari S, Astolfi ML, Moretti S, Curini R (2010), Talanta, 82:834–844.

Canepari S, Astolfi ML, Farao C, Maretto M, Frasca D, Marcoccia M, Perrino C (2013), Environmental Science and Pollution Research, 2013 DOI: 10.1007/s11356-013-2298-1 .

Carbone C, Decesari S, Mircea M, Giulianelli L, Finessi E, Rinaldi M, Fuzzi S, Marinoni A, Duchi R, Perrino C, Sargolini T, Vardè M, Sprovieri F, Gobbi GP, Angelini F, Facchini MC (2010), Atmospheric Environment, 44:5269-5278.

Cho S-H, Tong H, McGee JK, Baldauf RW, Todd Krantz Q, Ian Gilmour M (2009), Environmental Health Perspective, 117:1682–1689.

Dos Santos M, Gómez D, Dawidowski L, Gautier E, Smichowski P (2009), Microchemistry Journal, 91:133–139.

Draxler RR, Rolph GD (2010) HYSPLIT (HYbrid Single-Particle Lagrangian Integrated Trajectory) Model access via NOAA ARL READY Website (http://ready.arl.noaa.gov/HYSPLIT.php). NOAA Air Resources Laboratory, Silver Spring, MD.

Dutkiewicz VA, Qureshi S, Husain L, Schwab JJ, Demerjian KL (2006), Atmospheric Environment, 40:S347–S359.

EC: EU Air Quality Directive 2008/50/EC, 2008.

EC: EU Arsenic, cadmium, mercury, nickel and polycyclic aromatic hydrocarbons in ambient air Directive 2004/107/EC, 2004

Fernandez Espinosa AJ, Ternero Rodriguez M, Barragan de la Rosa FJ, Jimenez Sanchez JC (2002), Atmospheric Environment, 36:773–780.

Gietl JK, Lawrence R, Thorpe AJ, Harrison RM (2010), Atmospheric Environment, 44:141–146.

Harrison RM, Yin J (2000), Science of the Total Environment, 249:85–101.

Heal MR, Hibbs LR, Agius RM, Beverland IJ (2005), Atmospheric Environment, 39:1417–1430.

Hueglin C, Gehrig R, Baltensperger U, Gysel M, Monn C, Vonmont H (2005), Atmospheric Environment, 39:637–651.

Li R, Wiedinmyer C, Hannigan MP (2013), Science of the Total Environment, 456–457:346–358.

Limbeck A, Wagner C, Lendl B, Mukhtar A (2012), Analitica Chimica Acta, 750:111–119.

Marcazzan G M, Vaccaro S, Valli G, Vecchi R (2001), Atmospheric Environment, 35:4639-4650.

Marenco F, Bonansoni P, Carlzolari F, Ceriani M, Chiari M, Cristofanelli P, D'Alessandro A, Fermo P, Lucarelli F, Mazzei F, Nava S, Piazzalunga A, Prati P, Valli G, Vecchi R (2006), Journal of Geophysical Research, 111: D24202.

Marmur A, Park S-K, Mulholland JA, Tolbert PE, Russell AG (2006), Atmospheric Environment, 40:2533–2551.

Mukhtar A, Limbeck A (2013), Analitica Chimica Acta, 774:11– 25.

Oberdörster G (2001), International Archives of Occupational and Environmental Health, 74:1–8.

Oberdörster G, Oberdörster E, Oberdörster J (2005), Environmental Health Perspective, 113:823–839.

Öztürk F, Zararsız A, Dutkiewicz V A, Husain L, Hopke P K, Tuncel G (2009), Atmospheric Environment 61:463-475.

Pant P, Harrison RM (2013), Atmospheric Environment, (doi:10.1016/j.atmosenv.2013.04.028).

Perrino C, Canepari S, Catrambone M, Dalla Torre S, Rantica E, Sargolini T (2009), Atmospheric Environment, 43: 4766–4779.

Perrino C, Canepari S, Pappalardo S, Marconi E (2010), Chemosphere, 80:1291–1300.

Perrino C, Catrambone M, Dalla Torre S, Rantica E, Sargolini T, Canepari S (2013a), Environmental Science and Pollution Research, (DOI 10.1007/s11356-013-2067-1).

Pey J, Querol X, Alastuey A (2009), Atmospheric Research, 94:285–299.

Qureshi S, Dutkiewicz VA, Khan AR, Swami K, Yang KX, Husain L, Schwab JJ, Demerjian KL (2006), Atmospheric Environment, 40:S238–S251.

Reche C, Moreno T, Amato F, Viana M, van Drooge BL, Chuang H-C, Bérubé K, Jones T, Alastuey A, Querol X (2012), Ecotoxicology and Environmental Safety, 78:327–335.

Rodrıguez S, Querol X, Alastuey A, Viana M, Alarcon M, Mantilla E, Ruiz C R (2004), Science of the Total Environment, 328:95-113.

Sato K, Tamura T, Furuta N (2008), Journal of Environmental Monitoring, 10:211–218.

Sillanpää M, Saarikoski S, Hillamo R, Pennanen A, Makkonen U, Spolnikc Z, Van Grieken R, Koskentalo T, Salonen RO (2005), Science of the Total Environment, 350:119–135.

Svenningsson IB, Hansson H-C, Wiedensohler A, Ogren JA, Noone KJ, Hallberg A (1992), Tellus, 44B:556–569

Vecchi R, Marcazzan G, Valli G, Ceriani M, Antoniazzi C (2004), Atmospheric Environment, 38:4437–4446.

Viana M, Kuhlbusch TAJ, Querol X, Alastuey A, Harrison RM, Hopke PK, Winiwarter W, Vallius M, Szidat S, Prévôt ASH, Hueglin C, Bloemen H, Wåhlin P, Vecchi R, Miranda AI, Kasper-Giebl A, Maenhaut W, Hitzenberger R (2008), Aerosol Science, 39:827–849.

Voutsa D, Samara C (2002), Atmospheric Environment, 36:3583–3590.

Chapter 6- Sources of particulate matter: Receptor models

The last part of the present research work has been focused on the application of the receptor models aimed to the source apportionment of the PM collected in an industrial area. To this purpose the same data obtained from the field study conducted in the Po Valley, discussed in Chapter 5, were used. This part of the work was carried out at the University of Birmingham during the period February 2013-July 2013, under the kind supervision of Prof. Roy M. Harrison.

6.1 Introduction

Statistical models are more and more used in atmospheric sciences in order to achieve a full description of the sources contributing to the measured PM concentrations. They can be useful to understand under which process atmospheric particles are formed and how they are dispersed after the emission from a source. Indeed, models allow to express mathematically the processes that give rise to particulate matter and govern its lifetime in the atmosphere as well as to evaluate the natural or anthropogenic contributions of the measured concentration levels in ambient air. Particularly, source apportionment (SA) techniques aim to re-construct the impacts of the emissions from different sources of atmospheric pollutants, e.g., particulate matter, based on ambient data registered at monitoring sites (Viana et al., 2008 a). Among SA techniques, methods based on the evaluation of *monitoring data* consist of a basic numerical data treatment used to identify the main sources of the measured components. Most common applications investigate correlations between pollutants concentrations and meteorological parameters like wind direction and speed, temperature, relative humidity, solar radiation and air mass backward trajectories.

Also methods based on emission inventories and/or dispersion models to simulate aerosol emission, formation, transport and deposition can be used as SA technique. *Dispersion models* consist of a mathematical model that disperses (and may also chemically transforms) the emitted pollutant, generating a prediction of the resulting pollutant concentration at a point in space and time (Chow, 1995). Therefore it requires as input the source emissions and meteorological information. One of the factors affecting the accuracy of the results is then to provide a correct input to the dispersion models. For example, since different dispersion, transformation and deposition processes occur on different time scales, their importance depends on the associated spatial scales. Particularly, on a local scale only fast processes are important, which do not incorporate chemical reactions and aerosol formation, while, on regional or larger scales, the slower processes have to be included and,

consequently, chemical and/or physical transformations affecting the pollutant characteristics have to be described.

Nowadays the most used SA techniques are based on the application of *receptor models*. They are specified mathematical procedures for identifying and quantifying the sources of ambient air contaminants at a receptor site, primarily on the basis of concentration measurements at that site. These techniques use the principle of mass and species conservation and a mass balance approach can be used to identify and apportion sources of airborne PM in the atmosphere. Receptor models can be less labor intensive (i.e., less expensive) than extensive robust source-dispersion modeling: ambient data are available at many sites and do not require a representative source profile that sometime may not exist (Watson et al., 2002). One of the main differences among the available receptor models is the knowledge degree of the emission sources prior to the application of a specific model. Indeed model such as Chemical Mass Balance (CMB) requires the knowledge of the composition for all the relevant sources (Watson et la., 1990). However, these requirements are almost never completely achieved as some changes of the source profiles between the emitter and the receptor site often occur, so that the application of the CMB model is usually problematic.

An alternative to CMB is given by the multivariate models, e.g principal component analysis or PCA, positive matrix factorization or PMF, UNMIX, Multilinear Engine or ME, etc., (Viana et al., 2008 a). They require the input of data of multiple species for multiple time periods and extract information from all data simultaneously.

Furthermore, multivariate analyses essentially identify covariant sources. It is assumed that the co-variation comes from co-emission from a source, but it can also come from atmospheric processes that including meteorology and atmospheric chemistry (Viana et.al, 2008 b).

PCA and PMF are commonly used tools, because software to perform this type of analysis is widely available and detailed prior knowledge of the sources and source profiles is not required. Although the wide application of these models, some drawbacks have to be taken into account. Table 6.1 reports the positive and negative features specifically for PCA and PMF (http://www.integrated-assessment.eu/guidebook/principal_components_analysis; Paatero and Tapper, 1994).

Moreover, an alternative to the statistical data analyses is given by simpler models based purely on chemical analysis of major components of PM. Basically, chemical determinations are individually summed to obtain a mass closure and then grouped in order to determine the macro-sources of PM. (Almeida *et al*., 2006; Harrison *et al*., 2003; Perrino *et al*., 2007; Perrino *et al*., 2009; Rees *et al*., 2004) This latter approach has been widely described and discussed in Chapter 3 referring to the

mass balance closure including water analysis in PM.*Tab.6.1:Comparison between PCA and PMF models.*

PCA	
Strengths	*Weaknesses*
• PCA do not need the source emission composition as input; • It can help the identification of an important missing source.	• PCA requires large datasets on measured concentrations (preferably >100 samples); • Analysis is limited by the accuracy, precision, and range of species measured at the receptor locations (e.g. ambient monitoring) sites; • A determination must be made of how many factors to retain, and emission sources have to be deduced by interpreting these factors; • Vectors and components are usually related to broad source types rather than specific sources; • Analysis may generate negative loadings on some components (sources); this is physically impossible. • A large number of solutions can be obtained and it may not be clear whether an optimal solution has been found; • Results cannot be weighed to account for uncertainties in the measured data; • PCA models cannot properly handle missing data or and values below the detection limit (both of which commonly occur in environmental measurements). • Further Multi-linear Regression Analysis is required to quantify the sources to PM levels.
PMF	
Strengths	*Weaknesses*
• No need for *a priori* knowledge of source compositions; • Good to isolate minor contributors to mass; • No need to select "relevant" species; • Results CAN be weighted to account for uncertainties in each species and in each sample;	• Requires large data matrix; • Depends on source profiles which may vary with time; • Often "secondary" factors that are not true sources are isolated; • Gives a wide range of solutions for interpretation (need to determine which solutions make sense within the conceptual

• PMF ALLOWS to handle missing data or and values below the detection limit (both of which commonly occur in environmental measurements); • A non-negativity constraint is always used, since no source can contribute "negative" mass; • The robust mode is useful so that outliers do not significantly influence the solution; • PMF allows to quantify PM sources.	model); • Highly collinear sources are difficult to isolate;

6.1.1 Application of PMF receptor model to PM_{10} and $PM_{2.5}$ samples collected in Po Valley

Results of this work are being published by the journal Atmospheric and Air Quality Research.

The Po Valley, as widely discussed in Chapter 3/5, is a large industrialized and highly populated area located in the north of Italy.

Its adverse meteorological conditions, including weak circulation of air masses in the winter period, and alternation of hot-dry and humid days in summer (Bernardoni et al., 2011; Larsen et al., 2012) leads to the accumulation of pollutants in the local atmosphere, and consequently the European PM_{10} standard is exceeded in many cities located in Northern Italy (Larsen et al., 2012; Marcazzan et al., 2003). The further development of abatement strategies in this area is essential for the protection of both human health and the environment. One of the most powerful tools towards formulation of abatement policies is particulate matter source apportionment by combination of chemico-physical analyses of PM composition and statistical data analyses. As previously said PCA and PMF are the most important multivariate models as they do not require the knowledge of sources and emissions (Viana et al., 2008a).

A number of works in the literature relate to the source apportionment of PM_{10}, $PM_{2.5}$ and even PM_1 in several cities located in the Po Valley using different receptor models (Contini et al., 2012; Marcazzan et al., 2003; Stortini et al,. 2009; Vecchi et al., 2008). Most of them included as model variables only the total elemental concentration, excluding carbonaceous and ionic compounds. A fuller characterization of PM composition can assist identification and quantification of the sources.

In these cities, anthropogenic sources including traffic and industry make a significant contribution to the PM emissions. Industrial sources include a wide range of different elemental emissions, depending upon the characteristics of the plants present in the vicinity of the receptor site, e.g. steel mills, power plant, waste incinerators, etc. Also, emission sources from industrial areas are

particularly difficult to identify due to a lack of specific elemental tracer, making the source apportionment studies more difficult.

As already discussed in Chapter 5 the size fractionation and the chemical fractionation based on elemental solubility of PM may offer the possibilities to enhance the selectivity of the elements as source tracers. In this context the combination of a chemical fractionation methodology together with a receptor model could be beneficial in the identification of the PM sources within highly polluted areas. To this purpose PMF receptor model was performed to process the same PM_{10} and $PM_{2.5}$ data discussed in the previous chapter, including as model variables the extractable (soluble), the residual (insoluble) or both the fractions of some trace elements determined by means of the chemical fractionation methodology. Moreover PMF results were compared with those obtained by applying a mass closure method (widely discussed in Chapter 2) on the same data in order to examine the potential and the limitations of the two approaches.

6.2 Experimental

The sampling sites, sampling devices and chemical analysis are the same of those described in section 5.2 (Chapter 5) and 3.3 (Chapter 3). This part of the work related to the complete chemical characterization of PM: Macro-elements, inorganic ions, organic and elemental carbon and trace elements. Also, this elaboration involved only four Special Observation Periods (SOPs): January-February 2011, June 2011, January-February 2012 and May-June 2012.

Mass closure and macro-sources were calculated by using the same algorithms described in section 3.1 of Chapter 3. The results of this elaboration have been kindly provided by Doct. Cinzia Perrino of the Institute of Air Pollution (CNR, Montelibretti).

6.2.2 PMF model

PM_{10} and $PM_{2.5}$ sample data were processed using the PMF receptor model developed by Paatero et al. (1994). Here, a brief description of the theoretical concepts of this model. It uses a weighed least squares fit and the weightings are based on the known uncertainties of the elements in the data matrix (Paatero, 1997). Specifically, the mathematical model in matrix form is written as:

$$x_{ij} = \sum_{k=1}^{p} g_{ik} f_{kj} + e_{ij} \quad (1)$$

$$X = GF + E$$

Where x_{ij} is the concentration of the *j*-th measured species in the *i*-th samples, g_{ik} is the contribution of *k*-th factor to the *i*-th sample, f_{kj} is the concentration of the *j*-th species in the *k*-th factor profile and e_{ij} is the model error of the *j*-th measured species in the *i*-th samples. The goal is to find values for *G*, *F* and *p* that best reproduce *X* (Reff and Eberly, 2007).

The solution of this equation allows to know both the profile of the PM sources (factors) and the contribution of each source to each sample, on the base of the simple chemical analysis. In this study EPA PMF3.0 software was used for the analysis, available on the web. Site http://www.epa.gov/heasd/research/pmf/pmf_registration.html.

Separate data elaborations were performed for PM_{10} and $PM_{2.5}$ samples collected at all the three sampling sites (A, B, C, described in Chapter 5) resulting in 360 samples for PM_{10} and 360 samples for $PM_{2.5}$. For species analyzed by more than one analytical technique (see paragraph 3.3.2) only one method was chosen in order to avoid the double counting of these species (Reff and Eberly, 2007).

The use of an elemental fractionation methodology allows the improvement of the selectivity of most elements as source tracers, by discriminating combustive from mechanical-abrasive sources (Canepari et al., 2008, Canepari et al. 2009b, Canepari et al. 2010). In particular, the processed elements were chosen according to the results reported in the previous chapter, in which the dimensional distributions and solubility of the elements in the monitored area were examined in details: it was evidenced that the extractable fractions of As, Cd, Ni, Pb, Rb, Fe, Sb, Tl, V, Zn are generated by combustion sources in the fine particles, while the residual fraction of Ba, Cu, Fe, Sb, Mn, Ti are released as coarse particles by mechanical-abrasive sources. According to this, twenty-nine species were selected as PMF variables: OC, EC (thermo-optical analysis), Al Si, K (XRF), Cl^- NO_3^-, SO_4^{2-}, Na^+, NH_4^+ (Ion Chromatography), extractable fraction of As, Cd, Mg, Ni, Pb, Rb, Sb, Tl, V, Zn, residual fraction of Ba, Cu, Mn, Ti and both fractions of Fe, Sb. PM mass concentration was included in the input data matrix so that the model apportioned it to each factor; its uncertainty was tripled to avoid a large influence on the solution.

Data and uncertainties were handled in the same way for both size ranges. The uncertainties matrix was created using the analytical repeatability of the method calculated using twenty pairs of

equivalent real samples (Canepari et al., 2006 b; Canepari et al., 2009). Missing data were replaced with the species median concentration and their uncertainties were set to four times the median concentration. Data below detection limit were replaced with half of detection limit and their uncertainties were increased to 5/6 the detection limit (Polissar et al., 2008). Species were classified as "strong", "weak", and "bad" variables based on the signal-to-noise ratio, the shape of the distribution of scaled residuals and the "observed/predicted" plots (Paatero and Hopke, 2003; Reff and Eberly, 2007). All the factors found in the two analyses were independent, indicating the absence of a rotational ambiguity in the solution. As confirmation, PMF solutions with Fpeak value between -1 and 1 were explored. The resulting solutions were similar giving no further information about the factors' identification.

6.3 Results and discussion

6.3.1 PMF Source profiles

The minimum number of factors (p) to be chosen in the PMF analysis was evaluated calculating the maximum individual column mean (IM) and the maximum individual column standard deviation (IS) parameters from the scaled residuals matrix and the Q values, as suggested by Lee *et al*. (1999). These parameters gave information about the quality of the fit and were useful to determine the number of factors. Results (not shown) indicated that the number of factors to be studied was greater or equal to 6 for PM_{10} and greater or equal to 5 for $PM_{2.5}$. A p=6 solution and p=7 solution were chosen for PM_{10} and $PM_{2.5}$ respectively; in both cases, solutions with higher values of p were rejected as they evidently separated variables belonging to the same source in more than a factor.

The sources of PM_{10} and $PM_{2.5}$ and their chemical composition are shown in Figs. 6.1 and 6.2. The "crustal matter" source, accounting for about 20% of the PM mass concentration in both size fractions, was identified by high values of Al and Si. In both the profiles OC, EC and SO_4^{2-} were also included. Perrone *et al*. (2013) found these components mixed with crustal markers in $PM_{2.5}$, as the mineral particles can change their original composition during their ageing in the atmosphere, getting mixed/coated with inorganic ions, organics and black carbon. This may explain the higher PM concentration apportioned to this factor in the fine fraction. The "marine aerosol" source was identified by the presence of Na^+, Cl^- and Mg in both PM_{10} (5% of PM) and $PM_{2.5}$ (2% of PM).

A factor characterized by the presence of several elements in the soluble fraction (As, Cd, Pb, Fe, Tl, Zn) was found in PM_{10} and $PM_{2.5}$ accounting respectively for 10% and 4% of the PM

concentration. These elements are usually associated with different industrial emissions and are emitted by the several plants located in the area under study (Viana et al., 2008b; Contini et al., 2012). The factor was then named "industry". Chemical analyses of these elements showed that they all were almost wholly present in the fine fraction of PM (Canepari et al., 2013a). In this work the greater contribution of these species in the PM_{10} factor was probably due to the presence in the chemical profile of Al, Si and residual Fe and Mn, mainly present in the coarse fraction.

A factor identified by high concentration of OC, NO_3^-, SO_4^{2-} and NH_4^+ and a large contribution to extractable V and Ni occurred in PM_{10} (6%). These are indicators of secondary particles and of oil combustion (Vecchi et al. 2008). The same components were separated into two factors in $PM_{2.5}$, each one accounting for 7%.

A factor associated with three different sources was found in PM_{10} (50% of the mass concentration). The main species were NH_4^+ and NO_3^-, which identified a "secondary nitrate" source. In the same factor we found EC, OC, K and Rb, which are identified in literature as tracers of biomass burning (Gianini et al. 2012; Ducret- Stich et al., 2013). This factor also includes Zn together with EC, considered as tracers of traffic exhaust emissions (Viana et al., 2008a; Weckwerth, 2001). This factor was then named "secondary nitrate/biomass burning/exhaust particles".

In $PM_{2.5}$ the "secondary nitrate" source was resolved in a single factor, accounting for more than 40% of the mass concentration, while the biomass burning source, showing a high loading on K, OC and EC, was resolved in a factor unexpectedly including also Ba, Cu, Fe, Mn, Sb in the residual fraction (20% of PM concentration). These particles in their coarse fraction are mainly generated from mechanical-abrasive processes (brake wear) and can serve as indicators of non-exhaust traffic emissions (Harrison et al., 2004; Canepari et al., 2008; Gietl et al, 2010). The size distribution of brake wear extends into the fine fraction of PM, and it seems likely that PMF has failed to separate the biomass burning and brake wear signatures in $PM_{2.5}$.

The last factor, found only in PM_{10} and accounting for 13%, contributed substantially to Ba, Cu, Fe, Mn, Sb and Ti, all in the residual fraction. These elements are associated with brake and tyre wear, and the small percentages of Al and Si in the factor indicate a probable contribution from re-suspended road dust, in which soil is one of the components (Harrison et al., 2003; Viana et al. 2008a; Amato et al., 2011). It was called "brake and tyre wear/resuspended road dust" as it was clearly related to particles emitted by the non-exhaust traffic source.

Sources contributing to both PM_{10} and $PM_{2.5}$ were very similar, although the model separated them better in $PM_{2.5}$. The secondary nitrate source was the key component of PM composition but there was also a relevant anthropogenic contribution from biomass burning, industry and exhaust and

non-exhaust traffic sources, in agreement with the other studies performed in the Po Valley (Marcazzan et al., 2003; Vecchi et al., 2008; Bernardoni et al., 2011). Furthermore, the application of a chemical fractionation methodology was useful to identify in PM_{10} some sources that have similar composition in terms of total elemental concentration, since the extractable and the residual fractions of some elements correlated individually in different factors; this confirms that the two solubility fractions were emitted by different sources (e.g. natural crustal matter and re-suspended road dust, traffic exhaust and brake and tyre wear).

Unfortunately because some factors represented a mixture of emission sources, individual contributions of these sources could not be quantified.

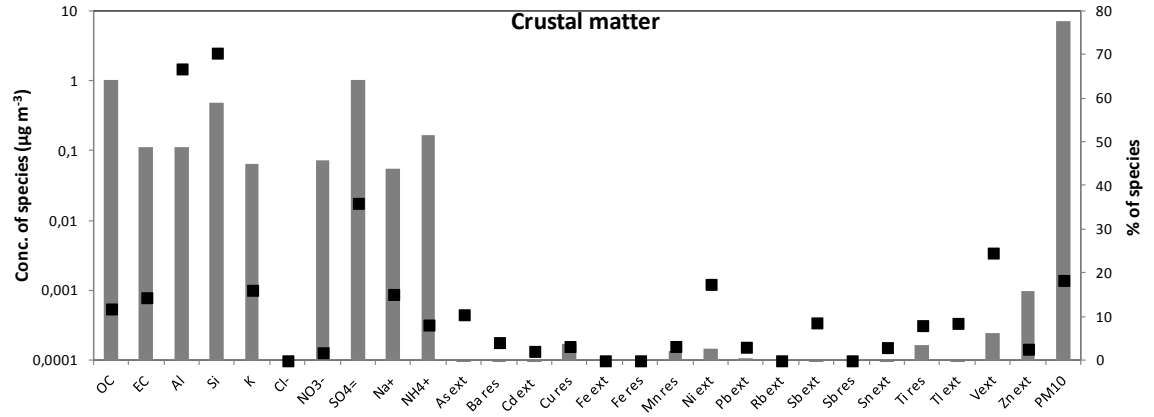
Crustal matter
Conc. of species (µg m-3)
% of species
10
1
0,1
0,01
0,001
0,0001
80
70
60
50
40
30
20
10
0
OC EC Al Si K Cl- NO3- SO4= Na+ NH4+ As ext Ba res Cd ext Cu res Fe ext Fe res Mn res Ni ext Pb ext Rb ext Sb ext Sb res Sn ext Ti res Tl ext V ext Zn ext PM10

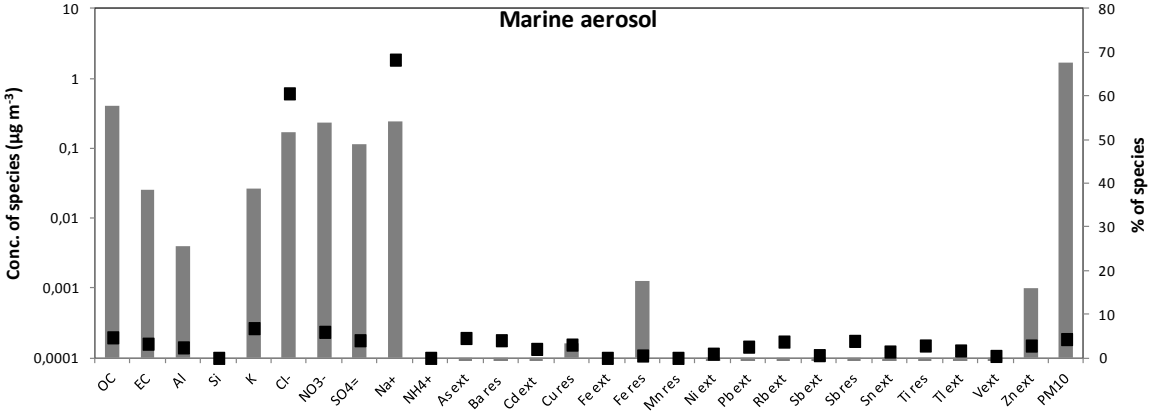
Marine aerosol
Conc. of species (µg m-3)
% of species
10
1
0,1
0,01
0,001
0,0001
80
70
60
50
40
30
20
10
0
OC EC Al Si K Cl- NO3- SO4= Na+ NH4+ As ext Ba res Cd ext Cu res Fe ext Fe res Mn res Ni ext Pb ext Rb ext Sb ext Sb res Sn ext Ti res Tl ext V ext Zn ext PM10

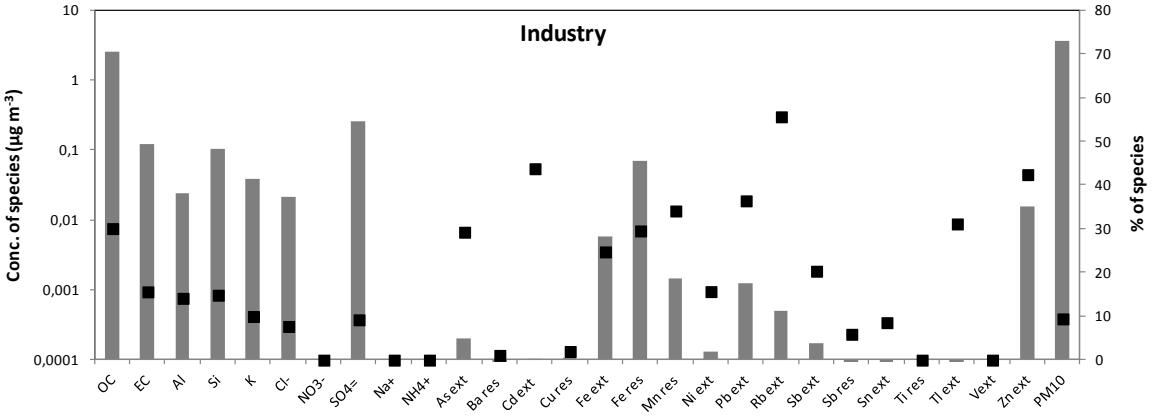
Industry
Conc. of species (µg m-3)
% of species
10
1
0,1
0,01
0,001
0,0001
80
70
60
50
40
30
20
10
0
OC EC Al Si K Cl- NO3- SO4= Na+ NH4+ As ext Ba res Cd ext Cu res Fe ext Fe res Mn res Ni ext Pb ext Rb ext Sb ext Sb res Sn ext Ti res Tl ext V ext Zn ext PM10

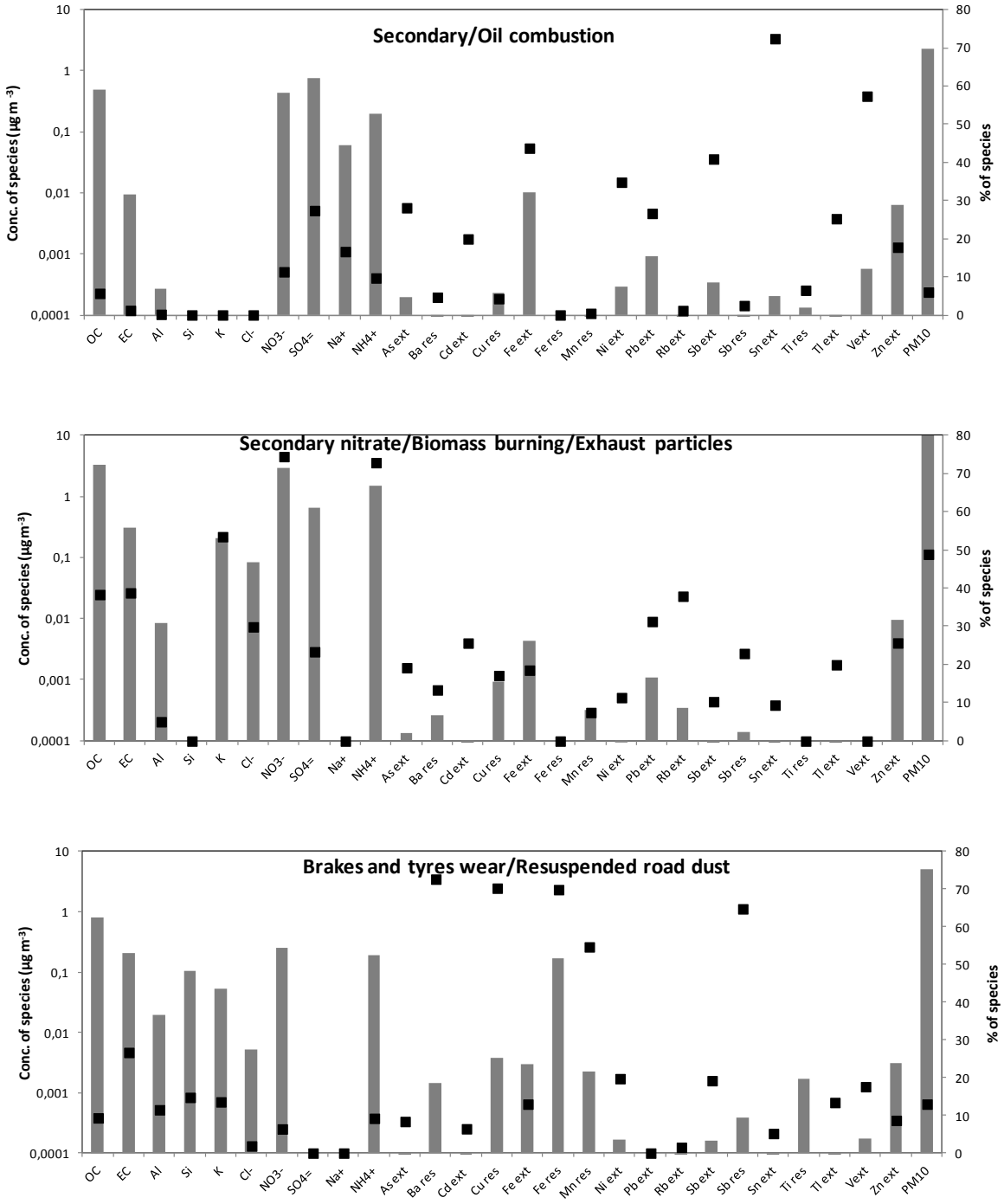

Fig.6.1: PMF source profiles of PM_{10}. The left side axis reports the concentration of each species in each factor ($\mu g/m^3$), the right side axis reports the percentage (%) of each species in each factor.

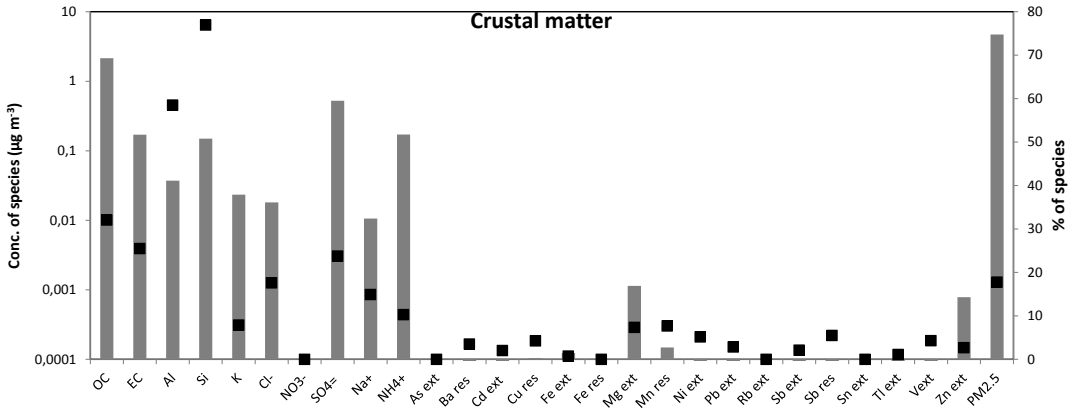
Crustal matter
Conc. of species (µg m-3)
% of species
10
1
0,1
0,01
0,001
0,0001
80
70
60
50
40
30
20
10
0
OC EC Al Si K Cl- NO3- SO4= Na+ NH4+ As ext Ba res Cd ext Cu res Fe ext Fe res Mg ext Mn res Ni ext Pb ext Rb ext Sb ext Sb res Sn ext Tl ext Vext Zn ext PM2.5

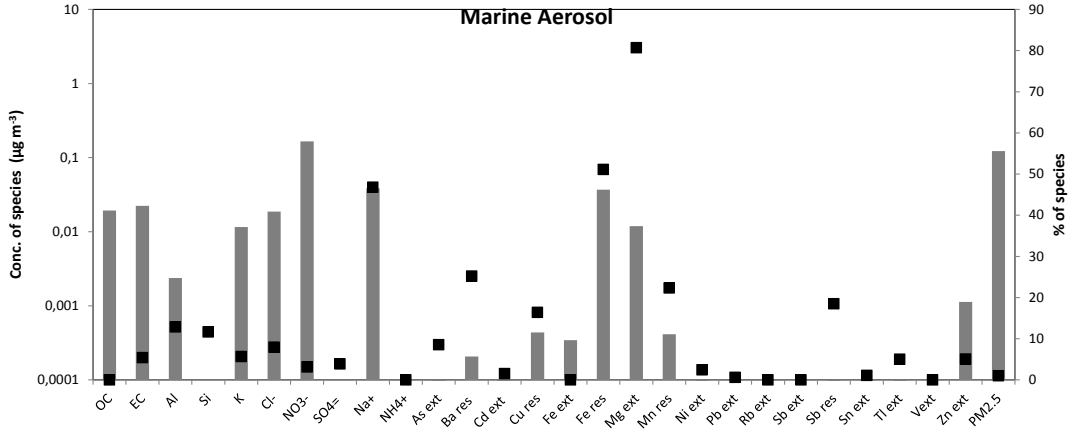
Marine Aerosol
Conc. of species (µg m-3)
% of species
10
1
0,1
0,01
0,001
0,0001
90
80
70
60
50
40
30
20
10
0
OC EC Al Si K Cl- NO3- SO4= Na+ NH4+ As ext Ba res Cd ext Cu res Fe ext Fe res Mg ext Mn res Ni ext Pb ext Rb ext Sb ext Sb res Sn ext Tl ext Vext Zn ext PM2.5

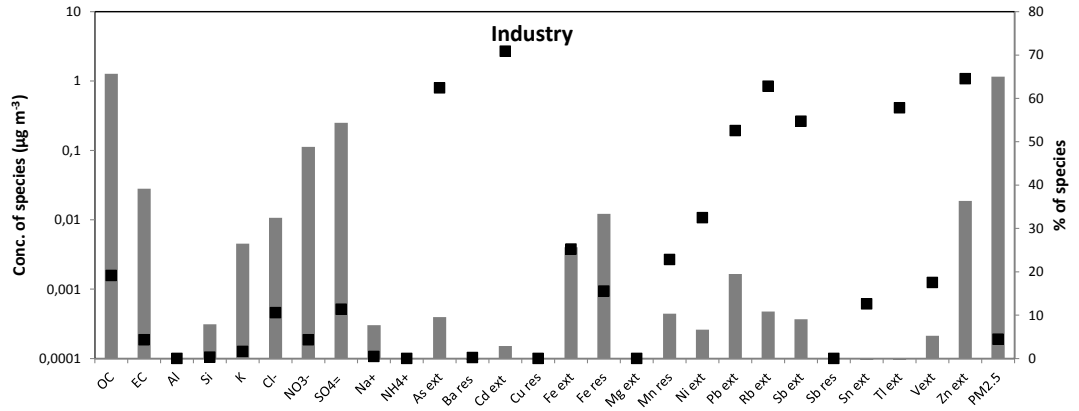
Industry
Conc. of species (µg m-3)
% of species
10
1
0,1
0,01
0,001
0,0001
80
70
60
50
40
30
20
10
0
OC EC Al Si K Cl- NO3- SO4= Na+ NH4+ As ext Ba res Cd ext Cu res Fe ext Fe res Mg ext Mn res Ni ext Pb ext Rb ext Sb ext Sb res Sn ext Tl ext Vext Zn ext PM2.5

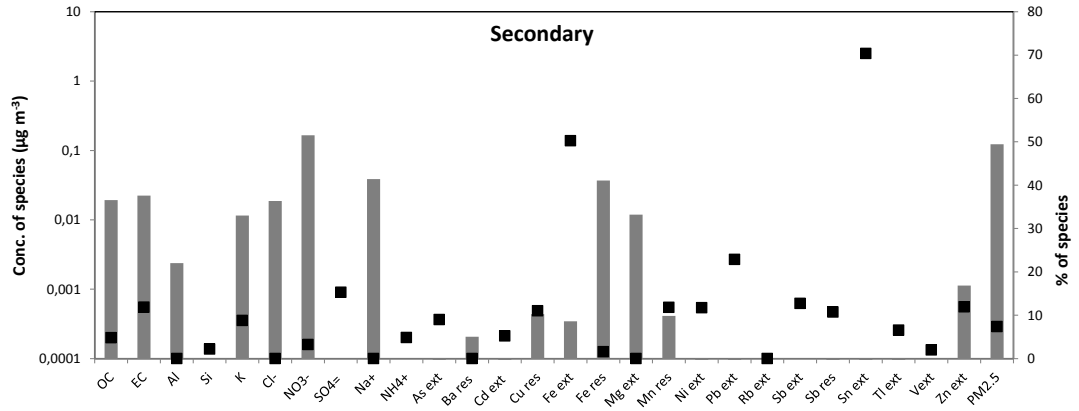
Secondary
Conc. of species (µg m-3)
% of species
10
1
0,1
0,01
0,001
0,0001
80
70
60
50
40
30
20
10
0
OC EC Al Si K Cl- NO3- SO4= Na+ NH4+ As ext Ba res Cd ext Cu res Fe ext Fe res Mg ext Mn res Ni ext Pb ext Rb ext Sb ext Sb res Sn ext Tl ext Vext Zn ext PM2.5

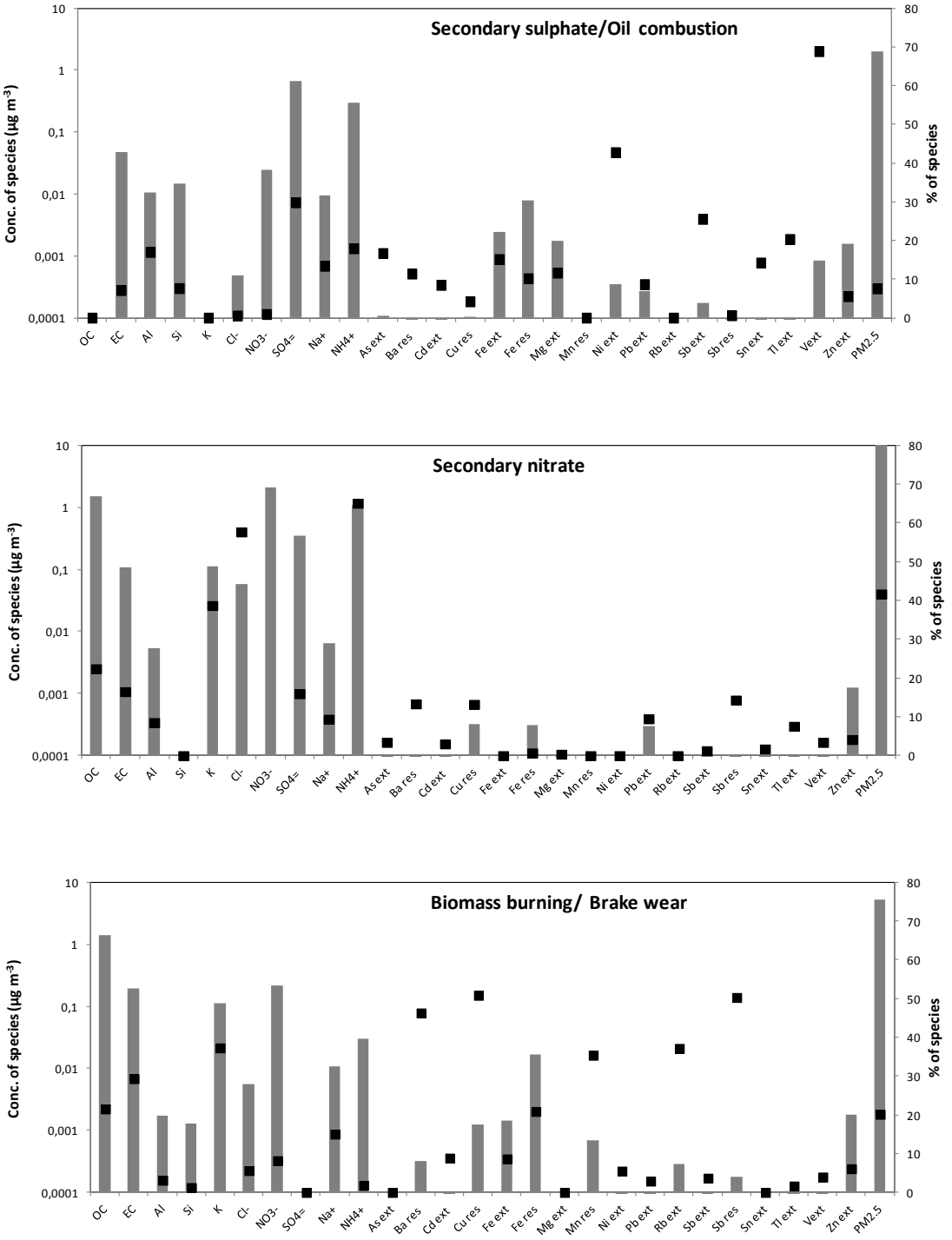

Fig.6.2: PMF source profiles of $PM_{2.5}$. The left side axis reports the concentration of each species in each factor (µg m^{-3}), the right side axis reports the percentage (%) of each species in each factor.

6.3.2 Spatial and temporal variation of sources identified by PMF

PMF model give also the possibility to study the temporal variation of each factor (source/es) during all the studied period. Time series of the factors were a useful aid to confirm the interpretation of the chemical profiles and to evaluate the seasonal trends and the differences among the sampling sites of the PM sources.

As an example, figure 6.3 shows the time evolution of crustal matter and marine aerosol sources in daily PM_{10} and $PM_{2.5}$ obtained in winter 2011 and summer 2012 for the sampling sites A, B and C. Source contributions at the three sites did not show very significant differences, confirming, also in this case, the homogeneity of the air masses in the area under study and the robustness of the analysis (Canepari et al., in press; Perrino et al., 2013a). The crustal matter source was higher in summer consistent with the dryness of the soil in this season. During summer 2012, the higher contribution of the crustal matter registered during the days of 19-22 June at all the sites was attributable to transport of mineral dust from the desert regions of North Africa towards Northern Italy. This episode was detected by the model BSC-DREAM8b (Dust REgional Atmospheric Model, Basart et al., 2012) and confirmed by the Hysplit model previously discussed. Marine aerosol contributions were higher in PM_{10}. This was an expected results, as the particles constituting the sea spray are most contained in the *coarse* fraction of PM.

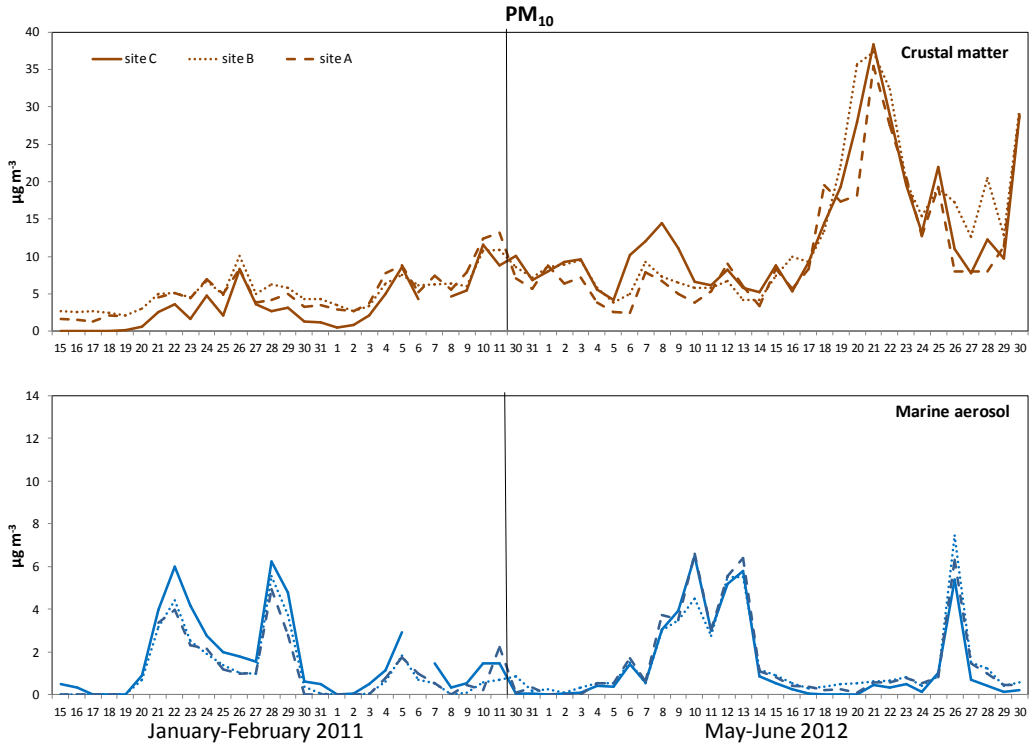

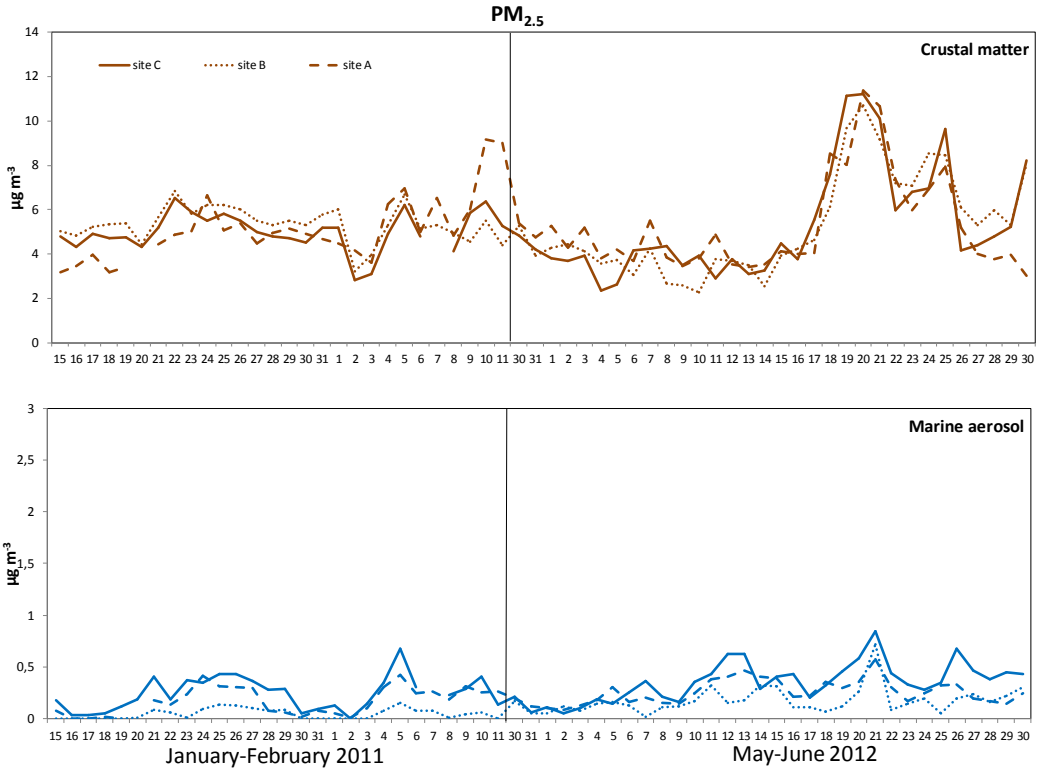

Fig.6.3: PMF time series of PM_{10} and $PM_{2.5}$ crustal matter and marine aerosol sources in winter 2011 and summer 2012 at sites A, B and C.

A seasonal pattern was not clearly defined as some intense advective phenomena that carried the particles from the sea to the inland areas occurred in both winter and summer periods (January 21-29, February 4-10, June 8-13 and June 26th), resulting in higher values.

Spatial and temporal variability of the other sources was difficult to interpret on the basis of time series only, because some factors resolved by PMF, particularly in PM_{10}, were associated with a mixing of different sources. It is well known that one of the limitations of this model is the inability to separate sources which co-vary in time (Viana et al., 2008b).

Covariation of the sources was mainly due to the particular meteorological conditions encountered during the cold months within the studied area, where the weak circulation of the air masses associated with high atmospheric stability led to the homogenous accumulation of pollutants. This was confirmed by comparing the source contributions with the natural radioactivity time pattern. As an example, Fig. 6.4 shows the time pattern of the PM_{10} secondary nitrate/biomass burning/exhaust traffic source at the three sites compared with the natural radioactivity pattern during winter

2011(upper panel) and the time pattern of PM_{10} brake and tyre wear/re-suspended road dust sources compared with natural radioactivity during summer 2012 (lower panel).

In winter, weak atmospheric mixing during both night and day corresponds to constantly high radioactivity values for many subsequent days. The upper graph shows a very close agreement between the temporal pattern of concentrations and natural radioactivity, confirming the modulation of these sources by the action of atmospheric stability. It has to be noted that during the first days of the winter 2011 an intense fog event occurred in Ferrara. This led to an increase in the average diameter of the particles (> 10 μm) that were thus excluded from the sampling head. For this reason, contributions were lower than expected on the basis of the natural radioactivity pattern (Canepari et al., 2013a). These ground-level sources, constant in time and homogeneously distributed in the monitored area, result to be the main contributors to the high PM concentrations registered in the winter period. Other sources, like brake and tyre wear/re-suspended road dust sources in $PM_{10,}$ were as much influenced by the mixing properties of the lower atmosphere but their time pattern was also dependent on the variability of the source emission rates.

In summer, the natural radioactivity pattern showed strong daily trends rather than long periods of atmospheric stability so there was no clear relationship of these sources to the radioactivity pattern (Fig. 6.4 lower panel) and the contributions of brake and tyre wear/re-suspended road dust were attributable mainly to traffic intensity. This contribution is higher during summer due to dryness conditions. Contributions of the secondary nitrate and biomass burning sources were instead lower, due to the higher temperatures enabling the volatilization of the secondary compounds, and the absence of domestic heating.

As regards $PM_{2.5}$ sources, PMF was able to better separate them and also in this case the winter trend showed a good agreement with the natural radioactivity for secondary nitrate, biomass burning, industry and secondary sources.

The time series of $PM_{2.5}$ industry, secondary and secondary sulphate/oil combustion sources for winter 2011 and summer 2012 appear in Figure 6.5.

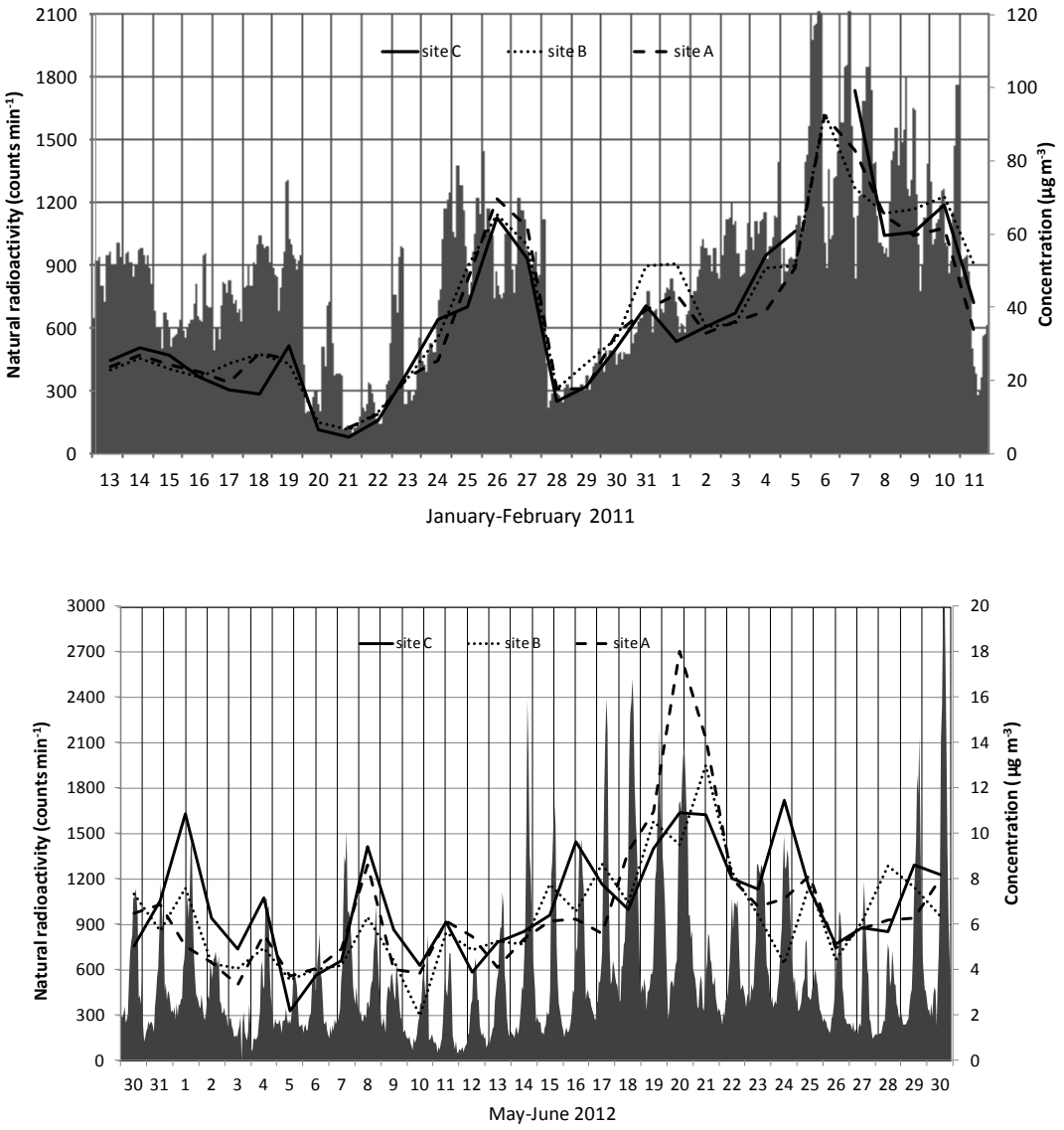

Fig.6.4:Upper panel: Comparison between natural radioactivity and PM_{10} secondary nitrate/biomass burning/exhaust particles source at sites A, B and C during winter 2011 (upper panel). Lower panel: Comparison between natural radioactivity and PM_{10} brakes and tyres wear/ resuspended road dust at sites A, B and C during summer 2012.

Values at the three sites were fairly similar confirming the low contribution of local point sources despite the closeness of the industrial area and their limited influence on the high concentrations of PM recorded in this area, as discussed in the previous Chapter regarding the elemental analysis. Industry showed higher contributions in winter, contributing to the worse air quality observed in the area of Ferrara during the cold months. Seasonal variability of the secondary factor was not clearly defined. High contributions were found in both winter and summer period. Secondary sulphate/oil combustion showed elevated values in summer. The correlation among Ni, V and SO_4^{2-} suggests

that secondary sulphate originated from the oxidation of SO_2 emitted primarily by the industry/power plants located in the monitored area, in particular the petrochemical plants. Secondary sulphates are formed mainly in summertime because of the higher photochemical activity in the Mediterranean basin (Vecchi et al., 2008). If the source is relatively local, it may be emitting above the mixed layer top in winter and hence not affecting local ground-level concentrations.

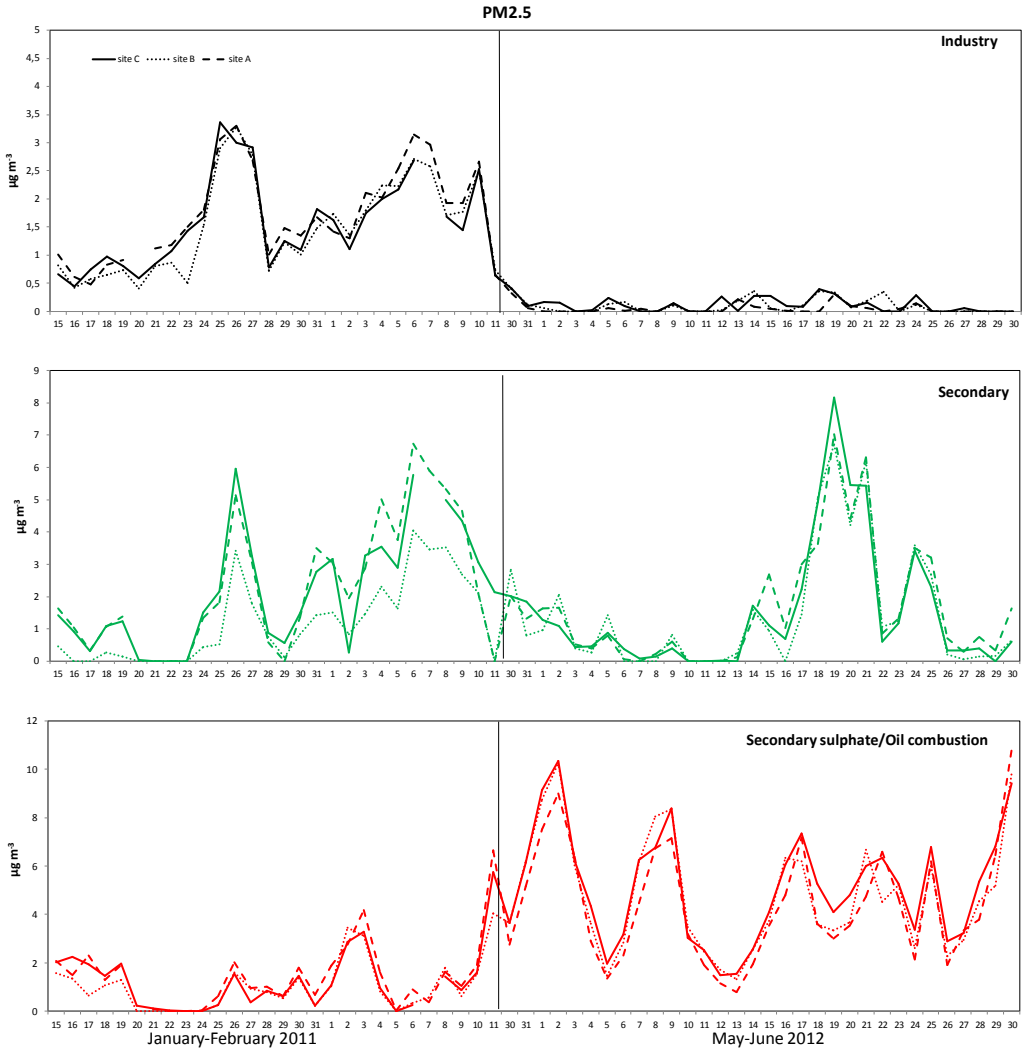

Fig.6.5: PMF time series of $PM_{2.5}$ industry, secondary and secondary/oil combustion in winter 2011 and summer 2012 at sites A, B and C.

6.3.3 Comparison between PMF and mass closure results

Results obtained by PMF were compared to those arising from mass closure (discussed in Chapter 3). Both the approaches, which are among the most widely used for studying the PM sources, allow the reconstruction of the sampled PM mass basing on very different principles. PMF values were obtained by adding the modeled concentration of each factor in each sample ($g_{i,k}$; eq.1). Mass closure considers the sum of concentration of major chemical components (only after conversion of elemental concentration to oxides). In both cases, the reliability of the results may be confirmed by the correspondence of the reconstructed mass with the total PM mass measured; in Fig. 6.6 we compare PM concentration as modelled by PMF and as reconstructed by the sum of the chemical analyses (mass closure) vs. the daily measured concentrations of PM_{10} and $PM_{2.5}$. In the case of PM_{10} we obtained a very similar agreement between the two approaches (R^2=0.94 for PMF, R^2= 0.93 for mass closure), while for $PM_{2.5}$ the PMF provided a higher correlation between measured and calculated data (R^2=0.93) than mass closure (R^2=0.90). Slopes of the curves were very close to 1 in PMF and around 0.7 in mass closure, whereas the intercept values were lower in PMF than in mass closure both for PM_{10} and $PM_{2.5}$. The lower values of the slope obtained in mass closure were most likely due to the presence of significant amounts of water in PM (Canepari et al. 2013b; Perrino et al. 2013b). By including the water determination in the mass closure, determined by the Karl-Fisher method optimized in our laboratory (see Chapter 2), the slope value becomes closer to 1. Separate measurements of water in samples rich in Saharan dust or secondary constituents showed a water content up to 10%. The PM mass reconstruction by PMF was not affected by this missing species and water was indirectly included in the source contributions.

A further comparison between the two approaches regarded the time pattern of the main sources. From the determination of the major components used for the mass closure only five macro-sources (MS; discussed in Chapter 3) were calculated, while PMF did not have any limitations in the number of factors that could have been found and included in the analysis also trace elements. This resulted in different sources identified with the two approaches, which impair a rigorous comparison. Anyway, for some common sources, the analogies and differences of the two approaches can be discussed.

As an example, in Fig.6.7 the daily variation of PM_{10} marine aerosol (upper graphs) and crustal matter (middle graphs) sources at site C during winter 2011 and summer 2012 are shown. The time pattern yielded by the two approaches were very similar for both sources, in winter and in summertime. However, PMF contributions were generally higher than those obtained by MS

calculation. For marine aerosol (MA) the average of the ratio MA_{PMF}/ MA_{MS} was 1.7 in winter and 1.2 in summer, while for crustal matter (CM) the average of the ratio CM_{PMF}/ CM_{MS} was 0.7 in winter and 1.8 in summer although the two series of data were well correlated (R^2= 0.7 for MA and CM in winter and R^2= 0.9 for MA and CM in summer). Similar results were obtained at sites A and B.

Large differences in the comparison between the results for marine aerosol obtained performing PCA and Mass Balance Analyses were found also by Almeida et al. (2006). They suggested that the discrepancy observed for the marine aerosol source was attributable to a poor mass closure that did not include all the components associated with sea spray, and to the reactions of NaCl with inorganic acids (HNO_3, H_2SO_4) that caused the loss of HCl, so that Cl^- was not totally present in particulate form at the sampling site. Nonetheless, the differences in our observations were too high to be explained only by these reasons and we suppose PMF overestimated the contribution of this source during severe sea salts events.

Also for the crustal matter source the discrepancy observed was only in small part explained by the assumption in the MS approach that all the elements were present as oxides. This difference could rather have been largely due to water and to other organic and inorganic species adsorbed on the surface of crustal particles, particularly during Saharan transport events (Canepari et al., 2013b; Perrone et al., 2013).

The MS approach included separate sources for secondary inorganic compounds, vehicular emission and organics, while PMF showed a mixed source comprising secondary nitrate/biomass burning/exhaust particles and did not show a single factor associated with organic compounds. Some previous studies have highlighted the difficulty of receptor models to detect and interpret sources of organics in the absence of speciated data on the organic matter (Viana et al., 2008a). The contribution of the organic compounds in PMF was assumed to be split between different factors and the main part was included in the nitrate/biomass burning/exhaust particles (see the factor profiles composition). Consequently, secondary inorganic compounds (SI), vehicular emission (VE) and organics macro-sources (O) were summed in order to compare them with the only source present in PMF (SI+VE+O in Fig. 6.7, lower panel). In winter a very good agreement between the two series of data was observed, the average of the ratio $(SI+VE+O)_{PMF}$/ $(SI+VE+O)_{MS}$ was 1. Conversely, in summer the SI+VE+O was higher in the MS calculation: the average $(SI+VE+O)_{PMF}/(SI+VE+O)_{MS}$ was 0.2. The good correlation in winter indicated that almost all the organics macro-source was constituted by the biomass burning products. The poorer relationship in summer was probably due to the low contribution of the biomass burning organics and to the

presence in the organics macro-source of a relevant amount of secondary (originated by photochemical oxidation) and biogenic compounds, which were not included in the considered PMF factor.

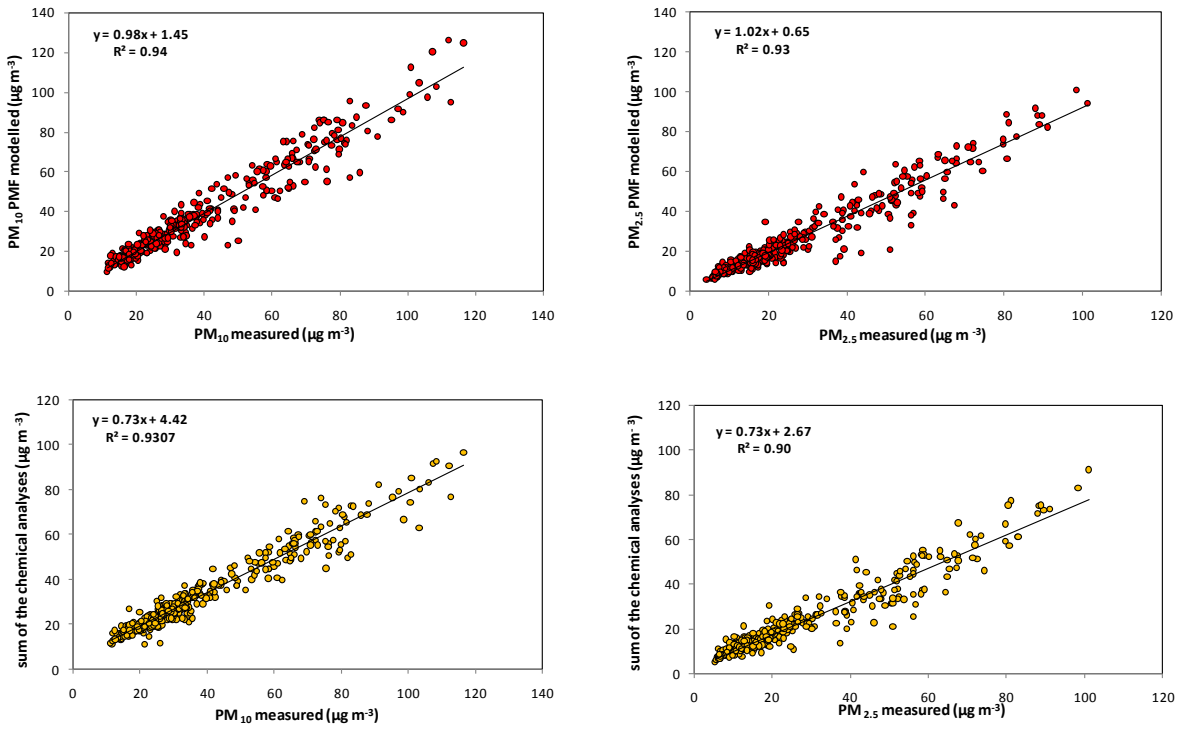

Fig.6.6: Correlation between measured and calculated concentrations of PM_{10} and $PM_{2.5}$ obtained with PMF and mass closure approaches.

Conclusions

Source apportionment carried out by the PMF model showed very similar sources for both PM_{10} and $PM_{2.5}$ although source separation was better in $PM_{2.5}$ samples. During the winter, the main sources of PM in the area of Ferrara were identified as secondary nitrate and biomass burning, accounting for about 40% and 20% of the $PM_{2.5}$ concentration respectively. In PM_{10} these sources were included in the same factor together with the exhaust particles, accounting, all together, for more than 50% of the total PM_{10} concentration. They were confirmed to be the main components responsible for the several exceedences of the PM_{10} daily limit value registered during the winter period in the area of Ferrara. Traffic and industry showed low contributions, despite the intensive industrial and urban activities around the monitored area. There were no significant differences of

the sources among the three sampling sites, confirming the spatial homogeneity of PM despite the close proximity of the sampling points to the industrial area.

We could explain the co-variation of some sources, especially in $PM_{10,}$ by comparing the daily trend of the source with the pattern of the natural radioactivity. In the winter months, a very good agreement was observed among homogeneously distributed sources (biomass burning, secondary nitrate, exhaust), whose temporal variations were modulated by the mixing properties of the lower atmosphere. In summer there was no clear correlation between the time pattern of the sources and the natural radioactivity, probably due to the more efficient convective atmospheric mixing during the daytime.

The comparison between PMF source contributions and macro-sources obtained by mass closure calculations showed that both approaches provided similar spatial and temporal variability of the main PM sources in the monitored area. However, some important discrepancies were found in comparing quantitative estimates of the individual sources. In particular, the PMF model tended to overestimate the source contributions of crustal matter and marine aerosol, above all when transport events occurred, with differences that could not have been explained even when considering the uncertainties in the calculation of the unmeasured species. While the PMF overestimation of the sea spray seemed to be an artifact, the differences in crustal matter seemed to be due to the adsorption of significant amount of water and other species (secondary inorganic ions, OC) on the crustal particles.

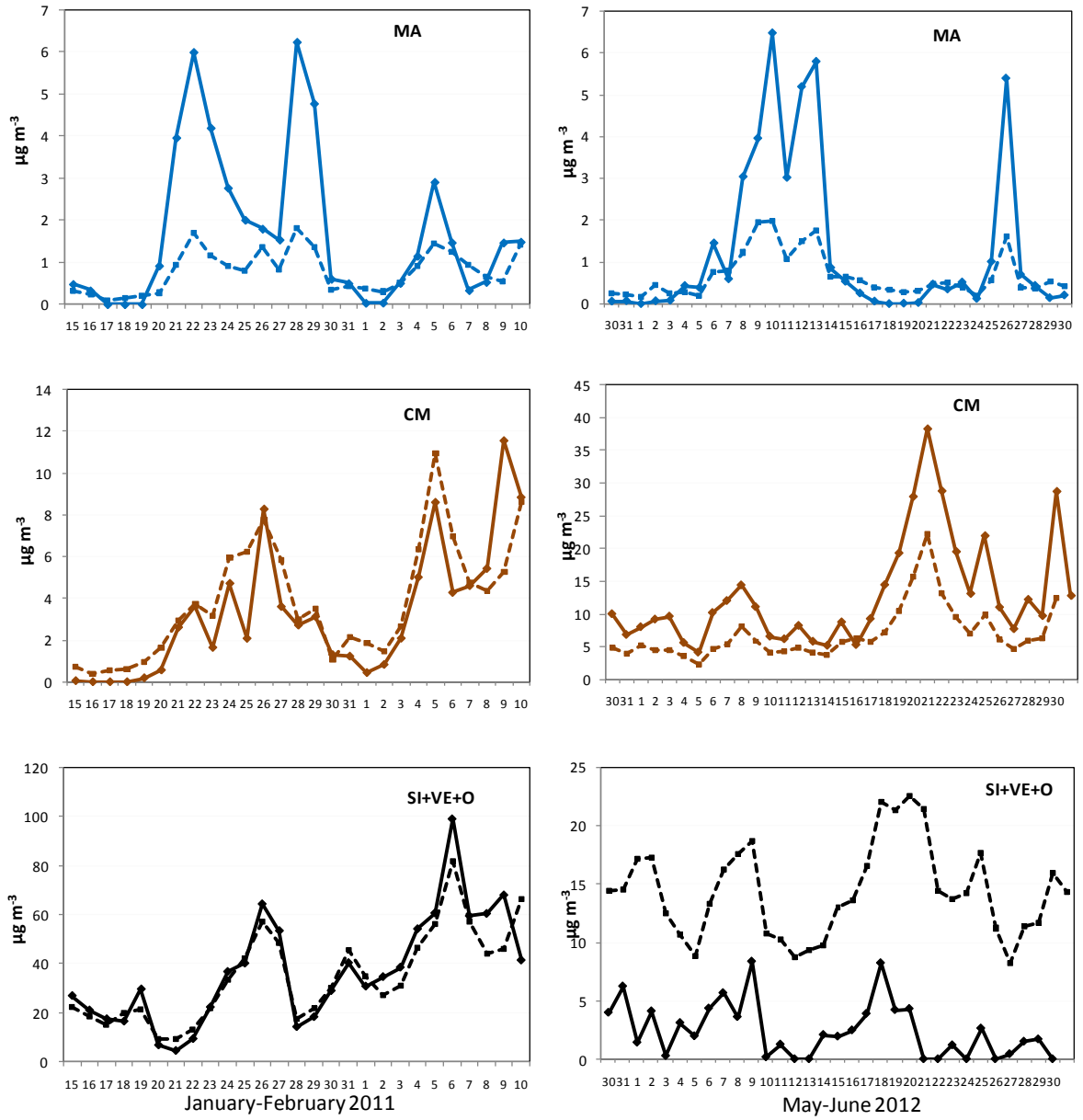

Fig.6.7: Daily variation of PM_{10} marine aerosol (MA, upper panel), crustal matter (CM, middle panel) and secondary inorganics+ vehicular emission+ organics (SI+VE+O, lower panel) sources at site C during winter 2011 and summer 2012. Solid line refers to PMF and dashed line refers to macro-sources calculation approach.

6.5 References

Almeida S M, Pio C A, Freitas M C, Reis M A, Trancoso M A (2006), Science of the Total Environment, 368: 663–674.

Amato F, Nava S, Lucarelli F, Querol X, Alastuey A, Baldasano J M, Pandolfi M,(2010), Science of the Total Environment, 408: 4309-4318.

Amato F, Pandolfi M, Moreno T, Furger M, Pey J, Alastuey A, Bukowiecki N, Prevot A S H, Baltensperger U, Querol X (2011), Atmospheric Environment, 45: 6777-6787.

Basart S, Pérez C, Nickovic S, Cuevas E, Baldasano J M (2012), Tellus, 64: 1-23.

Bernardoni V, Vecchi R, Valli G, Piazzalunga A, Fermo P (2011), Science of the Total Environment, 409: 4788-4795.

Canepari S, Cardarelli E, Giuliano A, Pietrodangelo A (2006a), Talanta, 69: 581–587.

Canepari S, Cardarelli E, Pietrodangelo A, Strincone M (2006b), Talanta, 69: 588–595.

Canepari S, Perrino C, Olivieri F, Astolfi M L (2008), Atmospheric Environment, 42: 8161–8175.

Canepari S, Perrino C, Astolfi M L, Catrambone M, Perret D (2009), Talanta, 77(5): 1821-1829.

Canepari S, Astolfi M L, Farao C, Maretto M, Frasca D, Marcoccia M, Perrino C (2013a), Environmental Science and Pollution Research, DOI: 10.1007/s11356-013-2298-1.

Canepari S, Farao C, Marconi E, Giovannelli C, Perrino C (2013b), Atmospheric Chemistry and Physics, 13: 1193–1202.

Castro L M, Pio, C A, Harrison R M , Smith D J T (1999), Atmospheric Environment, 33: 2771-2781.

Chan Y C, Simpson R W, McTainsh G H, Vowles P D (1997), Atmospheric Environment, 31: 3773–3785.

Chow J C (1995), Journal of Air Waste Management Association, 45: 320-382.

Contini D, Belosi F, Gambaro A, Cesari D, Stortini A M, Bove M C (2012), Journal of Environmental Science, 24(11): 1954-1965.

Ducret-Stich R E, Tsai M Y, Thimmaiah D, Kunzli N, Hopke P K, Phuleria H C (2013), Environmental Science and Pollution Research, DOI 10.1007/s11356-013-1682-1.

Gianini M F D, Gerhig R, Fisher A, Ulrich A, Wichser A, Hueglin C (2012), Atmospheric Environment, 59: 97-106.

Gietl J K, Lawrence R, Thorpe A J, Harrison R M (2010), Atmospheric Environment, 44: 141-146.

Harrison R M, Jones A M, Lawrence R G (2004), Atmospheric Environment, 38: 4531-4538.

Harrison R M, Jones A M, Lawrence R G (2003), Atmospheric Environment, 37: 4927-4933.

Hopke P K, Ito K, Mar T, Christensen W F, Eatough D J, Henry R C, Kim E, Laden F, Lall R V, Larson T, Liu H, Neas L, Pinto J, Stolzel M, Sush H, Paatero P, Thursto G D (2006), Journal of Exposure Science and Environmental Epidemiology, 16(3): 275-286.

Larsen B R, Gilardoni S, Stenstrom K, Niedzialek J, Jimenez J, Belis C A (2012), Atmospheric Environment, 50: 203-213.

Lee E, Chan C K, Paatero P (1999), Atmospheric Environment, 33: 3201-3212.

Marcazzan G M, Vaccaro S, Valli G ,Vecchi R (2001), Atmospheric Environment, 35: 4639–4650.

Marcazzan G M, Ceriani M, Valli G, Vecchi R (2003),Science of the Total Environment, 317: 137-147.

Paatero P. (1997), Chemometrics and Intelligent Laboratory Systems, 37(1): 23-35.

Paatero P, Tapper U (1994), Environmetrics, 5: 111-126.

Paatero P, Hopke P K (2003), Analitica Chimica Acta, 490 (1-2): 277-289.

Perrino C, Pietrodangelo A, Febo A (2001), Atmospheric Environment, 35: 5235–44.

Perrino C, Canepari S, Cardarelli E, Catrambone M, Sargolini T (2007), Environmental Monitoring Assessment, 128: 133-151.

Perrino C, Catrambone M, Pietrodangelo A (2008), Environmental International, 34: 621–628.

Perrino C, Canepari S, Catrambone M, Dalla Torre S, Rantica E, Sargolini T (2009), Atmospheric Environment, 43: 4766–4779.

Perrino C, Catrambone M, Dalla Torre S, Rantica E, Sargolini T, Canepari S (2013a), Environmental Science and Pollution Research, DOI 10.10077/s11356-013-2067-1.

Perrino C, Canepari S, Catrambone M (2013b), Aerosol and Air Quality Research. 13: 137-147.

Perrone M R, Becagli S, Garcia Orza J A, Vecchi R, Dinoi A, Udisti R, Cabello M (2013), Atmospheric Environment, 71: 176-186.

Polissar A V, Hopke P K, Paatero P, Malm W C, Sisler J F (1998), Journal of Geophysical Research, 103(15): 19045-19057.

Rees S L, Robinson A L, Khlystovd A, Stanier C O, Pandis S N (2004), Atmospheric Environment, 38: 3305–3318.

Reff A and Eberly S I (2007), Journal of Air Waste Management Association, 57: 146–154.

Stortini A M, Freda A, Cesari D, Cairns W R L, Contini D, Barbante C, Prodi F, Cescon P, Gambaro A (2009), Atmospheric Environment, 43: 6296-6304.

Terzi E, Argyropoulos G, Bougatioti A, Mihalopoulos N, Nikolaou K, Samara C (2010), Atmospheric Environment, 44: 2231–2239.

Turpin B J and Lim H (2001), Aerosol Science and Techonology, 35: 602–610.

Vecchi R, Chiari M, D'Alessandro A, Fermo P, Lucarelli F, Mazzei F, Nava S, Piazzalunga A, Prati P, Silvani F, Valli G (2008), Atmospheric Environment, 42: 2240-2253.

Viana M, Kuhlbush T A J, Querol X, Alastuey A, Harrison R M, Hopke P K, Winiwarter W, Vallius M, Szidat S, Prevot A S H, Hueglin C, Bloemen H, Wahlin P, Vecchi R, Miranda A I, Kasper-Giebl A, Maenhaut W, Hitzenberger R (2008a), Journal of Aerosol Science 39: 827-849.

Viana M, Pandolfi M, Minguillón M C, Querol X, Alaustey A, Monfort E, Celades I (2008b), Atmospheric Environment, 42: 3820-3832.

Viidanoja J, Sillanpää M, Laakia J, Kerminen V M, Hillamo R, Aarnio P, Koskentalo T (2002), Atmospheric Environment, 36: 3183-3193.

Watson J G (1984), Journal of Air Pollution Control Association, 34(6):619-623.

Watson J G, Robinson N F, Chew J, Henry R C, Kim B M, Pace T G, Meyer E L, Nguyen Q (1990), Environmental Software, 5: 38-49.

Watson J G, Zhu T, Chow J C, Engelbrecht J, Fujita E M, Wilson W E (2002), Chemosphere, 49:1093–1136.

Weckwerth G (2001), Atmospheric Environment, 35(32): 5525-5536.

Per la terza volta mi ritrovo nella mia stanza davanti al pc a sistemare grafici, tabelle, controllare pagine… e per la terza volta è arrivato il momento di ringraziare chi sta dietro ad ogni parola scritta in questa tesi. Tre anni sono volati e mi rendo conto adesso che forse sono stati quelli più belli, quelli più significativi… quelli trascorsi a fare ciò che veramente mi piace, quelli in cui ho vinto tante sfide con me stessa.

Comincio a dire un "GRAZIE" in generale a chi, in questi 3 anni, c'è sempre stato, a chi ad un certo punto ha deciso di cambiare strada…TUTTI ma proprio TUTTI mi hanno lasciato qualcosa, nel bene e nel male.

Ringrazio in primis i miei genitori, che mi hanno accompagnato anche in questo cammino, sostenendomi, lasciandomi libera di scegliere, ascoltandomi e consigliandomi ogni qualvolta si presentavano delle difficoltà che mi mettevano in crisi.

Ringrazio Moreno, il motivo principale per cui ricorderò sempre con gioia e piacere questi tre anni che, tra le altre cose, mi hanno regalato una persona tanto speciale e che ho la fortuna di avere al mio fianco ogni giorno. Grazie a lui ho capito cosa vuol dire veramente pensare "in due e per due", cosa significa fidarsi e poter contare su qualcuno che c'è sempre, anche quando riesco a dare il "peggio" di me (e lui può confermare che mi capita molto spesso!). Con la sua pazienza (infinita forse) è sempre pronto a starmi vicino ogni volta che divento paranoica, che vedo tutto "nero", che sono nervosa e scontrosa. Lo ringrazio anche per avermi accompagnato nell'esperienza in Inghilterra… perché senza di lui non sarei mai riuscita a rimanere da sola per così tanto tempo vivendo ogni giorno con il pensiero di trovarmi in una situazione "più grande" di me.

Ringrazio Silvia per avermi dato l'opportunità di conoscere un'amica, una persona con cui poter parlare di qualsiasi cosa, confrontarsi, ridere, scherzare, lavorare. Ma soprattutto la ringrazio perché il tempo passato a lavorare con lei mi è servito a capire qual è la strada che vorrei intraprendere. Ho trovato in lei una persona disponibile che mi ha stimolato e incoraggiato ad andare avanti anche quando pensavo di non farcela, fidandosi completamente di me. Spero di meritare sempre la sua fiducia e auguro a tutti di avere la fortuna di lavorare con una persona così... perché è bellissimo (e so per certo che è anche un'eccezione) tornare a casa la sera, sentirsi soddisfatti del proprio lavoro e pensare di essere "guidati" da una persona competente che stimi e che consideri un punto di riferimento.

Ringrazio tutti i ragazzi che ho conosciuto in laboratorio durante questi anni (Chiara, Irene, Valeria, Barbara, Mariano, Claudia, Angelo, Carolina, Stefano, Gabriele, Pia, Luigi… mi scuso se ho dimenticato qualcuno) per avermi regalato tanti sorrisi e per aver reso il lavoro divertente anche quando eravamo sommersi da migliaia di filtri!. Ma il mio "Grazie" più grande va a Melissa, Daniele e Giulia (Giulietta mia bella!) con i quali ho instaurato un rapporto che va ben oltre l'aspetto lavorativo. Mi ritengo molto fortunata ad avere incontrato delle belle persone come loro, a cui ho avuto ed ho l'onore di trasmettere tutto ciò che ho imparato. Spero di mantenere con loro questo rapporto anche quando sarà il momento per me di cambiare strada… (sperò un po' più in là!)

Ringrazio Elisabetta che mi ha visto “nascere” e “crescere” in laboratorio sin dalla mia tesi di laurea… e che continua ad esserci per me anche se non abbiamo più il tempo di una volta per stare insieme e consigliarci a vicenda.

Ringrazio Maria Luisa, anche lei presente sin dall’inizio, per avermi insegnato come fare le cose in laboratorio e per tutte le volte che le ha fatte insieme a me perché avevo paura di sbagliare e fare danni.

Ringrazio Cinzia per avermi dato la possibilità di lavorare anche con lei, per la sua disponibilità e per i suoi consigli preziosi.

Infine ringrazio Rosalba per avermi accolto tutte le sere con un sorriso quando rientravo a casa stanca, per avermi offerto un momento di svago nelle giornate più “buie”, ascoltando le mie confessioni nel bene e nel male. Un’amica vera che spero ci sarà sempre.